



University
of Glasgow

Del Rosario, Mario (2019) *Apicomplexan F-actin is required for efficient nuclear entry during host cell invasion*. PhD thesis.

<http://theses.gla.ac.uk/75066/>

Copyright and moral rights for this work are retained by the author

A copy can be downloaded for personal non-commercial research or study,
without prior permission or charge

This work cannot be reproduced or quoted extensively from without first
obtaining permission in writing from the author

The content must not be changed in any way or sold commercially in any
format or medium without the formal permission of the author

When referring to this work, full bibliographic details including the author,
title, awarding institution and date of the thesis must be given

Enlighten: Theses

<https://theses.gla.ac.uk/>
research-enlighten@glasgow.ac.uk

Apicomplexan F-actin is required for efficient nuclear entry during host cell invasion

By

Mario Del Rosario
Biologist, M.Res.

Submitted in fulfilment of the requirements for the
Degree of Doctor of Philosophy

School of Life Sciences
College of Medical, Veterinary & Life Science
Institute of Infection, Immunity & Inflammation
University of Glasgow

Abstract

The opportunistic pathogen *Toxoplasma gondii* is an obligate intracellular parasite part of the phylum *Apicomplexa*, able to infect all warm-blooded animals including humans. Invasion by apicomplexan parasites such as *Plasmodium falciparum* and *Toxoplasma gondii* to host cells requires the establishment and crossing through of a small ring-like junctional structure serving as an interface and stabiliser between the parasite and host cell plasma membrane. During the invasion process, the host cell possibly resist invasion to some degree, exerting force on the parasite's entry point as *de novo* actin polymerisation has been characterised in this location (Gonzalez *et al.*, 2009). Additionally, the parasite is required to generate force via an actomyosin motor to achieve host cell membrane penetration successfully, leading to mechanical deformation when the parasite is squeezing through the junctional ring. This actomyosin motor depends on a protein complex termed the glideosome, that pulls actin to achieve forward motility.

Actin plays a key role in the parasite's biology with important functions not only during invasion but also during replication, apicoplast maintenance and egress. Until recently, the lack of reliable F-actin sensors hampered the characterisation of actin dynamics during these processes. With the use of nanobodies with the potential to recognise actin (Periz *et al.*, 2017), a complex actin behaviour was uncovered allowing the assessment of *in vivo* dynamics through the parasite's lytic cycle. The uncovered flow of F-actin presented new opportunities to address debate over established hypothesis on parasite's actin and to extend the initial roles attributed to actin including the establishment of cytoplasmic actin pool through the parasite's life. Additionally, these F-actin dynamics were shown to be affected by traditional actin modulating drugs, as well as interference with actin binding factors resulting in abrogation of these dynamics and phenotypes associated with motility.

Additionally in this thesis, it is suggested that F-actin's role in invasion goes beyond powering the glideosome via force traction, but to facilitate nucleus passage and deformation. Real time and super resolution microscopy highlighted that during invasion events, the junction ring can oppose nucleus passage as parasites deficient of core components of the acto-myosin system have been shown to be incapable of withstand pressure exerted at the junction ring, leading

to blebbing and collapse of the invading parasite (Bichet *et al.*, 2016). Although some of these parasites are able to complete invasion, the dynamics are visibly affected suggesting more systems are at play during invasion.

The literature shows that other eukaryotic systems deploy nucleus protection and displacement mechanisms to facilitate migration through tight spaces by the concerted action of actomyosin complexes and cytoskeletal structures (Petrie *et al.*, 2012; Petrie and Yamada, 2015; McGregor, Hsia and Lammerding, 2016). This thesis proposes that the F-actin machinery facilitates nucleus passage through the junctional ring, offering a model for the dual contribution of F-actin forces by constricting and pushing/pulling the nucleus during host cell invasion by these apicomplexan parasites, sharing similar mechanism with those of larger eukaryotes.

Table of Contents

Abstract	2
Table of Contents	4
List of Tables.....	8
List of Figures	9
List of Accompanying Material.....	11
Figure copyright permissions	13
Acknowledgements.....	14
Author's Declaration	16
Publications arising from this work and collaborations	17
Conference Proceedings.....	17
Definitions/abbreviations	19
1 Introduction.....	21
1.1 The apicomplexan phylum and <i>Toxoplasma gondii</i>	21
1.2 Pathogenesis and clinical features.....	22
1.3 Lifecycle of <i>Toxoplasma gondii</i>	24
1.3.1 Lifecycle in the definitive host.....	25
1.3.2 Lifecycle in the intermediate host.....	25
1.3.2.1 The lytic cycle.....	25
1.4 Gliding motility	26
1.5 Invasion	28
1.6 Replication and egress.....	29
1.7 <i>Toxoplasma gondii</i> morphology	31
1.7.1 Ultrastructure	31
1.7.2 The apical complex and secretory organelles	33
1.7.2.1 The conoid and microtubule structures.....	33
1.7.2.2 Micronemes, rhoptries and dense granules	34
1.7.3 The Inner Membrane Complex	35
1.7.4 The nucleus.....	36
1.7.5 Apicoplast.....	36
1.8 <i>Toxoplasma gondii</i> : the model organism for genetic studies	38
1.8.1 Reverse genetics engineering and gene regulation.	38
1.8.1.1 Genetic level regulation.....	38
1.8.1.2 Transcriptional level regulation	39
1.9 Actin, a highly dynamic protein	40
1.9.1 Overview, structure in eukaryotic cells, nucleation and treadmilling. 40	
1.9.1.1 Actin in Apicomplexa	43

1.9.2	Actin polymerisation	45
1.9.2.1	Actin binding proteins (ABPs)	45
1.10	Efforts to visualise actin in Apicomplexan parasites	50
1.10.1	Endogenous tagging, antibodies against actin and chromobodies in <i>Toxoplasma gondii</i>	50
1.11	Mammalian cell migration and the role of actin and actin-related structures.	52
1.11.1	The role and mechanism of actin during cell motility in eukaryotes.	52
1.11.1.1	Motility on 2D surfaces and the core components facilitating this process.....	52
1.11.1.2	3D motility presents high plasticity in cell movement.....	55
1.11.2	Dynamics surrounding the nucleus during cell migration	56
1.12	Open questions regarding apicomplexan motility	59
1.12.1	The actomyosin motor and the linear motor model	59
1.13	Aims of this study	64
2	Materials and Methods.....	65
2.1	Equipment	65
2.2	Computer Software.....	66
2.3	Consumables, biological and chemical reagent	66
2.4	Kits.....	67
2.5	Buffers, solutions and media.....	67
2.6	Antibodies	70
2.7	Plasmids.....	71
2.8	Cell strains.....	71
2.8.1	Bacteria strains	71
2.8.2	<i>Toxoplasma gondii</i> strains.....	72
2.9	Mammalian cell lines.....	72
2.10	Molecular biology	72
2.10.1	Restriction endonuclease digest	72
2.10.2	Determination of nucleic acid concentrations.....	73
2.10.3	Plasmid transformation into bacteria	73
2.10.4	Isolation of plasmid DNA from bacteria.....	73
2.10.5	Small scale DNA plasmid extraction	74
2.10.6	Medium and large scale DNA plasmid extraction	74
2.10.7	Ethanol precipitation	74
2.11	Cell biology	74
2.11.1	<i>Toxoplasma gondii</i> tachyzoites and mammalian cells <i>in vitro</i> culturing	74
2.11.2	Trypsin/EDTA treatment of mammalian cell lines	75
2.11.3	Cryopreservation of <i>T. gondii</i> and thawing of stabilates.....	75

2.11.4	Transfection of <i>Toxoplasma gondii</i>	75
2.11.5	Transient transfections.....	75
2.11.6	Stable transfection.....	76
2.11.7	Isolation of clonal parasite lines by limited dilution.....	76
2.11.8	Inducing the <i>act1</i> KO	76
2.11.9	Fluorescence activated cell sorting	77
2.12	Tachyzoite phenotypic analysis	77
2.12.1	Immunofluorescence assay	77
2.12.2	Plaque assay	78
2.12.3	Time-lapse video microscopy.....	78
2.12.4	Inducing the conditional Cas9 <i>act1</i> cKO	78
2.12.5	Light microscopy	79
2.12.6	Flow analysis time-lapse microscopy.....	79
2.12.7	Parasite treatment with A23187 and BIPPO	79
2.12.8	Tight Junction assay	80
2.12.9	Live cell invasion	80
2.12.10	Correlative light-electron microscopy (CLEM)	81
2.12.11	Plasmodium Assays.....	81
2.13	Biochemistry	81
2.13.1	Preparation of parasite cell lysates	81
2.13.2	Sodium dodecyl sulphate polyacrylamide gel electrophoresis	82
2.13.3	Western blotting	82
2.13.4	Ponceau-staining	83
2.13.5	Immunostaining.....	83
2.13.6	Visualisation and quantification of the protein bands	83
2.14	Bioinformatics	83
2.14.1	Data and statistical analysis.....	83
2.14.2	Color-coded kymogram generation for particle dynamics analysis	84
2.14.3	Skeletonisation Analysis	85
2.14.4	Cell deformation analysis	85
2.14.5	Penetration Speed profile analysis	85
3	F-actin behaviour in <i>Toxoplasma gondii</i> through the lytic cycle.....	86
3.1	Expressing Chromobody-Emerald in <i>Toxoplasma gondii</i>	87
3.2	Cytoplasmic F-actin dynamics during <i>T. gondii</i> replication	90
3.3	F-actin accumulation on potential attachment points during parasite gliding motility	92
3.4	F-actin dynamics during parasite invasion into host cells.	94
3.5	The Actin Depolymerisation Factor (ADF) drastically alters <i>T. gondii</i> F-actin dynamics across the lytic cycle.	96

3.6	Discussion	104
4	F-actin in vivo dynamics analysis	107
4.1	F-actin live dynamics during replication; picking the best tool for image analysis on a very challenging subject.....	108
4.2	Skeletonisation analysis of F-actin: applying image processing methods to analyse Apicomplexan actin.	110
4.3	F-actin and kymograph analysis: a classic tool for actin flow analysis .	115
4.4	Limiting user input bias in flow analysis: KymographDirect and KymographClear.....	119
4.5	F-actin flow directionality on wild type parasites	121
4.6	Actin Depolymerisation Factor and Actin modulating drugs alters the F-actin flow in <i>Toxoplasma gondii</i>	123
4.7	F-actin flow analysis on extracellular parasites	126
4.8	Discussion	136
5	<i>Toxoplasma gondii</i> invasion dynamics: nuclear squeeze and the F-actin ring involvement in invasion	138
5.1	<i>Toxoplasma gondii</i> suffers mechanical stress during invasion	139
5.2	The nucleus acts as a limiting factor for parasite invasion; a potential explanation for abortive events	141
5.3	The F-actin ring is not present in all cases of invasion; parasite mutant lines invasion behaviour	143
5.4	<i>In vivo</i> analysis of F-actin dynamics and nuclear squeeze during <i>Toxoplasma gondii</i> invasion.	149
5.5	Super-resolution SIM analysis of invading parasites	152
5.6	Correlative Light-Electron Microscopy analysis of F-actin bundles association with the nucleus	155
5.7	<i>Toxoplasma gondii</i> F-actin-nucleus association.....	157
5.8	F-actin and nuclear squeeze invasion dynamics in other <i>Apicomplexan</i> parasites	159
5.9	Discussion	161
6	Discussion	163
6.1	F-actin flow, nucleation points and parasite replication.	164
6.2	Immobile extracellular parasites and actin flow.....	168
6.3	<i>Toxoplasma gondii</i> invasion: new perspectives on actin dynamics during invasion	172
6.4	Summary on findings and outlook.	176
7	Bibliography.....	178

List of Tables

Table 0.1 Copyright permissions obtained for figures reproduced from journal publications	13
Table 2.1. Buffers for DNA Analysis.....	67
Table 2.2. Buffers for Western blot analysis	68
Table 2.3. Buffers and media for bacterial culture	68
Table 2.4. Buffers and media for <i>T. gondii</i> tachyzoites and mammalian cell culture	68
Table 2.5. Primary antibodies	70
Table 2.6. Secondary antibodies, fluorescent ligands and stains	70
Table 3.1 Comparison between Act1 KO and Adf KD.....	104

List of Figures

Figure 1-1 Lifecycle of <i>Toxoplasma gondii</i>	24
Figure 1-2 <i>Toxoplasma gondii</i> lytic cycle.	26
Figure 1-3 <i>Toxoplasma gondii</i> invasion.	29
Figure 1-4 <i>Toxoplasma gondii</i> ultrastructure.	32
Figure 1-5 Structure of monomeric actin.	41
Figure 1-6 Actin nucleation.	42
Figure 1-7 Actin filament structure.	43
Figure 1-8 Actin binding factors in apicomplexan parasites.	50
Figure 1-9 Chromobody expression in <i>Toxoplasma gondii</i>	51
Figure 1-10 Major components of motile cells during migration.	54
Figure 1-11 3D motility plasticity to adapt to different situations.	56
Figure 1-12 Schematic of interactions between nuclear proteins and cytoskeleton.	58
Figure 1-13 Cytoskeletal organisation and dynamics around the nucleus during migration.	59
Figure 1-14 Linear motor model for <i>Toxoplasma gondii</i> actin-force generation.	63
Figure 3-1 Scheme for the generation of a chromobody EmeraldFP line.	88
Figure 3-2 Expression of the chromobody EmeraldFP in a RH wt line.	89
Figure 3-3 Chromobody EmeraldFP parasites during replication.	91
Figure 3-4 Types of 2-D gliding motility of <i>Toxoplasma gondii</i>	94
Figure 3-5 Invasion of RH parasites expressing chromobody EmeraldFP.	95
Figure 3-6 Generation of an adf cKD chromobody EmeraldFP.	97
Figure 3-7 Location of different organelles after tetracycline induction of adf cKD parasites.	101
Figure 3-8 Location of both the apicoplast and mitochondria after tetracycline induction on adf cKD parasites.	104
Figure 4-1 F-actin flow dynamics on <i>Toxoplasma gondii</i>	110
Figure 4-2 Optimisation of conditions for live and fixed microscopy to analyse F-actin localisation and dynamics in <i>T.gondii</i>	111
Figure 4-3 Workflow of a Skeletonisation procedure.	112
Figure 4-4 Skeletonisation process performed on time-lapse images of <i>Toxoplasma gondii</i>	114
Figure 4-5 Kymograph analysis of flowing particles.	116
Figure 4-6 Semi-automatic kymograph analysis of F-actin flow dynamics.	118
Figure 4-7 Example of an automatic kymograph analysis using KymographClear and KymographDirect	121
Figure 4-8 Automatic kymograph analysis using KymographClear and KymographDirect.	123
Figure 4-9 Flow analysis of RH chromobody EmeraldFP parasites treated with different Jasplakinolide concentrations and adf KD time course after ATc treatment.	126
Figure 4-10 F-actin flow in resting extracellular parasites.	130
Figure 4-11 Extracellular actin dynamics are shifted upon addition of A23187 or BIPPO.	133
Figure 4-12 Kymograph analysis of actin flow upon addition of A23187.	136
Figure 5-1 The parasite and its nucleus are deformed during invasion.	141
Figure 5-2 <i>T.gondii</i> nucleus can act as a limiting factor for invasion.	142
Figure 5-3 F-actin dynamics during <i>Toxoplasma gondii</i> invasion during fixed and live imaging.	146

Figure 5-4 F-actin dynamics during <i>Toxoplasma gondii</i> invasion.	148
Figure 5-5 Time lapse analysis of parasites that show accumulation of F-actin at the junction.	152
Figure 5-6 Super-resolution microscopy demonstrates formation of a F-actin cage around the nucleus during invasion.	155
Figure 5-7 Correlative Light and Electron microscopy during invasion.	156
Figure 5-8 Super-resolution microscopy demonstrates formation of a F-actin cage around the nucleus during invasion.	159
Figure 5-9 Plasmodium spp F-actin dynamics during invasion.	160
Figure 6-1 <i>Toxoplasma gondii</i> filamentous actin flow model in replicating parasites.	167
Figure 6-2 <i>Toxoplasma gondii</i> flow model in extracellular parasites.	171
Figure 6-3 Model of actin flow in highly polarised parasites during penetration.	174
Figure 6-4 Model of the proposed nuclear squeeze mechanism during apicomplexan invasion.	176

List of Accompanying Material

Movie S1. Actin flow during parasite replication. F-actin flow in multiple stages during replication. Imaging speed 7 fps.

Movie S2. Gliding motility and actin dynamics. F-actin dynamics during helical, circular and twirling gliding motility. Imaging speed 7 fps.

Movie S3. Invasion and F-actin dynamics. Invading parasite showing an F-actin ring during invasion. Imaging speed 7 fps.

Movie S4. Gliding motility during ADF depletion. ADF depletion causes a change in motility. Imaging speed 7 fps.

Movie S5. F-actin flow dynamics during ADF depletion. The dynamics of F-actin were analysed using skeletonisation modelling during ADF depletion. Imaging speed 7 fps.

Movie S6. F-actin dynamics are affected with Jasplakinolide treatment. Drug assay showing the degree F-actin dynamics are affected during JAS treatment. Imaging speed 7 fps.

Movie S7. F-actin dynamics are affected with the depletion of ADF. ATc treatment showing the F-actin dynamics changes once ADF is being depleted. Imaging speed 7 fps.

Movie S8. SR-SIM time-lapse of actin flow with skeletonisation analysis. Time-lapse of SR-SIM showing RH, myoAKO and adfKD parasites expressing chromobody EmeraldFP. Imaging speed 7 fps.

Movie S9. SR-SIM time-lapse of actin flow before and after calcium ionophore A23187 or BIPPO. Time-lapse of SR-SIM showing RH, myoAKO and adfKD parasites expressing chromobody EmeraldFP before and after calcium ionophore A23187 or BIPPO. Imaging speed 7 fps.

Movie S10. Wild type RH parasites invading HFF cells. Two time-lapse moving showing live invasion of RH wild type parasites. Imaging speed 7 fps.

Movie S11. Mutants parasite lines invading HFF cells. Parasite mutant lines myoA KO, act1 KO and mlc1 KO time-lapse moving showing live invasion of myoA KO parasites. Imaging speed 7 fps.

Movie S12. Abortive invasion by different parasite strains. Wild type RH, myoA KO, act1 K and mlc1 KO parasites time-lapse moving showing live abortive invasion of RH wild type parasites. Imaging speed 7 fps.

Movie S13. F-actin events during invasion. An F-actin ring appears during initial parasite penetration. However, the presence of an F-actin ring is not required in some cases. In rare cases such as capped invasion, the F-actin ring is also present. In mutants with abrogated F-actin dynamics such as adf cKD, the F-actin ring is

not present during invasion. Time-lapse moving showing live invasion of Cb-EmeraldFP parasites. The signal is F-actin Cb-EmeraldFP. Imaging speed 7 fps.

Movie S14. RH Chromobody EmeraldFP parasites invasion and F-actin dynamics during nucleus passage. Nucleus passage when the F-actin ring is present and absent. Time-lapse moving showing live invasion of Cb-EmeraldFP wild type parasites with an F-actin ring formation. Cb-EmeraldFP is shown in green, Hoechst staining is shown in magenta. Imaging speed 7 fps.

Movie S15. 3D rendering of RH and adf cKD Chromobody EmeraldFP parasites invasion with and without F-actin ring. 3D rendering using IMARIS software on invading Cb-EmeraldFP wild type and adf cKD parasites with an F-actin ring formation. Cb-EmeraldFP is shown in green, Hoechst staining is shown in magenta. Imaging speed 7 fps.

Movie S16. 3D rendering of RH Chromobody EmeraldFP parasites invasion with microtubule and TJ staining. 3D rendering using IMARIS software on invading Cb-EmeraldFP parasites with an F-actin ring formation. Cb-EmeraldFP is shown in green, Hoechst staining is shown in magenta, RON2 staining is shown in yellow and MT staining is shown in red. Imaging speed 7 fps.

Figure copyright permissions

Table 0.1 Copyright permissions obtained for figures reproduced from journal publications

Publisher	Journal	Reference journal title	Author (Year)	Figure No. in paper	Figure No. in this thesis	Copyright permission code
Springer Nature	Nature Reviews Microbiology	Modulation of innate immunity by <i>Toxoplasma gondii</i> virulence effectors	Christopher A. Hunter, L. David Sibley	Figure 1	Figure 1-1	4574820281685
Annual Reviews	Annual Review of Microbiology	Lytic Cycle of <i>Toxoplasma gondii</i> : 15 Years Later	Ira J. Blader, Bradley I. Coleman, Chun-Ti Chen, and Marc-Jan Gubbels	Figure 1	Figure 1-2	4574830301273
Springer Nature	Nature Reviews Microbiology	Gliding motility powers invasion and egress in Apicomplexa	Karine Frénal, Jean-François Dubremetz, Maryse Lebrun, Dominique Soldati-Favre	Figure 3	Figure 1-3	4574820835491
Annual Reviews	Annual Review of Microbiology	Lytic Cycle of <i>Toxoplasma gondii</i> : 15 Years Later	Ira J. Blader, Bradley I. Coleman, Chun-Ti Chen, and Marc-Jan Gubbels	Figure 1	Figure 1-4	4574830301273
The American Association for the Advancement of Science	Science	The Crystal Structure of Uncomplexed Actin in the ADP State	Ludovic R. Otterbein, Philip Graceffa, Roberto Dominguez	Figure 1	Figure 1-5	4575280621999
Annual Reviews	Annual Review of Biophysics	Actin structure and function.	Dominguez R and Holmes KC.	Figure 2	Figure 1-7	4575281092822
Elsevier	Current Opinion in Cell Biology	Multiple mechanisms of 3D migration: the origins of plasticity	Ryan J Petrie, Kenneth M Yamada	Figure 1	Figure 1-10	4580180282038
Elsevier	Current Opinion in Cell Biology	Squish and squeeze—the nucleus as a physical barrier during migration in confined environments	Alexandra Lynn McGregor, Chieh-Ren Hsia, Jan Lammerding	Figure 1	Figure 1-11	4575441474641
Elsevier	Current Opinion in Cell Biology	Squish and squeeze—the nucleus as a physical barrier during migration in confined environments	Alexandra Lynn McGregor, Chieh-Ren Hsia, Jan Lammerding	Figure 1	Figure 1-12	4575441474641
Springer Nature	Nature Reviews Microbiology	Gliding motility powers invasion and egress in Apicomplexa	Karine Frénal, Jean-François Dubremetz, Maryse Lebrun, Dominique Soldati-Favre	Figure 4	Figure 1-14	4670850372733

Acknowledgements

First of all, I want to thank my supervisor Prof. Markus Meissner for the all the support, guidance and discussion over the years. Markus, I'm very grateful for your generosity, motivation and contagious passion for science. Thank you for the opportunity to do this PhD.

My PhD education was possible thanks to the Ecuadorian government, as my scholarship was funded by SENESCYT in the *Universities of Excellence* program.

I also want to thank my second supervisor Prof. Andy Waters, for his suggestions and helpful advice that improved my development. I also want to acknowledge my PhD assessors Prof. Harry De Koning, Prof. Jeremy Mottram and Dr Meredith Stewart for your insight on my project and advice to further my research.

I'm grateful to all current and former members of the Meissner lab. From my start as a masters' student and through my PhD. I'm grateful with the invasion team in particular: Dr. Simon Gras, Dr. Gurman Pall, Dr. Javier Periz, Dr. Jamie Whitelaw, Dr. Sujaan Das and Dr. Fernanda Latorre-Barragan; all the brainstorming session were very helpful to steer my research in good track. I also want to thank my PhD first year supervisor Dr. Musa Hassan for his insightful comments and advice, and for teaching me the value of patience.

My PhD would have not been the same without my all the friends I made through the years: Jamie, Johannes, Simon, Chris, Matthew and Javier, I remember fondly all the laugh and general "nastiness" of our office in the level 6 of the GBRC. My time at the lab would not have been the same without Elena, Carmen and Mari, thank you for all the laughs and your friendship. Additionally, all my friends through the level 5 and 6 in the GBRC: Craig, Jim, Emma, Cat, Will, Dan Paape and Harris, Andrew, Sam, Patrizia, Federica, Jana and Alice and the whole of the McCulloch, Hammarton, Waters, Marti and Sheiner labs. I'm grateful for all the support from the staff of the Flow Core Facility, particularly Alana and Diane. I specially want to thank Chris, Leandro and Matthew for taking the time to read through my thesis and correct my silly mistakes, thank you guys, a lot.

To my surrogate family during all these years, Fernando and Anita. Your friendship and support were very welcome through this PhD. Jamie, I remember how welcomed you made me feel from the very first moment I started working at the lab during my masters to the great friend you became through the years, thank you, you are the most amazing Scotsman I have met during all my years in Glasgow. Leandro and Joana, your support, insight and friendship was very important during these years, thank you. Also, my other Ecuadorian family, Andrea and Fernanda. Thank you for your support through all these years. I also want to thank Johannes for his friendship and support, my time in Glasgow would not have been the same without you. We were the last men standing in the Glasgow-branch of our lab... I could not have asked for a better friend for it!

Thank you Natalia, for your friendship and the many laughs, it was amazing to have someone around who knows of good music. I still remember the San Juan bonfire in the meadow. Glasgow would not have been the same without Javier, thank you for your friendship and insight, for all the time we spent discussing about parasite invasion, actin and microscopy, but also about life in general. Also, thank you Leandro for all your help in the many microscope question I bothered you over the years, I learned much from you. Gurman, I'm very grateful for your help over the years and your sound advice. For your approachability and friendship, Elena and Chris, thank you.

My family has always been supportive of my academic studies. I want to thank my mother, Olga who has always encouraged me to pursue my passion. My sisters Veronica and Karina for always been there for me to give me courage. I also want to thank those no longer with us, my dad, the other Mario Del Rosario and the first Dr. from my family. You are still the beacon I look up to. My grandma Flora and my grandpa Igor, your unconditional love and warm is always with me.

Lastly, I want to thank my fiancé Helena. You are always there for me, cheering for me, caring for me. I only hope I can return all the love and support you have given me. We have been together through this journey and we are going to see it through, together.

Author's Declaration

I, Mario Del Rosario hereby declare that I am the sole author of this thesis and performed all of the work presented, with the following exceptions highlighted below. No part of this thesis has been previously submitted for a degree at this or another university.

Chapter 5:

Invasion and abortive events of *act1KO* appearing in Figure 5-2 and Movie S11-12 were captured by Dr. Jamie Whitelaw and Dr. Fernanda LaTorre-Barragan, College of Medical, Veterinary and Life Sciences, Institute of Infection, Immunity and Inflammation, University of Glasgow.

SR-SIM microscopy in Figure 5-6 and 5-8 were done in collaboration with Dr. Javier Periz, College of Medical, Veterinary and Life Sciences, Institute of Infection, Immunity and Inflammation, University of Glasgow.

Correlative Light and Electron microscopy in Figure 5-7 was done by Dr. Leandro Lemgruber, Imaging Technologist, College of Medical, Veterinary and Life Sciences, Institute of Infection, Immunity and Inflammation, University of Glasgow.

Plasmodium experiments done in Figure 5-9 by Dr. Sujaan Das, College of Medical, Veterinary and Life Sciences, Institute of Infection, Immunity and Inflammation, University of Glasgow and Dr. Oliver Lyth and Dr. Jake Baum, Department of Life Sciences, Imperial College London.

Chapter 6:

Invasion model in Figure 6-4 originally done by Dr. Javier Periz, College of Medical, Veterinary and Life Sciences, Institute of Infection, Immunity and Inflammation, University of Glasgow and modified by the author.

Publications arising from this work and collaborations

Mario Del Rosario, Javier Periz, Georgios Pavlou, Oliver Lyth, Fernanda Latorre-Barragan, Sujaan Das, Gurman S. Pall, Johannes Felix Stortz, Leandro Lemgruber, Jake Baum, Isabelle Tardieux and Markus Meissner. “Apicomplexan F-actin is required for efficient nuclear entry during host cell invasion”. Accepted - EMBO Reports (Production is currently taking place).

Javier Periz, Mario Del Rosario, Alexandra McStea, Simon Gras, Colin Loney, Lin Wang, Marisa L Martin-Fernandez, and Markus Meissner. “A highly dynamic F-actin network regulates transport and recycling of micronemes in *Toxoplasma gondii* vacuoles”. Nature Communications 10:4183 (2019)

Johannes Felix Stortz, Mario Del Rosario, Mirko Singer, Jonathan M Wilkes, Markus Meissner and Sujaan Das. “Formin-2 controls spatiotemporal polymerisation of actin filaments enabling segregation of apicoplasts and efficient cytokinesis in *P. falciparum*”. eLife 2019 8:e49030

Javier Periz, Jamie Whitelaw, Clare Harding, Simon Gras, Mario Igor Del Rosario Minina, Fernanda Latorre-Barragan, Leandro Lemgruber, Madita Alice Reimer, Robert Insall, Aoife Heaslip, Markus Meissner. “*Toxoplasma gondii* F-actin forms an extensive filamentous network required for material exchange and parasite maturation”. eLife 2017 6:e2411.

Conference Proceedings

Parts of the following thesis have been presented at the following conferences and various other local and national meetings.

XXIX Annual Molecular Parasitology Meeting in Woods Hole, MA, USA in September 2018.

- I gave a poster presentation on “Apicomplexan F-actin is required for efficient nuclear entry during host cell invasion”

EMBL Conference BioMalPar XIV: Biology and Pathology of the Malaria Parasite in the EMBL Heidelberg, Germany in May 2018.

- I gave an oral presentation on “Apicomplexan F-actin is required for efficient nuclear entry during host cell invasion”

EMBL Conference: BioMalPar XIII: Biology and Pathology of the Malaria Parasite in the EMBL Heidelberg, Germany in May 2017.

- I gave a poster presentation on “Apicomplexan F-actin is required for efficient nuclear entry during host cell invasion”

Definitions/abbreviations

°C	Degree Celsius	<i>E. coli</i>	<i>Escherichia coli</i>
Aa	Amino acid		
ADF <i>adf</i>	Actin depolymerisation factor	EDTA	Ethylene diamine tetraacetic acid
AID	Auxin-inducible degron	ER	Endoplasmic reticulum
AMA1	Apical membrane antigen 1	EtOH	Ethanol
Amp	Ampicillin	FBS	Fetal bovine serum
ADP	Adenosine diphosphate	fw	Forward
ATP	Adenosine triphosphate	FRM	Formin
BLAST	Basic Local Alignment Search Tool	g	Gram or Gravity (context dependent)
BIPPO	5-Benzyl-3-isopropyl-1H-pyrazolo[4,3-d]pyrimidin-7(6H)-one	GAP	Glideosome associated protein
bp	Base pair	gDNA	Genomic deoxyribonucleic acid
BSA	Bovine serum albumin	GFP	Green fluorescent protein
Ca ²⁺	Calcium	GOI	Gene of interest
CAT	Chloramphenicol acetyltransferase	GED	GTPase Effector Domain
cDNA	Complementary deoxyribonucleic acid	GPI	Glycophosphatidylinositol
Cas9	Caspase9	GTP	Guanosine triphosphate
Cb	Chromobody	h	Hour
Cb-Em	Chromobody EmeraldFP	H ₂ O	Water
CDPK	Calcium-dependent protein kinase	HEPES	4-(2-Hydroxyethyl)-piperazineethanesulphonic acid
CD	Cytochalasin D	HFF	Human foreskin fibroblast
CIP	Calf intestinal phosphatase	Hx or hxgprt	Hypoxanthine-xanthine-guanine phosphoribosyl transferase
C-terminal	Carboxyl terminal	IAA	indole-3-acetic acid
CRISPR	Clustered Regularly Interspaced Short Palindromic Repeats	IFA	Immunofluorescence analysis
DD	Destabilisation domain	IMC	Inner membrane complex
DHFR	Dihydrofolate reductase	IMM	Inner Mitochondrial membrane
DiCre	Dimerisable Cre	kbp	Kilo base pair
DMEM	Dulbecco's Modified Eagle's Medium	KD	Knockdown
DMSO	Dimethyl sulfoxide	kDa	Kilo Dalton
DN	Dominant negative	KO	Knockout
DNA	Deoxyribonucleic acid	rpm	revolutions per min
dNTP	Deoxynucleotide 5'-triphosphate	RT	Room temperature

LB	Luria-Bertani	rev	Reverse
LoxP	Locus crossover in P1	s	Second
M	Molar	SAG1	Surface antigen 1
MCS	Multiple cloning site	SD	Standard deviation
mg	Milligram	SDS-PAGE	Sodium dodecyl sulfate polyacrylamide gel electrophoresis
MIC	Micronemal protein	SEM	Standard of the mean
min	Minute	SOC	Super optimal broth with catabolite repression
ml	Millilitre	<i>spp.</i>	Species
mM	Milimolar	SSR	Site specific recombination
MPA	Mycophenolic acid	t	Time
mRNA	Messenger ribonucleic acid	<i>T. gondii</i> or <i>Tg</i>	<i>Toxoplasma gondii</i>
MT	Microtubule	TAE	Tris-acetate-EDTA
Myo	Myosin	TEMED	N,N,N',N'-tetramethylethylenediamine
NCBI	National Center for Biotechnology Information	TJ	Tight junction
ng	Nanogram	TM	Transmembrane
nm	Nanometer	Tris	Tris [hydroxymethyl] aminomethane
N-terminal	Amino terminal	U	Unit
o/n	Over night	UTR	Untranslated region
ORF	Open reading frame	UV	Ultraviolet
<i>P. falciparum</i>	<i>Plasmodium falciparum</i>	V	Volts
PBS	Phosphate buffered saline	v/v	Volume/volume percentage
PCR	Polymerase chain reaction	w/v	Weight/volume percentage
PFA	Paraformaldehyde	WB	Western blot
P _i	Inorganic phosphate	WHO	World health organisation
PM	Plasma membrane	WT	Wild-type
POI	Protein of interest	Xan	Xanthosine monophosphate
PV	Parasitophorous vacuole	X-Gal	5-bromo-4-chloro-3-indoyl- β -D-Galactopyranoside
PVM	Parasitophorous vacuole membrane	YFP	Yellow fluorescent protein
r	Resistant	μ g	Microgram
RB	Residual body	μ l	Microliter
RNA	Ribonucleic acid	μ m	Micrometer
RON	Rhoptry neck protein	μ M	Micromolar

1 Introduction

1.1 The apicomplexan phylum and *Toxoplasma gondii*

The apicomplexan phylum comprises a highly diverse group, with about 6000 species identified to date (Adl *et al.*, 2019). This group includes a diverse variety of protozoan parasites forming part of the coccidia, gregarines, hematozoa and cryptosporidia families, which are known to parasitise vertebrate and invertebrate hosts (Reid, 2015; Adl *et al.*, 2019).

Among apicomplexan parasites, the most notorious are the human pathogens *Plasmodium falciparum*, *Plasmodium vivax*, *Plasmodium ovale* and *Plasmodium malariae*, causative agents of malaria. These complex parasites use an Anopheles mosquito as a vector, completing their life cycle in many different organisms including humans. Malaria has long been considered a malaise of tropical countries (Adl *et al.*, 2007, 2019). However, new cases of other vector-borne diseases emerging in temperate climate countries have raised awareness of potential new risks of the disease. Strong efforts to control the disease have met with a good degree of success. Around 220 million cases of malaria are estimated worldwide, with around 400 thousand fatal cases according to the World Health Organisation (WHO), from a 2014 report. However, despite a reduction of malaria from 2015 to 2018, the disease still represents a global threat. This is exacerbated by an increase of drug resistant *Plasmodium falciparum* and *Plasmodium vivax* parasites that spread through a region complicating treatment efforts (Hanboonkunupakarn and White, 2016).

Another important apicomplexan parasite, often neglected by the public is *Cryptosporidium spp.*, the causative agent of cryptosporidiosis that can lead to severe gastrointestinal clinical pictures, resulting in high morbidity and mortality events, especially in children and other vulnerable groups (Adl *et al.*, 2007; Checkley *et al.*, 2015). It is distributed worldwide and like any other water-borne disease, it is more prevalent in developing countries. It is estimated that 20% of diarrheal episodes in children are caused by this pathogen in developing countries, and around 9% of diarrheal cases in developed countries, according to the WHO.

Most apicomplexan parasites, like any other parasite, require a specific host in order to survive. However, *Toxoplasma gondii* represents a special case. *T.gondii* has been observed to infect a wide range of warm-blooded organisms across the world ranging from birds, land and marine mammals and humans (Sibley *et al.*, 2009). However, most of these animals represent accidental hosts as the completion of the *T. gondii* life cycle depends primarily on rodents, birds and felids, the latter being its definitive host. A particular trait of *T.gondii* is the ability to invade almost every nucleated cell from warm-blooded hosts, explaining why so many incidental infections take place (Carruthers, 2002).

The success of *Toxoplasma gondii* is reflected by its worldwide distribution and the disease it causes; Toxoplasmosis is considered to affect around one-half of the world's population with prevalence rates by country ranging from 10 to 90% (Hill, Chirukandoth and Dubey, 2005; Pappas, Roussos and Falagas, 2009). A main characteristic of the clinical picture of Toxoplasmosis is the apparent lack of symptomatology in healthy individuals. However, it can result in life-threatening complications that can lead to fatalities in immunocompromised individuals along with foetal developmental complications during pregnancy (Hill, Chirukandoth and Dubey, 2005).

1.2 Pathogenesis and clinical features

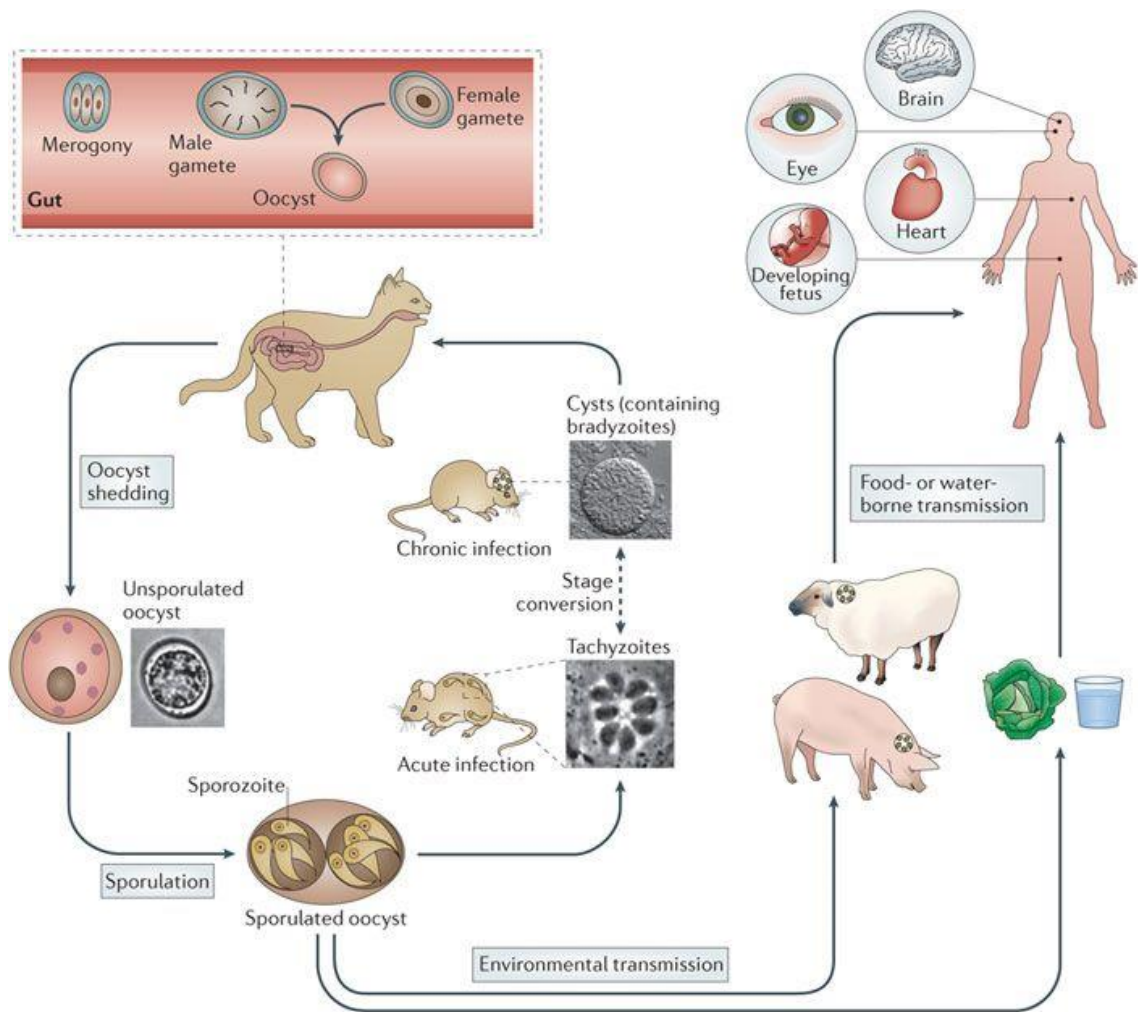
As mentioned in the previous section, life-threatening clinical conditions can arise from Toxoplasmosis. Luckily, severe manifestations of the disease are rare, with an estimate of 20000 severe cases of ocular toxoplasmosis emerging from 1 million new cases in the United States (Pappas, Roussos and Falagas, 2009; Flegr *et al.*, 2014). Unfortunately, the severity of the disease depends on the health and well-being of the population and developing countries see a higher number of severe toxoplasmosis cases than in developed nations. The main obstacle in providing accurate severe toxoplasmosis case numbers is that toxoplasmosis is usually incorrectly diagnosed or forms part of larger clinical pictures (Flegr *et al.*, 2014). Toxoplasmosis in healthy individuals is generally asymptomatic, with mild flu-like symptoms. If the disease occurs in immunocompromised individuals such as organ transplant and chemotherapy patients and those affected by diseases that weakens the immune system, several clinical pictures can develop (Montoya, 2002; Hill, Chirukandoth and Dubey, 2005; Flegr *et al.*, 2014). In adults, the

parasite will spread through the host body causing myocarditis, encephalitis, hydrocephalus and ocular toxoplasmosis, resulting in death in the most severe instances (Garweg, De Groot-Mijnes and Montoya, 2011; Kamerkar and Davis, 2012; Maenz *et al.*, 2014). Another threat from toxoplasmosis lies in pregnancy, as the parasite can traverse the placenta, colonising the foetus and resulting in congenital toxoplasmosis. Congenital toxoplasmosis can result in miscarriage or stillbirth (Montoya and Remington, 2008; Pappas, Roussos and Falagas, 2009). However, if the foetus survives severe impairments are often associated such as mental retardation, cognitive issues, seizures and organ enlargements.

Lastly, virulence varies within *T.gondii* parasites with four clonal strain types described: type I, II, III and haplogroup 12 predominantly in Europe, North America and Africa (Howe and Sibley, 1995; Khan *et al.*, 2011). These strain types are classified according to their virulence in mice with type I as a highly virulent strain and type II and III as less virulent strains (Sibley *et al.*, 2009). Different strains of the parasite produce different cytokine responses, triggering different physiological responses from the infected hosts (Sibley *et al.*, 2009; Behnke *et al.*, 2011, 2015). The virulence difference between types can be explained by the allelic combinations of the rhoptry proteins, specifically ROP18 and ROP5 (Ajioka and Boothroyd, 2009; Behnke *et al.*, 2015). Among the three haplotypes mentioned before, atypical strains that don't belong to their previous classification also exists. These groups represents haplogroups 4 - 15 and contain a cluster of around 150 genotypes (Minot *et al.*, 2012; Shwab *et al.*, 2014). These exotic or atypical haplotypes can occur anywhere in the world, South America and Africa appear to present the most diverse array of exotic haplotypes with the Northern hemisphere carrying a small amount of diversity (Sibley *et al.*, 2009; Yang *et al.*, 2013). This characteristic suggests that the areas with higher diversity allow more frequent sexual replication and recombination of parasites, possibly due to the biodiversity indexes of the regions. These atypical strains present differences in virulence, cytokine expression and host cell modulation which often results in a more severe disease than their Northern counterparts, ending in severe clinical pictures even in healthy individuals (Melo *et al.*, 2013). This is further demonstrated in the south of Brazil, where the highest prevalence of ocular toxoplasmosis can be found in the world (de Oliveira *et al.*, 2016).

1.3 Lifecycle of *Toxoplasma gondii*

Toxoplasma gondii includes two distinct stages in its lifecycle, alternating between the sexual reproduction stage limited to the intestine in its definitive host, felids, and the asexual stage occurring in virtually all nucleated cells from warm-blooded hosts (Gubbels, White and Szatanek, 2008).



Nature Reviews | Microbiology

Figure 1-1 Lifecycle of *Toxoplasma gondii*.

The lifecycle of *Toxoplasma gondii* is divided in a sexual stage in felid and an asexual stage in intermediate and incidental hosts. Taken from Hunter and Sibley 2012. License 4574820281685.

1.3.1 Lifecycle in the definitive host

The definitive host for *Toxoplasma gondii* allows sexual reproduction by the transmission of bradyzoites to the felid (Carruthers, 2002; Gubbels, White and Szatanek, 2008; Sibley *et al.*, 2009)(Figure 1-1).

The sexual reproduction stage starts by the host ingesting the infected mice. Once digestion starts, proteolytic enzymes will digest the infected prey tissue along with the bradyzoite cyst wall (Dubey, Lindsay and Speer, 1998). Once the parasites are able to burst out of the cyst, a new stage called the trophozoite will find and invade the felid's intestinal wall cells, followed by the formation of schizonts once the parasite starts cellular growth. Gametocytes are then formed, with micro and macrogametes fusing together and forming a single oocyst that is shed into the environment through faeces where the oocyst will remain in the environment, eventually making its way into mice and repeating the cycle again (Frenkel, Dubey and Miller, 1970; Dubey, Lindsay and Speer, 1998) (Figure 1-1).

When the sporulated oocyst makes its way into mice or other intermediate hosts, excystation of the sporozoites takes place, with sporozoites rapidly turning into tachyzoites that quickly disseminate through the host, starting the asexual cycle (Dubey, Miller and Frenkel, 1970).

1.3.2 Lifecycle in the intermediate host

As mentioned previously, *T.gondii* has a wide range of hosts that comprises all nucleated cells from warm-blooded hosts. In the intermediate hosts, the parasite is considered to undergo two stages: a lytic and a dormant stage (Blader *et al.*, 2015) (Figure 1-1).

1.3.2.1 The lytic cycle

The lytic cycle starts with the parasite moving towards the host cell, in an event called gliding motility (Black and Boothroyd, 2000; Heaslip *et al.*, 2011). Once it

finds a suitable host cell, it attaches to the host cell plasma membrane, re-orientates itself and then initiates invasion, establishing a parasitophorous vacuole (PV) where the parasite will undergo replication by endodyogeny. Endodyogeny is a type of cell replication where two daughter cells emerge from inside a single mother (Blader *et al.*, 2015). After several rounds of replication, the parasite will egress from the infected host cell to re-invade other neighbouring cells (Figure 1-2).

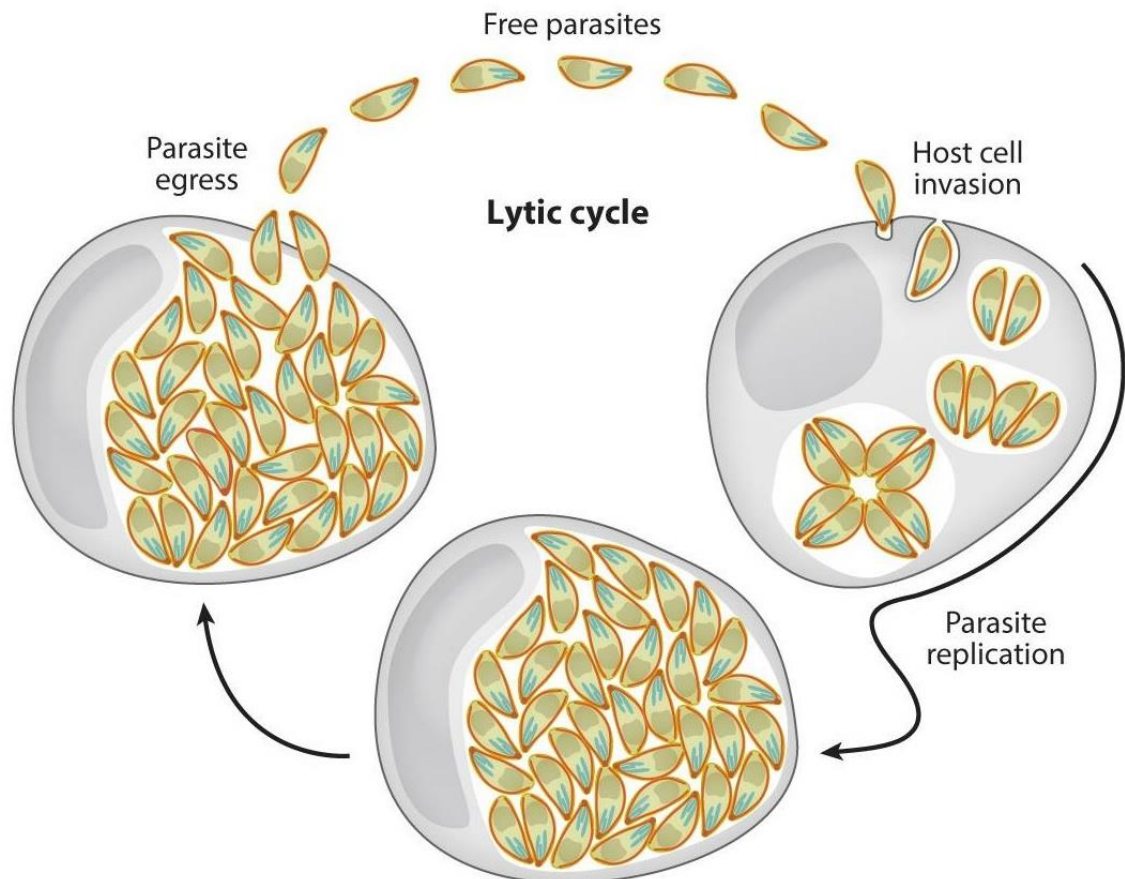


Figure 1-2 *Toxoplasma gondii* lytic cycle.

Toxoplasma gondii lytic cycle starts with gliding parasites that will localise a viable host cell. The parasite will then invade the host cell generating a parasitophorous vacuole structure where replication will take place. After several rounds of replication and after depleting the host cells resources, the vacuole will burst freeing the parasites where the cycle will repeat. Taken from Blader *et al.* 2015. License 4574830301273.

1.4 Gliding motility

Toxoplasma gondii zoites move across large areas in order to invade new cells (Heintzelman, 2015). This motility depends on an acto-myosin motor complex that allows the parasite to glide in what is known as gliding motility. The acto-myosin

motor complex, suggested to be located between the Inner Membrane Complex (IMC) and Plasma Membrane (PM) (Fréchal *et al.*, 2010) is thought to power motility by force generation through the concerted action of factors including structural and transmembrane proteins bound to the Inner Membrane Complex (IMC) such as glideosome-associated proteins (GAP) proteins (Harding *et al.*, 2016); a myosin A (MyoA) protein anchored in the GAPs powering the motor (Keeley and Soldati, 2004; Egarter *et al.*, 2014; Williams *et al.*, 2015); adhesion proteins such as micronemes (MIC) in the exterior that allow to bind to external substrates carrying transmembrane domains that allows to link the proteins to an unidentified linker (Carruthers and Tomley, 2008; Gras *et al.*, 2017), previously believed to be aldolase (Jewett and Sibley, 2003; Shen and Sibley, 2014) and now suggested to be a glideosome-associated connector (GAC) that binds actin (Jacot *et al.*, 2016); and short actin filaments generating traction alongside MyoA (Fréchal *et al.*, 2010; Whitelaw *et al.*, 2017). For a more in-depth description see section 1.12.1 of this chapter.

Gliding motility over a 2-D substratum has been heavily studied over the past 20 years and can be divided into three categories: helical motility, where the parasite moves in a helical manner propelling itself considerable distances in some cases; circular motility, where the parasite moves in a circular pattern; and twirling motility, where the posterior end of the parasite remains attached to a substrate and the other ends twirls in a circular fashion (Hakansson *et al.*, 2013; Heintzelman, 2015). In previous bio-mechanical studies in *Plasmodium* sporozoites using reflection interference contrast microscopy (RICM) and traction force microscopy (TFM), motility appeared to be defined by the dynamic turnover of discrete adhesion sites. These adhesion sites were described as strong adhesion points on both ends of the parasite and weaker attachment points along the body. This behaviour allows the parasite to attach and de-attach to the surface, resulting in rapid turnover of attachment sites and fast movement of the apicomplexan parasites (Münter *et al.*, 2009). During parasite gliding, surface antigen proteins (SAG1) from the parasite are left behind as trails along with a variety of other proteins. It has been highly speculated on how this motion is achieved based on the action of the linear motor along with the biological relevance of gliding itself.

Other studies tackling 3D motility using 3D matrices have been performed (Leung *et al.*, 2014), where an additional exclusive type of motility was described: a left-handed corkscrew motility. During this corkscrew motility, the parasite moves in fast and slow boosts, contradicting observations made in 2D gliding where the movement is more continuous. Taking this new type of motility into account, along with the fact that a 3D environment represents a better physiological representation, has led to the speculation that some forms of 2D motility are artefacts caused by asymmetric attachment to the surface (Leung *et al.*, 2014).

1.5 Invasion

Invasion is a multistep process (Figure 1-3), involving contact between the parasite and the host cell. Several proteins related to adhesins are released from the micronemes (e.g. AMA1, mic2) (Mital, 2005; Andenmatten *et al.*, 2013; Bargieri *et al.*, 2013) to mediate attachment. Attachment is followed by gliding motility of the parasite on the host cell surface by the glideosome complex (Kremer *et al.*, 2013). As stated before, *Toxoplasma gondii* is able to invade a wide range of hosts. Ubiquitously expressed host receptors, together with *T. gondii* own receptors allow invasion into many different host cells (Carruthers and Boothroyd, 2007).

The rhoptries excrete another set of proteins called rhoptry bulb (ROP) and rhoptry neck (RON) proteins (Alexander *et al.*, 2005). RON proteins are discharged into the host cell cytosol and then transported to the host cell membrane where, together with AMA1, they form a scaffold called the Tight Junction complex (TJ) (Meissner, Ferguson and Frischknecht, 2013). Following junction formation, ROP proteins are secreted to form the parasitophorous vacuole (PV) from the invagination of the host cell plasma membrane.

Similarly to parasite gliding motility, the most accepted hypothesis explains that invasion is powered by a linear motor system described in section 1.4 of this chapter. Parasite entry occurs by forward propulsion by the acto-myosin-dependant motility system into the host plasma membrane (Suss-Toby, Zimmerberg and Wardt, 1996). This mechanism creates an invagination of the plasma membrane of the host cell forming the PV (Charron and Sibley, 2004).

During this process, the AMA1-RON2 junction is translocated from the apical to basal end of the parasite concurrent with host cell penetration. Dense granule proteins are also involved in this step, working in the formation of the PV and subsequent host cell environment modulation for the next step in the life cycle (Sibley and Niesman, 1995; Shastri *et al.*, 2014; Heaslip, Nelson and Warshaw, 2016). This process takes an average of 30 seconds to complete (Whitelaw *et al.*, 2017). Following the final step in penetration, the newly formed PV will move closer to the mitochondria in an association believed to favour metabolic requirements of the parasite. Interestingly, this close mitochondrial association is only seen in type I parasites, as type II strains lack the MAF1 gene identified to be responsible for this association (Pernas *et al.*, 2014).

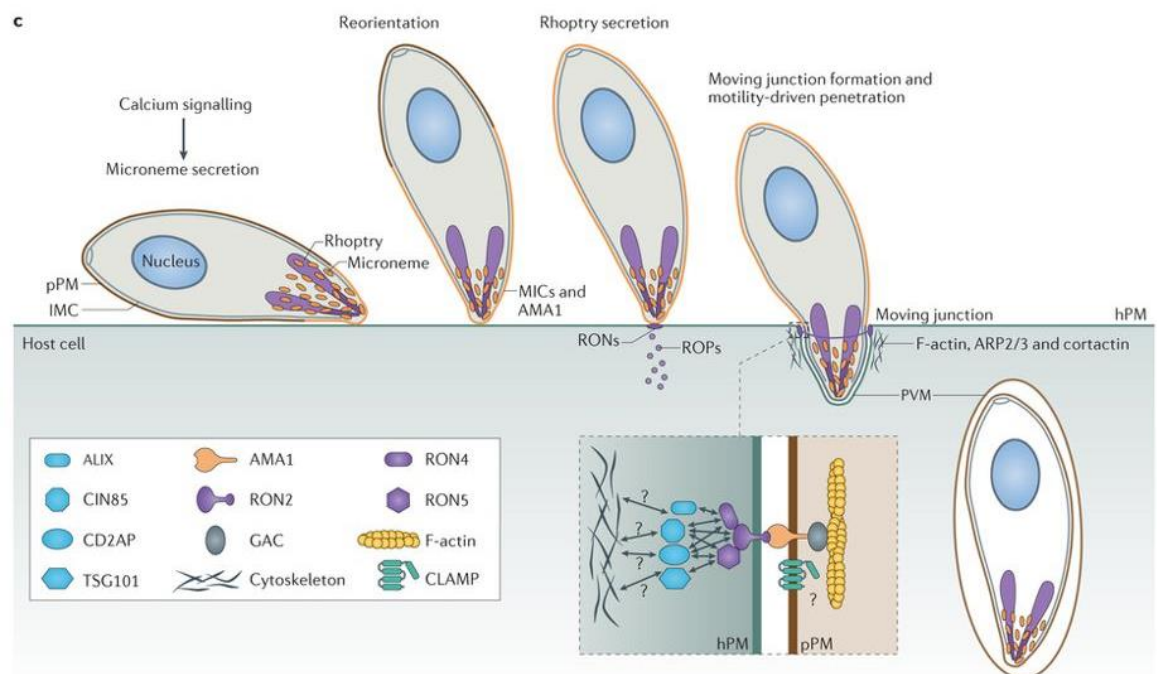


Figure 1-3 *Toxoplasma gondii* invasion.

Invasion starts with the parasite reorientation close to the host cell plasma membrane. The parasite will initiate microneme secretion along with RON complexes that will form the TJ. This will follow a penetration event where the parasite will enter the host cell. During this process other RON and ROP proteins will be secreted and will generate a parasitophorous vacuole membrane. Taken from Fréchal, Dubremetz, et al. 2017. License 4574820835491

1.6 Replication and egress

After the establishment of the PV, the tachyzoite encased in the PV undergoes several rounds of replication (Jones and Hirsch, 1972). The replication process

occurs through endodyogeny, which is when two daughter cells emerge from within the mother (Hu, 2002). Once the replication process starts, division of the centrioles and the interaction with the parasite cytoskeleton defines cell polarity (Nishi *et al.*, 2008; Agop-Nersesian *et al.*, 2010). At the beginning of DNA replication, components of the cytoskeleton are formed along with the conoid, spindle poles and intranuclear microtubules. The Inner Membrane Complex (IMC) is formed for each individual daughter and drives the cell division along with the parasite's microtubules (MTs) (Shaw *et al.*, 2000; Hu, 2002; Nishi *et al.*, 2008; Agop-Nersesian *et al.*, 2010). The organelles are then distributed between the daughter parasite cells beginning with the Golgi apparatus, apicoplast division and nuclear division.

During late phases, the ER and the mitochondria are divided, ending with the separation of all the organelles between the two nascent cells (Nishi *et al.*, 2008). Part of the micronemes and rhoptries are then recycled between the daughter cells along with newly synthesised ones (Nishi *et al.*, 2008). It is noteworthy to mention that each pair of daughter cells is joined together in the vacuole, and further joined to other daughter cells in actin-rich connections (Frénal, Jacot, *et al.*, 2017; Periz *et al.*, 2017). Severing of these connections during replication can lead to incorrect replication organisation or asynchronous replication of parasites in the PV (Frénal, Jacot, *et al.*, 2017). The replication cycle will continue doubling the number of cells every ~6 hours on average (Radke *et al.*, 2001; Gubbels, White and Szatanek, 2008).

Following replication, the host cell will reach a point where it can no longer support the rapidly dividing parasites. *T.gondii* potentially senses the imminent collapse of the host cell and induces egress triggered by external and internal factors (Gubbels, White and Szatanek, 2008; Frénal *et al.*, 2010; Roiko, Svezhova and Carruthers, 2014). Strong calcium accumulation occurs and the parasites activate their gliding complex, lysing out of the now acidic PV and host cell membrane (McCoy *et al.*, 2012; Roiko, Svezhova and Carruthers, 2014). The calcium peak is believed to trigger microneme secretion that disrupts the PV by the use of a perforin-like protein (PLP1) (Arrizabalaga *et al.*, 2004; Kafsack *et al.*, 2009; Garg *et al.*, 2015).

Calcium dependant processes such as calcium-dependant kinases like CDPK3 are required for egress (McCoy *et al.*, 2012). This calcium dependant pathway is triggered by changes in the parasitophorous vacuole environment of the parasite such as potassium levels. This is further hinted when parasites are treated with Calcium Ionophore A23187, a compound shown to affect the Na^+/H^+ ion channels in the parasite membrane (Arrizabalaga *et al.*, 2004; Caldas, de Souza and Attias, 2010). CDPK3 is also involved in triggering microneme secretion and myosin A activation by phosphorylation.

In addition to a rise in intracellular calcium, production of phosphatidic acid is also responsible for microneme secretion mediation (Bullen *et al.*, 2016). Factors such as transmembrane guanylate cyclases (GCs) and it's interacting partner unique GC organiser (UGO) along with cyclic guanosine monophosphate (cGMP)-dependent protein kinase G (PKG) trigger microneme secretion via the same calcium pathway mentioned before and are essential for parasite egress, motility and re-invasion. However, parasites lacking diacylglycerol kinase 2 (DGK2), responsible on generating phosphatidic acid in the parasitophorous vacuole can still egress suggesting the parasites possess several mechanisms regulating egress and microneme secretion. These mechanisms will be activated in different conditions, with harsher conditions able to bypass DGK2 activating microneme secretion via GC and UGO (Bisio *et al.*, 2019).

Lastly, genetic manipulation of core components of the acto-myosin motor generate impairment in egress, suggesting that gliding, invasion and egress are closely related to each other (Andenmatten *et al.*, 2013; Egarter *et al.*, 2014; Gras *et al.*, 2017; Whitelaw *et al.*, 2017).

1.7 *Toxoplasma gondii* morphology

1.7.1 Ultrastructure

The infective tachyzoite stage of the parasite is a crescent-shaped cell of approximately 6 μm long and 2 μm wide (Figure 1-4). The parasite possesses several conserved eukaryotic structures like nucleus, mitochondrion, ribosomes,

endoplasmic reticulum and Golgi complex (Figure 1-4). In addition, it also possesses special apically oriented organelles (Shaw and Tilney, 1999; Katris *et al.*, 2014) characteristic of the phylum such as the conoid and secretory organelles such as the rhoptries (ROPs) and micronemes (MICs), as well as other organelles such as dense granules that play a role in invasion (Mercier *et al.*, 2005; Kessler *et al.*, 2008; Behnke *et al.*, 2011; Sharma and Chitnis, 2013). They also possess a unique organelle called the apicoplast, which is a four membrane-bound plastid like organelle (Roos *et al.*, 1999; Waller and McFadden, 2005; Lim and McFadden, 2010). The parasite is additionally enveloped by membranous structures: the Inner Membrane Complex (IMC) and plasma membrane (PM) (Agop-Nersesian *et al.*, 2010; Fréna1 *et al.*, 2010).

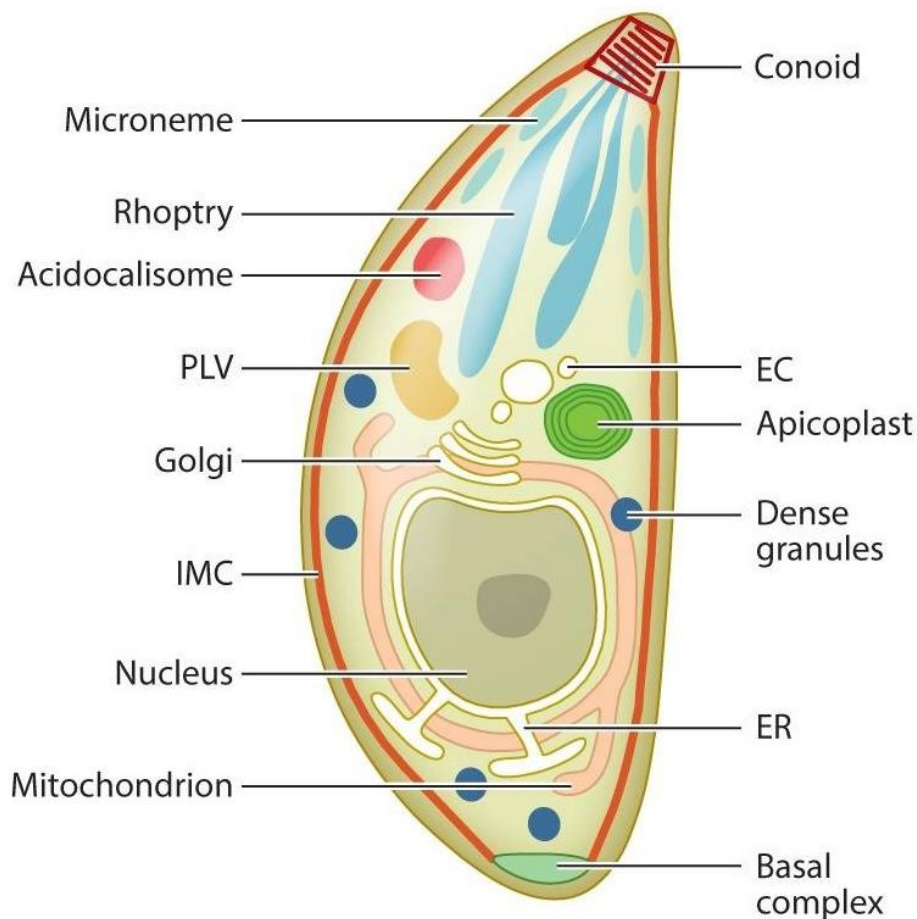


Figure 1-4 *Toxoplasma gondii* ultrastructure

The crescent shape characteristic of *Toxoplasma gondii* is easily distinguishable. Apical oriented organelles especially involved in the parasite's invasion such as dense granules, micronemes, conoids and rhoptries are present. Common organelles such as Golgi body, the ER and the mitochondrion are also present with the addition of the highly characteristic apicoplast, which is a metabolic organelle unique to this phylum. Taken from Blader *et al.* 2015. License 4574830301273.

1.7.2 The apical complex and secretory organelles

1.7.2.1 The conoid and microtubule structures

The conoid of apicomplexan parasites is a hollow cone-shaped structure. It is bound to the cytoskeleton by close interaction with microtubules in two apical polar ring structures (Dubey, Lindsay and Speer, 1998; Speer and Dubey, 1998). The cone structure itself is composed of 14 tubulin fibres and it is extended in conditions where tachyzoites are extracellular (Hu, 2002). Conoid extension is believed to depend on the close interaction of actin and myosins and it is believed to function in environmental sensing and invasion (Shaw and Tilney, 1999; Del Carmen *et al.*, 2009).

Microtubules (MTs) comprise 22 filamentous structures that extend 2/3 of the length of the parasite in a spiral pattern (Morrissette, Murray and Roos, 1997; Shaw *et al.*, 2000; Morrissette and Sibley, 2002). The microtubules are further bound to the IMC by GAPM proteins conferring cell shape stability (Harding *et al.*, 2019).

Toxoplasma gondii possesses three α and three β tubulin isotypes alongside carrying genes for γ , δ and ϵ tubulin. Only γ tubulin is expressed in tachyzoites (Xiao *et al.*, 2010; Morrissette, 2015). β tubulin is expressed in similar levels through different stages of the parasite, the α isotype expression levels vary, hinting at different roles in individual stages (Morrissette, 2015).

Subpellicular microtubules are composed of 13 lateral associated protofilaments, which are $\alpha 1$ and $\beta 1$ heterodimers assembled head-to-tail. Sub-pellicular microtubules originate from the conoid from polar rings that constitute the microtubule organising centre (MTOC). From the MTOC, the plus-end or the extending face of MTs grow from the apical end of the parasite (Russell and Burns, 1984). From this point onwards, microtubules extend in a left-handed rearward spiral.

The main role of microtubules is believed to be structural as their association with the IMC is crucial during parasite replication, as the packaging of daughter cells in endodyogeny is coordinated by the growth of cortical microtubules and the IMC.

Microtubule depolymerising drugs such as oryzalin results in abnormal IMC assembly, resulting in non-viable daughter cells (Morejohn *et al.*, 1987; Shaw *et al.*, 2000; Morrissette and Sibley, 2002; Nishi *et al.*, 2008).

Lastly, several proteins decorate microtubules such as SPM1, ICMAP1, TrxL1 and TLAP2 that are parasite specific. These proteins are hypothesised to confer a highly stable nature to these microtubules when compared to other eukaryotes (Heaslip, Ems-McClung and Hu, 2009; Tran *et al.*, 2012; Liu *et al.*, 2013).

1.7.2.2 Micronemes, rhoptries and dense granules

Highly regulated microneme secretion is essential for invasion and egress processes (Carruthers and Tomley, 2008). Calcium signal peaks are often associated with these processes (Borges-Pereira *et al.*, 2015) and microneme secretion has been linked with the activation of ion channels in the parasite along with CDPK3 (McCoy *et al.*, 2012). Microneme synthesis requires trafficking through the endosomal pathway and proteolytic protein maturation by rhomboid (ROM) proteases (Sheiner, Dowse and Soldati-Favre, 2008; Shen *et al.*, 2014). In the current literature, about 50 microneme proteins have been described, with many of them sharing functional mechanisms with adhesin proteins (Carruthers and Tomley, 2008; Nishi *et al.*, 2008; Sheiner *et al.*, 2010). These adhesin proteins allow the parasite to attach to substrates or receptors to allow gliding motility, invasion and egress.

Rhoptries are club-shaped organelles numbering between 8-10 per parasite (Carey *et al.*, 2004; Butcher *et al.*, 2011; Lei *et al.*, 2014). They are formed by an upper neck containing RON proteins and a bulbous compartment harbouring ROP proteins (Bradley *et al.*, 2005; Lamarque *et al.*, 2011). Through sequential secretion of both RON and ROP proteins, host cell penetration and maintenance of the PV is possible (Beck *et al.*, 2014). Additionally, ROP proteins have been suggested to act as virulence factors, secreted into the host cell cytosol to regulate the host immune-related processes such as early activation of immune-related GTPases (IRGs) that impede association with the PV, avoiding membrane damage (Behnke *et al.*, 2012; Niedelman *et al.*, 2012; Lei *et al.*, 2014).

Dense granules are electron dense organelles localised throughout the cytoplasm. Dense granule proteins (GRA) are important factors secreted upon invasion and relocated in the PV membrane (PVM) for correct assembly and maintenance (Mercier *et al.*, 2005). Since they closely interact in the PVM, it has also been suggested that they possess a role in host cell response modulation (Gold *et al.*, 2015). This function is perhaps essential for long-term survival of the parasite as a recent study uncovered a dense granule-resident effector called Toxoplasma E2F4-associated EZH2-inducing gene regulator or TEEGR (Braun *et al.*, 2019). The immune system of the host has a negative feedback system to maintain immunological homeostasis (Z. Liu *et al.*, 2015). TEEGR is able to modulate this system by negatively regulating NF- κ B, steering the infected host inflammatory response towards a Th1 response. Although the Th1 response appears to promote rapid clearance of tachyzoites, the parasite seems to favour it, as this effect allows the parasite to make it to immune privileged sites, escaping other inflammatory immune responses in the process (Braun *et al.*, 2019).

Additionally, dense granules are responsible for the generation of membranous nanotubular networks (MNN) in the PV, as genetic ablation of the *gra2* gene resulted in the disruption of this network leading to vacuole disorganisation (Mercier, 2002). The MNN is formed post-invasion and rapidly expands with each replication round (Mercier, 2002). In a relatively recent study, dense granule movement was characterised to depend on myosin F using filamentous actin bundles as tracks for transport (Heaslip, Nelson and Warshaw, 2016).

1.7.3 The Inner Membrane Complex

Covering almost the entire body of the parasite with the exception of the conoid and basal body, the inner membrane complex (IMC) is composed of alveoli, which are membranous sacs located underneath the plasma membrane (Morrissette, Murray and Roos, 1997; Mann and Beckers, 2001) (Figure 1-4). The IMC is supported by the highly organised subpellicular network on the cytoplasmic side that connects to the IMC via IMC-anchored GAPM proteins (Morrissette, Murray and Roos, 1997; Harding *et al.*, 2019). Previous experiments measured the space between the IMC and PM with ranges from 22 - 30 nm (Kudryashev *et al.*, 2010).

The glideosome-associated protein GAP45 connects both the PM and IMC, and it is believed to be responsible for the structural integrity of the space as depletion of GAP45 proteins lead to the IMC detaching from the PM (Egarter *et al.*, 2014). Additionally, GAP40 and GAP45 are anchored in the IMC, with critical roles in the biogenesis of the IMC (Bosch *et al.*, 2012; Harding *et al.*, 2016). More importantly, the area between the IMC and PM has been hypothesised to be the area where the glideosome machinery is located (Frénal *et al.*, 2010).

1.7.4 The nucleus

The nucleus is probably the most defining feature of the majority of cells, as it harbours most of the genetic material needed for survival (Lammerding, 2011). Most nuclei in eukaryotic cells contain nuclear envelope proteins (NE) present in both the inner and outer NE lipid bilayer. This NE can also be an extension of the endoplasmic reticulum (ER) with common connected spaces between the two (Isermann and Lammerding, 2013). Core proteins responsible to keep the nucleus together are present in most cells. Filamentous protein networks exist on the inner face of the NE with a main core protein named lamin. Lamin supports nuclear architecture, prevents membrane blebbing and allows organisation of nuclear pore complexes (NPCs) (Dahl, 2004; Lammerding, 2011). As important as lamins are for the nucleus, they are not universal, as organisms lacking lamin exist such as *Saccharomyces cerevisiae*. In this case, partial function is performed by a different set of protein including Mlp1 and Esc1, allowing nuclear structure stabilisation (Georgatos, Maroulakou and Blobel, 1989).

Toxoplasma gondii is another organism lacking lamin proteins, albeit orthologs are believed to exist. Little work has been carried out in the parasite and, thus, ample information remains to be found.

1.7.5 Apicoplast

The apicoplast is a product of secondary endosymbiosis that represents a relic of an its cellular evolution. This organelle probably started as a cyanobacteria that was engulfed by an eukaryotic cell and managed to survive (primary endosymbiosis), forming a symbiotic relationship that benefited both organisms creating a photosynthetic eukaryotic organism. From this point, a descendant of

this photosynthetic organism was also engulfed by a heterotrophic eukaryote, forming a newly symbiotic relationship (secondary endosymbiosis) (McFadden, 2001; Yoon *et al.*, 2002; Weber and Linka, 2011).

Four membranes surround the apicoplast (Figure 1-4). The most external one originates from the phagosome, the third membrane is a relic from a red algal plasma membrane and the remaining two membranes constitute the outer and inner membranes of the ancestral chloroplast (Waller and McFadden, 2005; Lim and McFadden, 2010). Since it is a heavily modified organelle, the photosynthetic capabilities no longer exist, although it is still essential for the survival of the parasite as it is necessary for fatty acid biosynthesis (FASII) (Ramakrishnan *et al.*, 2012), isoprenoid precursors via the DOXP pathway, iron harbouring and heme synthesis (Seeber and Soldati-Favre, 2010; Nair *et al.*, 2012; van Dooren, Kennedy and McFadden, 2012).

During replication, the apicoplast is divided and segregated by the action of myosin F and actin (Egarter *et al.*, 2014). Incorrect division, segregation or apicoplast loss leads to the parasite slowly dying due to the inability to generate required metabolites in a process termed “delayed death phenotype” (Frénal, Jacot, *et al.*, 2017). Even though parasites that lack an apicoplast are capable of invasion, they shortly die if at least one of the parasites in a vacuole lacks an apicoplast. Upon severing connections between parasites such as the nanotubular network and cytoskeletal elements (Mercier, 2002; Frénal, Jacot, *et al.*, 2017), the parasites are no longer able to share metabolites leading to the same delayed death phenotype for the vacuole (Frénal, Jacot, *et al.*, 2017). It is important to note that in *Plasmodium spp.* the apicoplast shares very similar features to those found in *T. gondii*. However, apicoplast loss can be supplemented with isopentenyl phosphate (IPP), allowing *Plasmodium* merozoites to survive. This feature is not present in *Toxoplasma* tachyzoites, suggesting at least some functions are different between apicomplexan parasites (Yeh and DeRisi, 2011).

1.8 *Toxoplasma gondii*: the model organism for genetic studies

Toxoplasma gondii, when compared to other apicomplexan parasites represents a simple genetical system. Taking into account the ease of culturing parasites, fast replication cycles and high transfection efficiency, *T.gondii* represents a prime example of a model organism for apicomplexan parasites.

Although many different novel approaches are used in apicomplexan parasites, within this thesis the DiCre and Tet systems were employed for the characterisation of actomyosin mutants and thus, will be the focus of this chapter.

1.8.1 Reverse genetics engineering and gene regulation.

1.8.1.1 Genetic level regulation

To dissect key components of the *Toxoplasma* invasion machinery, the generation of conditional knockout (KO) mutants is vital. Currently, two regulators at the genetic level can be used for the generation of knockout mutants, the DiCre system and CRISPR/Cas9 system (JIMÉNEZ-RUIZ *et al.*, 2014). The DiCre system is based on recombination of specific sites using a dimerisable Cre recombinase protein that recognizes and performs an excision of DNA that is flanked by two identical sequences called LoxP sites (Andenmatten *et al.*, 2013).

The DiCre enzyme is divided into two inactive fragments fused to one of the rapamycin binding proteins (FRB and FKBP); when rapamycin (RAPA) is added as a ligand, effectively reconstituting the active enzyme, the LoxP-flanked Gene of interest (GOI) is excised, usually replaced by a YFP coding sequence to assess correct excision (Andenmatten *et al.*, 2013).

Using this strategy, the generation of conditional KOs in *Toxoplasma gondii* becomes highly efficient, allowing the proper study of phenotypes resulting from these mutants (Egarter *et al.*, 2014; Whitelaw *et al.*, 2017). Mutants that have been generated using this system can be divided into two main groups, ones that are still viable after KO of the gene of interest, and those that are not. Among the

former, examples include the *myoAKO*, which is less efficient than the wild type during invasion, cannot egress properly and grows slowly in culture, but does not present organelle defects (Andenmatten *et al.*, 2013; Egarter *et al.*, 2014).

Those that cannot survive for long periods of time after KO of the GOI are essential, and thus they need to be induced shortly before working with them, such as the *act1KO*, which presents a severe decrease in invasion, a defect in the replication of the apicoplast due to the depletion of actin and which are completely blocked in egress (Whitelaw *et al.*, 2017). In some cases, they are viable up to 5 days in culture. The *gap45KO* presents a change in cell morphology, making parasites rounder when extracellular. However, they still can invade, although at a much lower rate than the wild type (Egarter *et al.*, 2014).

1.8.1.2 Transcriptional level regulation

One of the most widely used methods in *Toxoplasma gondii* is the use of tetracycline-inducible systems. Originally created as a tetracycline-repressor system (Tet-R) and later adapted to a tetracycline-transactivator system (Tet-TA) (Meissner *et al.*, 2001). The tetracycline-dependant transactivator 1 (TATi) is constitutively expressed from a strong gene promoter. TATi can bind to TetO-sequences (tetracycline operator sequences) that are placed upstream of a minimal promoter. This minimal promoter is the tet-responsive promoter that activates transcription. Once anhydrotetracycline (ATc) is added, conformational changes of TATi will take place, abolishing TetO binding and turning transcription off. This technology allowed the initial wave of genetic engineering studies in *Toxoplasma gondii* and was later adapted to *Plasmodium falciparum* (Meissner *et al.*, 2001, 2005; Meissner, Schlüter and Soldati, 2002).

1.9 Actin, a highly dynamic protein

1.9.1 Overview, structure in eukaryotic cells, nucleation and treadmilling.

Actin is a highly versatile molecule involved in several house keeping processes in cells such as cell motility, cell division, cytokinesis, tracking and maintenance of cell shape among others (Visa and Percipalle, 2010; Dominguez and Holmes, 2011; Pollard, 2016). The involvement of actin in many key processes explains why it is one of the most abundant proteins in eukaryotic cells. It is a single molecule (monomeric actin, 42 kDa (Kabsch *et al.*, 1990)) capable of forming microfilaments (F-actin) that are tightly regulated (Pollard, 2016). The actin monomer is composed of 4 subdomains and can shift between an ATP-bound and an ADP-bound state linked to subdomain 2 (Kabsch *et al.*, 1990; Pollard, 2016). Thanks to this property, the architecture conformation of filamentous actin varies depending on the interaction of monomers in different states. Adenosine triphosphate (ATP) is localised in a cleft between subdomains 2 and 4 forming ATP-bound actin, which is capable of forming stable bonds with other ATP-bound actin monomers (Pollard, 1986; Kovar *et al.*, 2006). This ATP can be hydrolysed to generate ADP-bound actin, which becomes less stable over time and prone to dissociation between actin monomers (Pantaloni, Carlier and Coue, 1984).

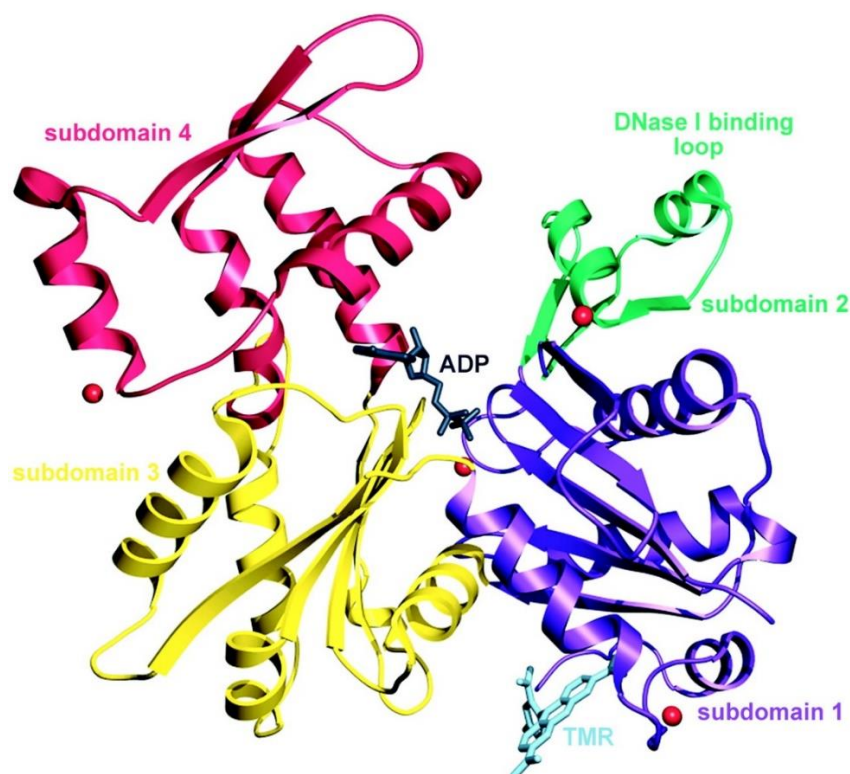


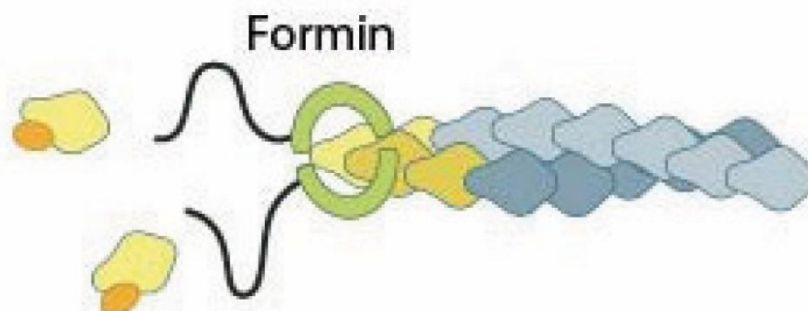
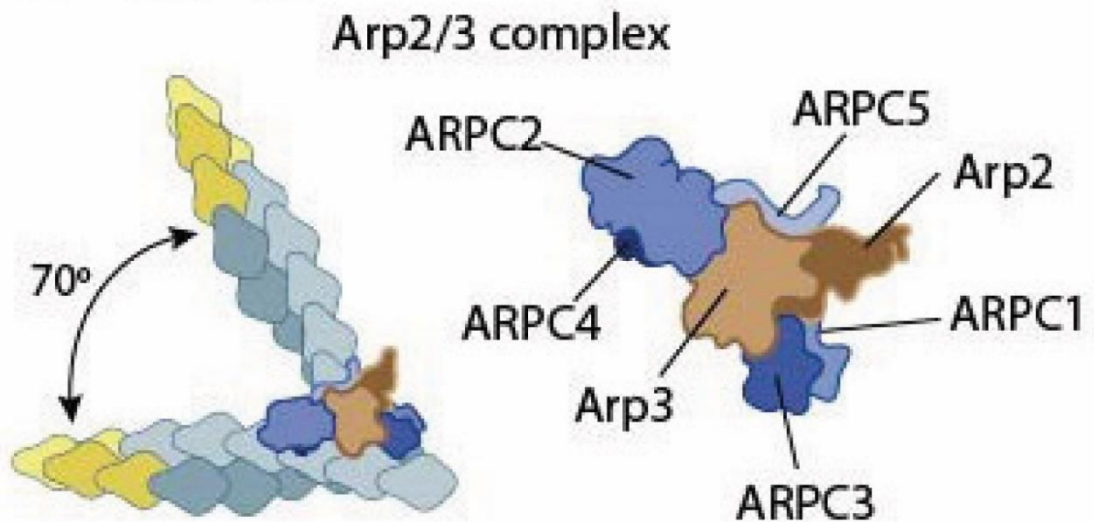
Figure 1-5 Structure of monomeric actin.

Monomeric actin comprises 4 subdomains along with the ADP binding site and the DNase binding loop 1. Taken from Otterbein, Graceffa, and Dominguez 2001. License 4575280621999.

Stable ATP-bound actin monomers can nucleate, usually by combining three monomers that can rapidly become unstable if no further interactions occur with nucleation factors (Welch and Mullins, 2002). Nucleation factors such as formins and the Arp2/3 complex provide stabilisation to the dimer or trimer actin complex promoting polymerisation in a thermodynamically stable fashion (Pollard, 2007) (Figure 1-6 A). After the initial nucleation lag phase, the elongation phase occurs with ATP-bound actin monomers binding to both ends of the nascent filament. One key point in this event is the different rates of polymerisation, as actin monomers binding to the barbed (+) end will promote polymerisation with 3-5 times more affinity than the pointed (-) end of the filament (Nishida and Sakai, 1983; Bugyi and Carlier, 2010). The event where new actin monomers are bound to the nascent filament is limited by the available quantity of actin monomers in the cytosol. The actin monomer concentration is known as the critical concentration (C_c). Low monomer concentration will prohibit further actin polymerisation (Pantaloni, Carlier and Coue, 1984). However, if a high concentration of actin monomers is present, rapid polymerisation will occur with rates far exceeding polymerisation events when compared to depolymerisation ones (Pollard, 1984; Kovar *et al.*, 2006). Upon actin polymerisation initiation, free actin monomers will be up-taken by the nascent actin filament in order to increase the filament size. Once the availability of actin monomers decreases, filament elongation will decrease in speed, eventually stopping altogether (Pollard and Borisy, 2003). To avoid this result, actin molecules will be depolymerised from one end of the filament to provide the medium with available actin monomers. This process is tightly regulated by a separate set of proteins called Actin Binding Proteins (ABPs) (Pollard, 2016). Once the concentration reaches an equilibrium, the C_c will maintain stable rates of polymerisation and de-polymerisation events called treadmilling (Cleveland, 2004; Bugyi and Carlier, 2010) (Figure 1-6 B). Once the filament is stably going through polymerisation/de-polymerisation, the ATP bound to actin will be cleaved by hydrolysis, releasing phosphate (P_i), which results in ADP-bound actin; the slow release of P_i results in destabilisation of the

actin filament, usually at the pointed (-) end (Pollard, 1984; Murakami *et al.*, 2010) (Figure 1-6 B).

A Nucleation



B

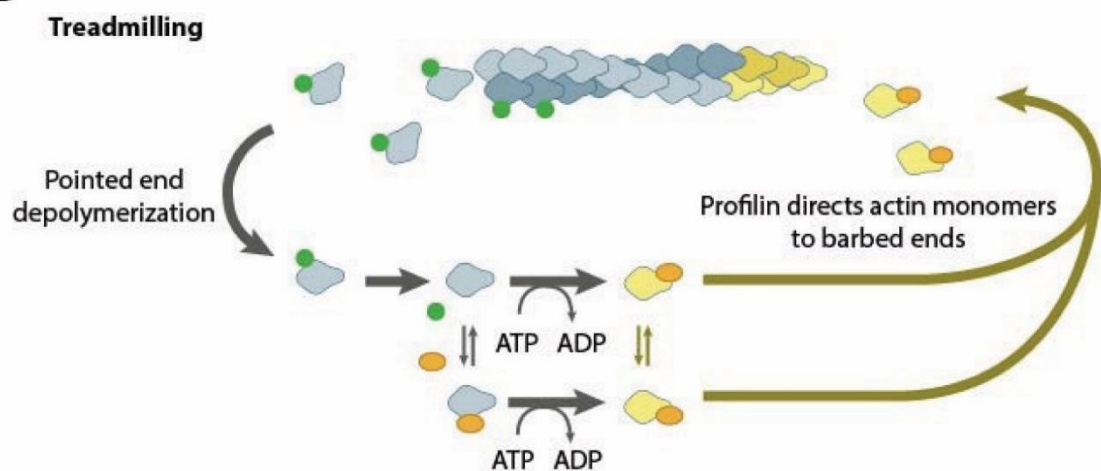


Figure 1-6 Actin nucleation.

A. Actin monomers are nucleated when trimers or tetramers are reached. This mechanism can be promoted by nucleating proteins such as the Arp2/3 complex and formins. **B.** Actin treadmilling occurs once the critical concentration of actin monomers is in equilibrium and the ratio of incorporated actin monomers in the barbed (+) end is the same as the actin monomers that disassociates from the pointed (-) end of the filament. Taken from (MBINFO, 2019). Creative Commons Attribution 4.0 International License.

The resulting actin filaments can form a wide variety of structures to fulfil their diverse roles. These filaments are structured as two protofilaments intertwined forming a right-handed helix with a diameter close to 7-10 nm (Dominguez and Holmes, 2011) (Figure 1-7). The structure and length of the filamentous structures depends on several factors including C_c and the actin binding proteins (ABPs) that can modulate length and filament conformation. ABPs possess different functions such as increasing the availability of monomeric actin in the medium via severing or depolymerisation in the case of the ADF/Cofilin family of proteins (Bamburg, 1999; Kanellos and Frame, 2016) and increasing the rate of monomeric actin incorporation into the elongating end of the filament in the case of the Profilin family of proteins, among others (Yarmola and Bubb, 2006; Birbach, 2008). These actin filaments are usually arranged into parallel bundles, with the filaments orientating into the same direction; antiparallel, where the filaments face opposite directions; and dendritic networks where the filaments form a lattice structure (Chhabra and Higgs, 2007).

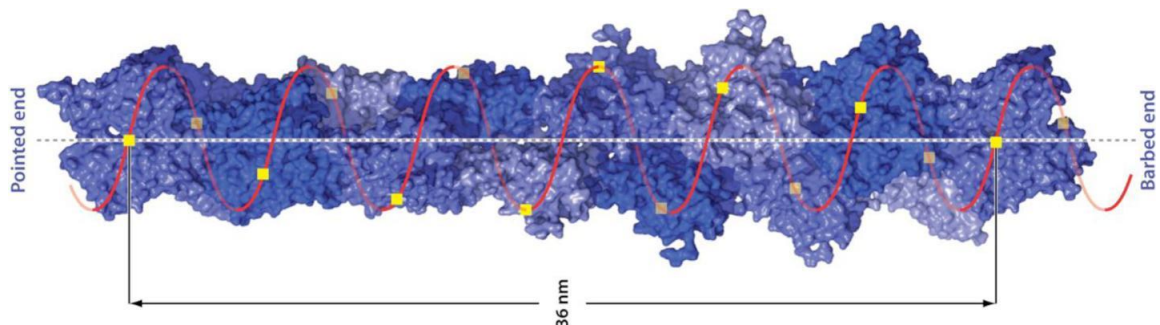


Figure 1-7 Actin filament structure.

The filamentous structure of actin follows a double right-handed helix. Taken from Dominguez and Holmes 2011. License 4575281092822.

1.9.1.1 Actin in Apicomplexa

In most eukaryotes, actin possesses 3 distinct isoforms: α -, β - and γ -actin (Garrels and Gibson, 1976). Different cell types possess different actin isoforms depending on function such as α -actin working in muscle cells and β - and γ -actin in most of the other cells (Herman, 1993). Apicomplexan actin is highly divergent compared to canonical actins. While only one copy *act1* can be found in case of *T. gondii* and

other coccidians (Dobrowolski, Niesman and Sibley, 1997), in the case of *Plasmodium spp* 2 actin isoforms (ACTI and ACTII) are present in the genome (Wesseling *et al.*, 1988; Siden-Kiamos, Louis and Matuschewski, 2012; Vahokoski *et al.*, 2014). ACT1 is the main isoform, ubiquitously expressed in all lifecycle stages of the parasite, while ACT2 appears to be expressed in specific phases such as the mosquito and gametocyte stage, being essential for the male gametocyte flagellated form (Vahokoski *et al.*, 2014). TgACT1 and PfACT1 appear to be closely related (with 93% gene sequence similarity). However, they appear to be highly divergent from the actin isoforms of other eukaryotes sharing 83% with beta (β) and gamma (γ) mammalian actin (Dobrowolski, Niesman and Sibley, 1997). Several of these amino-acid differences are predominantly located on the surface of actin monomers, suggesting monomers from different organisms would not be compatible with *P.falciparum* ones. Curiously, rabbit-skeletal actin was capable of forming filaments by polymerising on both ends of *P. falciparum* actin short-filaments (Schmitz *et al.*, 2010).

Additionally, *T.gondii* actin has been reported to be predominately in a monomeric state, accounting for around 97% of the total actin in the parasite (Dobrowolski, Niesman and Sibley, 1997). Most efforts to visualise filamentous actin have proven unsuccessful, strengthening this view. However, the most accepted hypothesis explains that short actin filaments are localised between the PM and IMC to power the glideosome (Keeley and Soldati, 2004). One of the explanations offered explains that *T.gondii* F-actin forms short unstable filaments that are difficult to capture (Sahoo, 2005; Schmitz *et al.*, 2005, 2010). A different polymerisation model has also been proposed, where actin polymerises without the need of critical concentration or nucleation in an isodesmic manner (Skillman *et al.*, 2013). This isodesmic model requires actin to be polymerised with equal affinity between all monomers independent of filament length as the formation of dimers or filamentous structures would be equally energetically viable (Skillman *et al.*, 2013). This view directly challenges the cooperative model of actin polymerisation where critical concentration is required to polymerise and elongate actin filaments and would imply that TgACT1 is unique among all other actin molecules described to date (Cooper *et al.*, 1983).

New evidence suggest that apicomplexan F-actin behaves similarly to other eukaryotes, as apicomplexan actin dynamics are affected by genetic deletion mutants of factors that bind actin, suggesting that actin polymerisation does depend on critical concentration regulation (Periz *et al.*, 2017). Additionally, new reports suggest filamentous actin polymerisation in *Plasmodium falciparum* behaves in a similar fashion as canonical actin polymerisation (Das *et al.*, 2017; Kumpula *et al.*, 2017). In this study, Kumpula *et al.* 2017 showed that apicomplexan actin polymerisation occurs following the cooperative model, similarly to the rabbit actin used for comparison. It is important to note that the experiments resulted in shorter filament lengths due to higher depolymerisation rates, supporting the hypothesis that filamentous actin structures in apicomplexan parasites are more unstable when compared to other eukaryotes (Schmitz *et al.*, 2005, 2010; Vahokoski *et al.*, 2014; Kumpula *et al.*, 2017). A subsequent crystallography study done by the same group, provided evidence that magnesium binding activates *PfAct1* monomers prior to polymerisation by a slight flattening of the monomer structure that was reversed upon phosphate release. This process, controlled by the A-loop, switches filament structures into stable and unstable conformations. This characteristic results in short filamentous structures due to an overabundance of nucleation caused by a very short polymerisation lag-phase and fragmentation of F-actin (Kumpula *et al.*, 2018).

1.9.2 Actin polymerisation

1.9.2.1 Actin binding proteins (ABPs)

Efficient actin polymerisation and adapting actin elongation for different functions requires an intricate interplay of a vast repertoire of proteins that regulate actin dynamics (Pollard, 2016). These factors possess a wide range of functions from nucleation, capping, polymerisation, branching, depolymerisation, severing and bundling of actin filaments (Carlier and Pantaloni, 1997; Arber *et al.*, 1998; Pollard and Borisy, 2003; Campellone and Welch, 2010; Li *et al.*, 2010; Jayo *et al.*, 2016; Sadhu and Chatterjee, 2016). Additionally, other factors are also involved in translocation and force generation by using actin filaments, such as myosin proteins (Sellers, 2000; Gaskins *et al.*, 2004). Since canonical eukaryotes contain a very high number of these factors, this section will

focus on apicomplexan parasites, especially *Toxoplasma gondii*, that possess a limited number of known and well-characterised ABPs.

Initiating nucleation in order to promote actin polymerisation is usually enabled by a set of specialised proteins referred to as nucleation factors (Campellone and Welch, 2010). These nucleation factors are required to bypass the initial requirement to dimerise or trimerise actin monomers that precludes actin nucleation and posterior polymerisation. In most eukaryotes, nucleation factors such as the Arp 2/3 complex, Wiskott-Aldrich syndrome protein (WASP), WH2, Spire and formins are used to enhance polymerisation rates by nucleation initiation (Machesky and Gould, 1999; Pollard, Blanchoin and Mullins, 2002; Kheir, 2005; Mullins *et al.*, 2013). The mechanisms used vary with the proteins, but they usually share common features such as actin binding domains and the ability to attract more actin monomers that will initiate nucleation.

In apicomplexan parasites, a strikingly small number of nucleation factors are conserved with no Arp2/3 complex to be found along with the associated proteins involved such as WASH/WAVE/WASP (Goley and Welch, 2006). The Arp2/3 complex not only promotes nucleation but also mediates nucleation for actin branching, a feature apparently missing from apicomplexan actin (Bugyi and Carlier, 2010). Among all the listed nucleation factors, only formins appear to be conserved in the phylum (Daher *et al.*, 2010). Formins are large multi-domain proteins that bind to the barbed end of filamentous actin promoting filament length and controlling actin polymerisation (Pollard, 2007). Evidence of cooperation between formin complexes and profilin has been shown, where profilin provides the formin complex with ATP-bound actin monomers (Craig and Pollard, 1982; Kovar and Pollard, 2004; Bugyi and Carlier, 2010) (Figure 1-8). Formin binds to the barbed (+) end of filaments, preventing capping, and their proline-rich formin homology 1 (FH1) domain interacts with profilin to achieve monomer integration into the filament. Another domain called formin homology 2 (FH2) participates in nucleation and barbed (+) end filament binding for new monomers (Evangelista, 2003; Higgs and Peterson, 2005) (Figure 1-8). In *Toxoplasma gondii*, 3 formins have been described in the literature (Daher *et al.*, 2010). While earlier results suggested that Formin 1 and 2 were localised in the pellicle of the parasites (Daher *et al.*, 2012), a recent study provided evidence

that formin 1 (FRM1) (Tosetti *et al.*, 2019) is localised in the apical end of the parasite, formin 2 (FRM2) (Stortz *et al.*, 2019; Tosetti *et al.*, 2019) in the central area of the parasite between the nucleus and the apicoplast and formin 3 (FRM3) (Tosetti *et al.*, 2019) in the residual body during replication. So far, nucleation centres seen in parasite live actin dynamics have been linked to these formin complexes, as they localised in the same regions previously described. For more information regarding the location of formins and nucleation centres refer to chapter 4 and 6.

Previous work in the extracellular life stage of the parasite provided evidence that FRM1 is responsible for actin nucleation during gliding, invasion and egress, as genetic deletion mutants were impaired in these functions (Tosetti *et al.*, 2019), while FRM2 and 3 provided no deleterious effect (Stortz *et al.*, 2019; Tosetti *et al.*, 2019). On the other hand, FRM2 ablation resulted in a loss of the central nucleation centre along with apicoplast inheritance defects in the form of incorrect apicoplast division and translocation, with the majority of the plastid structures ending up in the residual body (Stortz *et al.*, 2019; Tosetti *et al.*, 2019). These results suggest a role in intracellular replicating parasites along with FRM3. Although *Plasmodium falciparum* parasites only possess 2 formin genes, a similar effect was also reported. Genetic knockouts of formin 1 or 2 resulted in a similar loss of the central polymerisation centre, resulting in apicoplast accumulation in the residual body (Stortz *et al.*, 2019) and Pfformin1 was shown to be localised moving along the junctional ring during invasion (Baum *et al.*, 2008).

Another important aspect of nucleation and actin polymerisation is monomer sequestering, as it can artificially modulate the critical concentration to control polymerisation. This sequestration effect works to either promote or inhibit polymerisation. Apicomplexa possess two identified monomer sequestering proteins, a single copy of profilin (Kucera *et al.*, 2010) and the Srv2/cyclase-associated protein (CAP) (Hunt *et al.*, 2019).

The function of profilin relies on binding to actin monomers for sequestering, catalysing the exchange of a ADP to a ATP actin-bound state. This mechanism is possible by altering the nucleotide-binding site facing the cytosol (Zhao *et al.*, 2013). This mechanism promotes the abundance of monomeric actin molecules that are available to join elongating filaments. They are believed to work

alongside formin complexes, promoting rapid actin polymerisation (Tanaka, 2000). However, the apicomplexan formin FH1 domain appears to be vestigial, suggesting profilin-formin interaction is either weak or does not take place (Higgs and Peterson, 2005; Daher *et al.*, 2010). This would further indicate that apicomplexan profilin primarily functions as an actin monomer sequestering protein. Genetic deletion mutants of profilin were reported to cause defects in gliding and invasion. However, no effect in replicating parasites was reported (Plattner *et al.*, 2008; Kucera *et al.*, 2010). It has also been reported that apicomplexan profilin can function as an inducer of IL-12 in mice (Plattner *et al.*, 2008; Kucera *et al.*, 2010; Morgado *et al.*, 2011). This effect is thought to occur during invasion, as the parasite would secrete profilin through an unknown mechanism to affect the immune response from the host cell.

CAP homologue protein has been associated with monomer sequestration in apicomplexan parasites (Hunt *et al.*, 2019). Its location in *T.gondii* has been identified in the apical region, while extracellular parasites show a cytoplasmic location (Hunt *et al.*, 2019). A recent study in *T.gondii* cyclase associated protein (CAP), reported that a knock-out mutant led to significant defects in parasite-to-parasite communication but not to division synchronicity. This was further explained as a defect in the formation of a residual body in the vacuole while still maintaining connections between daughter cells (Hunt *et al.*, 2019).

Another important regulator of actin polymerisation is the mechanism to release unstable ADP-actin monomers into the cytosol. The actin depolymerisation factor (*adf*) is an actin binding protein more likely related to actin severing and thus, depolymerisation. Mammalian ADF proteins are difficult to categorise since they are known for performing several functions, such as severing and depolymerisation (Bamburg, 1999; Wolf *et al.*, 2015). In some cases, the literature is rather ambiguous, where it has been shown that under specific circumstances, such as aggregated states of the protein, it can promote stabilisation between filaments (Maciver and Hussey, 2002; Wiggan *et al.*, 2012; Wang *et al.*, 2013). It usually remains in two states. The first is a phosphorylated state that possesses a low affinity for actin and is usually labelled as inactive. This state possesses low severing/depolymerisation potential and has been linked to form protein aggregates thought to function as a binding complex for several actin filaments

(Wang *et al.*, 2013). The second one is a de-phosphorylated state possessing high affinity for actin and the ability to sever filaments (Arber *et al.*, 1998; Van Troys *et al.*, 2008; Goyal *et al.*, 2013). In *Toxoplasma gondii*, the ADF protein has been linked to actin monomer sequestering and severing (Yadav *et al.*, 2011) (Figure 1-8), as depletion of ADF generates actin accumulation in both ends of the parasite (Mehta and Sibley, 2011). This effect was further observed with a total abrogation of the actin dynamics, leading to a phenotype similar to the act1KO parasite with weak and erratic gliding motility, severe invasion reduction, asynchronisation of replication and egress defects (Mehta and Sibley, 2011). A more in-depth characterisation of the ADF depletion mutant can be found in chapter 3.

Besides actin severing, apicomplexan parasites possess a reduced repertoire of bundling proteins. Coronin, a protein suggested to work in cross-linking filaments to create F-actin bundles has been described for Apicomplexa (Kallio and Kursula, 2014; Salamun *et al.*, 2014; Bane *et al.*, 2016). Coronin is considered to provide dual mechanisms working to promote actin polymerisation in the barbed (+) end alongside actin severing via coordination with cofilin proteins (Bane *et al.*, 2016) (Figure 1-8). Another function lies in rapid cytoskeletal remodelling to promote cell motility and endocytosis (Chan, Creed and Bear, 2011). In Apicomplexa, coronin can bind F-actin and has been suggested to promote F-actin bundling (Bane *et al.*, 2016). A cellular role has been suggested in the directionality of motility and invasion in *Plasmodium falciparum* parasites, where deletion of the gene lead to un-directed movement and invasion defects (Olshina *et al.*, 2015; Bane *et al.*, 2016). In *T.gondii* parasites, deletion mutants presented no clear phenotype with slight effects on gliding and invasion (Salamun *et al.*, 2014; Bane *et al.*, 2016). However, in both apicomplexan parasites coronin accumulation in the basal end has been described in invasion events, leading to hypothesise of additional functions of coronin not currently explored. Additional bundling proteins found in other eukaryotes appeared to be absent including, but not limited to, actinin, filamin, spectrin, tropomyosin and fascin, the latter being a vital filament cross-linking protein in the F-actin-nucleus interface (Villari *et al.*, 2015). This general absence suggest coronin might be involved in other mechanisms not described or additional not yet identified F-actin bundling proteins exist in the parasite.

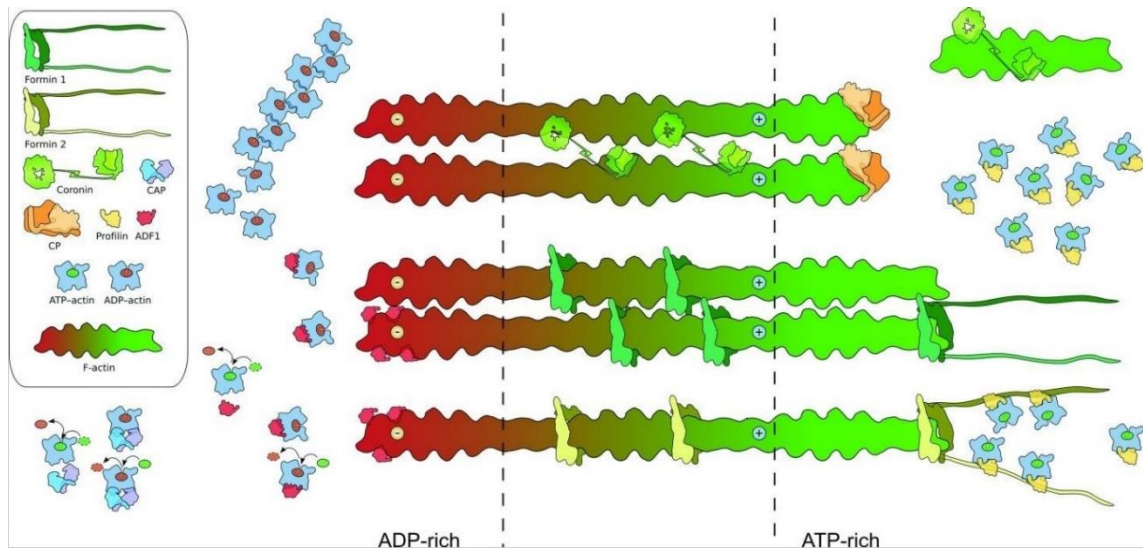


Figure 1-8 Actin binding factors in apicomplexan parasites.

Many different actin binding factors facilitate and control actin polymerisation. Formins allow rapid nucleation while profilin promotes sequestering and incorporation of new ATP-bound actin monomers. ADF severs and depolymerises ADP-bound monomers while Coronin sequesters and promotes actin bundling. Taken from E.-P. Kumpula and Kursula 2015. Creative Commons Attribution 4.0 International License.

1.10 Efforts to visualise actin in Apicomplexan parasites

1.10.1 Endogenous tagging, antibodies against actin and chromobodies in *Toxoplasma gondii*.

One of the main difficulties in visualising apicomplexan actin is the failure of classical methods proven to work for mammalian actin. Initial approaches, such as fusing a GFP protein to actin molecules via genetic manipulation, resulted in the inability to differentiate cytoplasmic GFP-actin and F-actin (Angrisano, Delves, *et al.*, 2012). Methods as simple as tagging actin with a fluorescent protein to the use of molecular probes such as LifeAct (Riedl *et al.*, 2008) proved to be unfruitful (Dr. Javier Periz, *personal communication*). This is likely due to the apicomplexan actin architecture, shown to be highly unstable. Antibodies targeting actin or F-actin provided mixed results, as the majority of the antibodies targeting actin resulted in cytoplasmic staining (Fréchal *et al.*, 2010; Angrisano, Riglar, *et al.*, 2012). Electron microscopy provided limited results, managing to visualise short actin filaments in some cases (Dobrowolski, Niesman and Sibley, 1997; Shaw and Tilney, 1999). The situation changed with the use of a new

technology in the form of Nanobodies (Rocchetti, Hawes and Kriechbaumer, 2014; Panza *et al.*, 2015). These Nanobodies represent single domain antibodies that, although smaller in size than regular antibodies, still retain their ability to bind to specific epitopes. The nanobodies can be fused to fluorescent proteins, called Chromobodies that can be engineered to bind to specific structures even in *in vivo* systems (Panza *et al.*, 2015). Using engineered Actin Chromobodies co-expressed in the parasite allowed visualisation of F-actin in live parasites for the first time in Apicomplexan parasites (Figure 1-10) (Periz *et al.*, 2017). The extent of the usefulness of the chromobody will be discussed in the next chapters of this thesis characterising replication, gliding and invasion of both fixed and live parasites.

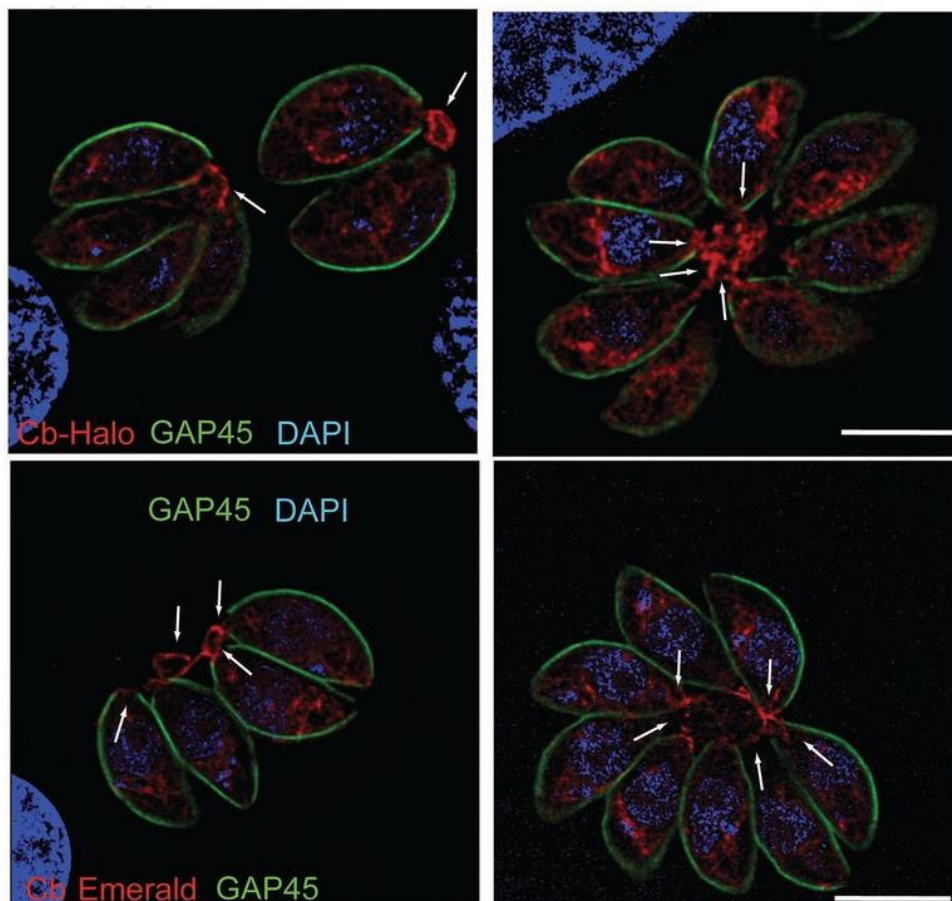


Figure 1-9 Chromobody expression in *Toxoplasma gondii*.

Chromobody-Halo targeting F-actin in *Toxoplasma gondii* parasites uncovers actin dynamics both connecting parasites in a nanotubular network in the vacuole and actin dynamics in the cytoplasmic part of the cells. Taken from Periz *et al.* 2017. Creative Commons Attribution 4.0 International License.

1.11 Mammalian cell migration and the role of actin and actin-related structures.

1.11.1 The role and mechanism of actin during cell motility in eukaryotes.

Cell migration comprises cycles of steps that allow a cell to move. Different migration modes are present in eukaryotes relying on the same machinery used in different ways depending on the type of matrix used. This plasticity in migration depends largely on the degree of actomyosin contractility and the relative amounts and strength of the cell-matrix adhesions (Wolf *et al.*, 2003; Petrie and Yamada, 2016).

2D and 3D motility present key differences in motility, with 2D surface motility presenting interesting findings on how lamellipodia protrusions are formed and actomyosin-driven contractility that allows the cell to push forward (Petrie and Yamada, 2015). However, in 3D matrices the cells displayed varying types of motility that allow cells to migrate. Additionally, 3D motility not only represents more physiological conditions during motility, but also allows cell motility assessment in cells previously believed to be unable to move due to the lack of cell-to-surface adhesions (Petrie and Yamada, 2016).

1.11.1.1 Motility on 2D surfaces and the core components facilitating this process

During 2D motility, the cell senses cues that guide the formation of protrusions called lamellipodia at the front of the cell by means of adhesion proteins in the extracellular matrix (ECM) (Stricker, Falzone and Gardel, 2010). This is followed by the formation of new focal adhesion points at the front that firmly attaches the cell to the substrate (Chacko, Zanicchi and Diaspro, 2013; Schiffhauer *et al.*, 2016). Now, rearward traction of the focal adhesion points at the front occurs by an actomyosin complex and, lastly, these focal adhesion points now at the rear are disassembled permitting forward movement (Brangwynne, MacKintosh and Weitz, 2007; Krause and Wolf, 2015). These steps require dynamic assembly and disassembly of many elements including actin and the cytoskeleton (Maiuri *et al.*, 2015).

Lamellipodia formation consists of actin branching and elongation, resulting in a mesh resembling a lattice at the front of the moving cell (Pantaloni, Le Clainche and Carlier, 2001; Pollard and Borisy, 2003) (Figure 1-11). The branching is mediated, as mentioned in the previous section, by the Arp2/3 complex, which nucleates filamentous actin branching by attaching to a main filament (Machesky and Gould, 1999). Following the branching activity, an elongation step occurs mainly by polymerisation promoting in the barbed (+) end of the nascent filament by Profilin-1 (Pfn-1) sequestering and transport of actin monomers (Kovar, 2006; Le Clainche and Carlier, 2008; Zhao *et al.*, 2013). Pfn-1 works alongside the Rho effector formin (mDia) that nucleates actin, promoting rapid polymerisation at the barbed (+) end.

In this process capping and depolymerisation events occur to guarantee a steady supply of actin monomers. Capping proteins such as CapZ prevent filament extension at the barbed (+) end and gelsolin severs unstable filaments into smaller ones (Maciver and Hussey, 2002; Dos Remedios *et al.*, 2003). ADF/cofilin, a sever/depolymerisation protein with a high affinity for ADP-bound actin, promotes depolymerisation of these short filaments (Chan, Creed and Bear, 2011).

The focal adhesion points function as adhesive contact points between the ECM and the cell (Stehbens and Wittmann, 2012). This is done by transmembrane domains of integrins that interact with various linkers that include, but are not limited to, talin, vinculin, actinin and integrin-linked kinases, which in turn interact with actin and other cytoskeletal proteins (Schoenwaelder and Burridge, 1999; Gu *et al.*, 2011; Lippert and Wilkins, 2012; Vogel *et al.*, 2014).

Additionally, intermediate filaments (IF) are also present, providing structural integrity to the cytoplasm and mechanical resistance (Bindschadler *et al.*, 2004; Dupin, Sakamoto and Etienne-Manneville, 2011; Gregor *et al.*, 2014). These IF are linked directly to the protrusion focal contacts, suggesting that they might regulate adhesion dynamics (Schwarz and Leube, 2016). IF are vital for cell contraction, allowing the cell to move; fibroblasts that lack IF proteins such as vimentin exhibit impaired contractile activity (Maier, Traenkle and Rothbauer, 2016). The nucleus is another important aspect where IFs are implicated, since lamin proteins are type IV intermediate filament proteins (Mckee, Kirschner and Caput, 1986; Georgatos, Maroulakou and Blobel, 1989). Lamins influence nucleus

rigidity and thus the ability of the nucleus to be squeezed or transported during migration (Dahl, Ribeiro and Lammerding, 2008; Schäpe *et al.*, 2009) (Figure 1-11).

Microtubules (MTs) are able to resist high compressive loads and for this reason they are essential for the cell's structural integrity (Wilson and Holzbaur, 2012; Villari *et al.*, 2015). During lamellipodia formation, certain MTs named pioneer microtubules extend into the protrusion to assist in pushing the membrane forward (Waterman-Storer and Salmon, 1999; Stehbens and Wittmann, 2012). Additionally, evidence exists that microtubules are used as tracks where membrane vesicles are delivered or recycled, facilitating communication between different areas of the cell (Etienne-Manneville, 2013). Microtubules are also involved in the formation of the focal adhesion sites where MTs interact directly with fascin, which are responsible for actin binding and bundling (Villari *et al.*, 2015). These mechanisms regulate fascin-dependant control over focal adhesion points, which in turn regulate migration speed, among other things (Figure 1-11).

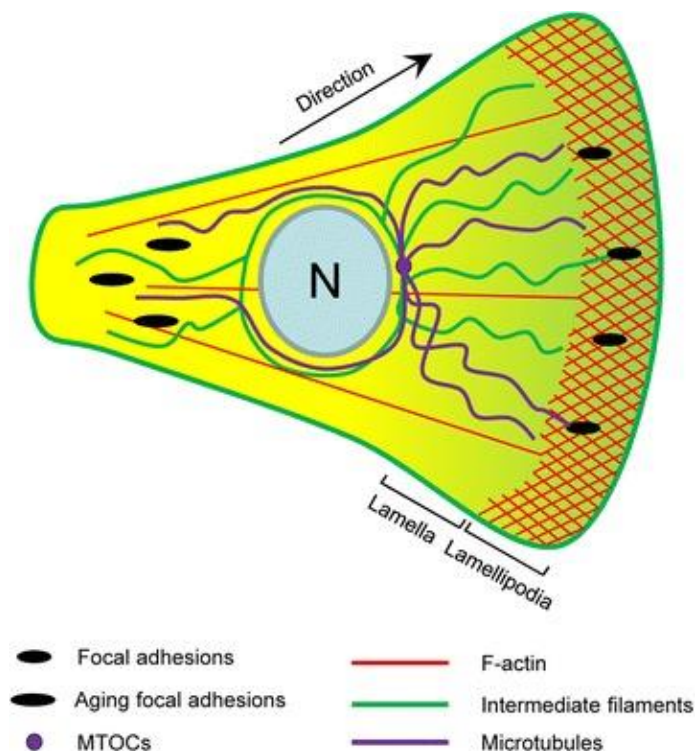


Figure 1-10 Major components of motile cells during migration.

Cell motility occurs by lamellipodia extension and protrusion via F-actin, intermediate filaments and microtubules. Taken from D. D. Tang and Gerlach 2017. Creative Commons Attribution 4.0 International License.

1.11.1.2 3D motility presents high plasticity in cell movement

Different cell types present distinct motility mechanisms in order to move through 3D environments (Sahai and Marshall, 2003; Wolf *et al.*, 2003). The different types of cell motility are usually classified into 1. actomyosin and pressure-driven protrusion; 2. actin polymerisation-driven protrusion and; 3. retrograde flow-driven movement (Figure 1-12).

During 3D motility in matrices that allows adhesion such as dermis or fibroblast-derived substrates, another type of protrusion called lobopodial protrusion occurs by pressure generated by the translocation of the nucleus in a piston-like phenomenon (Petrie, Koo and Yamada, 2014). While lamellipodia protrusions are predominantly driven by F-actin polymerisation, lobopodial protrusion occurs by membrane blebbing (Figure 1-12) (Charras *et al.*, 2006; Tinevez *et al.*, 2009; Ridley, 2011). Intracellular hydrostatic pressure is generated by the piston-like use of the nucleus by actomyosin contraction causing rupture of the actin cortex (Tinevez *et al.*, 2009) or actin-plasma membrane link (Charras *et al.*, 2006). Without support, intracellular pressure build-up occurs generating a membrane bleb that grows in size until the actin cortex structure is re-established. This function goes into a cycle, allowing directional migration where RhoA, a small GTPase protein in the Rho family triggers actomyosin contractility that in turn pulls the nucleus forward via nesprin 3, a nucleoskeleton-cytoskeleton linker protein (Petrie *et al.*, 2012; Petrie, Koo and Yamada, 2014).

In type I collagen gels, cell migration occurs by low-pressure lamellipodial protrusions, similarly to 2D migration. To do so, Rac1 directs Arp2/3 nucleation and branching activity allowing the membrane to be pushed into the matrix (Figure 1-12). During this type of motility, the intracellular pressure is both lower and uniform in the cell and, although actomyosin contractility plays a minor role, it is still required specifically for pulling the nucleus forward (Petrie *et al.*, 2012; Thomas *et al.*, 2015).

In certain cases, integrin-based adhesion is not required for migration in 3D environments (Y.-J. Liu *et al.*, 2015). For example, if a non-adhesive cell is compressed between two surfaces, rapid actomyosin retrograde flow without strong force generation underneath the plasma membrane creates force enough

to push the cell forward. Additionally, the osmotic engine model explains that the cell's plasma membrane semi-permeability allows the active transport of water from the front of the cell to the back, propelling the cell forward. This active water transport is mediated by ion channel pumps and aquaporins alongside myosin II contractility, driving protrusions at the front of the cell (Figure 1-12) (Chen *et al.*, 2012; Chi *et al.*, 2014; Stroka *et al.*, 2014; Oelz, Rubinstein and Mogilner, 2015).

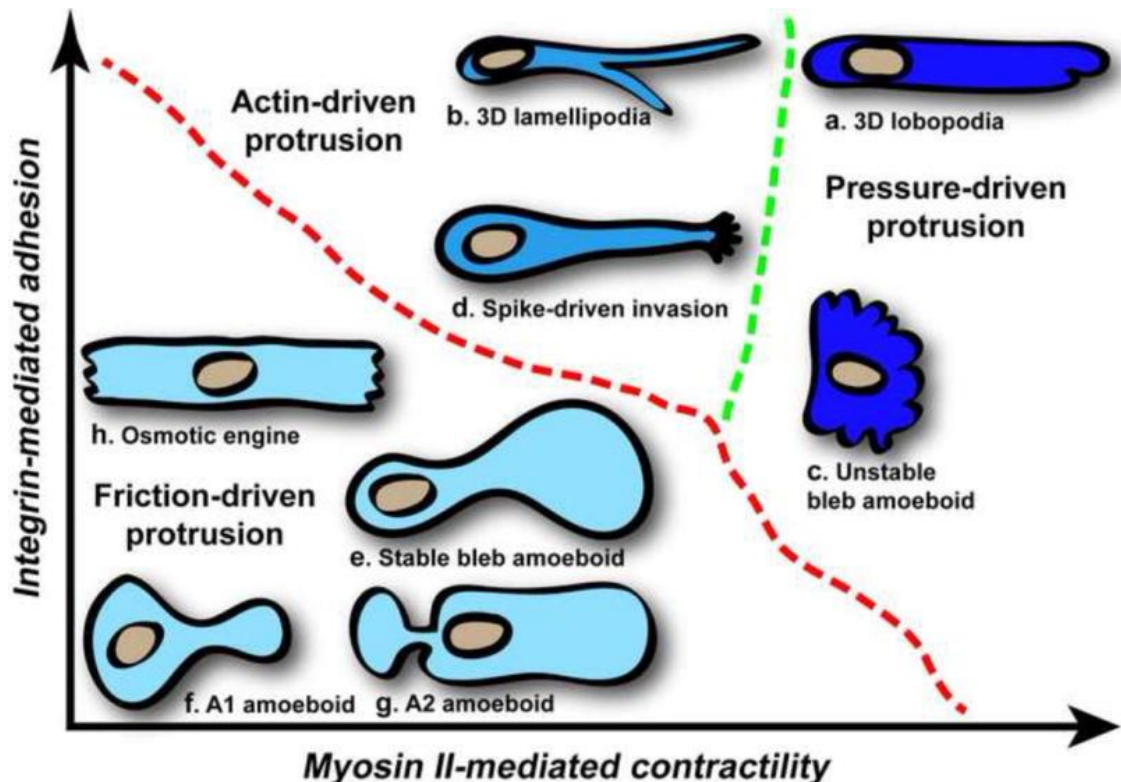


Figure 1-11 3D motility plasticity to adapt to different situations.

In 3D environments, motility adapts and displays a diverse array of modes of migration sharing similar mechanisms with 2D migration in some cases. Taken from Petrie and Yamada 2016. License 4580180282038.

1.11.2 Dynamics surrounding the nucleus during cell migration

As mentioned in 1.7.4, the nucleus is essential in all cells as it harbours the genetic material and therefore helps in the development, maintenance and repair of the cell. Given the size and rigidity of the nucleus, it is a major factor impacting motility as demonstrated by many experiments where the shape and size of the

nucleus impacted a cell's ability to traverse confined spaces (Gomes, Jani and Gundersen, 2005; Wu *et al.*, 2014; Krause and Wolf, 2015; Petrie and Yamada, 2015; Thiam *et al.*, 2016). In most cases, the nucleus can be deformed to allow passing through confined spaces. However, the deformability is limited by the rigidity of the nucleus (Lammerding, 2011). Nucleus rigidity is governed mainly by lamins, a type of intermediate filament that shapes the nucleus as well (Schäpe *et al.*, 2009). Lamins are also involved in organization of chromatin, transcription regulation and the DNA damage response. Lack of lamin proteins in a nucleus leads to a phenotype where the nucleus is less rigid and is easily deformed, while an increase in lamin expression leads to more nucleus rigidity and the inability to deform the nuclear shape (Kong *et al.*, 2012; Lautscham *et al.*, 2015). Another factor involved in nuclear shape and rigidity is chromatin. Chromatin can be found in two states in the nucleus: euchromatin, which is considered “open”, or available for transcription, and heterochromatin, which is considered “closed” and is not transcriptionally active (Wolffe and Hayes, 1999; Murakami, 2013). Promoting an increase in euchromatin results in a less rigid, more deformable, nucleus, suggesting heterochromatin might be another factor involved in nuclear rigidity (Iyer *et al.*, 2012; Schreiner *et al.*, 2015).

During cell migration, the nucleus needs to be translocated along with the cell and in some cases, the nucleus also needs to undergo deformation to adapt to confined spaces the cell might be migrating through (Mak, Reinhart-King and Erickson, 2013; Krause and Wolf, 2015; Jayo *et al.*, 2016). In order to achieve this, the nucleus needs to interact with the cytoskeleton through linker proteins connecting the nuclear envelope with cytoskeletal proteins. The linker of nucleoskeleton and cytoskeleton (LINC) complex enables the transmission of these mechanical stimuli in the nuclear envelope (Isermann and Lammerding, 2013; Revach *et al.*, 2015; Arsenovic *et al.*, 2016) (Figure 1-13).

During cell migration, the nucleus is usually positioned in the rear. By mechanical contractility by an actomyosin complex and intermediate filaments, the nucleus is believed to be pushed forward (Wu *et al.*, 2014). During 3D motility assays, actomyosin contractibility along with integrin-mediated traction in the lamellipodia are required to push the nucleus forward through narrow passages (Krause and Wolf, 2015). Additionally, non-muscle myosin II (NMIIA) actomyosin

bundles interact with vimentin and bind to nesprin-3a proteins of the LINC complex to facilitate this forward pull (Fukata *et al.*, 2001; Wang, Li and Tang, 2006; Thomas *et al.*, 2015). Microtubules also associate dynein/kinesin complexes directly with LINC proteins (Sellers, 2000; Schiffhauer *et al.*, 2016) (Figure 1-13).

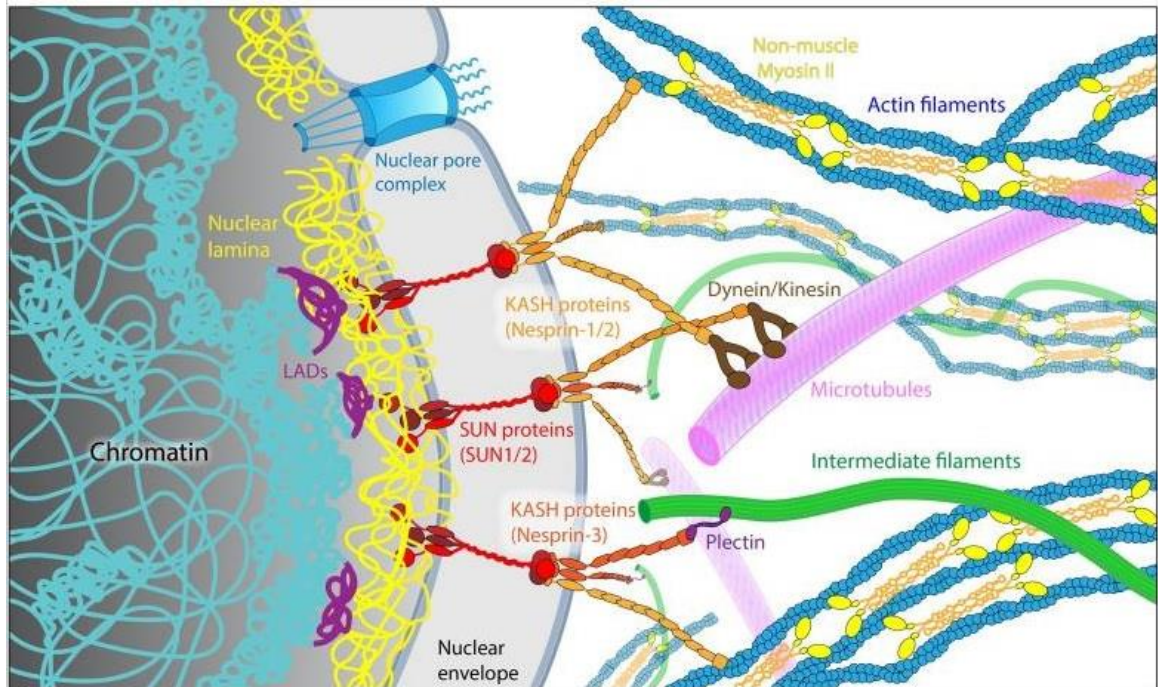


Figure 1-12 Schematic of interactions between nuclear proteins and cytoskeleton.

Several nuclear envelope proteins interact with actin and other cytoskeletal proteins. This includes nesprin, SUN and lamin with Dynein/Kinesin, actin, intermediate filaments and microtubules. This interaction allows the nucleus to be protected, deformed and moved. Taken from McGregor, Hsia, and Lammerding 2016. License 4575441474641.

As the cell migrates through a narrow passage, the nucleus is observed to take up most of the space in the narrow region, effectively separating the cell in two: a front and a rear portion (Davidson *et al.*, 2014). Two mechanisms are believed to play a role in this situation. The first is an osmotic pressure difference caused by the polarised distribution of the cell, where Na^+/H^+ pumps, along with aquaporins located in the plasma membrane on both sides of the cell, can alter water permeation driving migration and nuclear movement (Stroka *et al.*, 2014). The second mechanism is the nucleus itself as, during narrow passage, the nucleus divides the cell into two compartments. Actomyosin contractibility along with nesprin 3 linkers pulls the nucleus forward causing pressure build-up at the front of the cell allowing “passive” movement and converting the nucleus into a piston

of sorts that does not depend on lamellipodia mediation (Petrie, Koo and Yamada, 2014) (Figure 1-14).

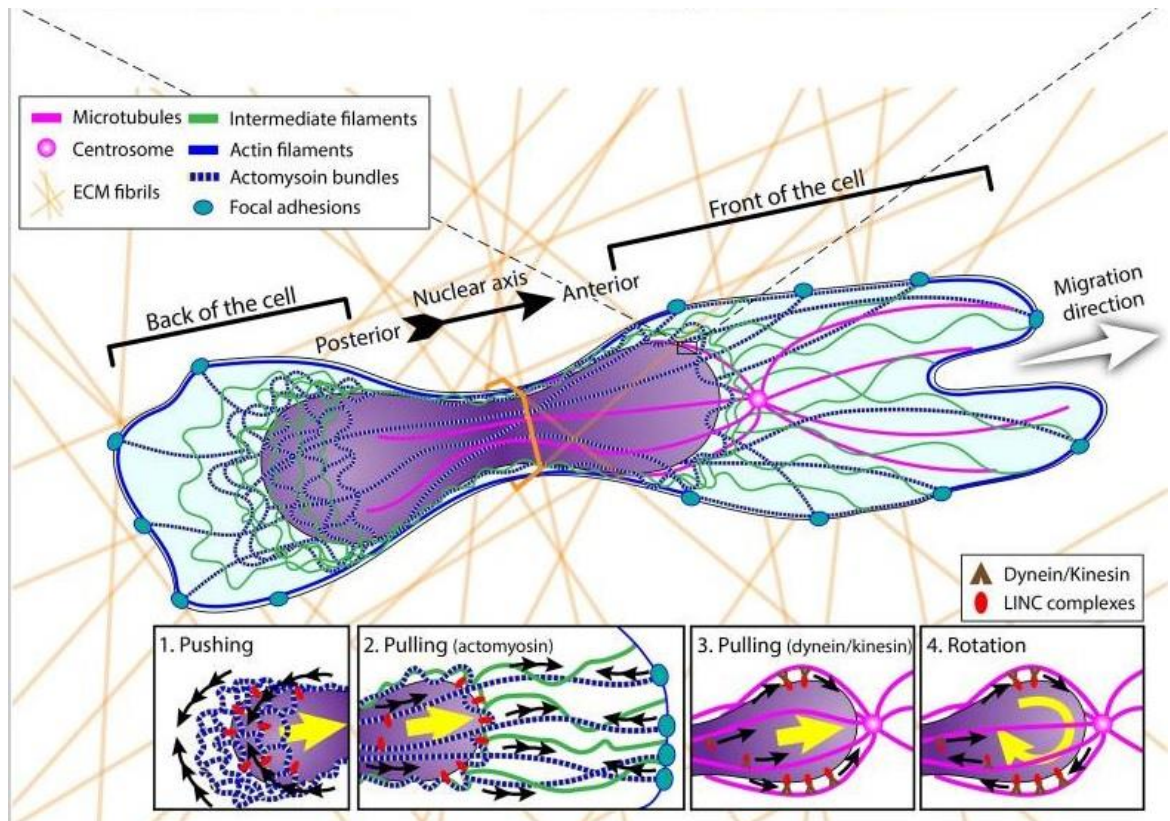


Figure 1-13 Cytoskeletal organisation and dynamics around the nucleus during migration. An interplay of actin, intermediate filaments and microtubules along with nuclear envelope proteins allow the nucleus to be deformed and the nucleus to be pushed and pulled to facilitate cell migration. Taken from McGregor, Hsia, and Lammerding 2016. License 4575441474641.

1.12 Open questions regarding apicomplexan motility

1.12.1 The actomyosin motor and the linear motor model

Apicomplexan parasites present a unique type of motility that does not require cytoskeletal shape changes and is substrate-dependent. This motion, called gliding motility depends on an actomyosin motor also known as the glideosome. This glideosome relies heavily on actin filaments and a type of myosin XIV called myosin A, unique to these parasites.

The exact molecular mechanism of the glideosome, along with orientation of the complex has been debated for years (King, 1988; Tardieux and Baum, 2016). The most accepted model predicts the myosin motor to be anchored to the Inner

Membrane Complex (IMC) of the parasites, displacing short actin filaments linked to adhesion proteins to gain traction and generate force. This model is believed to face the plasma membrane (PM), essentially being in the pellicular region of the parasite between the IMC and PM (Tardieux and Baum, 2016). However, other models over the years has been proposed including a reverse topology model, where the glideosome is anchored to the plasma membrane (King, 1988) and a free orientation model, where filamentous actin is bound to the PM by F-actin bundling proteins including coronins and formins (Daher *et al.*, 2010; Olshina *et al.*, 2015; Bane *et al.*, 2016; Tardieux and Baum, 2016). This free orientation model would work by generating force via myosin A, translocating the membrane patch linked to F-actin and adhesions without the necessity of a linker protein and resulting in forward displacement. Additionally, an osmotic gradient model powered ion pumps and aquaporins that does not depend on actin or myosin was also proposed (Egarter *et al.*, 2014). Although this model would explain why parasites lacking glideosome components can still glide and invade, actin and myosins remain important, suggesting osmotic-driven motility could be complementing glideosome-powered gliding. Lastly, a fountain-flow model was recently proposed, where surface proteins secreted by the parasite are recycled via endocytosis in an endocytic-secretory cycle. This model does not rely on actin as membrane flow was not affected by interference with the actomyosin system but would work alongside with it, linking microneme secretion, recycling and gliding motility together (Gras *et al.*, 2019).

The glideosome is composed of several basic proteins (e.g. adhesins, MyoA, MLC1, GAP45, GAP50, GAP40, GAPM and an unidentified linker) believed to be key for invasion (Keeley and Soldati, 2004; Heintzelman, 2015) (Figure 1-15). Among the main components of the glideosome, myosin A does not present a C-terminal tail as is typical of mammalian myosin XIV proteins; instead it possesses a neck, which biochemical studies have shown to bind to myosin light chain (MLC1) along with three essential light chains (ELC1 and ELC2) (Agop-Nersesian *et al.*, 2009; Fréchal *et al.*, 2010; Heaslip *et al.*, 2010). The myosin A motor has been suggested as the main driving force behind gliding motility and invasion (Dowse and Soldati, 2004; Gonzalez *et al.*, 2009). In vitro kinetic assays suggest myosin A can interact and move towards the barbed (+) end of actin filaments further hinting at a close interaction (Gilk *et al.*, 2009; Tang *et al.*, 2014). Since myosin A lacks the C-

terminal tail, the concerted action of MLC1, ELC1 and ELC2 is believed to promote the myosin A arm movement, characteristic of other myosin XIV proteins (Williams *et al.*, 2015; Yusuf *et al.*, 2015; Green *et al.*, 2017).

The C-terminal domain of GAP45 is necessary and sufficient to recruit MLC1 and, indirectly, myosin A to the IMC (Fréchal *et al.*, 2010), functioning to anchor the complex to the IMC. Having the myosin A-MLC1-ELC1-ELC2 complex anchored to the IMC is necessary to generate force in order to move the motor forwards. Another protein, GAP45, is vital for gliding, invasion, and egress and it is believed to work to maintain the structural integrity and space between the IMC and PM (Agop-Nersesian *et al.*, 2009). GAP40 and 50 are also essential components of this anchor and have been suggested to work in the biogenesis of the IMC (Harding *et al.*, 2016).

Adhesin proteins are also necessary to provide traction and transient adhesion to substrates or the host cell plasma membrane (Soldati, Dubremetz and Lebrun, 2001). These adhesins, such as AMA1 and MIC2, are secreted by micronemes during gliding, invasion and egress, and it is believed that they can bind to a wide range of ligands including heparin sulphate and other proteoglycan derivatives (Soldati, Dubremetz and Lebrun, 2001; Mercier *et al.*, 2005; Huynh, Boulanger and Carruthers, 2014; Katris *et al.*, 2014; Howard *et al.*, 2015). The cytosolic tail domain of these adhesin proteins has been suggested to act as a linker to the actomyosin motor complex (Figure 1-15). In addition, other linkers have also been suggested, with the GAC connector as the most recent (Jacot *et al.*, 2016), linking the adhesin proteins with the actomyosin motor complex.

Taken together, the current linear motor model forms a complex where short actin filaments produce the force to achieve rearward movement. This force production is generated by an IMC-anchored myosin A motor that would walk or displace short actin filaments that are constantly polymerised and depolymerised by the interplay of actin binding proteins. This process would be enough to generate force transmission into the adhesin domains in the PM resulting in forward movement. However, reverse genetic studies have shown that the lack of several of these components does not completely stop mutant parasites from gliding, invading or egressing, but merely affects the efficiency (Egarter *et al.*, 2014; Whitelaw *et al.*, 2017). Mutants lacking myosin A, microneme 2 and AMA1 can be

maintained in *in vitro* cultures (Andenmatten *et al.*, 2013; Bargieri *et al.*, 2013; Egarter *et al.*, 2014; Gras *et al.*, 2017), suggesting other proteins or mechanism(s) can complement their function. These results would suggest either that the linear motor model needs to be revised, or that a different system exists to complement gliding motility and invasion.

Additionally, views that *T.gondii* invasion is exclusively driven by the parasite, while the host cells remains passive, have been disproven. During invasion, the host actin cytoskeleton is modulated at the attachment point by both *Toxoplasma gondii* and *Plasmodium berghei* parasites (Gonzalez *et al.*, 2009; Delorme-Walker *et al.*, 2012). Moreover, the invasion entry point in the host cell accumulates F-actin believed to be regulated by parasite's factors secreted during invasion (Baum *et al.*, 2008; Gonzalez *et al.*, 2009; Sweeney *et al.*, 2010). In cases where *toxofilin* or *myosin A* is genetically suppressed, the parasites are unable to remodel the host cortical actin resulting in parasites that are stuck with half of their body outside the host cell, triggering host cell membrane protrusions that surround the parasite, pulling them inside and completing invasion (Delorme-Walker *et al.*, 2012; Bichet *et al.*, 2016)

Regardless of the proposed model, the importance of the glideosome for motility is clear and the correct assembly of the complex and the true orientation in the parasite's cytoplasm remains to be elucidated.

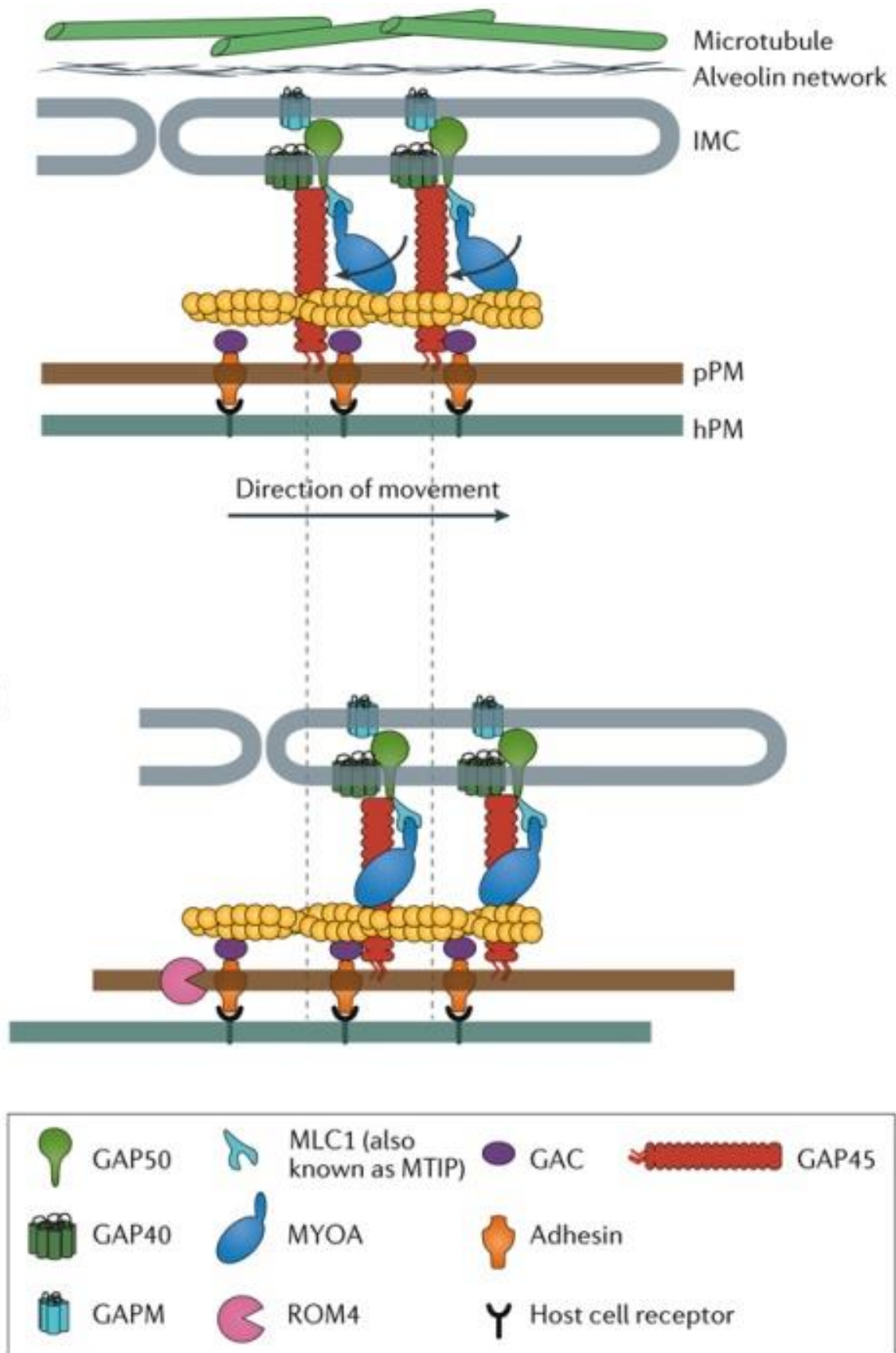


Figure 1-14 Linear motor model for *Toxoplasma gondii* actin-force generation.

The glideosome complex. It is composed of the five proteins MyoA, MLC1, GAP50, and GAP40 which are key for invasion. MyoA doesn't present a tail but it binds to the myosin light chain (MLC1). GAP45 recruits MLC1 and MyoA indirectly to the IMC. Adapted from Fréna, Dubremetz, *et al.*, 2017. License 4670850372733.

1.13 Aims of this study

The glideosome model predicts even translocation of short F-actin filaments from the apical tip of the parasite to the posterior pole. This F-actin translocation generates force and traction, powering motility and invasion. However, direct visualisation of F-actin dynamics was not possible.

In earlier studies, it was found that most of the parasite's F-actin shows a highly dynamic behaviour within the cytosol, suggesting important roles in this location. Here, using conditional mutants for the acto-myosin system of *Toxoplasma gondii* combined with the expression of chromobodies that recognise actin, analysis of the distribution, dynamics and functions of F-actin during intracellular parasite growth, motility and invasion were assessed.

In summary, this project aims to:

Characterise the actin dynamics in both intra- and extracellular parasites using fixed and live imaging via image analysis and data processing;

Address how depletion of actin related proteins or addition of compounds targeting actin affect these dynamics;

Re-assess invasion dynamics in terms of live actin visualisation;

Explore how mechanical stress affects invasion, and more importantly how the nucleus is managed during this event;

Elaborate a potential new invasion model based on the newly characterised actin dynamics.

2 Materials and Methods

2.1 Equipment

Table 2.1. Equipment

Applied Precision	DeltaVision® Core microscope
BD Biosciences	Syringes, Needles (23-25 gauge), FACS tubes with cell strainer cap
BioRad	Agarose gel electrophoresis equipment, UV transilluminator, SDS-PAGE system, Blotting apparatus (Transblot SD and Mini transblot electrophoretic transfer cell), gel documentation system, gene Pulser Xcell, Micropulser, S3e™ Cell sorter
BTX	Electroporation cuvettes and system (ElectroSquare Pore 830)
Eppendorf	Thermocycler (Mastercycler Eppgradient), Thermomixer compact
Fished Scientific	Ultrasound water bath FB15047
GE healthcare	Nitrocellulose membrane (Hybond ECL),
Grant	Water bath
Heraeus Instruments	Incubator
Ibidi	15 µ-Slide 10.8 Luer collagen IV chambers
KD scientific	Syringe pump
Kuehner	Shaking incubator (ISF-1-W)
Li-COR	Odyssey CLx
Lonza	4D-Nucleofactor™X electroporation unit, Single 100 µl Nucleovette™
Milipore	MilliQ water deionising facility, 3 µm Millipore filters
Photometrics	CoolSNAP HQ2CCD camera
Sanyo	CO ₂ - incubator tissue culture
Satorius	Analytical balances
Sciquip	Sigma 6K 15 centrifuge (1150 rotor and 12500 rotor)
StarLab	ErgoOne Single & Multi-Channel pipettes, StarPet Pro pipette controller
Stuart	Heat block, Roller mixer, Orbital Shaker
ThermoFisher scientific	CO ₂ - incubator tissue culture, Nanodrop spectrophotometer, Centrifuge (sorvall legend XFR), Table top centrifuge Heraeus Pico 21, Tabletop cooling centrifuge Heraeus Fresco 21, Invitrogen™ DynaMag™ magnets.
Zeiss	Axioskop 2 (mot plus) fluorescence microscope with AxioCam MRm CCD camera, Primo Vert (light microscope), Axiovert 40 CFL fluorescence microscope with AxioCam ICc1, Axiovert A1 fluorescence microscope with AxioCam IMc1, ELYRA PS.1 Super-resolution microscope, sCMOS pco SIM camera, Plan Apochromat 63x lens

2.2 Computer Software

Table 2.2. Software

Adobe Systems Inc.	Adobe design premium CS4
AcaClone software	pDraw32
Applied Precision	SoftWoRx explorer and SoftWoRx suite
BioRad	ProSort™
Carl Zeiss Microscopy	Zen Black and Zen blue
CLC Bio	CLC Genomics Workbench 6
GraphPad software Inc.	GraphPad Prism version 7.3
Li-COR	Image Studio 5.0
Microsoft Corporation	Windows 7, Microsoft Office 2010
<i>National Institute for Biotechnology Information (NCBI)</i>	Basic Local Alignment search tool (BLAST) (Altschul <i>et al.</i> , 1990)
<i>National Institute of Allergy and Infectious Diseases (NIAID)</i>	ToxoDB (Kissinger <i>et al.</i> , 2003; Gajria <i>et al.</i> , 2008)
National Institutes of Health	ImageJ (Rueden <i>et al.</i> , 2017), Fiji (Schindelin <i>et al.</i> , 2012)
New England Biolabs (NEB)	NEB tools™: Double Digest Finder, Enzyme Finder, NEBCutter®, NEBBioCalculator®, Tm Calculator
OligoCalc	Oligo Analysis tool (Kibbe, 2007)
PerkinElmer	Volocity 3D Image Analysis Software
Thermo Scientific	Thermo Scientific web tools: Tm Calculator
Glyph and Cogg, LLC	Mendeley Desktop 1.19.3
University of Utah	ApE Plasmid Editor v2.0.53c Copyright© by M. Wayne Davies
BioEdit	BioEdit Sequence alignment editor
Institut Pasteur and France	Icy Imaging software 1.9.10.0 (De Chaumont <i>et al.</i> , 2012)
Biolmaging	

2.3 Consumables, biological and chemical reagent

Table 2.3. Biological and chemical reagents

Clontech	Shield-1
Formedium	Tryptone, yeast extract
Li-COR	Chameleon Duo Pre-stained protein ladder
Life technologies	Phosphate buffered saline 1X (PBS), Trypsin/EDTA (0.05%), PureLink® RNA mini kit, DNaseI, Platinum Taq DNA Polymerase High Fidelity, NuPage SDS loading buffer and reducing agent, Sodium bicarbonate, Ultrapure agarose
Marvel	Milk powder (skimmed)
Melford	Agar, dithiothreitol, IPTG, X-Gal
NEB	DNA ladder (1 kb), All Restriction enzymes and associated buffers, T4 DNA ligase, Taq polymerase, Phusion® and Q5® high-fidelity DNA polymerase, Calf intestinal phosphatase (CIP)

Phenix Products	Research	GelRed nucleic acid stain
Promega		pGEM®-T Easy vectors system
Roche		MgSO ₄ × 7H ₂ O, potassium hydroxide, paraformaldehyde
Sigma		Ammonium persulfate, Bromophenol blue sodium salt, Casein hydrolysate, Dulbecco's Modified Eagle Medium (DMEM), Ficoll, Ethylene glycol tetraacetic acid, Ponceau S, Isopropanol, Sodium dodecyl sulfate (SDS), dimethyl sulfoxide (DMSO), N,N,N',N'-tetramethylethylenediamine, Triton X-100, Rapamycin, beta mercaptoethanol, Tween20, Giemsa stain, RNase-ZAP, L-glutathione reduced, Adenosine 5'-triphosphate disodium salt hydrate, Glutamine, 30% acryl-bisacrylamide mix, Sodium deoxycholate, K ₂ HPO ₄ , Magnesium chloride, Bleomycin (BLEO), Ampicillin sodium salt, Gentamicin, Xanthine, Chloramphenicol (CAT), Indole-3-acetic acid sodium salt (IAA, Auxin)
Southern Biotech		Fluoromount G (with and without DAPI)
Thermo Scientific		Bovine serum albumin (BSA), Ethylene diamine tetraacetic acid, Glycerol, Glycine, Methanol, Tris, Sodium chloride, 40 nM FluoSpheres® Carboxylate-Modified Microspheres, Platinum Taq DNA Polymerase High Fidelity, Restore Western blot stripping buffer, Invitrogen™ Dynabeads™ magnetic beads.
VWR		CaCl ₂ × 2 H ₂ O, Glacial acetic acid, Ethanol, HEPES, Potassium chloride, Na ₂ HPO ₄ , KH ₂ PO ₄
Zeiss		Immersion oil

2.4 Kits

Table 2.4. Nucleic acid extraction and amplification kits

Qiagen	Spin Mini-prep, Plasmid Midi-prep, MinElute PCR Purification MinElute, QIAquick gel extraction kit, DNeasy blood and tissue
Roche	PureLink® RNA isolation mini kit, high Pure PCR product purification
Thermo scientific	Maxima SYBR green/ROX qPCR Mater Mix

2.5 Buffers, solutions and media

Table 2.1. Buffers for DNA Analysis

50X TAE buffer	2 M Tris, 0.5 M Na ₂ EDTA, 5.71% glacial acetic acid (v/v)
5X loading dye	15% Ficoll (v/v), 20 mM EDTA, 0.25% Bromophenol Blue in H ₂ O
NEB 1 kb + DNA ladder	150 µl 1kb ladder (1 µg/µl), 300 µl 5X DNA loading buffer, 1050 µl H ₂ O

Table 2.2. Buffers for Western blot analysis

RIPA buffer	50 mM Tris-HCl (pH 8.0), 150 mM NaCl, 1 mM EDTA, 0.5% sodium deoxycholate, 0.1% SDS (w/v), 1 % triton X-100 (v/v)
4X separating gel buffer	1.5 M Tris-HCl (pH 8.8), 0.4% SDS (w/v)
Separating gel	8-15% of 30% acryl-bisacrylamide, 25% 4X separating gel buffer, 0.1% APS 10% (w/v), 0.2% TEMED (v/v)
4X stacking gel buffer	0.5 M Tris/HCl (pH 6.8), 0.4% SDS (w/v)
Stacking gel	4% of 30% acryl-bisacrylamide, 25% 4X stacking gel buffer (v/v), 0.1% APS 10% (w/v), 0.2% TEMED (v/v)
SDS PAGE running buffer	25 mM Tris, 192 mM glycine, 0.1% SDS (w/v)
Transfer buffer for wet blot	48 mM Tris, 39 mM glycine, 20% methanol (v/v)
Blocking solution	0.2% Tween (v/v), 3% skimmed milk powder (W/v), 0.037g SDS (W/v)
Washing solution (PBS-Tween)	0.2% tween (v/v) in 1X PBS
1 M DTT	3.085 g 1,4-dithio-DL-threitol (DTT) in 20 ml 10 mM NaAc (pH 5.2)
10 % APS	1 g ammonium persulfate in 10 ml H ₂ O

Table 2.3. Buffers and media for bacterial culture

LB medium	10 g/l tryptone, 5 g/l yeast extract, 5 g/l NaCl
LB agar	1.5% (w/v) agar in LB medium
SOB medium	2% tryptone (w/v), 0.5% yeast extract (w/v), 0.05% NaCl (w/v), 2.5 mM KCl, 10mM MgCl ₂
SOC medium	20 mM glucose in SOB medium
NYZ broth	5 g/l NaCl, 2 g/l MgSO ₄ *7H ₂ O, 5 g/l yeast extract, 10 g/l casein hydrolysate, pH adjusted to 7.5 with NaOH
Ampicillin (1000X)	100 mg/ml in H ₂ O
IPTG (100 µl/petri dish)	100 mM IPTG in H ₂ O
X-Gal (20 µl/petri dish)	50 mg/ml in N,N-dimethylformamide

Table 2.4. Buffers and media for *T. gondii* tachyzoites and mammalian cell culture

DMEM _{COMPLETE}	500 ml DMEM, 10 % FCS (v/v), 2 mM glutamine, 20 µg/ml gentamicin
DMEM Fluorobrite _{COMPLETE}	500 ml DMEM, 10 % FCS (v/v), 2 mM glutamine, 20 µg/ml gentamicin
2 x Freezing solution	25 % FCS (v/v), 10 % DMSO (v/v) in DMEM _{COMPLETE}
Electroporation buffer (Cytomix)	10 mM K ₂ HPO ₄ /KH ₂ PO ₄ , 25 mM HEPES, 2 mM EGTA pH 7.6, 120 mM KCl, 0.15 mM CaCl ₂ , 5 mM MgCl ₂ with 5 mM KOH adjusted to pH 7.6, 3 mM ATP, 3 mM GSH
Giemsa staining solution	10 % Giemsa stain (v/v) in H ₂ O

MPA (500X)	12.5 mg/ml in methanol
XAN (500X)	20 mg/ml, 1M KOH
Pyrimethamine (1000X)	1 mM in EtOH
Shield-1 (1000X)	1 mM in 70 % EtOH
Rapamycin (1000X)	50 μ M in DMSO
ATc (1000X)	0.5 μ g/ml
FACS buffer	1 % FCS, 1 mM EDTA in PBS
PFA fixing solution	4 % PFA (w/v) in PBS
PFA Cytoskeletal Buffer CB1	MES pH 6.1 10mM 138 mM KCL 3mM MgCl 2mM EGTA 5% PFA
PFA Cytoskeletal Buffer CB2	MES pH6.1 10 mM KCL 163.53 mM MgCl 3.555 mM EGTA 2.37 mM Sucrose 292 mM NH ₄ CL 50 mM
PFA quenching solution	0.2 % triton X-100 (v/v) in PBS
Permeabilisation solutions	0.1 % Saponin (v/v) in PBS
Blocking solution	% BSA (w/v) in permeabilisation solution
Endo buffer	44.7 mM K ₂ SO ₄ , 10 mM Mg ₂ SO ₄ , 106 mM sucrose, 5 mM glucose, 20 mM Tris, 0.3 5 % (w/v) BSA, pH 8.2
Gliding buffer	1 mM EGTA, 100 mM HEPES in HBSS
Hoechst 33342	
EM fixation solution	2.5 % Glutaraldehyde (v/v), 4 % Paraformaldehyde (w/v) in 0.1 M Phosphate buffer, pH 7.4

2.6 Antibodies

Table 2.5. Primary antibodies

Name	Species	Dilution		Source	Reference
		IFA	WB		
Catalase	Rabbit	(-)	1:3000	Soldati, D.	(Ding, Clayton and Soldati, 2000)
GAP45	Rabbit	1:1000	(-)	Soldati, D.	(Frénal <i>et al.</i> , 2010)
HA	Rat	1:500	1:1000	Roche	Commercial
HA	Mouse	1:100	(-)	Cell signaling	Commercial
HSP60	Rabbit	1:2000	(-)	Sheiner, L.	(Agrawal <i>et al.</i> , 2009)
IMC1	Mouse	1:1000	(-)	Ward, G.	(Wichroski <i>et al.</i> , 2002)
TOM40	Rabbit	1:2000	(-)	Van dooren, G.	Commercial
Rop2,4	Mouse	1:500	(-)	Dubremetz, JF.	(Sadak <i>et al.</i> , 1988)
<i>T. gondii</i> ACT1 polyclonal	Rabbit	1:500	1:500	Baum, J.	(Angrisano, Riglar, <i>et al.</i> , 2012)
Mic2 6D10	Mouse	1:500	n.t.	Carruthers, V.	(Huynh <i>et al.</i> , 2003)
Rop1	Mouse	1:200	n.t.	Sibley, L. D.	(Sadak <i>et al.</i> , 1988)
Rop5 T53E2	Mouse	1:1000	n.t.	Dubremetz, J.F.	(Sadak <i>et al.</i> , 1988)
RON4 TS6H1	Rabbit	1:500	n.t.	Lebrun, M.	(Leriche and Dubremetz, 1991)
RON2	Rabbit	1:500	n.t.	Lebrun, M.	(Besteiro <i>et al.</i> , 2009)
GAP40	Rabbit	1:250	n.t.	Soldati, D.	(Green <i>et al.</i> , 2017)
Gra7	Rabbit	1:500	n.t.	Delauw, M. F.	(Dunn <i>et al.</i> , 2008)
SAG1 (Toxoplasma)	Rabbit	1:1000	n.t.	ABCAM	Commercial
SAG1 _{monoclonal}	Mouse	1:1000	n.t.	Lourido, S	(Burg <i>et al.</i> , 1988)

Table 2.6. Secondary antibodies, fluorescent ligands and stains

Name	Species	Dilution			Source
		IFA	WB	Live-IM	
Alexa Fluor350 mouse	anti-Goat	1:3000	(-)	(-)	Life Technologies
Alexa Fluor488 mouse	anti-Goat	1:3000	(-)	(-)	Life Technologies

Alexa mouse	Fluor594	anti-	Goat	1:3000	(-)	(-)	Life Technologies
Alexa mouse	Fluor633	anti-	Goat	1:3000	(-)	(-)	Life Technologies
Alexa rabbit	Fluor350	anti-	Goat	1:3000	(-)	(-)	Life Technologies
Alexa rabbit	Fluor488	anti-	Goat	1:3000	(-)	(-)	Life Technologies
Alexa rabbit	Fluor594	anti-	Goat	1:3000	(-)	(-)	Life Technologies
Alexa rabbit	Fluor633	anti-	Goat	1:3000	(-)	(-)	Life Technologies
Alexa	Fluor350	anti-rat	Goat	1:3000	(-)	(-)	Life Technologies
Alexa	Fluor488	anti-rat	Goat	1:3000	(-)	(-)	Life Technologies
Alexa	Fluor594	anti-rat	Goat	1:3000	(-)	(-)	Life Technologies
IRDye680RD Mouse		anti-	Goat	(-)	1:5000	(-)	Li-Cor
IRDye800CW Mouse		anti-	Goat	(-)	1:5000	(-)	Li-Cor
IRDye680RD Rabbit			Goat	(-)	1:5000	(-)	Li-Cor
IRDye800CW Rabbit		anti-	Goat	(-)	1:5000	(-)	Li-Cor

2.7 Plasmids

Table 2.7. Main plasmids used in this study for cloning and expression in *T. gondii*

Expression vector	Resistance	Reference
Chromobody-Emerald FP	-	(Heaslip, Nelson and Warshaw, 2016; Periz <i>et al.</i> , 2017)

2.8 Cell strains

2.8.1 Bacteria strains

Table 2.8. *Escherichia coli* competent cells for plasmid transformation

XL10-Gold	Stratagene	Chemically competent
DH5 α	NEB	Chemically competent

2.8.2 *Toxoplasma gondii* strains

Table 2.8: *T. gondii* strains used in this study

Strain (full name)	Selectable Marker	Reference
<i>RHΔhxgprt</i>	-	(Donald and Roos, 2006)
<i>RHΔku80</i>	-	(Huynh and Carruthers, 2009)
<i>RH chromobody</i>	-	(Periz <i>et al.</i> , 2017)
<i>Emerald</i>	HX	(Mehta and Sibley, 2011)
<i>ADF cKD</i>	HX	This study
<i>ADF CKD chromobody</i>	DHFR	This study
<i>Emerald</i>	HX	(Egarter <i>et al.</i> , 2014; Whitelaw <i>et al.</i> , 2017)
<i>MyoAKO chromobody</i>	-	(Periz <i>et al.</i> 2019)
<i>Emerald</i>	-	
<i>Act1 cKO</i>	-	
<i>RH myoA-SNAP</i>	-	

2.9 Mammalian cell lines

Toxoplasma gondii tachyzoites were cultured in Human Foreskin Fibroblast (HFF) up to passage 23. The fibroblast cells are allowed to grow into monolayers, where growth is arrested due to contact inhibition. These cells were used for routine parasite culture. HFF can be commercially acquired from ATCC.

2.10 Molecular biology

2.10.1 Restriction endonuclease digest

Digestion of DNA by endonucleases was done for plasmid verification and linearization of vectors prior transfection. All restriction processes were done following the standard protocol of 1 hour. Restriction enzymes and buffers were supplied by NEB®.

Isolated DNA from bacterial cultures was verified using 100ng of DNA for diagnostic digests.

Stable transfections were done by vector linearization using a single restriction enzyme. An Amaxa[®] nucleofector was used for transfections where up to 20 µg of DNA from a vector was used, following standard protocol from the manufacturer.

2.10.2 Determination of nucleic acid concentrations

Concentration of nucleic acids was assessed by using a nanodrop spectrophotometer. An absorbance at 260 nm was used to determine potential chemical or protein contaminants (Desjardins and Conklin, 2010).

2.10.3 Plasmid transformation into bacteria

Bacterial transformation was done by employing chemically competent *E. coli* to increase plasmid vector copies. Bacterial competent cells were thawed on ice prior to transfection. 50 µl of bacteria was used per transformation, where 5 µl of the vector was mixed and incubated for 10 minutes. After incubation, the mixture was heat-shocked at 42°C for 30 sec, followed by an additional incubation on ice for 2 minutes. 500 µl of NZY broth was supplemented to promote bacterial cultures recovery at 37°C in a temperature-controlled shaker. Once the cultured has recovered, the culture was plated on LB-ampicillin agar plates, and incubated at 37°C overnight in an incubator. Lastly, the colonies were screened by analytical digest if required.

2.10.4 Isolation of plasmid DNA from bacteria

Overnight bacterial cultures were separated from the growth media and accumulated by sedimentation using a centrifuge. The resulting pellet was resuspended in a buffer comprising of EDTA and RNase A. This mixture was subsequently complemented with a lysis buffer (SDS and NaOH) to allow cell breakage and protein denaturation. The NaOH provokes disruption of hydrogen bonds between DNA bases, effectively separating double-stranded DNA (dsDNA) into single-stranded DNA (ssDNA). The lysis reaction needs to be controlled, as longer reactions can result in DNA degrading. To stop the reaction, a buffer containing potassium acetate is used to neutralise the alkalinity of the lysis buffer allowing ssDNA to be maintained. The high salt concentration precipitates cellular debris that is discarded by pelleting them using centrifugation. The supernatant containing the desired plasmid was purified by silica columns using a QiAprep spin

Miniprep and Midiprep kits (Qiagen®). The vector was eluted in ultra-pure distilled water.

2.10.5 Small scale DNA plasmid extraction

If small amounts of plasmid DNA was required, 4 ml of bacterial cultures were incubated at 37°C overnight. The cultured was pelleted by centrifugation and processed as described in 2.10.4. The resulting plasmid DNA was eluted in 50 µl in ultra-pure distilled water.

2.10.6 Medium and large scale DNA plasmid extraction

If large amounts of plasmid DNA were required, 50 ml overnight cultures were done at 37°C. The cultures were pelleted and the same procedure described in 2.10.4 was used. The plasmid DNA was eluted with 200 µl in ultra-pure distilled water.

2.10.7 Ethanol precipitation

Plasmid DNA was precipitated by ethanol precipitation before transfection. The vector elute was complemented with 1/3 of 3M sodium acetate (pH 5.2) and 3 volumes of ice-cold ethanol 100%. The mixture was left at -80 °C for 1 hour and the centrifuged at 13000 RPM at 4 °C for 20 minutes. The sample was centrifuged twice with 70% ethanol to remove excessive salts. Lastly, the ethanol was discarded and the sample was air-dried before resuspension in P3 buffer.

2.11 Cell biology

2.11.1 *Toxoplasma gondii* tachyzoites and mammalian cells *in vitro* culturing

Human Foreskin Fibroblasts (HFFs) monolayers were used to culture *Toxoplasma gondii* tachyzoites. Routine culturing was done using Dulbecco's modified Eagle's medium (DMEM), supplemented with 10 % fetal bovine serum (FBS), 4 mM L-Glutamine and 10 µg/ml gentamycin. Both HFFs and parasites were grown at 37°C and 5% CO₂ in a humidified incubator. Parasite lines were maintained over time by passing recently lysed extracellular tachyzoites to confluent HFF monolayers. If the parasites needed to be artificially released from the vacuole, mechanical

methods were employed by scratching the infected HFF monolayer followed by passing the HFF/parasite suspension in the media through a 25 G syringe thrice.

2.11.2 Trypsin/EDTA treatment of mammalian cell lines

Routine HFF cells were cultured by Matthew Gow, providing consistency in the cultures. The cells were split 1:4 by washing three times with PBS to remove residual medium and cell debris and then trypsin proteases was used for 5 minutes to facilitate cell detachment from the culturing flask. This was followed by adding DMEM_{COMPLETE} to distribute the new cell passage to other culturing vessels.

2.11.3 Cryopreservation of *T. gondii* and thawing of stabilates

Parasite stabilates were created by freezing large intracellular vacuoles. To facilitate parasite viability after thawing, heavily infected HFF monolayers were scraped and mixed with freezing medium (table 2.5.4). The mixture was transferred to 2 ml cryotubes and transferred to -20°C immediately. After the sample is frozen, the cryotubes were transferred to -80°C where they can be store for up to 6 months. If long term preservation was required, storage in liquid nitrogen is necessary.

To recover viable cultures from stabilates, the frozen samples were thawed at 37°C and added into confluent monolayers of HFFs.

2.11.4 Transfection of *Toxoplasma gondii*

Electroporation is the technique of choice for both transient and stable transfections of *Toxoplasma gondii* (Kim and Boothroyd, 1995). In the work presented in this thesis, an Amaxa electroporator was used as it provided the highest transfection efficiency as it uses the commercial Amaxa nucleofector P3 buffer.

2.11.5 Transient transfections

Toxoplasma gondii is able to be transiently transfected with circular exogenous DNA. This DNA, usually a plasmid is not integrated into the genome and is able to stay extra-chromosomal for a few generations before being lost (Suarez *et al.*,

2017). Through this study, transient transfections were done using the Amaxa nucleoporator. 10^6 parasites were transfected per condition using the P3 Lonza buffer and 20 μg of plasmid DNA. The transfectants were culture in 6-cm dishes or coverslips and maintained plasmid DNA expression by up 96 to hours.

2.11.6 Stable transfection

For stable transfections, plasmid DNA was linearised by restriction digestion. Stable transfections require either random or targeted insertions of DNA into the genome of the parasite. During random integration, the exogenous DNA is incorporated into the genome by the parasite's non-homologous end joining (NHEJ) repair mechanism, mediated by the Ku80 enzyme (Donald and Roos, 2006). During random integration, adding the same restriction enzyme to the mixture that is being transfected facilitates integration efficiency as the enzyme activates the DNA repair mechanism resulting in high integration efficiency. This method is called restriction enzyme mediated insertion (REMI) (Black *et al.*, 1995).

During this study, the chromobody EmeraldFP vector was transfected and randomly integrated using the method described above. The parasites were then cultured for 5 days before mechanical egress was done. Remaining HFF cells were lysed by syringing via a 25 G needle and the samples was filtered by 3 micron Millipore filter (Millipore Merck). It was then sorted by FAC, as described in 2.5.7.

2.11.7 Isolation of clonal parasite lines by limited dilution

Isolates of stable, clonal parasite lines was done through limited dilution of a stable pool using a 96-well plate. 5 to 7 days after cell infection, plaque formation was noticeable and wells with individual plaques were selected. These wells were assessed by light fluorescent microscopy and labelled as clonal lines if they presented 100% chromobody EmeraldFP expression.

This method was also repeated by FAC sorting, where 3 positive events were sorted into each well in a 96-well plate.

2.11.8 Inducing the *act1* KO

The *act1* KO was induced by the addition of 50 nM rapamycin (RAPA) to the parental LoXAct1 line. The induction lasted for 4 hours at 37 °C, 5 % CO₂ (Andenmatten *et al.*, 2013). RAPA is able to bind the two halves of the Cre-recombinase that recognises the LoxP sites, effectively excising the *act1* gene in between the sites. Since the induction of the DiCre could reach rates as low as 50%, 2.5 % Dextran sulfate in DMEM_{COMPLETE} was used during induced parasite culturing. Dextran sulfate isolates egressed parasites by blocking re-invasion of extracellular parasites. It works by binding glycans impeding parasite-host interaction in surface receptors. Since the *act1* KO population cannot egress on their own (Andenmatten *et al.*, 2013; Periz *et al.*, 2017), the induced parasite remained in culture. This cycle was repeated every 48 hours. This particular mutant was used in the experiments depicted in Figure 5-2.

2.11.9 Fluorescence activated cell sorting

Since no drug selection was used to obtain chromobody EmeraldFP parasites, Fluorescence activated cell sorting (FACS) was used to enrich the population by sorting. For this end, parasites were mechanically egressed and the HFF were lysed by syringing as described in 2.5.4. Either a S3e™ Cell Sorter (Bio-Rad Laboratories, Inc.), sorter using a 488 nm laser or a BD FACS Aria III (BD-BioSciences) were used to sort GFP positive parasites. The parasites were sorted into 5 ml tubes. The equipment was calibrated prior sorting by using ProLine™ universal calibration beads (Bio-Rad Laboratories, Inc.). The gates were adjusted by using controls for host cell debris, GFP positive and GFP negative parasites. The BD FACS Aria III was also capable of sorting 3 positive events into individual wells in a 96-well plate. This allow to save time in obtaining clonal lines.

2.12 Tachyzoite phenotypic analysis

2.12.1 Immunofluorescence assay

Immunofluorescence analysis (IFA) was performed to determine localisation of proteins and to assess expression of mutant parasites. Immunofluorescence analysis was done by using HFF cells grown on cover slips inoculated with *T. gondii*; infected HFF monolayers were fixed in 4% paraformaldehyde for 20 min at room temperature, and washed once with PBS. Next, coverslips containing parasites

were blocked for 40 min in permeabilising conditions (0.1% Saponin, 2% BSA in 1X PBS). Probing with primary antibodies was performed for 60 min in a wet chamber: coverslips were placed upside down into a petri dish that contained a wet paper towel, parafilm and 30 μ l drops of primary antibody diluted in blocking solution. Afterwards, coverslips were washed 4 times and incubated with secondary antibodies in blocking buffer for 1 hour. Finally, coverslips were washed 4 times with PBS, and fixed using Fluoromount™ containing DAPI. All procedures were performed at room temperature.

2.12.2 Plaque assay

1×10^3 parasites were inoculated on confluent HFF monolayers grown in 6-well plates. The plates were incubated at 37°C, 5% CO₂ for 7 days. After this time, monolayers were gently washed once in PBS and fixed with cold methanol for 20 min. Fixative was removed and cultures were stained with Giemsa (1:10 in H₂O) for 45 min, then washed three times with PBS. Images were acquired using Axiovert 40 fluorescence microscope with AxioCam. When required, plaque size was measured using ImageJ software and normalized to the appropriate control.

2.12.3 Time-lapse video microscopy

Video microscopy was conducted with the DeltaVision Core microscope, equipped with a temperature and gas control chamber which was used to maintain culture conditions (37°C and supplying 5% CO₂). Parasites were grown in glass bottom live cell dishes (Ibidi μ -dish^{35mm-high}). Obtained videos were analysed using SoftWoRx® or Fiji software.

2.12.4 Inducing the conditional Cas9act1 cKO

The act1 cKO parasite strain was obtained by addition of 50 nM of rapamycin to the parental lines. The strain was incubated for 1 h at 37 °C and 5% CO₂ and cultured as described previously (Whitelaw *et al.*, 2017). To decrease the population of un-induced parasites, the culture medium was replaced by DMEMcomplete supplemented with 2.5% dextran sulphate after 24 h to inhibit re-invasion of WT parasites.

2.12.5 Light microscopy

Widefield images were acquired in z-stacks of 2 μm increments and were collected using an Olympus UPLSAPO 100 \times oil (1.40NA) objective on a Delta Vision Core microscope (AppliedPrecision, GE) attached to a CoolSNAP HQ2 CCD camera. Deconvolution was performed using SoftWoRx Suite 2.0 (AppliedPrecision, GE). Video microscopy was conducted with the Delta Vision Core microscope as above. Normal growth conditions were maintained throughout the experiment (37 $^{\circ}$ C; 5% CO₂). Further image processing was performed using FIJI for ImageJ (NIH) and Icy Image Processing Software (Institut Pasteur) (De Chaumont *et al.*, 2012).

Super-resolution microscopy (SR-SIM) was carried out using an ELYRA PS.1 microscope (Zeiss) as described previously¹². 3D rendering and model views were generated using Imaris software (Bitplane, Oxford Instruments) using the acquired SR-SIM files.

2.12.6 Flow analysis time-lapse microscopy

To discriminate parasite orientation, 500nm of SiR tubulin was added to parasite cultures 1 hour before the experiment. To prepare tachyzoites for the assay, 1 \times 10⁶ mechanically freshly released live parasites per dish were washed 3 times with PBS and incubated a minimum of 10 minutes in serum-free DMEM medium. Cytochalasin D was added 30 minutes before imaging in a concentration of 2 μM . The samples were then imaged by widefield microscopy using a Delta Vision Core microscope or Super-resolution microscopy (SR-SIM) using an ELYRA PS.1 microscope.

2.12.7 Parasite treatment with A23187 and BIPPO

Calcium ionophore A23187 was added to live parasite dishes using with a final concentration of 2 μM . BIPPO was similarly used with a final concentration of 5 μM . The parasites were imaged by light microscopy immediately after adding A23187 or BIPPO.

2.12.8 Tight Junction assay

For the assay 3×10^6 mechanically freshly released parasites per well were incubated in 200 μ l Endo Buffer (44.7 mM K_2SO_4 , 10 mM $MgSO_4$, 106 mM sucrose, 5 mM glucose, 20 mM Tris- H_2SO_4 , 3.5 mg/mL BSA, pH 8.2) for 10 minutes at 37° C degrees. The parasites were then allowed to settle into confluent layer of HFFs for 3 minutes at room temperature. This step was followed by 20 minutes incubation at 37° C. The supernatant was carefully removed and replaced by pre-warmed culture media. The samples were further incubated for 5 minutes to allow invasion.

This was followed by fixing the samples using two different buffers: Cytoskeleton buffer (CB1) (10 mM MES pH 6.1, 138 mM KCL, 3 mM MgCl, 2 mM EGTA, 5% PFA) and Cytoskeleton buffer (CB2) (10 mM MES pH 6.1, 163.53 mM KCL, 3.555 mM MgCl, 2.37 mM EGTA, 292 mM Sucrose). These buffers were mixed in a 4:1 ratio respectively and subsequently used for fixation for 10 minutes. The samples were then treated with a PFA quenching solution (50 mM NH_4CL) for 10 minutes followed by PBS washing for three times. A minimum total of 40 parasites were counted for each sample in three biological replicates. The tight junction assay involving several mutants and wt in Fig. 5-3C employed a multiple comparison two-way ANOVA using Tukey's multiple comparison test with a p-value of <0.0001

2.12.9 Live cell invasion

Parasites were mechanically released using 23 G needle and filtered prior to inoculation on a confluent layer of HFFs, grown on glass bottom dishes (MaTek). The dish was then transferred to the DV Core microscope (AppliedPrecision, GE) and maintained under standard culturing conditions. Images were captured at 1.4 frames per second in DIC using an Olympus apochromat 60x oil objective. Images were analysed using the Icy Image Processing software (Institut Pasteur) (De Chaumont *et al.*, 2012). Penetration speed profiles were obtained for 18 independent invasion events for RH Cb-EmeraldFP and Cb-EmeraldFP parasites. The statistical analysis of RH wt Invasion events in Fig. 5-4C was done by unpaired two-tailed t-test in 28 total parasite invasion events that were captured across three different biological replicates.

2.12.10 Correlative light-electron microscopy (CLEM)

Cells were grown in gridded glass bottom petri dishes (MaTek) and infected with Cb-EmeraldFP or RH parasites. Invading parasites were imaged with SR-SIM in an ELYRA PS.1 microscope (Zeiss, Germany) with a Plan-Apochromat 63x oil (1.4 NA) objective. After imaging, the material was fixed in 2.5% glutaraldehyde and 4% paraformaldehyde in 0.1 M Pipes buffer (TAAB, UK). To increase the contrast of cytoskeleton elements, 1% tannic acid was added to the fixation solution. After an overnight incubation, the material was processed for transmission electron microscopy as described previously (Loussert, Forestier and Humbel, 2012). Thin sections of the same areas imaged in SR-SIM were imaged in a Jeol 1200 transmission electron microscope (JEOL, Japan).

2.12.11 Plasmodium Assays

The Cb-EmeraldFP sequence was cloned and transfected into *P. Falciparum* 3D7 parasites, and parasites were cultured in RPMI 1640 supplemented with Albumax (Invitrogen). Schizonts were collected on a bed of 70% Percoll as previously described (Das *et al.*, 2017). The schizonts were allowed to egress in a medium containing blood at 1% haematocrit and merozoites at various stages of invasion were fixed in 4% paraformaldehyde with 0.0075% glutaraldehyde as previously described (Das *et al.*, 2017). The junction was stained with a RON4 antibody and the nucleus stained by DAPI. Cb-EmeraldFP labelled actin filaments were fluorescent in the green range. For image acquisition, z-stacks were collected using a UPLSAPO 100x oil (1.40NA) objective on a Delta Vision Core microscope (Image Solutions - Applied Precision, GE) attached to a CoolSNAP HQ2 CCD camera. Deconvolution was performed using SoftWoRx Suite 2.0 (Applied Precision, GE). An Elyra S1 microscope with Super resolution Structured Illumination (SR-SIM) (Zeiss) was used for super-resolution dissection of AMA1 staining on the merozoite surface.

2.13 Biochemistry

2.13.1 Preparation of parasite cell lysates

For western blot analysis, parasites were mechanically released and syringed as described in 2.11.1 10^7 parasites were used for each sample and centrifuged at

1500 g for 5 minutes at 4°C. The samples were then washed two times in cold PBS. The parasites were then lysed on ice to prevent protein denaturation and degradation with 8 µl of RIPA (Table 2.5.2) buffer for 5 minutes. Insoluble material was removed by centrifugation at 4°C for 10 minutes at maximum RPM. The supernatant was then transferred to fresh vial and 1.2 µl (Invitrogen©) of reducing agent was added along with 3 µl NuPage® 4x loading dye. Each sample was boiled 10 minutes at 95 °C

2.13.2 Sodium dodecyl sulphate polyacrylamide gel electrophoresis

Separation of proteins was done by using sodium dodecyl sulphate polyacrylamide gel electrophoresis (SDS-PAGE) (Laemmli, 1970). The SDS-polyacrylamine gel was poured in a 1.5 mm thick glass cassette at 8%. APS and TEMED were added as a polymerisation catalyst. The resolving gel was poured first and isopropanol added on top to even out polymerisation in the surface. After the polymerisation was done, the isopropanol was discarded and a stacking mixture was added on top along with a 10-well comb. Gel cassettes were assembled in the Bio-Rad© mini-PROTEAN® Tetra Cell using 1 x SDS running buffer. The parasite lysate sample was loaded along with 1 µl of Chameleon™ Duo protein ladder (Li-COR) to assess gel migration and protein size. The samples ran at 90 V for 10 minutes through the stacking gel. The voltage was then increased to 120 V (for 50 minutes) to allow protein separation on the resolving gel.

2.13.3 Western blotting

For the blotting, the samples were transferred from the SDS-gel to Hybond® ECL™ nitrocellulose membranes (Sigma-Aldrich®), by a wet transfer method. To achieve this, membranes and the gel were sandwiched together and surrounded by 3 Whatman filter paper on each side along with a foam pad. This construct was pre-soaked in transfer buffer. This construct was ran in a Bio-Rad© mini-PROTEAN® Tetra Cell using a transfer buffer (See Table 2.5.2). The protein transfer was done at 100 V for 60 minutes maintaining low temperatures using ice in a cold room to prevent overheating.

2.13.4 Ponceau-staining

The transferred was verified by Ponceau staining. This was done by staining the membranes with a Ponceau S solution for 5 minutes at room temperature (RT) while shaking. Following visualisation, the staining was removed by washing with PBS twice and one time with the transfer buffer.

2.13.5 Immunostaining

The resulting membrane was blocked 1 hour in 3% skimmed milk in PBST (Table 2.5.4) at RT while shaking. The membranes were then incubated for 1 hour in a wet chamber with a primary antibody diluted in 1 mL of blocking buffer. This was followed by washing three times with PBST and then left to incubate with a secondary antibody (IRDye® LiCor®) diluted in 6 mL blocking buffer for an additional 1 hour while shaking. Lastly, the membrane was washed three times in PBST and once in PBS.

2.13.6 Visualisation and quantification of the protein bands

Membrane was scanned using the Li-Cor® Odyssey® equipment. This system allows highly accurate quantitative infrared detection of the protein of interest.

2.14 Bioinformatics

2.14.1 Data and statistical analysis

All primary data was entered using Microsoft Excel and then processed by GraphPad Prism® 7.03. Additionally, Statistical analysis was performed using GraphPad Prism® 7.03. For group comparison, the P value was calculated using an unpaired Student's t-test. When multiple groups were compared, the P value was determined using One-way or Two-way ANOVA accompanied by Dunnet's or Tukey's multiple comparison test as described in each figure legend.

2.14.2 Color-coded kymogram generation for particle dynamics analysis

Fourier-filtered Color-coded kymograms were generated using the KymographClear plugin on ImageJ and published in Mangeol, Prevo, & Peterman, 2016.

KymographClear is an ImageJ macro toolset designed to extract kymograph based on particular Region of Interest (ROI) from image sequences (Mangeol, Prevo and Peterman, 2016). This is done by first generating a maximum-intensity collapsed image from the source sequence. An ROI track can then be defined by the user, which will allow the macro to generate a kymograph based in the defined track. Another macro from the same plugin, can be used for background correction. One particular advantage of the KymographClear macro is the use of Fourier filtering for the kymograph, which not only allows discrimination of anterograde, retrograde and static signals, but also presents it in a colour-coded manner (Red for anterograde, green for retrograde and blue for static). These generated data are then saved and can be imported into another software for further analysis.

KymographDirect is a stand-alone software that allows automatic kymograph analysis, limiting user input bias. It is designed to work along with the data generated by KymographClear and can efficiently work with data at even low Signal to Noise Ratio (SNR). The software can be programmed to correct bleaching during image acquisition and can read the background correction data obtained in the prior step. The trajectories of the moving particles are then calculated for both velocity and intensity along the complete track and presented in graph form and can also be exported as text files to workbooks. The intrinsic works of the software and the algorithms it uses to detect the trajectories of moving particles are beyond the scope of this work and the author would recommend revising the original publication for more information of the inner works of this software (Mangeol, Prevo and Peterman, 2016). A more detailed protocol can be found on the author's website: <https://sites.google.com/site/kymographanalysis/>

2.14.3 Skeletonisation Analysis

The skeletonisation process was done in ImageJ FIJI using the Skeletonisation processing plugin (Doubé *et al.*, 2010). The sample was binarized by thresholding. A skeletonisation algorithm is then employed by the plugin which converts the thresholded signal into pixels, reducing the total width but not the length. The time-lapse profile was collapsed (Z-Project) to define the F-actin structures and their dynamics over the course of the time-lapse. The plugin can be accessed by: <https://imagej.net/AnalyzeSkeleton>

2.14.4 Cell deformation analysis

Samples were captured using SR-SIM and widefield microscopy as previously described. The deformation was then analysed with Zen blue software (Zeiss) by measuring the size of the parasite body and nucleus when going through a tight junction. A total of 100 parasites per biological replicate were measured for each condition for RH in Fig. 5-1B and a total of 30 parasites per biological replicate were measured for the mutant in Fig. 5-1C,D. Statistical analysis was carried out by ordinary one-way ANOVA, using Tukey's multiple comparison test with a p-value of <0.0001.

2.14.5 Penetration Speed profile analysis

Movies obtained were analysed using Icy Image Processing software (Institut Pasteur) (De Chaumont *et al.*, 2012) with the Manual Tracking plugin. The methodology used consists in tracking the apical end of the parasite through the duration of penetration. The resulting data was then exported to GraphPad PRISM7 Software for subsequent analysis.

3 F-actin behaviour in *Toxoplasma gondii* through the lytic cycle

To begin analysing actin dynamics in Apicomplexan parasites, improved tools needed to be developed or adapted from other fields of biology. Previously, several methods were tried including endogenously tagging actin with GFP and using antibodies with different epitopes leading to different interpretations and concerns regarding to specificity of the respective tag or antibodies in immunofluorescent assays (Morisaki, Heuser and Sibley, 1995; Jewett and Sibley, 2003; Drewry and Sibley, 2015). Using a conditional *act1* cKO, antibodies from various labs were tested for their specificity (Andenmatten *et al.*, 2013; Whitelaw *et al.*, 2017). While many cross-reacted, an antibody preferentially recognising *Plasmodium* filamentous actin from the Baum lab (Angrisano, Riglar, *et al.*, 2012) was also shown to positively stain for *Toxoplasma* F-actin (Periz *et al.*, 2017; Whitelaw *et al.*, 2017).

A recent study in our lab using actin specific nanobodies fused to different epitope or fluorescent tags allowed for the first time the analysis of F-actin localisation and dynamics in *Toxoplasma gondii* (Periz *et al.*, 2017). These nanobodies are derived from the heavy chain fragment of regular antibodies obtained from the *Camelidae spp.* family (Rothbauer *et al.*, 2006; Muyldermans *et al.*, 2009) and were originally fused to an Red Fluorescent Protein tag to allow live imaging of actin filament dynamics without adverse effects on cell fitness (Rothbauer *et al.*, 2006). From this point on, actin nanobodies has been successfully used in different organisms such as plants (Rocchetti, Hawes and Kriechbaumer, 2014) and, even endogenous expressed protein in living zebrafish (Panza *et al.*, 2015), where no detrimental effect was observed.

These nanobodies, aptly named chromobodies, are primed to recognise epitopes of the actin protein and thus, were able to label filamentous actin in live parasites. This uncovered several, previously unknown functions and locations of F-actin through the parasites lytic cycle, including a massive actin nanotubular network connecting parasites within the same vacuole (Periz *et al.*, 2017). Importantly, F-actin antibodies raised in the Baum lab (Angrisano, Riglar, *et al.*, 2012) detected similar structures in wild type parasites, indicating that the chromobody does not significantly alter F-actin dynamics (Periz *et al.*, 2017).

One of the major issues with the first version of the actin chromobody expression in *Toxoplasma gondii* was the nature of the fluorescent tag. The first generation used a HALO-tag (Promega) which is a self-labelling protein tag, that can be covalently bound to a ligand that carries a chromophore. While this fluorescent dye is bright, it also creates a considerable amount of background noise during imaging, making detection of fast F-actin dynamics in the parasite difficult. Therefore, a new chromobody vector was designed by a collaborator where the HALO tag was replaced by a modified GFP protein called Emerald Fluorescent Protein (EmeraldFP) (Figure 3-1 A) (Ilagan *et al.*, 2010; Heaslip, Nelson and Warshaw, 2016) and randomly integrated into the parasite's genome.

3.1 Expressing Chromobody-Emerald in *Toxoplasma gondii*

In order to obtain a clonal population of parasites expressing the actin chromobody EmeraldFP, FAC sorting was used (Figure 3-1B). After 72 hours (a time point, where stable integration of the construct into the genome is expected and episomal expression is reduced (Donald and Roos, 1993)), the parasites were sorted once to increase the population of transgenic parasites. These parasites were further enriched by two sorting steps and clonal parasites were obtained by limiting dilution of the sorted population. The parasites undergoing FACS, were analysed by comparing the SSC and FCS to controls (host cell debris, fluorescent-negative parasites and GFP parasites) (Figure 3-2 A). Parasites with a clear population difference were selected across two rounds of sorting (R3 Figure 3-2 B,C) to obtain a clonal population.

Upon analysis of the resulting clonal line, the parasites showed similar characteristics to the HALO tag (Periz *et al.*, 2017) without the excessive background noise of the TMR dye (Figure 3-2 D). This advantage was used to visualise dimmer details of the signal inside each individual parasite, such as smaller and weaker filamentous actin structures (red arrowhead Figure 3-2 E). The phenotype of this line was compared to wild type parasites and no significant differences were obvious in host cell invasion, replication or egress, demonstrating that expression of Chromobody has no toxic effects and therefore can be used to study F-actin in the parasite (Figure 3-2 F-H).

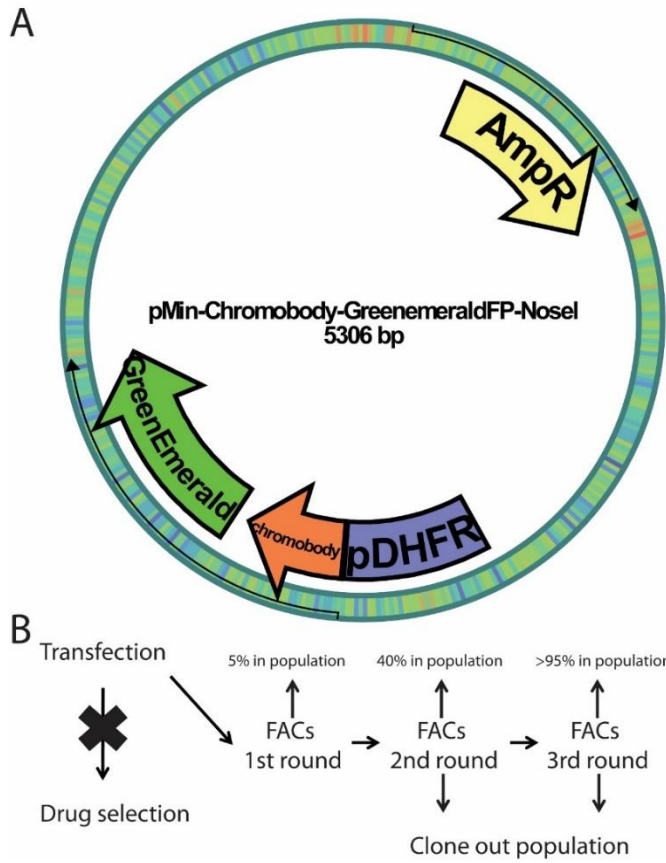
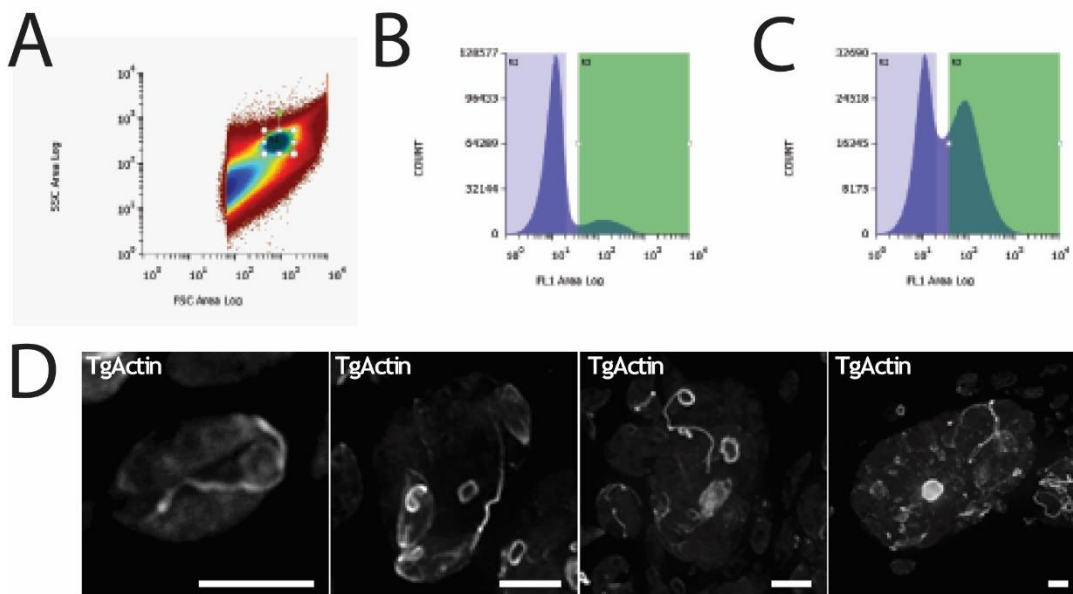


Figure 3-1 Scheme for the generation of a chromobody EmeraldFP line

A. Plasmid map depicting the chromobody EmeraldFP cassette on a DHFR promoter. **B.** FAC sorting work flow to obtain a fluorescent population. Since no drug selection was used a population of transfected parasites were sorted over 3 rounds to obtain a high prevalence of parasite positively expressing the chromobody EmeraldFP cassette. Once the population was sufficiently enriched, clonal lines were generated by limiting dilution.



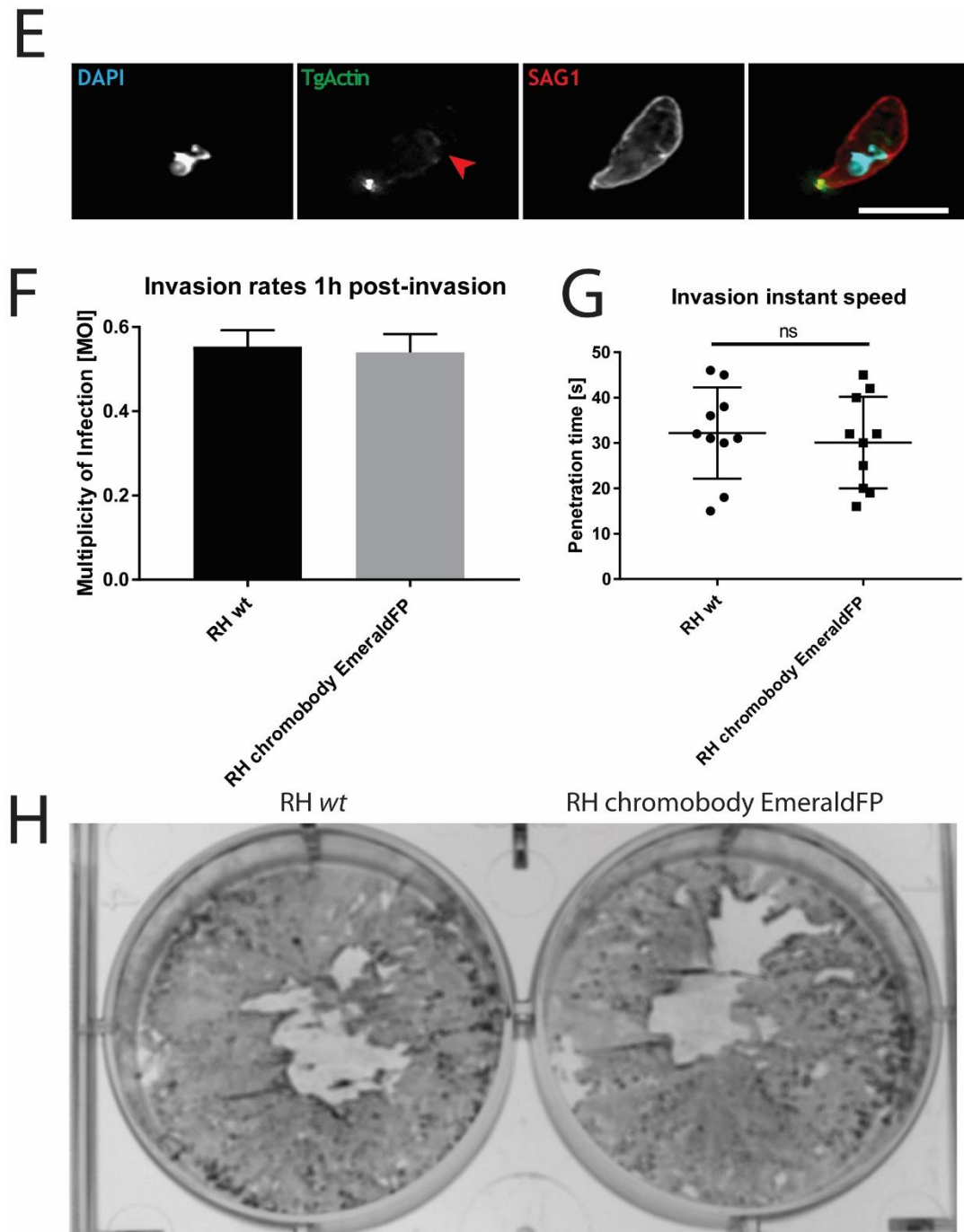


Figure 3-2 Expression of the chromobody EmeraldFP in a RH wt line.

A. Schematic depicting the population chosen for sorting based on the FSC and SSC. Controls were used to determine the correct values for parasites. **B,C.** Example of FACS strategy. **B.** shows obtained population directly (96 hours) after transfection. **C.** Shows enrichment of parasites expressing Chromobody after 2 rounds of sorting. **D.** Replicating parasites expressing chromobody EmeraldFP depicted in different stages. Note that the EmeraldFP not only stains an impressive nanotubular F-actin network, but also finer structures within the parasites. **E.** Extracellular parasites expressing chromobody EmeraldFP attached to a surface. Majority of F-actin is localised at the posterior pole, where the parasite is attached to the surface. However, signal can also be seen close to the centre or the nucleus of the parasite (red arrowhead). DAPI is shown in blue, TgActin Chromobody EmeraldFP in green and sag1 in red. **F.** Invasion rates of RH wild type and RH chromobody EmeraldFP parasites. **G.** Invasion instant speed of RH wild type and RH chromobody EmeraldFP parasites in live imaging. **H.** Plaque assay comparing RH wild type and RH chromobody EmeraldFP parasites. Scale bars represent 5 μ m.

3.2 Cytoplasmic F-actin dynamics during *T. gondii* replication

Once parasites expressing chromobody were established to behave identically when compared to the parental wild type line, *in vivo* replication actin dynamics were analysed. This was done by imaging different vacuoles in different stages (Figure 3-3). Based on the cases that were observed, F-actin is highly dynamic and found in different locations within the parasite. While actin was predicted to act mainly between the IMC and the PM of the parasite (Jewett and Sibley 2003; Drewry and Sibley 2015; D.M. Wetzel, S. Håkansson, K. Hu, D. Roos 2003), analysis of F-actin dynamics with the chromobody presented a majority of detectable F-actin to be found below the IMC, within the cytosol of the parasite, both during the intra- and extracellular stage of the parasite (red, green and yellow arrowheads, Figure 3-3, Movie S1).

During parasite replication (Figure 3-3 A-E), actin is accumulated at 3 points across the parasite body (Movie S1). It is hypothesised that these points act as centres for actin polymerisation, as large concentrations of F-actin can be observed being translocated from these points to the rest of the body of the parasite. The first centre is located in the central area of the parasite, close to the Golgi, showing F-actin translocation from the cytoplasm to the periphery (red arrowhead). The second centre is located at the apical end, which appears to further supply F-actin to the periphery (yellow arrowhead). Lastly, a third centre located close to the basal end in the residual body (green arrowhead). This last point appeared to receive the influx of F-actin originating in the previous centres and moving into the RB. The observed F-actin dynamics followed a pattern better described as a “flow”, showing somewhat fast dynamics akin to mammalian actin (Pollard and Borisy, 2003; Pollard and Cooper, 2009; Gardel *et al.*, 2010). However, the directionality is impossible to discern by eye, needing more in-depth analysis in order to address directionality and speeds (Movie S1). An in-depth analysis of the actin flow can be found in Chapter 4 of this thesis.

One of the main differences between parasite replication stages lies within the nanotubular network (Figure 3-3 A-E). As parasites replicate and the vacuoles becomes bigger, the more intricate and complex the nanotubular network appears, showing similar results as described in a previous study (Periz *et al.*,

2017). It is of particular importance to note that these actin accumulation centres have been linked to the location of formins in *Toxoplasma gondii* (Stortz *et al.*, 2019; Tosetti *et al.*, 2019), protein complexes that function as nucleation initiation points for F-actin polymerisation.

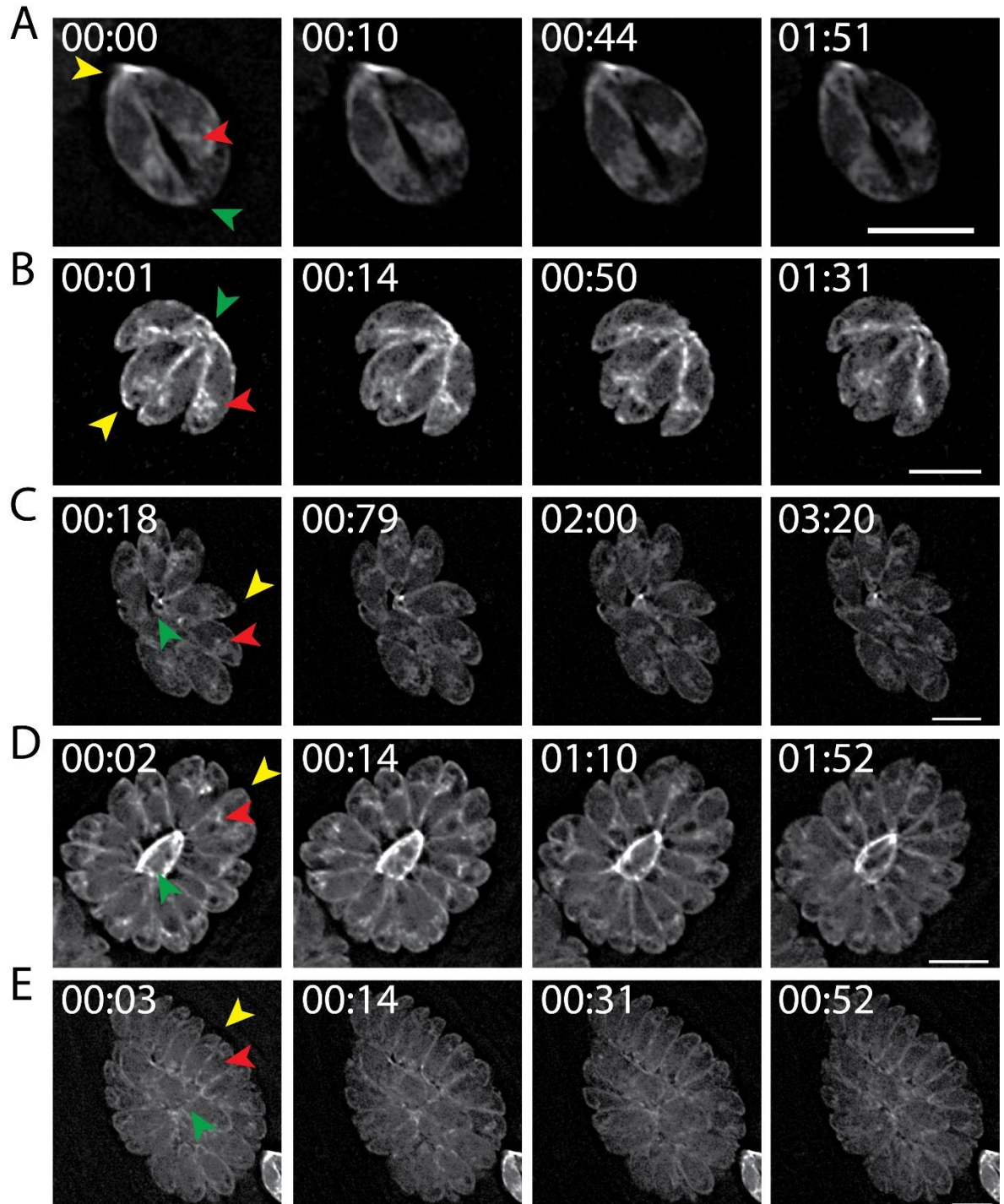


Figure 3-3 Chromobody EmeraldFP parasites during replication.

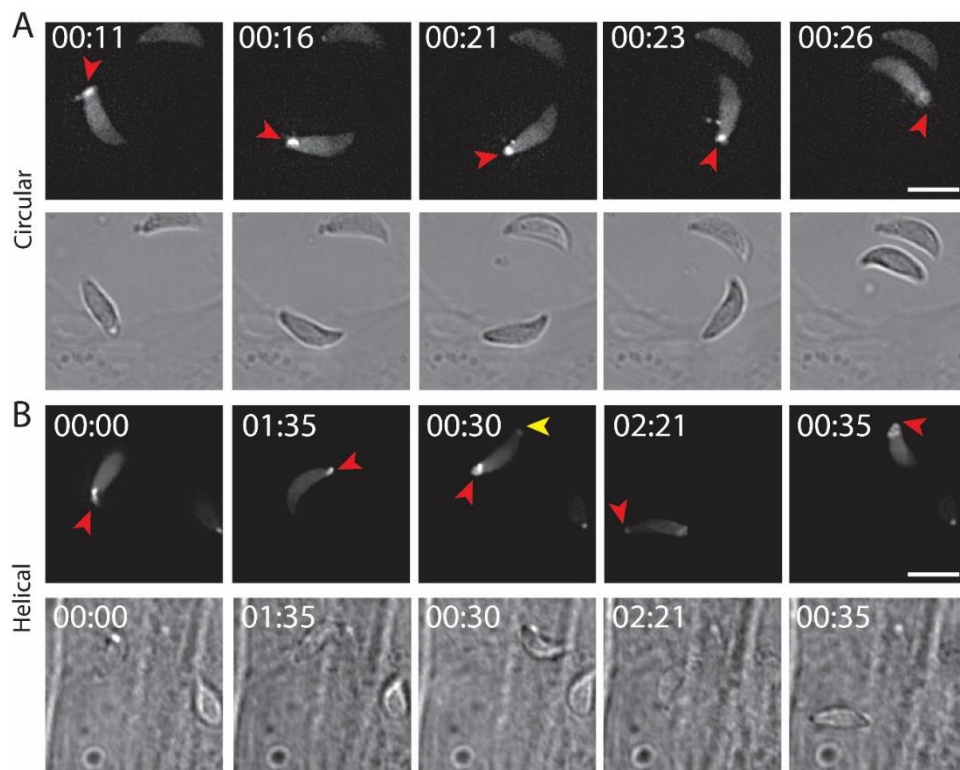
A-E. The replicating parasites present a highly dynamic behaviour of F-actin as a flow that moves around the periphery and centre of the parasite. A-E. Regardless of the replication stage (2 to 32 stage), the parasite present 3 centres of F-actin accumulation: the apical end (yellow arrowhead), the central region (red arrowhead) and the basal end (green arrowhead). Stills generated from Movie S1. Numbers indicate minutes:seconds; and Scale bars represent 5 μm .

3.3 F-actin accumulation on potential attachment points during parasite gliding motility

Toxoplasma gondii moves across large areas in order to invade new cells (Heintzelman, 2015). This type of movement termed gliding motility over a 2-D substratum has been heavily studied over the past 20 years. Gliding motility can be divided into three categories: helical motility, where the parasites moves in a helical manner propelling itself considerable distances in some cases; circular motility, where the parasite moves in a circular pattern; and twirling motility, where the posterior end of the parasite remains attached to a substrate and the other ends twirls in a circular fashion (Wetzel *et al.*, 2003; Heintzelman, 2015). In previous bio-mechanical studies in *Plasmodium* sporozoites using reflection interference contrast microscopy (RICM) and traction force microscopy (TFM), motility appeared to be limited by the dynamic turnover of discrete adhesion sites. These adhesion sites were described as strong adhesion points on both ends of the parasite and weak attachment points along the body. This behaviour allows the parasite to attach and de-attach with ease in a stick-and-slip motion, allowing fast movement turnover which results in the characteristic rapid motility of apicomplexan parasites (Münter *et al.*, 2009). It has been speculated on how this motion is achieved, based on the action of a linear motor as large eukaryotic cells make use of focal adhesion points and actin retrograde flow for traction force generation to achieve migration. In this case, F-actin is polymerised at the leading edge of the lamellipodia and flow towards the cell body generating traction force via pulling of adhesion proteins that are tethered to the ECM (Mendez, Kojima and Goldman, 2010; Stehbens and Wittmann, 2012; Horzum, Ozdil and Pesen-Okvur, 2014).

Using RH parasites expressing a chromobody EmeraldFP, further characterisation of the actin dynamics of gliding parasites was conducted. Circular motility exhibits a strong accumulation of F-actin at the posterior end of the parasite (red arrowhead Figure 3-4 A, Movie S2). This accumulation can be observed during the entire circular motility as shown in the still images and movies. During helical motility, strong actin accumulation can be observed at the posterior end (red arrowhead Figure 3-4 B, Movie S2). However, accumulation at the anterior end can also be observed in certain stages of the movement (yellow arrowhead still 00:30). These observations are consistent with the previously mentioned study

done in *Plasmodium* sporozoites (Münter *et al.*, 2009), where the parasite achieves motility via focal attachment points. During twirling motility, only the posterior end of the parasite that remains attached to the substrate can be seen with F-actin accumulation (green arrowhead Figure 3-4 C, Movie S2). This attachment is joined by several points of F-actin that appear as “dots”. This is particularly apparent once the parasite starts to twirl where two F-actin accumulation points can be seen at the beginning (green arrowhead 01:41), increasing to three dots later during the event (green arrowhead 01:43). Once the parasites start to twirl, these F-actin accumulation points seem to orbit around a single point in the centre (green arrowhead 01:47 - 01:50; Movie S2). Taking the work presented in Münter *et al.*, 2009 and the F-actin accumulation points in both ends of the parasite described in this work, it can be hypothesised that F-actin accumulates at these attachment points, allowing the parasite to stick to a substrate and transfer the force for motility. It is possible that accumulation of adhesin proteins and elements such as micronemes, are concentrated at these points, along with accumulation of actin. However, further experiments to characterise whether these F-actin accumulation points can be related to attachment are required to dissect the attachment machinery of the parasite.



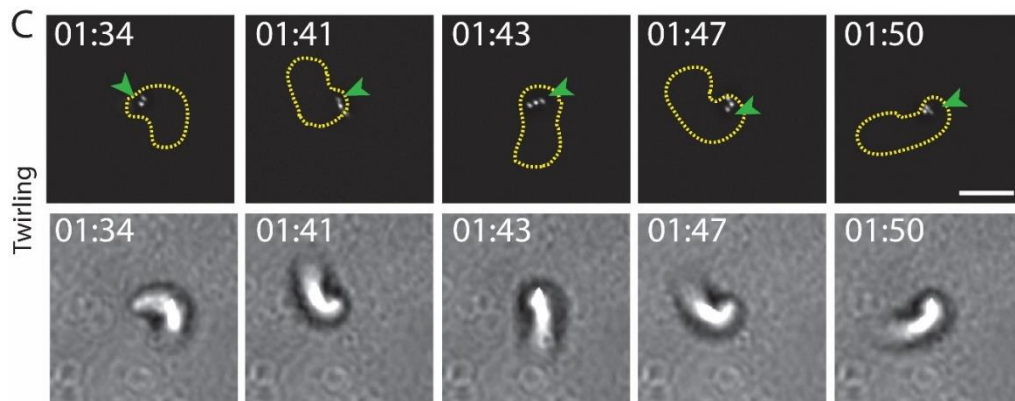


Figure 3-4 Types of 2-D gliding motility of *Toxoplasma gondii*.

A. Circular gliding motility. The parasite accumulates F-actin on the basal end prior to initiate movement. This accumulation lasts through the whole duration of the motion. The accumulation of F-actin appears to be related to motility (red arrowhead). **B.** Helical gliding motility. The parasite accumulates F-actin on the basal end prior to movement. During the helical motion (00:30), apical location of F-actin is visible at the apical tip, potentially coinciding with attachment formation at the apical tip. Note that this accumulation disappears, once the parasite detaches at the apical pole, although this could be explained as the parasite moving out of focus (00:33), Similar motility behaviour has been previously described as “stick and slip” where both ends of the parasite allow attachment (by focal adhesion points that corresponds well with the rich F-actin accumulation in this case) and minor adhesion through the parasite body (undetected). **C.** Twirling gliding motility. The parasite firmly attaches at the posterior end to the substrate and twirls around its axis. F-actin signals, potentially corresponding to attachment sites, with multiple signals appearing that coincide with motion initiation (green arrowhead, 01:34). This culminates with several F-actin signal points orbiting around a more stable site (green arrowhead, 01:43 – 01:50). Yellow lines indicate the parasite shape. Stills generated from Movie S2. Numbers indicate minutes:seconds; and Scale bars represent 5 μm .

3.4 F-actin dynamics during parasite invasion into host cells.

Invasion is key to the survival of obligate intracellular pathogens like *Toxoplasma gondii*. Forming part of the lytic cycle, this step allows the parasite to enter the host and replicate in order to propagate. During invasion, actin’s major role is believed to power the invasive step via an acto-myosin complex localised between the IMC and PM. (Meissner, Schlüter and Soldati, 2002; Bichet *et al.*, 2014; Drewry and Sibley, 2015; Tardieux and Baum, 2016).

Unexpectedly though, our results suggest that during invasion (Figure 3-5, Movie S3), F-actin is accumulated at the back of the parasite before penetration in a similar fashion to gliding motility (red arrowhead 00:08). Moreover, once the parasite starts the penetration process, an F-actin ring is visible at the apical tip at the onset of invasion (yellow arrowhead 00:23). The F-actin ring appears close to the tight junction throughout invasion, similar to what was previously published

in invading *Plasmodium* merozoites (Angrisano, Riglar, *et al.*, 2012). This F-actin ring will remain throughout the entire penetration process until the parasite is inside (00:23 - 00:40). Once this process is complete, the parasite will perform a twist motion that will seal and separate the parasitophorous vacuole from the host plasma membrane via the RON complex. This complex is reported to allow membrane scission at the tight junction-plasma membrane interface (Pavlou *et al.*, 2018), finishing the invasion step.

A more in-depth analysis of the dynamics involved in invasion, particularly pertaining actin and the entry of the parasite into the host cell can be found in Chapter 5.

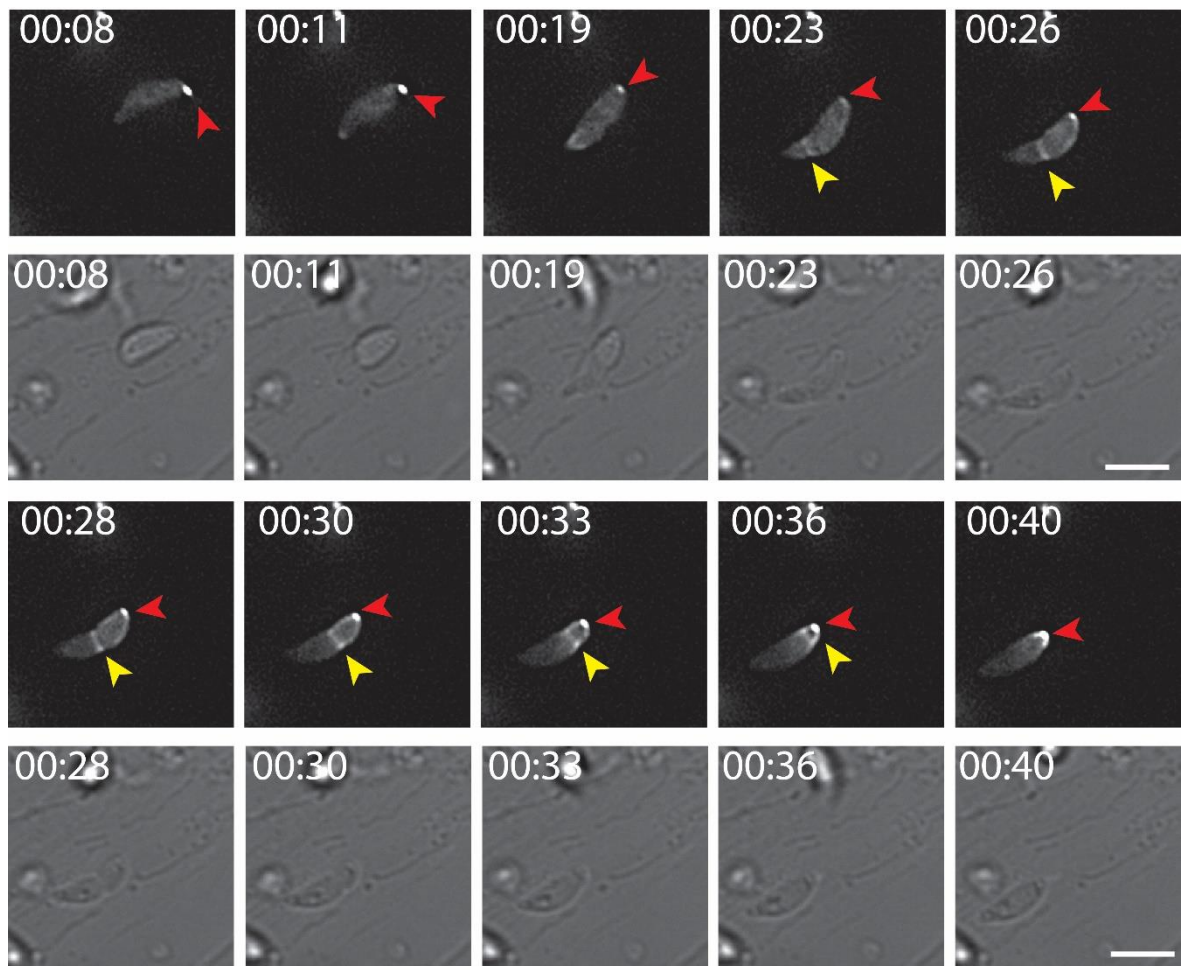


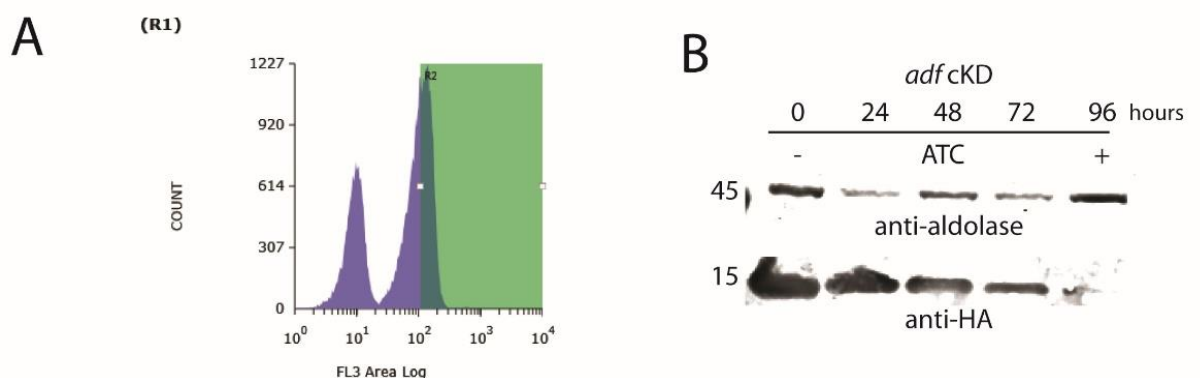
Figure 3-5 Invasion of RH parasites expressing chromobody EmeraldFP.

The parasite shows F-actin accumulation akin to gliding motility (red arrowhead). At the onset of invasion, an F-actin ring can be seen appearing at the apical tip of the parasite (yellow arrowhead, 00:23). This F-actin ring continues following the TJ until the invasion process finishes and the ring reaches the posterior end F-actin accumulation (yellow arrowhead, red arrowhead; 00:36 – 00:40). Stills generated from Movie S3. Numbers indicate minutes:seconds; and Scale bars represent 5 μm .

3.5 The Actin Depolymerisation Factor (ADF) drastically alters *T. gondii* F-actin dynamics across the lytic cycle.

Having validated that F-actin dynamics can be analysed using chromobodies, the consequences of interfering with F-actin regulatory proteins, such as ADF, on F-actin dynamics was desired to be explored.

The actin depolymerisation factor (*adf*) is an actin binding protein more likely related to actin severing and thus, depolymerisation. Mammalian *adf* proteins are difficult to categorised since they are known for performing several functions, such as severing of G-actin and depolymerisation of F-actin (Bamburg, 1999; Wolf *et al.*, 2015). In some cases, the literature is rather contradictory where they show that under specific circumstances such as aggregated states of the protein can promote stabilisation between filaments (Maciver and Hussey, 2002; Wiggan *et al.*, 2012; Wang *et al.*, 2013). It usually remains in two states, a phosphorylated state that possess a low affinity to actin, usually labelled as an inactive state that can form aggregates, believed to function as a binding complex for several actin filaments (Wang *et al.*, 2013). The second one is a de-phosphorylated or active state possessing high affinity for actin and the ability to sever filaments (Arber *et al.*, 1998; Van Troys *et al.*, 2008; Goyal *et al.*, 2013).



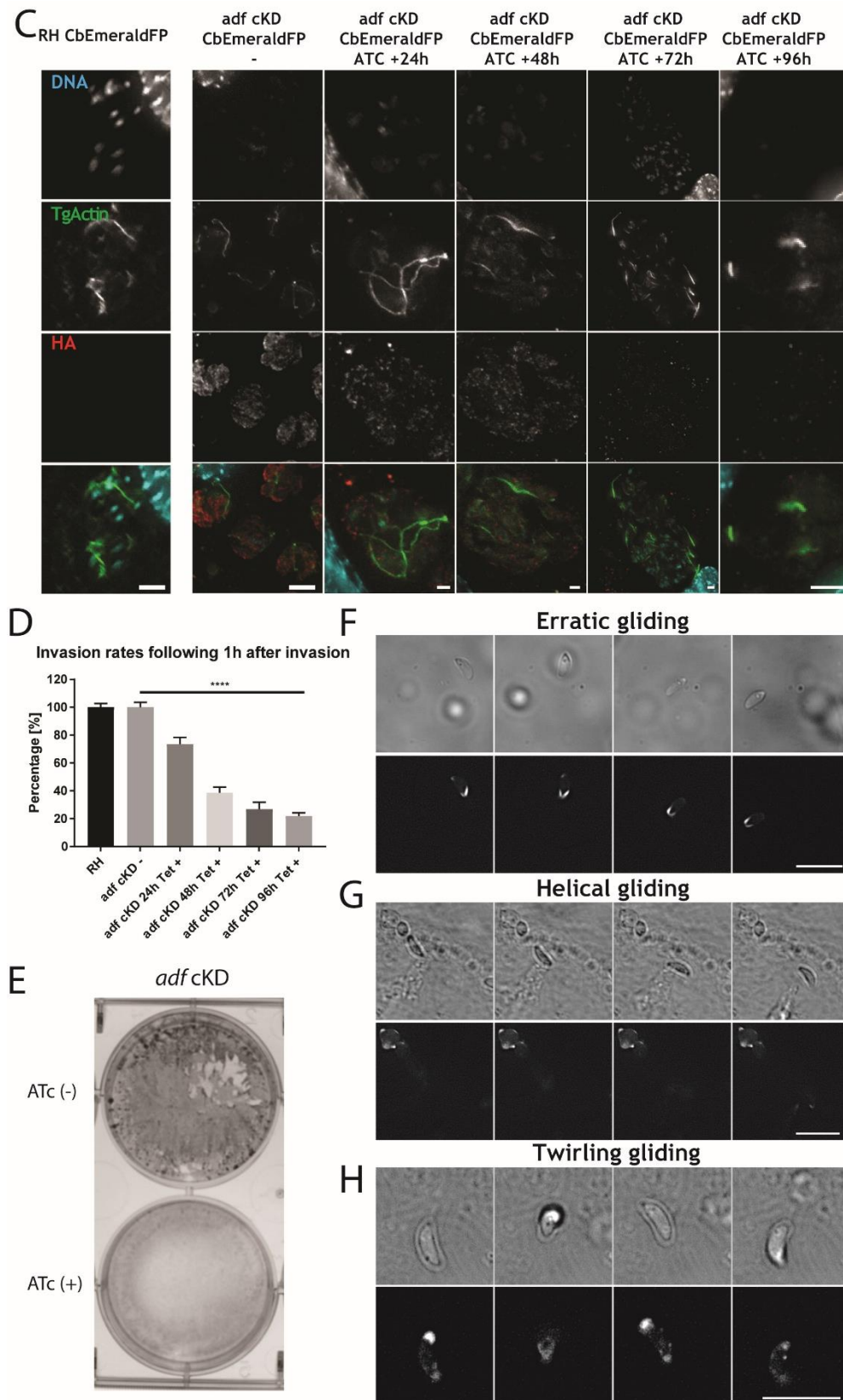


Figure 3-6 Generation of an *adf cKD* chromobody EmeraldFP.

A. After several rounds of FAC sorting, a highly enriched population is sorted and cloned out to obtain clonal lines of *adf cKD* expressing CbEmeraldFP. **B.** Western blot depicting depletion of the ADF-HA protein after addition of anhydrotetracycline (ATc). After 96 hours of ATc induction, the protein reaches background expression levels. Aldolase works as a loading control. **C.** IFA demonstrating knockdown of ADF-HA. Similar to (B), 96 hours after tetracycline induction, the HA signal drops significantly. Note that F-actin dynamics changes during this process, with strong accumulation of F-actin at the posterior pole and almost complete abolishment of dynamics. DNA is represented as

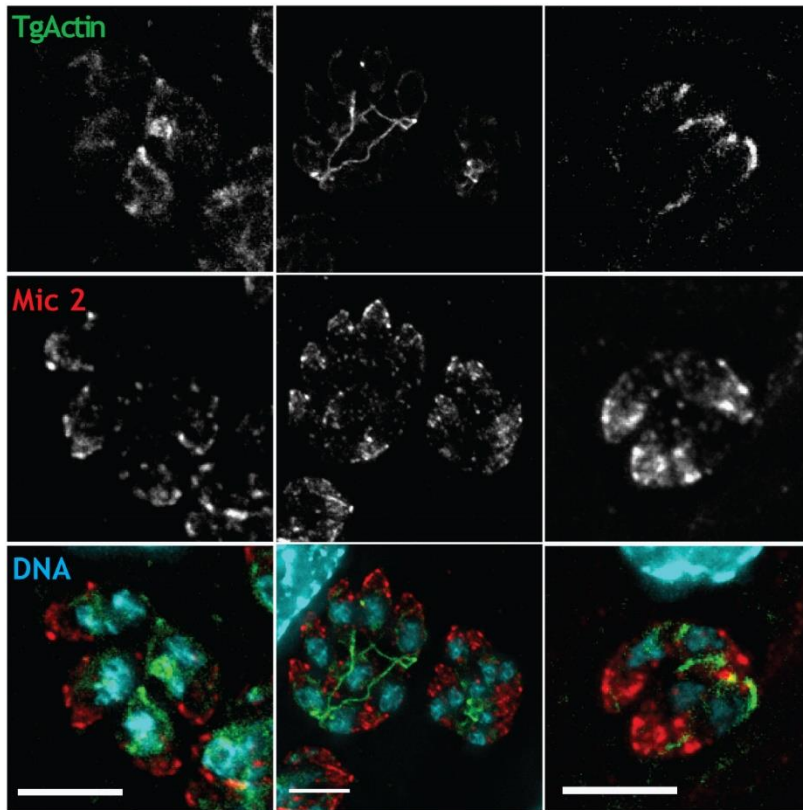
cyan, TgActin with the chromobody EmeraldFP in green and HA in red. **D.** Invasion rates of the *adf* chromobody EmeraldFP after tetracycline induction 1 hour following parasite invasion. The invasion rates of the parasite are reduced after tetracycline induction. 96 hours post-induction, the invasion rates are reduced to around 20%. **E.** Plaque assay comparing *adf* chromobody EmeraldFP parasites with and without ATc induction. **F.** Erratic gliding behaviour seen after 96 hours of tetracycline induction. The parasites appear to be unable to glide properly. **G.** Helical gliding behaviour appears to be reduced as the parasite cannot complete full helical gliding. **H.** Twirling gliding behaviour is presented with slower and weaker movement. This reduction in movement can be explained due to the accumulation of F-actin on both ends and the disappearance of usual F-actin dynamic behaviour. Stills generated from Movie S4. Scale bars represent 5 μm .

In *Toxoplasma gondii*, *adf* has been linked to actin severing (Mehta and Sibley, 2011), mimicking the same effect of Jasplakinolide after protein depletion. This effect is paired with an important decrease in egress, invasion and showing erratic motility (Mehta and Sibley, 2011). Since the chromobody-EmeraldFP provided important data regarding actin dynamics on the parasite, analysing how the dynamics would be affected by de-regulation of actin binding factors would allow the dissection of these dynamics in a more in-depth fashion. (Yadav *et al.*, 2011)

The *adf* tetracycline inducible mutant (*adf* cKD) (Mehta and Sibley, 2011) was chosen, as this line was previously characterised using actin antibodies. This line also possesses a Hemagglutinin marker (HA) fused to the ADF protein, which can be used to assess depletion. In order to obtain a line that expressed chromobody-EmeraldFP, the same chromobody vector previously described in 3.1 was transfected following standard protocols. 5 days after transfection, the parasite line was sorted by FACs as described above in 3.1 (Figure 3-6 A). After selecting a clonal line of *adf* cKD chromobody-EmeraldFP parasites, a western blot was done to assess the down-regulation potential of the line (Figure 3-7 B), along with immunofluorescent assays to show diminishment of the protein marker (Figure 3-7 C). In both cases, 96 hours after tetracycline induction, protein levels were significantly reduced in both IFAs and western blot analysis.

As previously stated, the *adf* cKD showed a decrease in invasion capability after protein depletion (Figure 3-6 D). This effect starts to become severe after 48 hours, where invasion is reduced by more than 50%. By 96 hours, invasion reaches levels of around 20% when compared to RH parasites, confirming previous results (Mehta and Sibley, 2011).

A RH CbEmeraldFP *adf* CbEmeraldFP *adf* KD CbEmeraldFP
- ATC +96h



B RH CbEmeraldFP *adf* CbEmeraldFP *adf* KD CbEmeraldFP
- ATC +96h

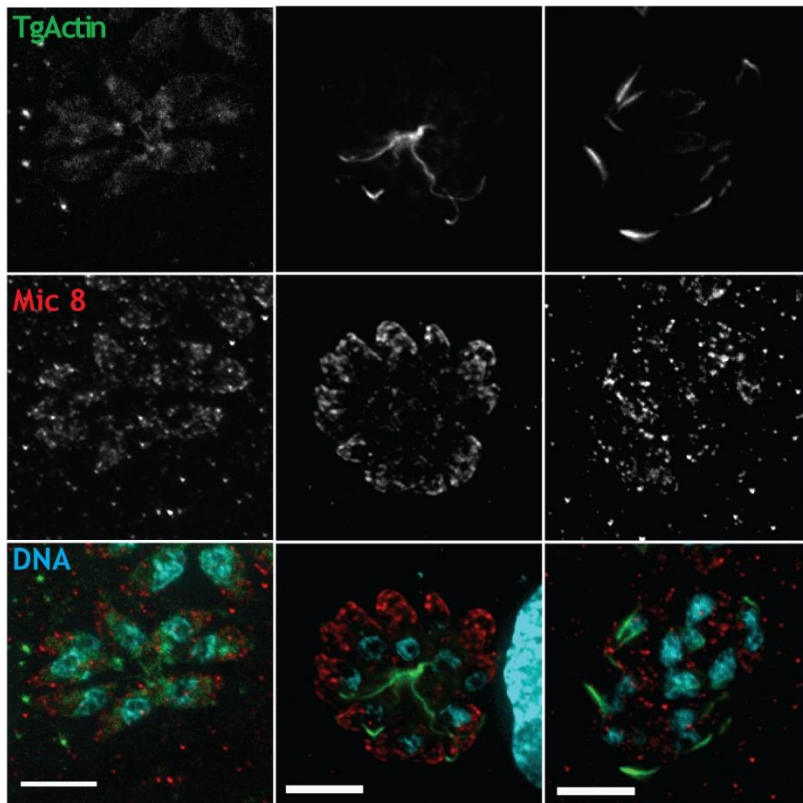


Figure 3-7 Location of different organelles after tetracycline induction of adf cKD parasites.

A. Mic2 location on adf cKD parasites. The usual location towards the apical end. After 96 hours of tetracycline induction, the location seems similar to non-induced parasites. **B.** Mic8 location in adf cKD parasites. The usual location of the micronemes towards the apical end. After 96 hours of tetracycline induction, the location seems to be disorganised in comparison to non-induced parasites. **C.** Rop1 location in adf cKD parasites. The usual location of the rhoptry proteins is around the centre to apical region. After 96 hours of tetracycline induction, the location seems similar to non-induced parasites. **D.** Rop2/4 location on adf cKD parasites. The usual location of the rhoptry proteins are around the centre to apical region. After 96 hours of tetracycline induction, the location seems similar to non-induced parasites. Actin was labelled by stable chromobody Emerald expression (green). Anti-mic2 antibodies labelled microneme 2 (red), Anti-mic8 antibodies labelled the microneme 8 (red), anti-ROP1 labelled rhoptries 1 (red), anti-ROP2/4 antibodies labelled the rhoptries 2/4 (red). Scale bars represent 5 μm .

Since invasion was impaired, analysis of F-actin dynamics in gliding parasites upon knockdown of ADF was done as downregulation of the glideosome components have previously shown defects in both gliding and invasion (Andenmatten *et al.*, 2013; Egarter *et al.*, 2014; Whitelaw *et al.*, 2017). After inducing the parasites for 96 hours, the parasites mobility capacity is severely impaired (Figure 3-6 E-G, Movie S4), confirming previous data (Mehta and Sibley, 2011). The hallmarks of gliding motility such as, helical motility is severely reduced (Figure 3-6 F, Movie S4), while circular motility is absent. Twirling motility is still present, albeit decreased. Another type of motility is present, termed erratic gliding. This type of gliding was previously described to be a type of serpentine-like unorganised motility (Mehta and Sibley, 2011)(Figure 3-6 E). Since the motility found in our study was consistent with Mehta and Sibley 2011, no further gliding motility quantification analysis was done.

In all examples, the previous highly dynamic F-actin behaviour was lost. Instead, accumulation of F-actin at the posterior and to a lesser extent the apical pole was observed. Adding to the previously stated hypothesis, the attachment and erratic gliding appeared to be weaker and more transient. If the parasite attachment points depended on F-actin dynamic turnover in both ends, stabilisation of F-actin would lead to improper attachment formation.

Furthermore, organelle changes upon ADF depletion were analysed (Figure 3-7 A-D; Table 3.1). Although the knockdown parasite grow similarly to un-induced parasite, the replication appears to be un-organised similarly as previous reports for the *act1* KO (Whitelaw *et al.*, 2017). Since the F-actin connections between daughter cells are likely disturbed, asynchronous replication was expected as

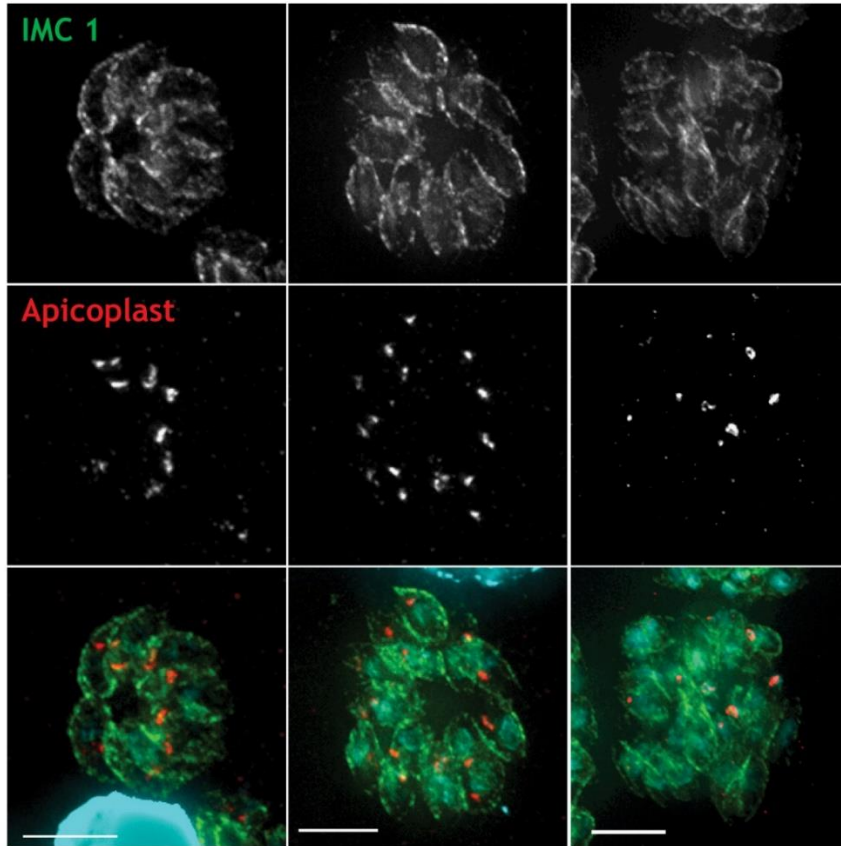
pointed out in past experiments where severance of these parasite-to-parasite connections lead to unorganised growth (Frénal, Jacot, *et al.*, 2017).

Similarly to previous results with the *act1* KO (Whitelaw *et al.*, 2017), no major differences for markers of the rhoptries were detected (Rop1 and Rop2/4) (Figure 3-7 A,C,D). Similar distribution of the micronemal protein MIC2 appeared normal. However, MIC8, another micronemal protein, previously shown to be localised in a different subset (Kremer *et al.*, 2013), appeared to be slightly mis-localised and found around the parasite with no strong apical accumulation upon induction (Figure 3-7 B).

Previous reports that the *act1* KO mutant presented an apicoplast inheritance defect linked ACT1 and apicoplast division (Andenmatten *et al.*, 2013; Whitelaw *et al.*, 2017). After *adf* cKD, the apicoplast showed an unusual phenotype coupled with organelle enlargement, hinting at a defect of apicoplast division and inheritance. This was more apparent since not every parasite had an apicoplast in the vacuole (Figure 3-8 A).

Since mitochondria division has been previously linked to actin in higher eukaryotes (Hatch, Gurel and Higgs, 2014; Hatch *et al.*, 2016), the phenotype during ADF depletion was also assessed (Figure 3-8 B). However, the mitochondria appeared normal after induction. This result not necessarily demonstrates that actin is not involved, but its function is at least not vital for correct mitochondria division (Melatti *et al.*, 2019).

A RH CbEmeraldFP *adf* CbEmeraldFP *adf* KD CbEmeraldFP
 - ATC +96h



B RH CbEmeraldFP *adf* CbEmeraldFP *adf* KD CbEmeraldFP
 - ATC +96h

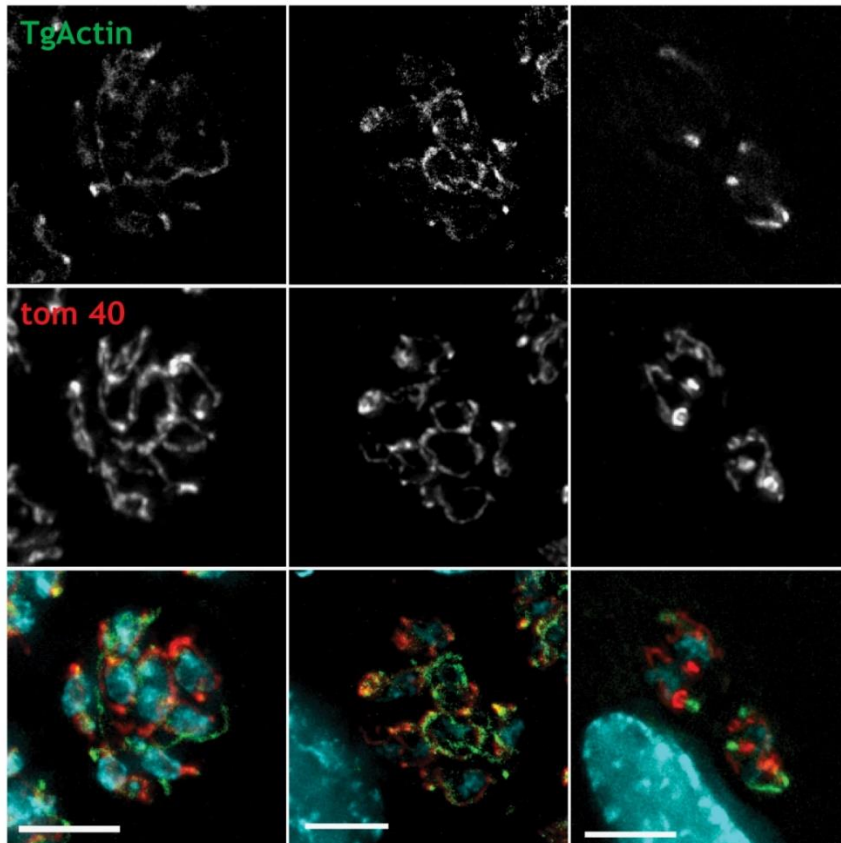


Figure 3-8 Location of both the apicoplast and mitochondria after tetracycline induction on *adf* cKD parasites.

A. The apicoplast inheritance is not affected with the chromobody EmeraldFP. Following 96 hours of tetracycline induction, the inheritance of the apicoplast is affected. This is showed with enlarged apicoplast that seems to not divide and the absence of apicoplast on several daughter cells. **B.** The mitochondria division does not appear to be affected by depletion of the *adf* protein. Anti-IMC1 antibodies labelled the Inner Membrane Complex 1 (green), Anti-HSP60 antibodies labelled the apicoplast (red); actin was labelled by stable chromobody Emerald expression (green), anti-tom40 antibodies labelled the mitochondria (red). Scale bars represent 5 μ m.

	<i>wt</i>	<i>Act1</i> KO	<i>Adf</i> KD
actin dynamics	normal	absent	abrogated
replication	synchronised	asynchronised	
apicoplast inheritance	normal	inheritance defect	
microneme organisation	normal		MIC8 slightly mis-localised
rhoptries organisation	normal		
mitochondria defect	no		

Table 3.1 Comparison between *Act1* KO and *Adf* KD

Table comparing wild type, *act1* KO and *adf* KD phenotypic analysis of replicating parasites.

3.6 Discussion

This chapter focused on characterisations done with tools previously developed in the Meissner lab. While the original chromobody-Halo tag construct is very useful, low signal to noise ratio made imaging difficult, especially with dimmer structures such as small filamentous actin structures. Here a new parasite line was generated in RH wild type parasites by transfecting with a vector carrying the chromobody fused to an EmeraldFP construct that can be selected using FACs (Figure 3-1 A-C)

and behaves as *wt* parasites regarding their lytic cycle (Figure 3-1 F-H). Using an enhanced GFP variant, the EmeraldFP proved to be invaluable in F-actin research in Apicomplexan parasites as the high signal-to-noise ratio made imaging easier, which allowed visualisation of dimmer F-actin structures than the ones originally described in Periz *et al.*, 2017.

Actin chromobodies uncovered for the first time in apicomplexan parasites, a highly dynamic behaviour of F-actin. This was first observed during parasite replication, where a flow of actin can be seen across the body of the parasite (Figure 3 A-E). It is noteworthy to mention, that within this highly dynamic flow of actin, three distinct points where F-actin appears to accumulate/polymerise can be observed. These points then appear to distribute actin to neighbouring locations. Based on these observations, originally three actin nucleation points were hypothesised to exist within the parasite, one in the central area (where FRM2 is located), one in the apical end (where FRM1 is located) and another one in the residual body (where FRM3 is located) (Stortz *et al.*, 2019; Tosetti *et al.*, 2019).

With these new tools at hand, characterisation of the dynamic behaviours of F-actin during invasion and motility was carried out, as they are powered by actin-dependent processes. The main hypothesis in the field is that the linear motor model uses a myosin class XIV protein to displace actin filaments in order to generate the force for movement. This acto-myosin complex would then allow the parasite to establish an even more complex structure along with adhesin proteins to achieve attachment and stability (Meissner, Schlüter and Soldati, 2002; Carruthers and Boothroyd, 2007; Sharma and Chitnis, 2013; Tardieux and Baum, 2016).

F-actin can be seen at positions where the parasite is likely to attach to the surface. However, further examination is required using more specialised microscopy such as RICM and TFM together with adhesion proteins tagged with fluorescent markers. F-actin dynamics during motility are even more interesting during twirling motion, as F-actin accumulation points appear to orbit around a sole point (Figure 3-4 D). This dynamic behaviour of F-actin might suggest the action of a myosin such as Myosin C, since it is localised at the posterior pole (Frénal *et al.*, 2014).

At this point it is unclear how the glideosome would be involved in the generation of force for Twirling motility, since the force must be exclusively generated at the posterior pole and the F-actin accumulations appear to be formed directly at the posterior end and not as suggested by the linear motor model (Tosetti *et al.*, 2019) by polymerisation of F-actin at the apical tip and translocation to the posterior pole.

4 F-actin in vivo dynamics analysis

Whereas capturing images or time-series for visual clues is highly important in biological systems, obtaining quantitative, statistically meaningful data from captured images can be challenging as Signal to noise ratio (SNR), speed, sample variability, focus and intensity can provide a wide range of variables that can render data useless or very difficult to process (Sailem, Cooper and Bakal, 2016). Even when data can be extracted from images, poor data quality can lead to wrong interpretations. Thus, generating high-quality data is a challenge that cannot be underestimated.

The process to analyse quantitative data obtained by microscopy uses mathematical models that often require information that is both laborious and time-consuming to extract. Analysing these data can also become biased. Hence, over the years researchers have tried to automatize this process with success (Saxton and Jacobson, 2002; Chenouard *et al.*, 2010; Chiba *et al.*, 2014; Mangeol, Prevo and Peterman, 2016).

Analysis such as single particle tracking can be useful to follow moving particles during time-lapse microscopy, allowing extraction of valued data comprising speed, intensity, direction and linearity of movement (Saxton and Jacobson, 2002; Jaqaman *et al.*, 2008). Moreover, advance methods can determine whether particles fuse together to form a single particle or separate to form 2 independent ones, allowing an extra layer of complexity to the analysis. However, for time-lapse images with high particle density, these methods are inefficient and inaccurate as keeping track of multiple particles that are moving in different directions is beyond the current limitations of the mathematical models they are based on (Mangeol, Prevo and Peterman, 2016).

For this end, analysis of moving particles by separation of the movement into its basic components (displacement and time), allows accurate extraction of data as it is simplified and easier to read. Kymographs use this principle allowing researchers to measure particle movement with high success, (Vallotton and Small, 2009; Chiba *et al.*, 2014; Mangeol, Prevo and Peterman, 2016). Actin flow measurement and actomyosin contractibility leading to the dynamic clustering of receptors (Yi *et al.*, 2012), actomyosin coordination in organelle arrangement

(Trivedi *et al.*, 2014) and, filopodial behaviour assessment by analysis of the growth cones (Kato *et al.*, 2002) are but a few examples of the use of kymograph in actin dynamics analysis.

Since the goal of our experimentation was to determine the speed, direction and intensity of the flow of actin molecules in *Toxoplasma gondii*, generation of stable, low SNR samples was desired to generate good data analysis. For this end, replicating parasites were selected as the parasites remain almost immobile, facilitating reliable flow measurements without any additional data manipulation.

4.1 F-actin live dynamics during replication; picking the best tool for image analysis on a very challenging subject

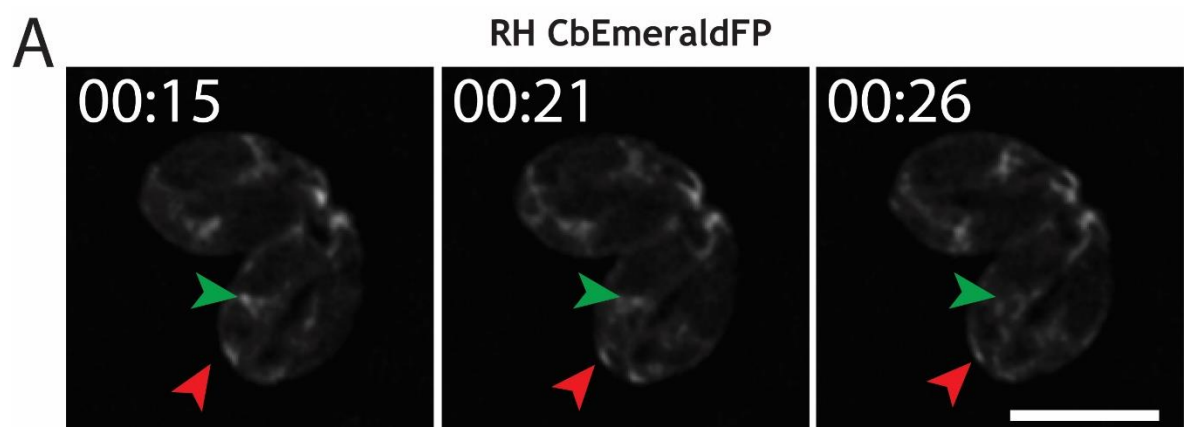
As mentioned in the previous chapter, actin dynamics were observed in replicating parasites with a tendency to accumulate at specific points, named *nucleation centres* as shown in RH parasites expressing chromobody EmeraldFP (red and green arrowheads, Figure 4-1 A, B, Movie S5). These nucleation centres appear to act as points where filamentous actin is nucleated, elongated and subsequently translocated to other areas. Upon depletion of ADF, it is believed the polymerisation critical concentration is shifted, as available monomeric actin is expected to be lowered causing a halt in new polymerisation (red and green arrowheads, Figure 4-1 C).

While analysis of time lapse movies by eye can already reveal information caused by depletion of actin binding proteins, such as ADF, other more delicate differences in F-actin dynamics might not be obvious in this way. Therefore, quantifiable methods are needed to obtain quantifiable data for F-actin dynamics and localisation.

Automatic tracking tools designed to follow individual particles are usually effective in ideal conditions, such as high SNR, fast framerate and good spatial resolution. In contrast, more challenging data is often misinterpreted, failing to provide accurate readings to reliably interpret the biology behind the phenomenon (Saxton and Jacobson, 2002; Jaqaman *et al.*, 2008).

Other tools such as kymographs, which are images that represent spatial position over time are generally more suited for the chaotic nature of dynamic actin-flows, as it can reliably dissect movement events of multiple particles at the same time. Yet, their time-consuming nature and difficult reproducibility are often a major obstacle for proper use (Chiba *et al.*, 2014). Besides these issues, kymograph comprise one of the most widespread tools used in the actin field, with more than dozens of articles citing different uses and methods (Snow *et al.*, 2004; Ou *et al.*, 2005; Chenouard *et al.*, 2010; Wei *et al.*, 2012; Horzum, Ozdil and Pesen-Okvur, 2014).

The mathematical and computational field is rapidly evolving, allowing the creation of better tools for data and image analysis. Tools such as optical flow analysis, which can accurately follow particle trajectories and trace their direction are available for large cells. Unfortunately, analysing particles by optical flow in small cells such as *Toxoplasma gondii* remains a challenge. Other tools more readily applicable to smaller organisms such as automatic tracking of kymographs have become more common, allowing faster analysis and reducing user input bias in the system and improving reproducibility (Mangeol, Prevo and Peterman, 2016). Therefore, one aim of this thesis was to optimise and adapt kymograph analysis for the use in apicomplexan parasites, such as *Toxoplasma gondii*.



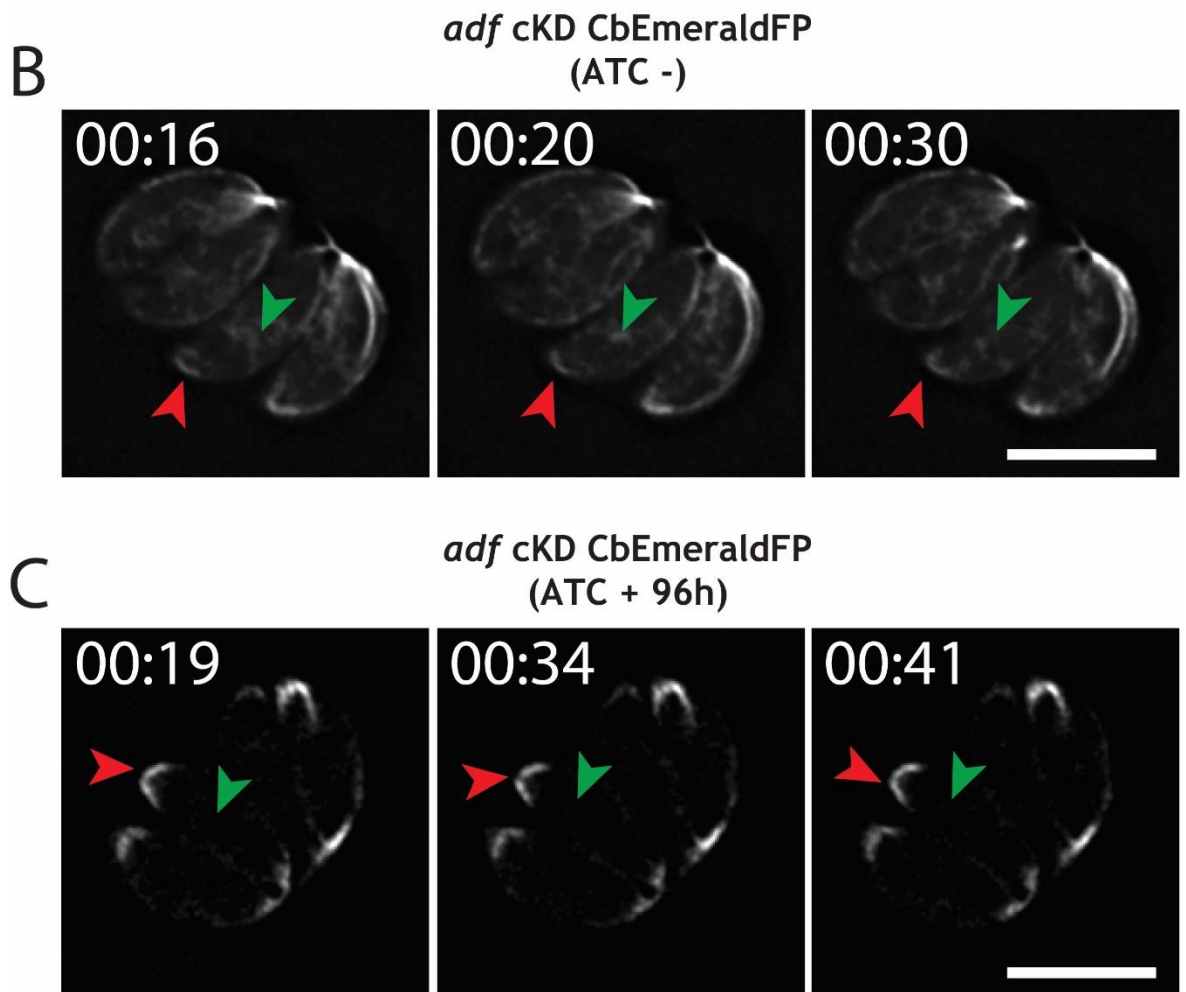


Figure 4-1 F-actin flow dynamics on *Toxoplasma gondii*.

A. RH chromobody Emerald replicating parasites in time-lapse images. An apical nucleation centre (red arrowhead) and a nucleation centre in the central area of the parasite (green arrowhead) can be seen. **B.** *adf* cKD chromobody Emerald replicating parasites in time-lapse images. An apical nucleation centre (red arrowhead) and a Golgi area nucleation centre (green arrowhead) can be seen. In this un-induced state, the F-actin dynamics appear to closely resemble the *wt* dynamics. **C.** *adf* cKD chromobody Emerald replicating parasites in time-lapse images. The apical nucleation centre (red arrowhead) and the Golgi area nucleation centre (green arrowhead) disappeared. In this induced state, the F-actin dynamics appear to come to a complete stop as no dynamics are apparent, with intense F-actin accumulation in both poles. Stills generated from Movie S5. Numbers indicate minutes:seconds; and Scale bars represent 5 μm .

4.2 Skeletonisation analysis of F-actin: applying image processing methods to analyse Apicomplexan actin.

Producing low quality data using microscopy can lead to poor analysis and incorrect interpretation of data. Issues such as low SNR due to high unspecific fluorescence in the sample can lead to incorrectly definitions of intensity profiles, masking our targeted signal or affecting subsequent processes such as deconvolution or mathematical image reconstruction. Even though processes such

as deconvolution are designed to reduce unspecific or out of focus signal, limitations in the algorithm often results in loss of data or even the creation of artefacts (Chomik *et al.*, 1997; Markham and Conchello, 2001).

Different conditions were tested to obtain optimal SNR and parasites kept in Fluorobrite medium instead of DMEM, presented better SNR as Fluorobrite is a non-fluorescent medium (Figure 4-2 A,B).

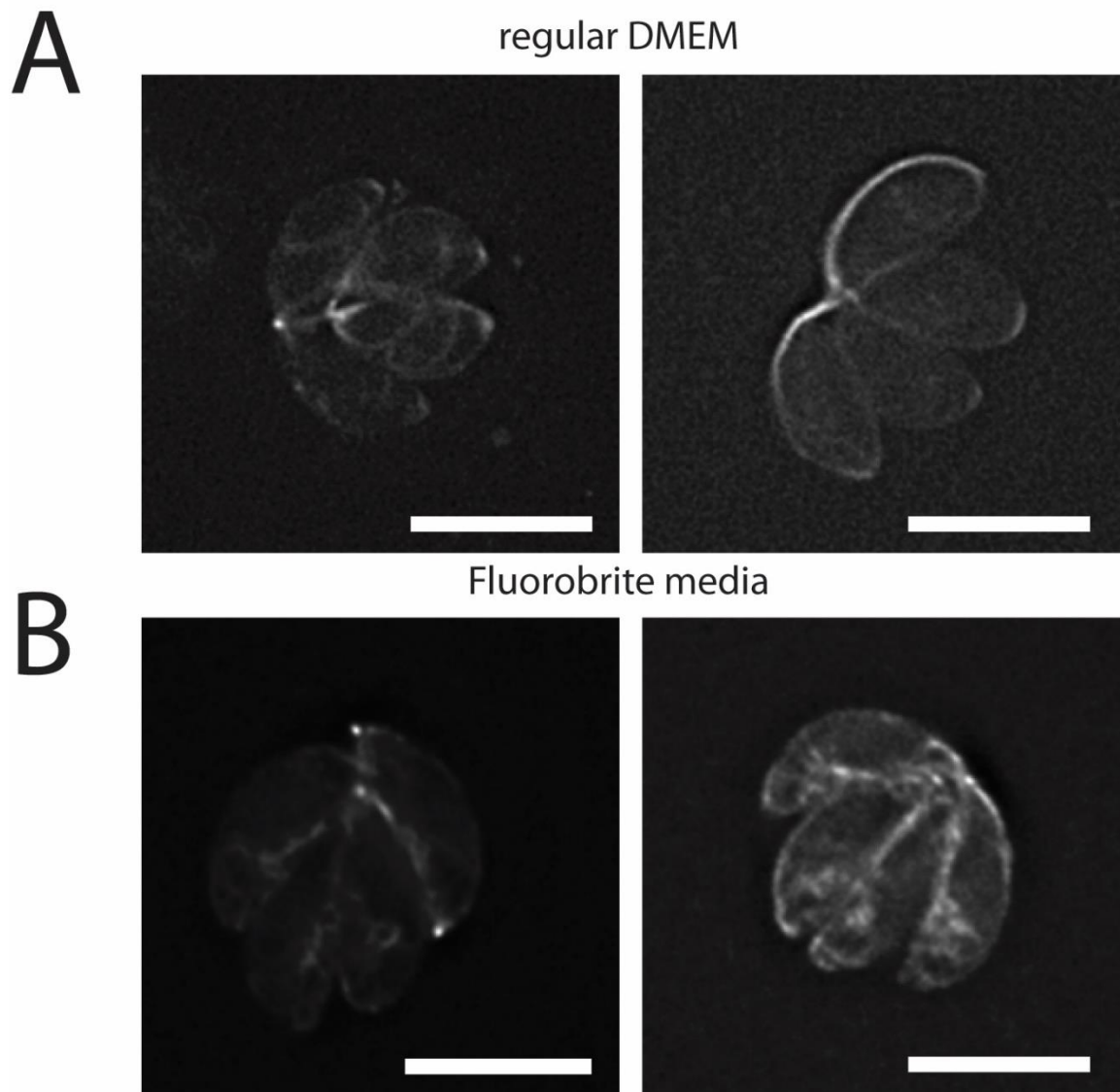


Figure 4-2 Optimisation of conditions for live and fixed microscopy to analyse F-actin localisation and dynamics in *T.gondii*

A. The commonly used DMEM media (supplemented with 10% FBS, 5% L-glutamine) can produce a high amount of SNR during acquisition due to autofluorescence. **B.** When a non-auto fluorescent medium is used (Fluorobrite supplemented with 10% FBS, 5% L-glutamine), the SNR is increased, allowing better data acquisition. Scale bars represent 5 μm .

Skeletonisation tools were originally designed for the automatic generation of models based on histological sections from high-resolution light microscopy data

(Arganda-Carreras *et al.*, 2010). These tools were found to be superior to previous techniques that relied on manual registration and/or rigid-body analysis of images (manually comparing two or more tissue image sections to align them), which were acquired using different platforms, methods and acquisition ending in complex reconstruction processes that were prone to artefacts and errors. Different methods that could be employed without manual registration were also used with limitations, particularly on the extension of a small reconstructed area (Arganda-Carreras *et al.*, 2010; Doube *et al.*, 2010).

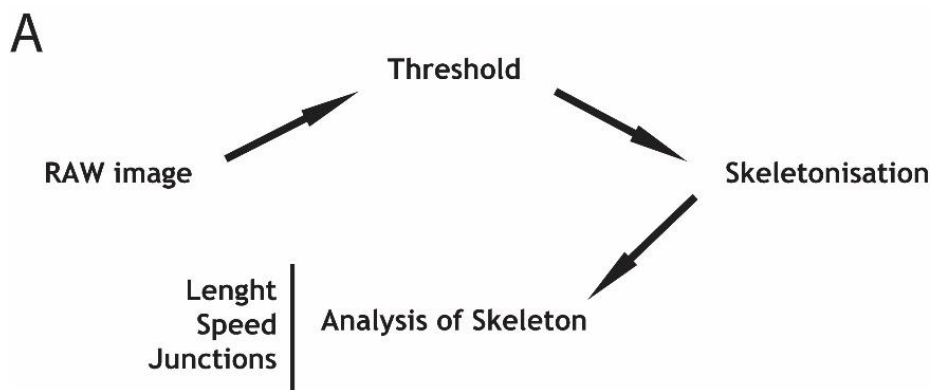


Figure 4-3 Workflow of a Skeletonisation procedure.

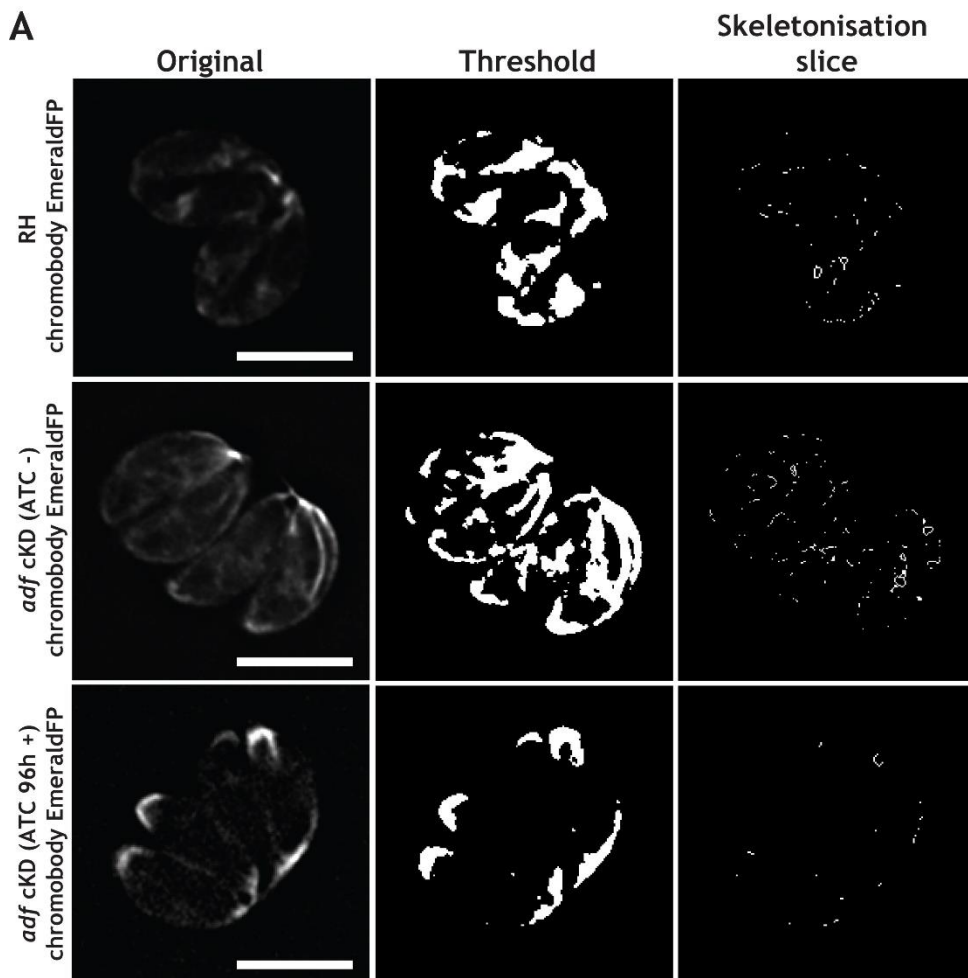
The workflow of Skeletonisation starts with the original image that is binarised via thresholding. This new image is then skeletonised and analysed.

With increasing computational power, better techniques were designed, requiring less or no-manual input along with high-resolution imaging resulting in reliable 3D reconstruction of whole tissues. This early method required high resolution in the z-axis where the samples were automatically segmented and registered; using the contours of the sample as a basis, the algorithm would then group images together to be reconstructed in 3D, creating realistic structures based on tissue samples (Arganda-Carreras *et al.*, 2010). This same method has been adapted to work in 2D, allowing analysis of 2D time-lapse imaging.

The skeletonisation method used in this study follows a similar principle applied to 2D samples (Figure 4-3, 4-4 A, Movie S5), where the sample is binarized by thresholding (Threshold, Figure 4-4 A). A skeletonisation algorithm is then employed which converts the thresholded signal into pixels, reducing the total width but not the length (Skeletonisation slice, Figure 4-4 A). Following the pixel conversion, the new skeletonised profile can be measured and characterised, generating a new colour-coded skeleton profile that labels the pixels (orange),

the branching points where two or more pixels emerge (purple) and the end points of branches (green) (Figure 4-4 B). The resulting process can be applied to time-lapse microscopy generating profiles useful to follow structural changes and displacement over time. This time-lapse profile can also be projected to define F-actin structures and their dynamics over the course of the movie (Skeletonisation collapse and colour-coded, Figure 4-4 B, Movie S5).

Since this process was developed to work in bone structures generated from thresholded images, limitations are present in the form of lack of width measurements (only length can be reliably measured) and the inability to measure intensity profiles of the signal. These disadvantages are counter-balanced with the ability to measure branch length, number of branches, junctions and branch ends. The resulting data hint that the filamentous actin flow occurs continuously inside the cytosol, as F-actin pools appeared to be formed inside the parasite cytosol in several examples.



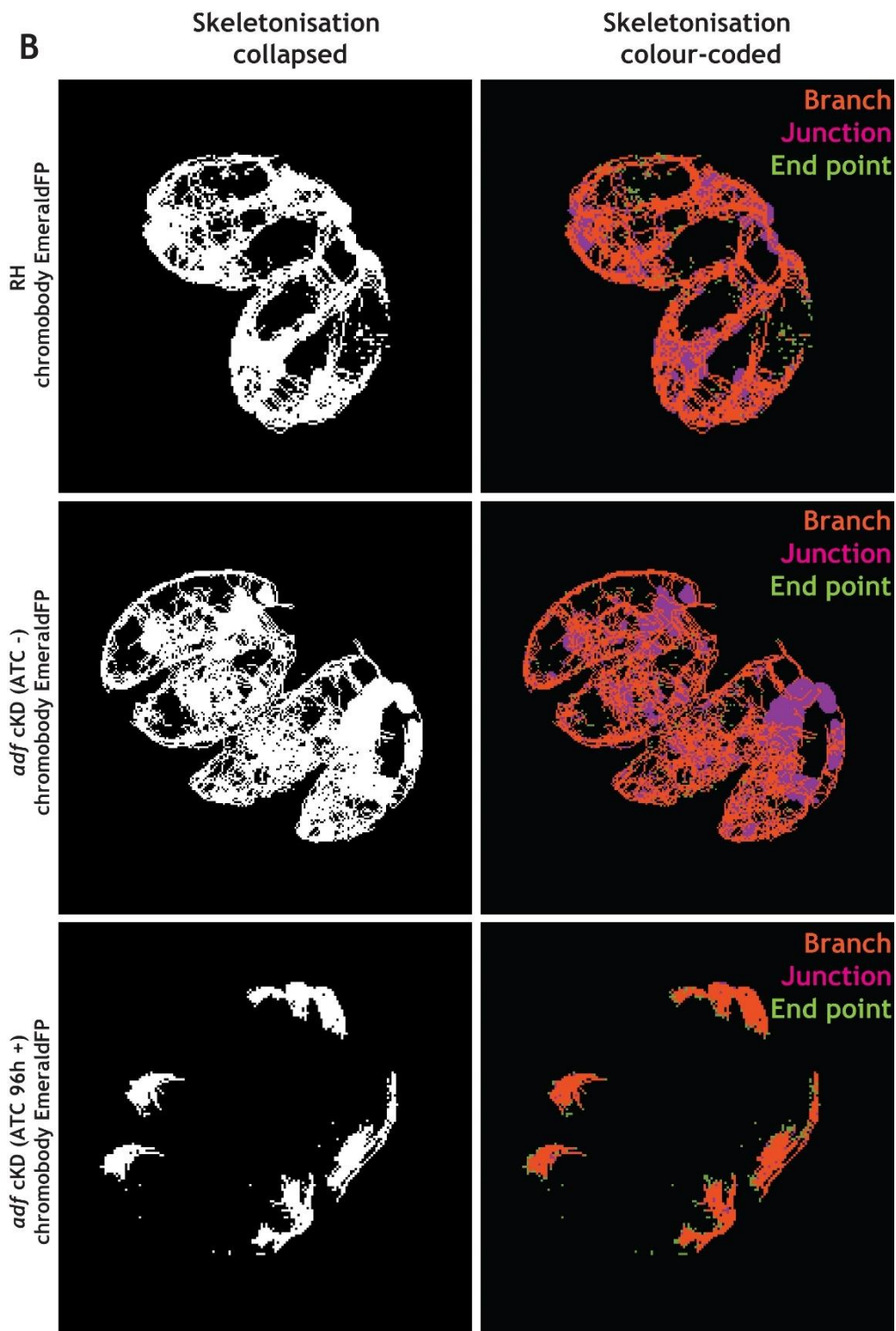


Figure 4-4 Skeletonisation process performed on time-lapse images of *Toxoplasma gondii*.
A. The images are transformed using a Threshold function with the Otsu algorithm to maintain consistency between samples. From these binary images, the Skeletonisation process is carried out. The resulting structures can then be used to follow locations where actin signal was found. **B.** The skeletonisation process can be complemented with the generation of a 3 colour-coded image depicting the branches (orange), purple (junctions) and the ends of branches (green). Stills generated from MovieS5. Scale bars represent 5 μ m.

4.3 F-actin and kymograph analysis: a classic tool for actin flow analysis

Kymographs are representations of time-lapse dynamic processes on a single image that allows the separation of speed into the minimal components (Space and time) (Chiba *et al.*, 2014). They are generated by plotting the intensity across all images of a stack along a given line (using the movie presented in Figure 4-4 A). Subsequent time points will stack at the bottom, allowing measurements of the process by following the displacement in the plot (Figure 4-5 A).

To start measuring the space-time plot, vectors are drawn to facilitate calculation of the components involved in the dynamic (yellow lines, Figure 4-5 A). These vectors are then measured in order to obtain the values of the vector (A_v or Anterograde vector and R_v or Retrograde vector slopes). The first step is to calculate the angles α_1 and α_2 , which are then used to calculate β_1 and β_2 (Figure 4-5 A). The vectors are then calculated by applying the tangent of the β angle of the respective vector, multiplied by the division of L and d (L and d are the pixel dimensions for both frame and space required to convert the system into units of time and length) (Smal *et al.*, 2010; Mukherjee *et al.*, 2011). It is also possible to obtain a vector comprised by the sum of the absolute values of both vectors that represent the total velocity of the dynamic, called PR_v (Polymerisation result) (Figure 4-5 A).

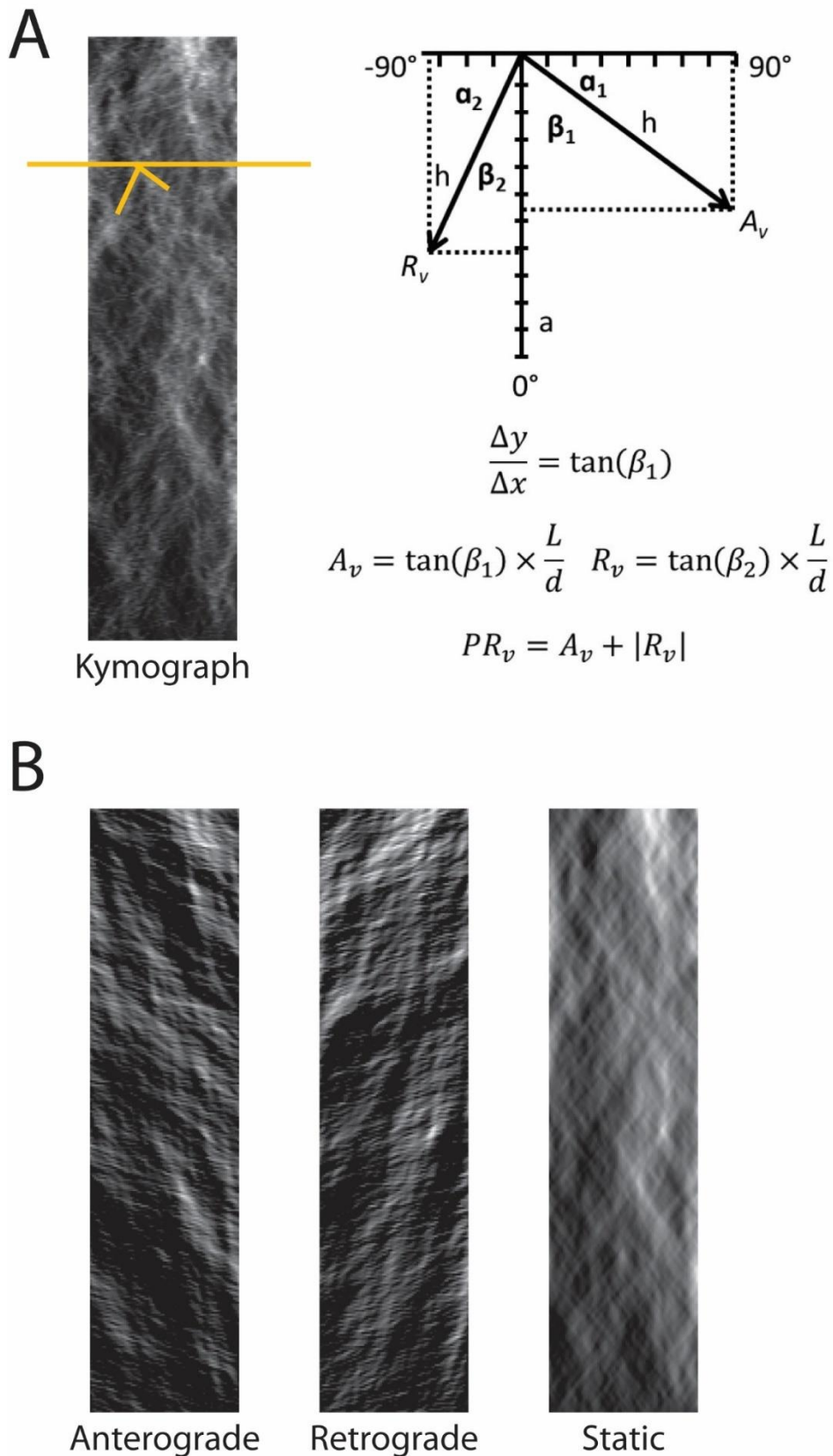


Figure 4-5 Kymograph analysis of flowing particles.

A. Kymograph generated from Figure 4-4 A, where vectors (yellow lines) are drawn to obtain the potential angles. This can be represented in a xy axis chart, where α and β angles are defined and calculated by dividing the difference between the x and y coordinates. The speed vectors (R_v and A_v) are then calculated with the tangent function of the β angle multiplied by the division of the pixel distance and time values. This can be further processed to obtain the joined vector speed by the sum of both vectors by adding the absolute values of each. **B.** By using a similar process in a

mathematical algorithm called Fourier filtering, it is possible to divide a kymograph into forward and backwards motion. A similar procedure can be done to obtain a filtered static signal image. The vector diagram was inspired by Actin dynamics in microtubule mutants (Baker and Straube, 2013).

A similar principle can be used to physically separate a kymograph into its directional components, meaning that it is possible to generate forward, backwards and even static kymographs of a single dynamic (Chenouard *et al.*, 2010). This function is usually achieved by Fourier filtering, which uses the Fourier transform of a kymograph. The Fourier transform decomposes an image into frequencies where the sine and cosine components are measured. These frequencies can then be attenuated or amplified, ending in an inverse-transformation of the resulting wave. This process can be used to delete and reconstruct signals, effectively masking one signal and amplifying the ones that are interesting (Figure 4-5 B) (Chow, Davey and Mulcahy, 1997; Jameson *et al.*, 2009; Hlavac, 2011; Gozalez and Woods, 2013; Dougherty, 2018).

By using automatic processes to measure and calculate these vectors, a semi-automatic process can be employed to quickly obtain values of dynamic movement (Figure 4-6). After drawing a ROI line (yellow dotted line, Figure 4-6 A), kymographs were obtained and were immediately Fourier-filtered to obtain individual kymographs for each direction of movement. A few ROI lines were then traced following the flow movement patterns of actin, allowing speed calculation (red and green lines, Figure 4-6 B). The measured tracks showed higher speeds in individual tracks for anterograde movement (going from the parasite RB to the apical end) (Figure 4-6 C). However, more events were found in the retrograde flow (Figure 4-6 D), with an average slower speed. By adding both absolute values of anterograde and retrograde flows, a total polymerisation rate between 0.75 to 1 $\mu\text{m/s}$ was obtained. It is important to mention that these values are not absolute and only show relative differences between individual conditions (such as conditional mutants or drug treated parasites), when compared to WT parasites. In order to obtain more meaningful values, movies need to be standardised with *in vitro* polymerisation assays. However, for the objectives of this study, where mutants and F-actin dynamics should be compared and relative differences determined, it was decided that this tool is sufficient.

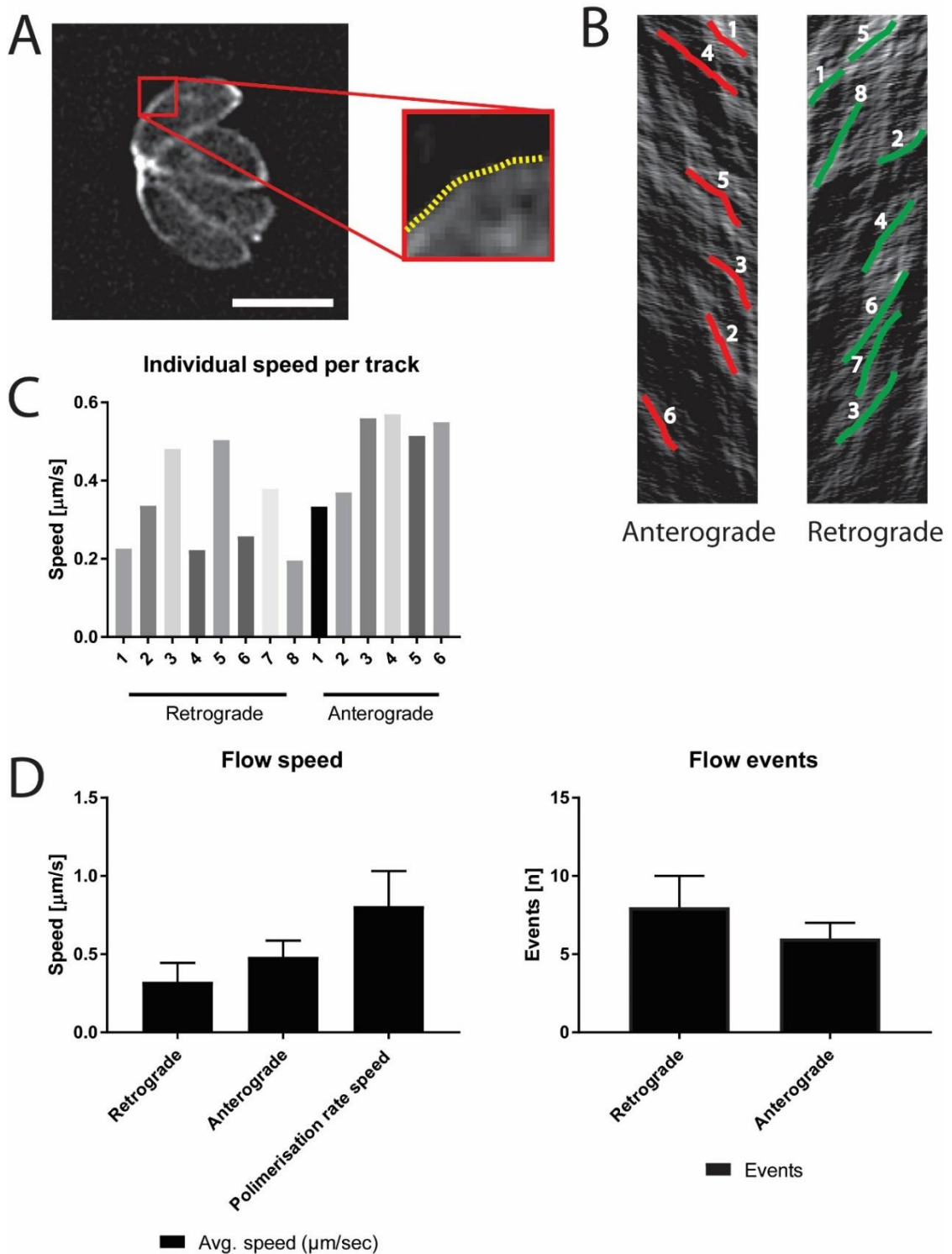


Figure 4-6 Semi-automatic kymograph analysis of F-actin flow dynamics.

A. A kymograph is performed by tracing a path (yellow dotted line) along the periphery of the parasite. **B.** The resulting kymograph (also shown in Figure 4-5 B) is then Fourier filtered into both anterograde and retrograde kymographs. ROI tracks were then traced along the flow of particles to measure the speed. The red ROIs represent forward, or anterograde movement and the green ROIs represent backwards or retrograde movement. **C.** These ROIs are then processed in the open software Icy, where motion data is obtained for each ROI track. In the case of the retrograde flow, more events are recorded with a slightly lower speed, while the anterograde flow appears to have less events with a slightly increase in speed. **D.** The individual tracks can then be averaged, and the data compared between flows. The flow appears to be bi-directional with a higher load in the retrograde flow, meaning that more F-actin particles are flowing from the apical end to the posterior end. Scale bars represent 5 µm.

4.4 Limiting user input bias in flow analysis: KymographDirect and KymographClear

One of the major issues faced when working with kymograph is the reliability of the measurements. Since this is a user-driven process, it is prone to bias and lack of reproducibility (Doggett and Breslin, 2011; Chiba *et al.*, 2014; Mangeol, Prevo and Peterman, 2016). Efforts to automate these processes are few, as most groups using kymograph tools often create ImageJ plugins or macros limited to their conditions.

KymographClear is an ImageJ macro toolset designed to extract kymograph based on particular ROI from image sequences. Since reducing user input bias was desired, the method described in Mangeol, Prevo and Peterman, 2016a was used. For a more in-depth procedure, see the materials and methods section 2.14.2 (Chapter 2).

The data processing workflow (Figure 4-7 A) starts with the generation of a max-intensity projected image from time-lapse imaging, which will be used to trace an ROI wished to be analysed as a kymograph in KymographClear (red and green spotted line, Figure 4-7 B). A kymograph will be generated presenting all the trajectories in the time-lapse (Kymograph resulting from both red and green ROIs, Figure 4-7 B). Although this process tries to limit user input bias, it is not excluded entirely, as user input is necessary for tracing the ROI and subsequent analysis in KymographDirect. KymographDirect will then be used to load the resulting data, and the automatic traces the software creates, are then adjusted by the user to closely resemble the kymograph (software interface where traces are automatically generated by KymographDirect, Figure 4-7 B). This data is then exported to workbooks for posterior analysis and statistics (Figure 4-7 B). This analysis can be used to assess time-average plots to discriminate the location of the signal along the track, which is clearly shown to be consistent in the peripheral area of the parasite, but not in the cytoplasmic region, as a distinct peak is depicted that belongs to the potential nucleation centre in the central region of the parasite (Figure 4-7 B).

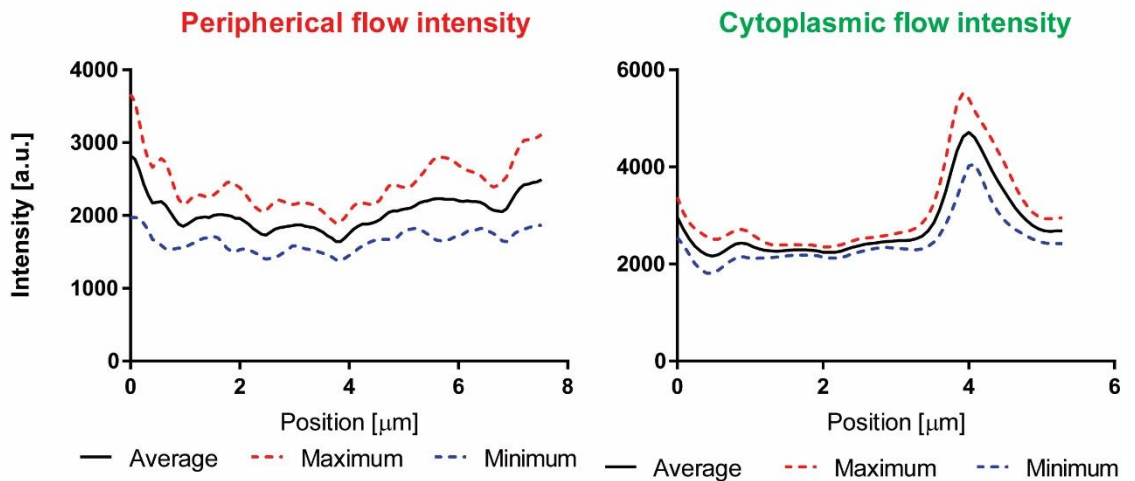
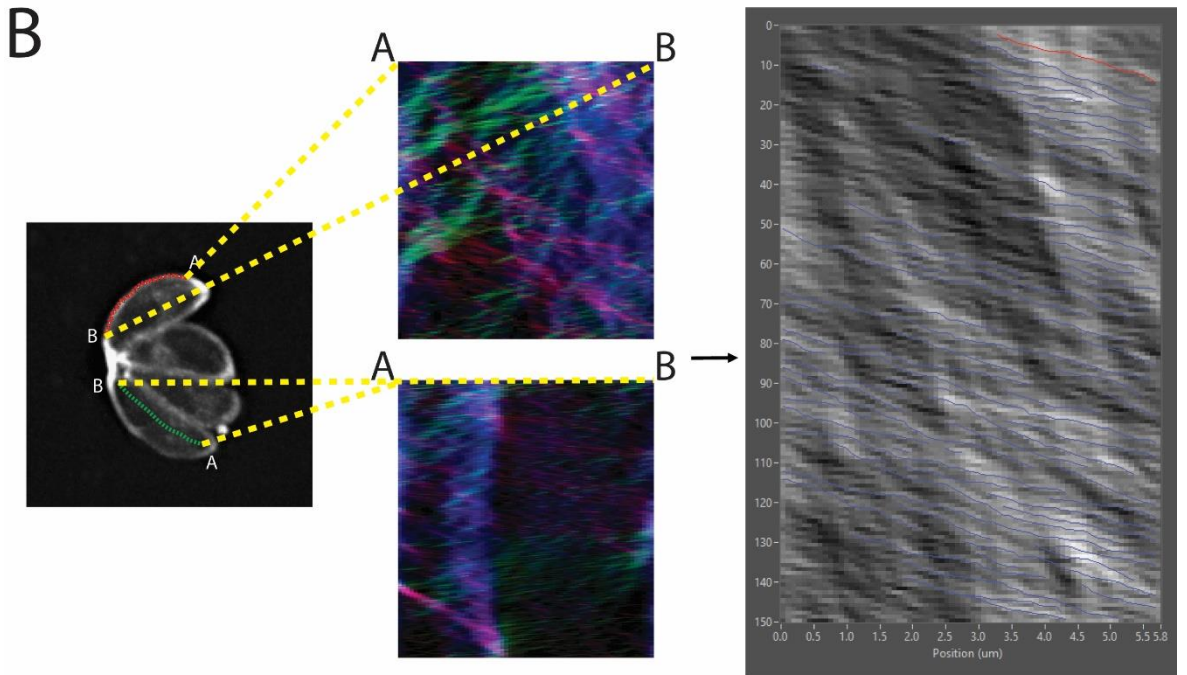
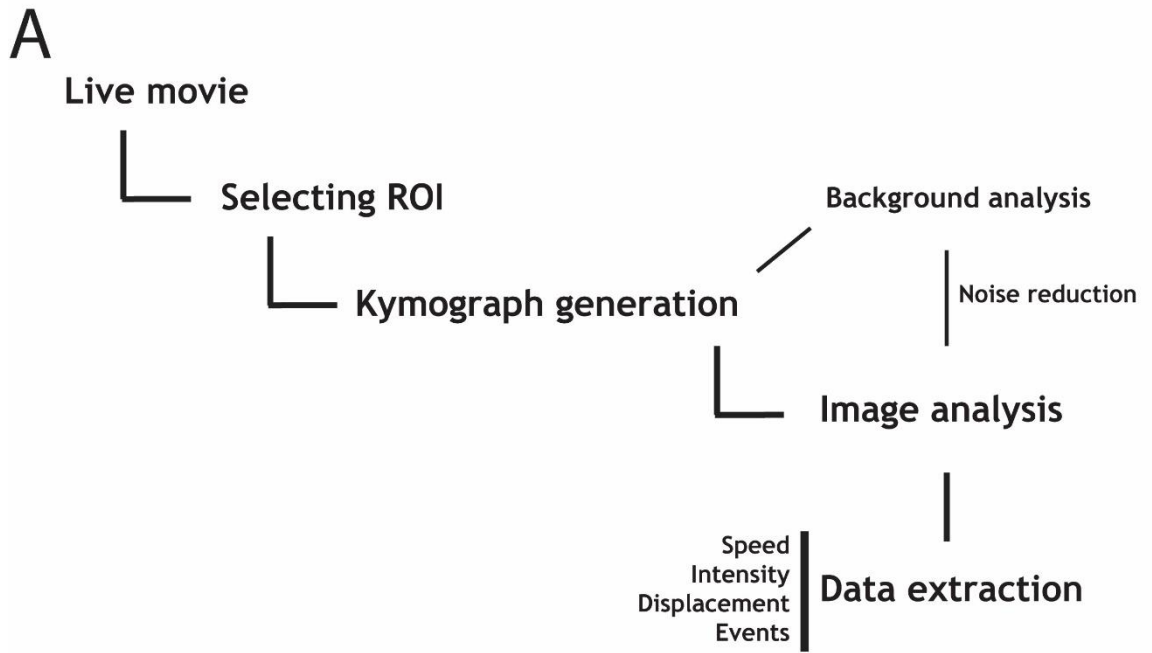


Figure 4-7 Example of an automatic kymograph analysis using KymographClear and KymographDirect

A, B. Workflow for KymographClear and KymographDirect analysis. An ROI track is traced (red dotted line for peripheral and green dotted line for cytoplasmic analysis), and a kymograph is generated using KymographClear. In the same process, background signal can also be recorded for posterior use. KymographDirect can then be used to process the gathered data (automatic tracing of ROI tracks) and then exported to text files or workbooks. The resulting data can then be plotted as the time-average intensity plots shown in the example, where the cytoplasmic signal appears to fluctuate through the periphery, while the cytoplasmic condition presents a very distinct peak where the central area nucleation centre lies.

4.5 F-actin flow directionality on wild type parasites

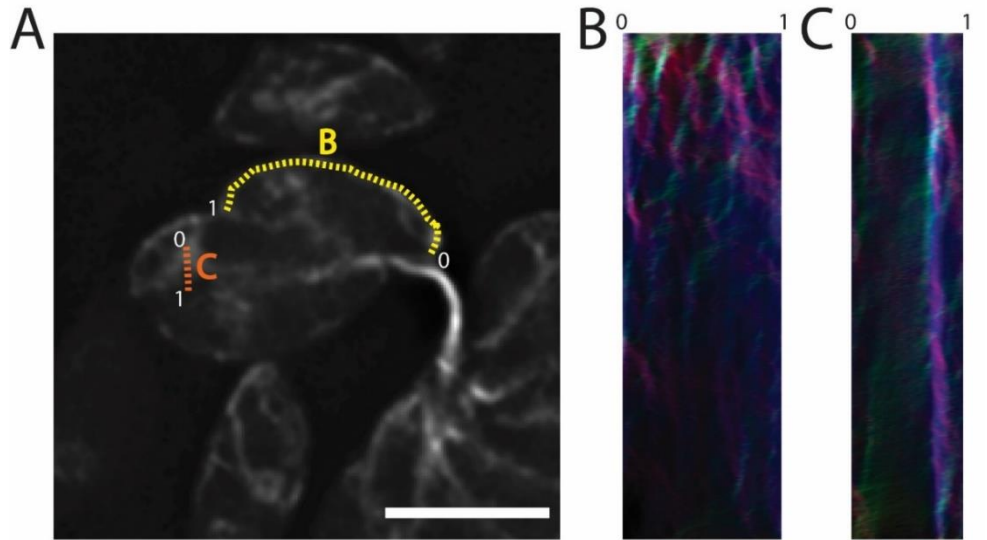
Analysing the flux of F-actin in replicating parasites is required to address the directionality of the flow. As F-actin dynamics occur through the parasites body, two areas of interest are present for this study: the actin flux from the central region of the parasite to the periphery and the actin flux at the periphery of the parasite (red ROI for the periphery and green ROI for the central region flux, Figure 4-8 A).

The two ROI generated very distinct kymographs (Figure 4-8 B,C), with defined flux going in two directions, as previously shown in Figure 4-5 B. Both kymographs are then analysed in KymographDirect until the traces used for analysis closely resemble the kymograph in question.

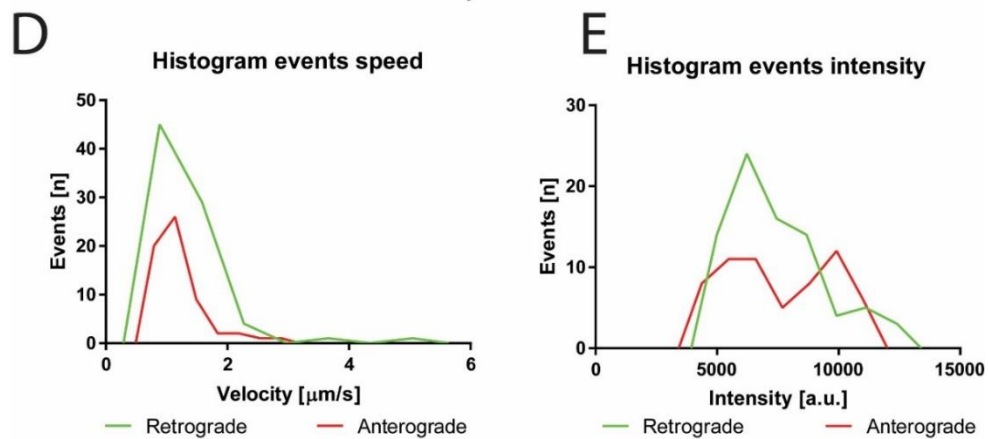
The peripheral analysis shows intense bi-directional flow of F-actin, with many events going into both directions (Figure 4-8 C). However, the majority of the events in terms of speed and intensity correspond to the retrograde flow (Figure 4-8 C, D, E). This means that a higher F-actin flux moves from the apical end to the basal end in a retrograde fashion independently of parasite gliding motility. Since this event occurs in intracellular parasites, it supports the idea that F-actin dynamics can play a role in vesicular transport as suggested in previous works (Heaslip, Nelson and Warshaw, 2016; Periz *et al.*, 2017).

Upon analysing the central region flow, intense F-actin flow was observed, going from the nucleation centre in the central region to the periphery (Figure 4-8 C, F, G). This is apparent when comparing the retrograde with the anterograde flow speed and intensity, as higher numbers of events that are both faster and more intense (Figure 4-8 F, G) can be observed for the flow going from the nucleation

centre in the central region to the periphery. These data support our observations that the F-actin flow predominantly follows a retrograde flow, with the nucleation centre in the central region supplying most of the flow for this process in the periphery.



Peripheral flow



Cytoplasmic flow

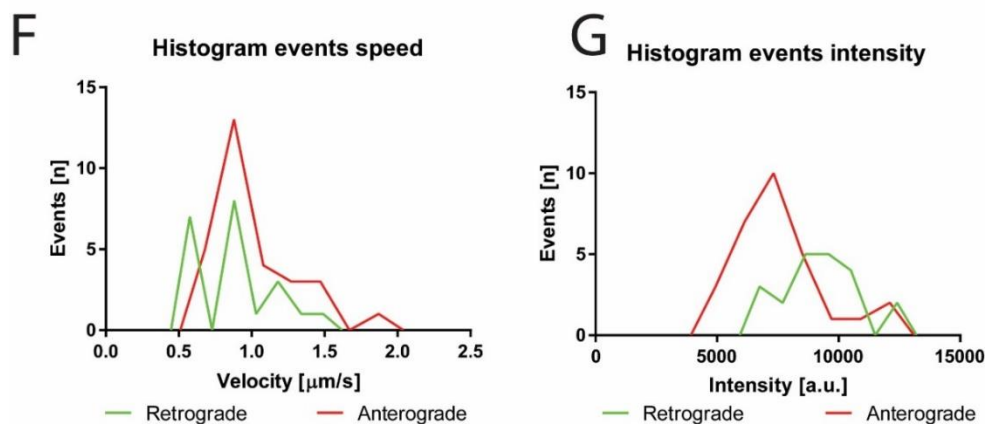


Figure 4-8 Automatic kymograph analysis using KymographClear and KymographDirect.

A. An ROI track is traced for cytoplasmic flow (red dotted line) or peripheral flow (green dotted line). **B.** The resulting kymograph of the peripheral ROI track. **C.** The resulting kymograph of the cytoplasmic ROI track. **D.** In the peripheral track, a bi-direction flow was encountered, stronger retrograde flow in terms of events and speed was found. **E.** In the peripheral track, stronger retrograde flow in terms of events and intensity was found. The peripheral actin flow appears to flow in both directions, yet it is predominantly retrograde. **F, G.** The cytoplasmic flow presents stronger anterograde flow, meaning it goes from the nucleation centre to the periphery. This was true in terms of number of events, speed and intensity suggesting the nucleation centre is feeding the F-actin peripheral flow. Scale bars represent 5 μm .

4.6 Actin Depolymerisation Factor and Actin modulating drugs alters the F-actin flow in *Toxoplasma gondii*

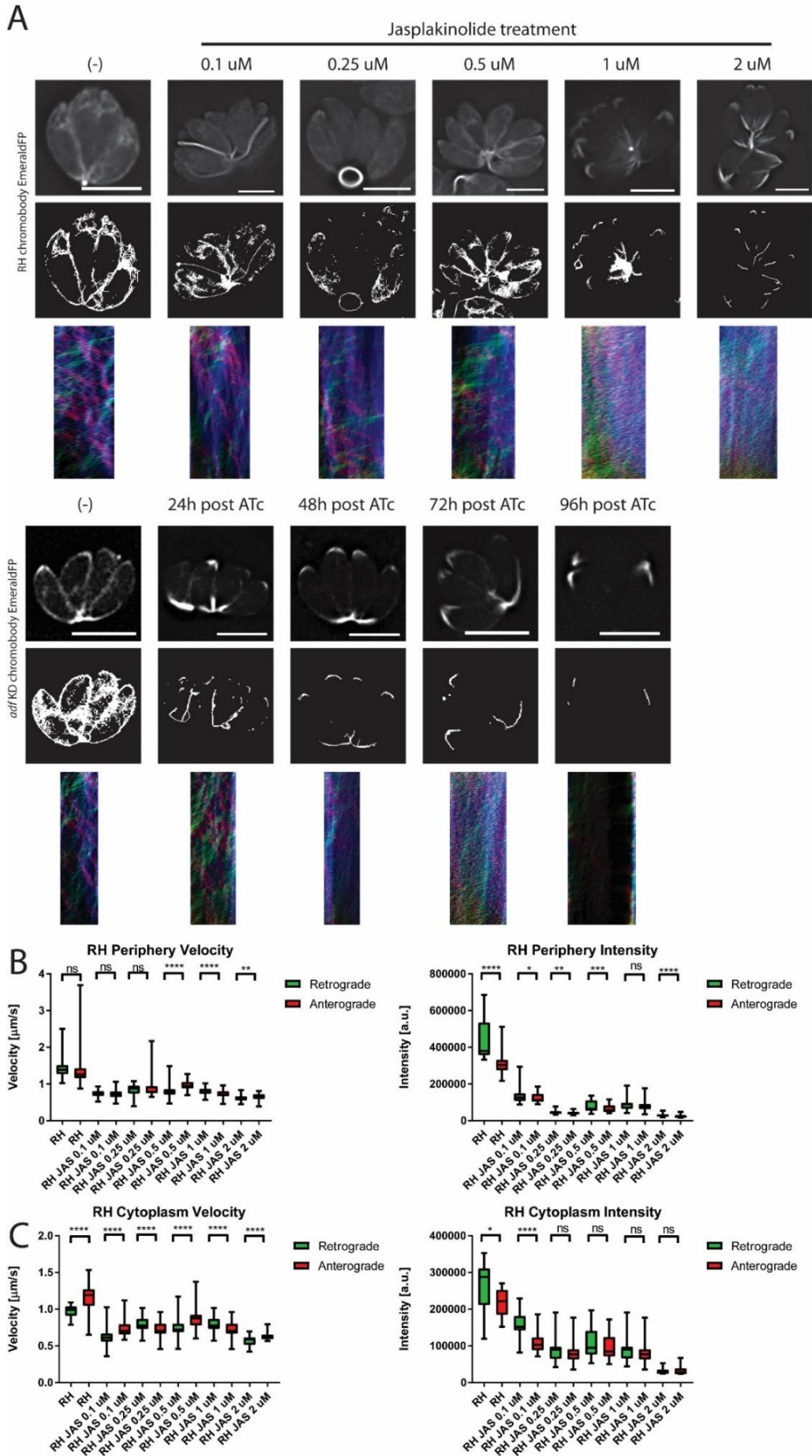
Next, we wished to assess the applicability of the adapted algorithms to the effects of actin stabilisation drugs, such as Jasplakinolide (JAS) as this drug has been used for several years in the actin field and its effect is well documented in *Toxoplasma gondii* (Wetzel *et al.*, 2003; Mehta and Sibley, 2011). Jasplakinolide is a toxin isolated from *Jaspis johnstoni* capable of generating new actin binding sites, decreasing the critical concentration required for nucleation from tetramer to trimers (Bubb *et al.*, 2002; Gavin and Holzinger, 2003). This characteristic leads to an increase in actin polymerisation that eventually results in filament stabilisation. In *T.gondii*, the effects mimics results observed in the ADF depleted mutant with accumulation of F-actin in both the apical and basal end. This phenotype is paired with conoid extension and erratic motility (Wetzel *et al.*, 2003; Mehta and Sibley, 2011).

A change in F-actin structure and polymerisation by actin modulation drugs is expected based on previous reports (Periz *et al.*, 2017; Whitelaw *et al.*, 2017). Upon the addition of 1 μM of JAS, the parasites presented a reorganisation of F-actin akin to what was shown in previous studies (Mehta and Sibley, 2011; Yadav *et al.*, 2011). This reorganisation is rapid, triggering translocation of actin filaments to both ends of the parasite (Figure 4-9 A, Movie S6). The extension of the conoid as previously described (Poupel and Tardieux, 1999; Shaw and Tilney, 1999) was also encountered, presenting a particular F-actin-rich tip. Kymograph obtained from these parasites depict a striking change in the actin flow dynamics. With the use of actin depolymerisation drugs or transcription disruption, such as

increase of JAS concentrations or ADF depletion, particle trajectories are replaced by static and a signal void in the case of the *adf* KD 96 hours post induction (Figure 4-9 A, Movie S7).

During the JAS drug concentration assay of *wt* parasites, the flux of actin consistently changed with increasing concentrations of the drug (Figure 4-9 B, C). Analysis in the peripheral and cytoplasmic flow of F-actin shows a drastic effect upon low concentrations of JAS, as 0.1 μM of the drug is enough to cause a severe change in both speed and intensity of the actin flow. Additionally, this result is paired with actin flow change, where the rates appear to even out in both speed and intensity. In both cases, a concentration as low as 0.1 μM of JAS appears to lead to severe changes in the actin flow, with higher concentration only having a small effect until reaching 2 μM . It is important to note that even small concentrations of JAS are enough to affect the flow, causing complete abrogation.

Since the *adf* KD chromobody EmeraldFP strain of *Toxoplasma gondii* presented a similar phenotype to JAS, flow analysis was carried out in a time course after ATc treatment. Upon treatment with ATc, F-actin dynamics changed due to the diminishing ADF concentration/presence, even in the first 24 hours where the intensity of both cytoplasmic and peripheral actin flow was severely affected (Figure 4-9 D, E). The speed was also affected to a lesser degree, showing a modest decrease during the first 24 hours. By 48 hours, the actin flow is severely disrupted in both speed and intensity as the parasites visually resemble the already mentioned phenotype of actin accumulation on both ends.



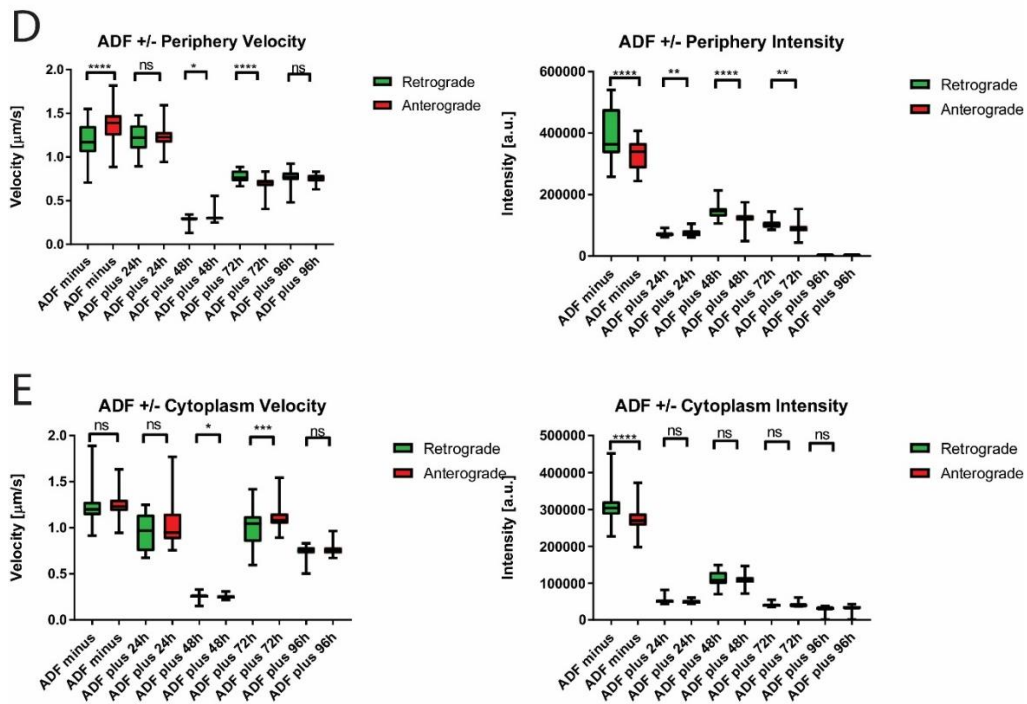


Figure 4-9 Flow analysis of RH chromobody EmeraldFP parasites treated with different Jasplakinolide concentrations and *adf* KD time course after ATc treatment.

A. Parasites treated with JAS presented a changed phenotype at a concentration as low as 0.1 μM . The flow appears to be more affected starting from 0.25 μM and from 1 μM and on, the flow appears to be completely abrogated. In the case of *adf* KD, following ATc treatment, stronger actin accumulation in the form of thicker nanotubular filaments can be observed as soon as 24 hours after ATc treatment. By 72 hours, the flow appears to completely stop in a similar fashion as JAS treatment. **B, C.** Peripheral and cytoplasmic actin flow analysis of JAS treated parasites. Following what we can observe by eye, treatment with JAS as little as 0.1 μM is enough to induce a major decrease in the actin flow. This effect becomes critical when using 1 μM JAS as the flow appears to be completely gone. **D, E.** In the case of the *adf* KD ATc time course treatment, both the peripheral and cytoplasmic actin flow dynamics appear to be reduced in intensity starting in the first 24 hours following ATc treatment, by 72 hours the effect appears to reach a maximum point without further decrease after 96 hours. The speed appears to be affected starting from 48 hours post ATc treatment. The speed reaches the minimum speed by 96 hours where it appears to present a complete abrogation of the F-actin flow dynamics. Stills generated from MovieS6 and 7. Scale bar represents 5 μm .

4.7 F-actin flow analysis on extracellular parasites

Analysing dynamic F-actin flow in replicating parasites is relatively easy. In contrast analysis in extracellular parasites is complicated due to motility of parasites, making kymograph analysis difficult and less reliable.

For this reason, analysis of extracellular parasites in a resting state were done by both skeletonisation and kymographs (Figure 4-10, Movie S8). Extracellular

parasites in a resting state appear to behave in a similar fashion as intracellular parasites in regard to the actin dynamics (Figure 4-10 A). Two distinct nucleation centres can be seen in the apical end (yellow arrowhead) and the central region (red arrowhead) in both *wt* and *myoA* KO. In the case of *adf* KD parasites, most of the actin dynamic is disrupted, with intense F-actin accumulation on both ends (Figure 4-10 A). Skeleton analysis confirmed that all actin structures form a continuous network across the parasite, showing the same areas of F-actin accumulation at the apical end (yellow arrowhead) and the central region (red arrowhead) (Figure 4-10 A). This was further shown with time-averaged intensity plots using kymographs to assess the dynamics of actin flow (Figure 4-10 B). Two distinct nucleation centre intensity peaks can be identified in the apical end (0 μm) and the central region (around 2 μm) in both *wt* and *myoA* KO. In the case of *adf* KD parasites, strong F-actin intensity peaks are observed on both ends (0 and 7 μm).

Following these results, the effect of compounds known to stimulate microneme secretion were tested (Figure 4-11, Movie S9). Calcium ionophore A23187 is a known trigger for egress in *Toxoplasma gondii*, where it can trigger egress as little as 2 hours after invasion (McCoy *et al.*, 2012), this effect also activates parasite gliding motility in a *TgCDPK3* dependent manner due to microneme secretion (Garrison *et al.*, 2012; McCoy *et al.*, 2012). 5-Benzyl-3-isopropyl-1H-pyrazolo[4,3-d]pyrimidin-7(6H)-one shortened to BIPPO (Howard *et al.*, 2015), is a drug capable of inhibiting 3',5'-cyclic nucleotide phosphodiesterases (PDEs) that are responsible for the breakdown of cyclic nucleotides such as cAMP and cGMP (Howard *et al.*, 2015). This mechanism is believed to be responsible in the activation of microneme secretion and egress by modulating the signal pathway of PKG-dependant processes.

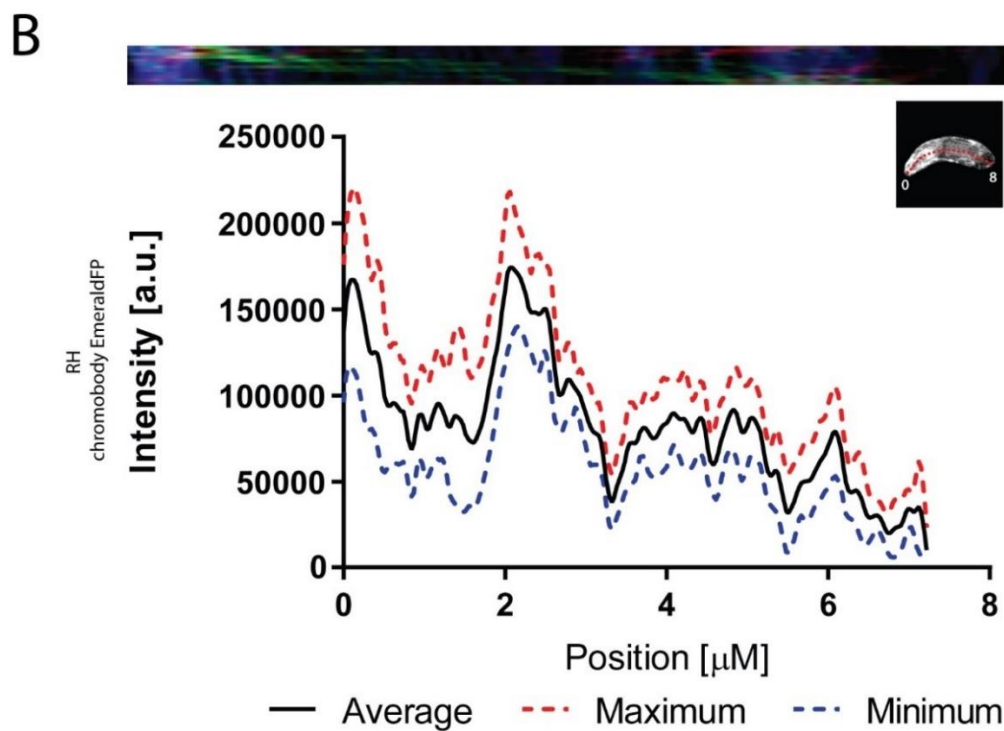
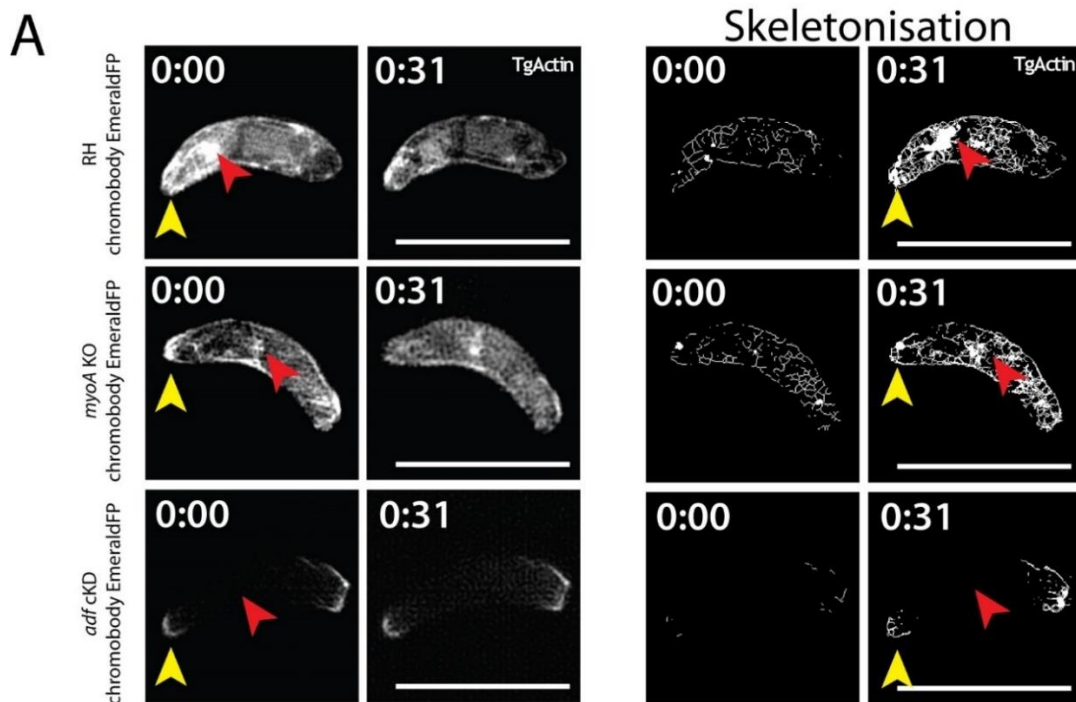
Skeletonisation analysis was done upon addition of A23187 or BIPPO, where actin relocalisation to the anterior and posterior end was observed in RH wild type parasites and the DMSO control. Curiously, A23187 seemed to favour actin accumulation at the apical tip, while BIPPO favoured accumulation at the basal end (Figure 4-11 A, B). Parasites treated with cytochalasin D, presented remarkable cytosolic signal before and after A23187 or BIPPO treatment. These results were expected, as cytochalasin D is capable of binding barbed (+) ends of

filamentous actin in a similar effect to capping, preventing further polymerisation (Figure 4-11 A) (Scherlach *et al.*, 2010). No further changes upon treatment with A23187 or BIPPO were observed in the case of the *adfKD*. It is worth mentioning that *adfKD* presented prior accumulation in both ends of the parasite due to the depletion of ADF, leading to stabilisation of actin (Figure 4-11 A, B). The *myoAKO*, presented actin flow dynamics akin to wild type parasites before treatment. However, upon adding either A23187 or BIPPO, relocalisation of actin occurred. This relocalisation manifested as accumulation in the apical end along with the initial 1/3 of the parasite's periphery (Figure 4-11 A, B).

Since both A23187 and BIPPO presented effects on actin relocalisation, parasites were counted following treatment with these compounds (Figure 4-11 C). Following immediate A23187 treatment, both RH Cb-EmeraldFP and DMSO RH Cb-EmeraldFP and DMSO control presented a preferential accumulation in the apical end (~60%), with some events showing basal accumulation (~20%) (Figure 4-11C). Non-induced *adfKD* parasites resembled RH parasites regarding their F-actin relocation. When RH Cb-EmeraldFP and DMSO control parasites were treated with BIPPO, preferential actin relocalisation occurred towards the basal end (~60%), with some parasites showing accumulation in the apical end (~20%) (Figure 4-11C). *MyoAKO* parasites treated with either A23187 or BIPPO presented the same accumulation in the apical end, with F-actin accumulation in the first third of the parasite's periphery (~70%) (Figure 4-11 C). Parasites treated with either JAS or CD, did not present changes upon addition of either A23187 or BIPPO. This effect was not surprising, as changes in the actin dynamics are expected to impede correct polymerisation and translocation of actin. Similarly, the *adf KD* parasites following 96 hours of ATc treatment, did not present changes. Appearing as having both apical and basal signal for F-actin in both A23187 and BIPPO treatment (Figure 4-11C).

Kymograph analysis also identified the intensity profiles of peripheral actin signal on parasites treated with Ca²⁺ Ionophore A23187 (Figure 4-12 A, B). Kymograph analysis using BIPPO is not shown as a similar effect was observed in actin relocalisation. Kymographs depicting the intensity profiles of actin dynamics along the periphery remains similar between wt and *myoA KO*, while the *adf KD* shows a lack of dynamics across the entire parasites body (Figure 4-12 A). Upon

addition of Ca²⁺ ionophore A23187, strong accumulation at the apical tip can be observed in wt, while the *myoA* KO shows strong dynamics in the first half of the peripheral area close to the apical tip. For *adf* KD, the F-actin accumulation in both ends is independent of calcium ionophore A23187 or BIPPO addition (Figure 4-12 B).



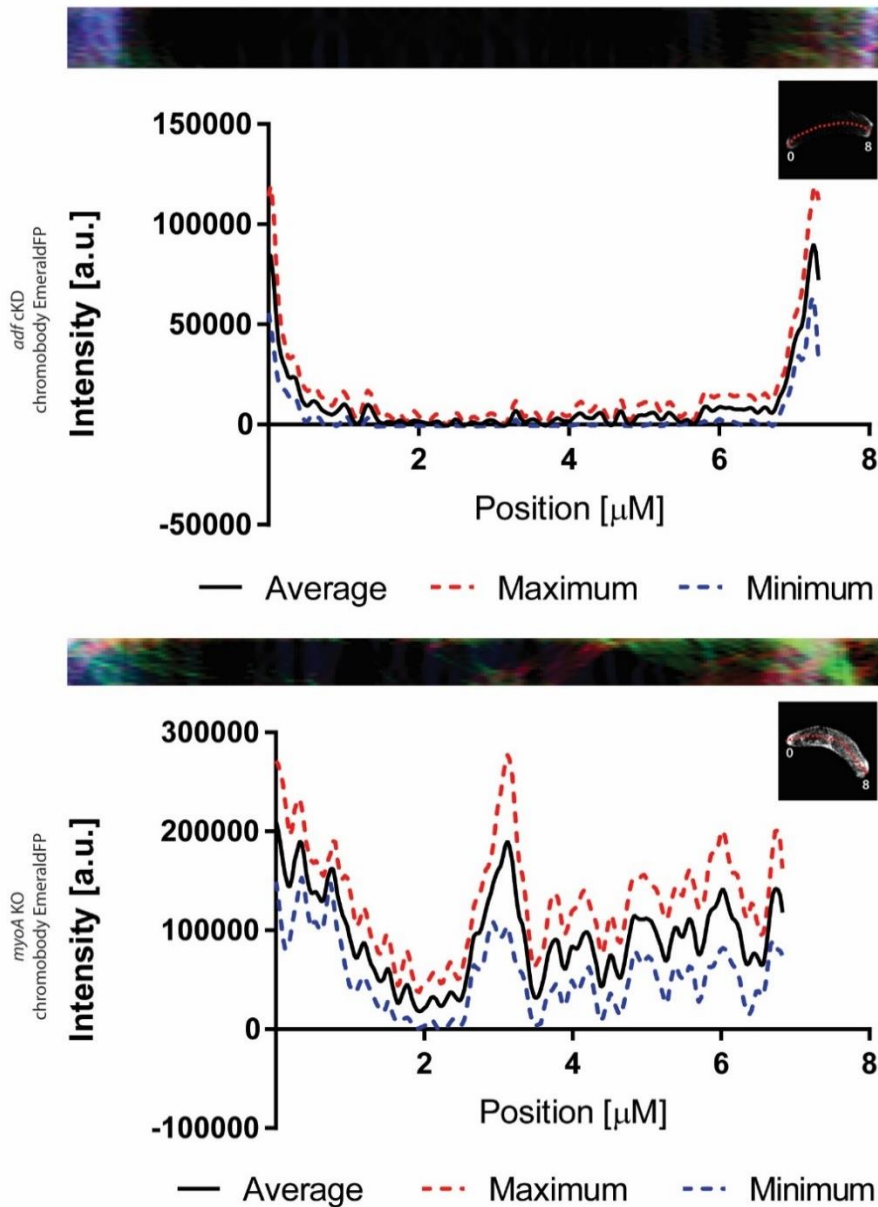
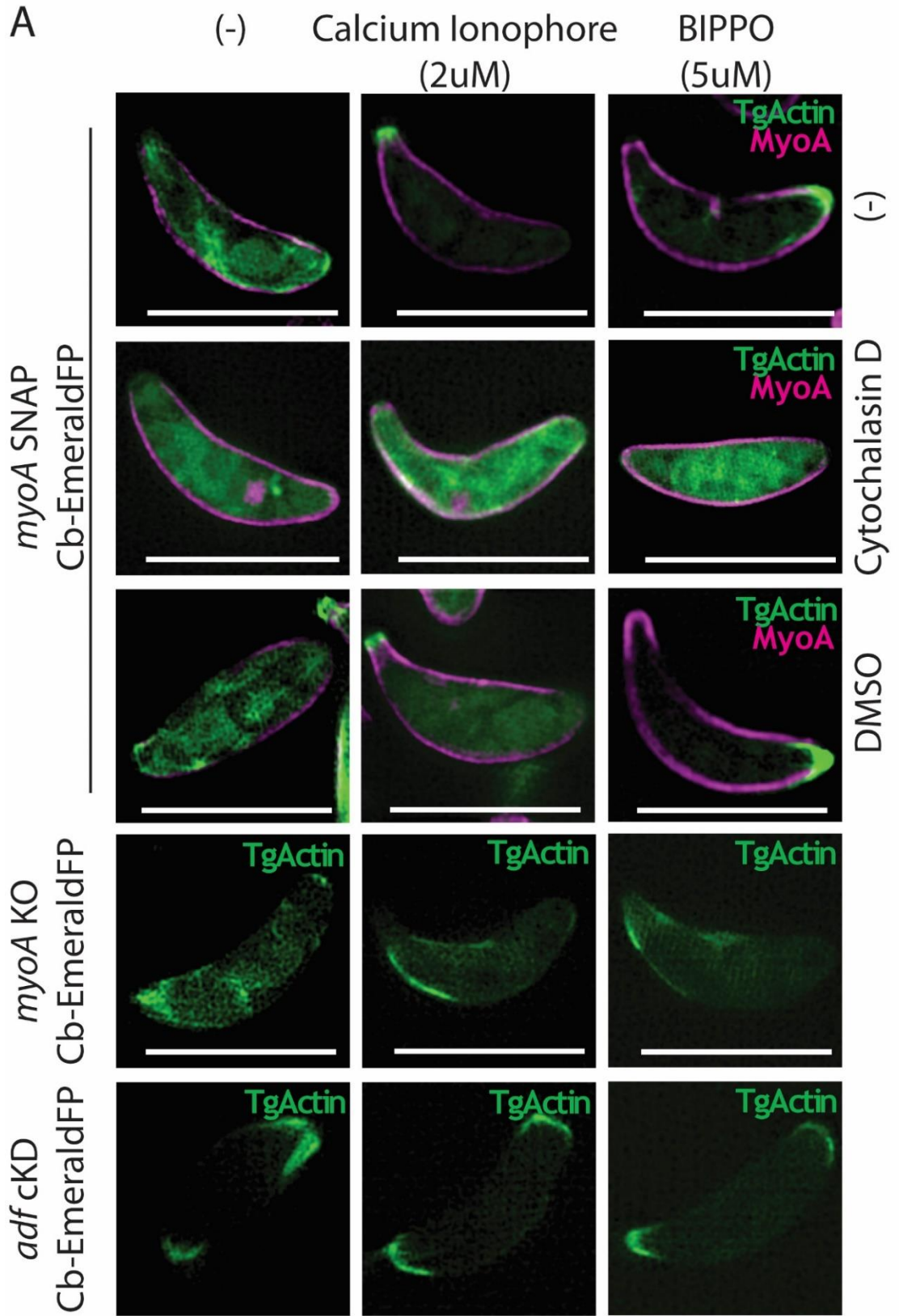
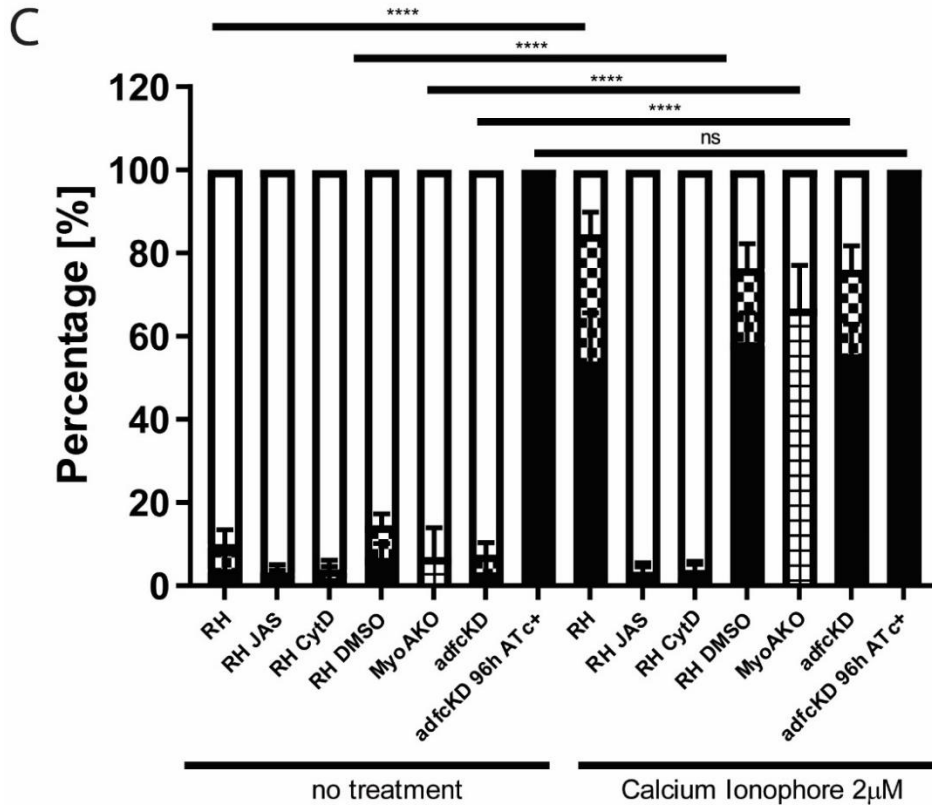
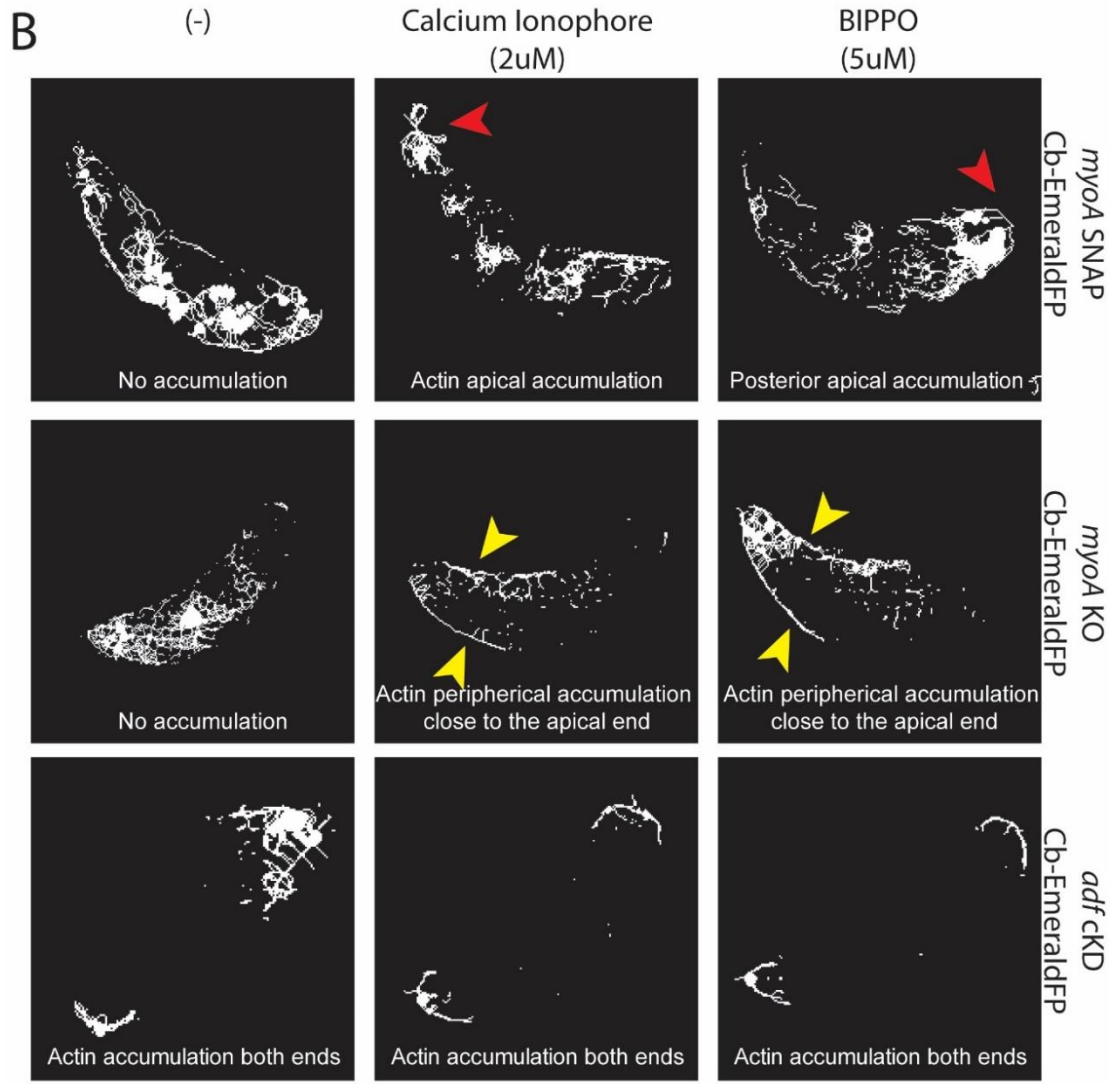


Figure 4-10 F-actin flow in resting extracellular parasites.

A. Stills depicting actin flow in extracellular RH, *myoA* KO and *adf* KD parasites expression chromobody EmeraldFP. F-actin flow can be seen transitioning from the Golgi region nucleation centre into the periphery in both RH and *myoA* KO. For *adf* KD, the flow appears to be abrogated and cannot be observed. Red arrowhead marks the Golgi region nucleation centre, while the yellow arrowhead marks the apical end nucleation centre. The skeletonisation process of the time-lapse images depicts areas where the actin chromobody signal is more common. Over time, the signal appears to accumulate in specific areas of the parasites, as previously observed. Red arrowhead marks the Golgi region nucleation centre, while the yellow arrowhead marks the apical end nucleation centre. **B.** The kymograph was generated by tracing a line in the middle of the parasite's body (red line). The colour-coded kymograph represents forward movement (red), backwards movement (green) and static (blue). The intensity profile generated from the kymograph corroborate our previous observation of accumulation points in the body of the parasite over time. These accumulation points are similar between RH and *myoA* KO chromobody EmeraldFP. In the case of *adf* KD, accumulation was only found in both ends of the parasites. The colour-coded kymograph represents forward movement (red), backwards movement (green) and static (blue). Stills generated from MovieS8. Numbers indicate minutes:seconds; and Scale bars represent 5 μm .





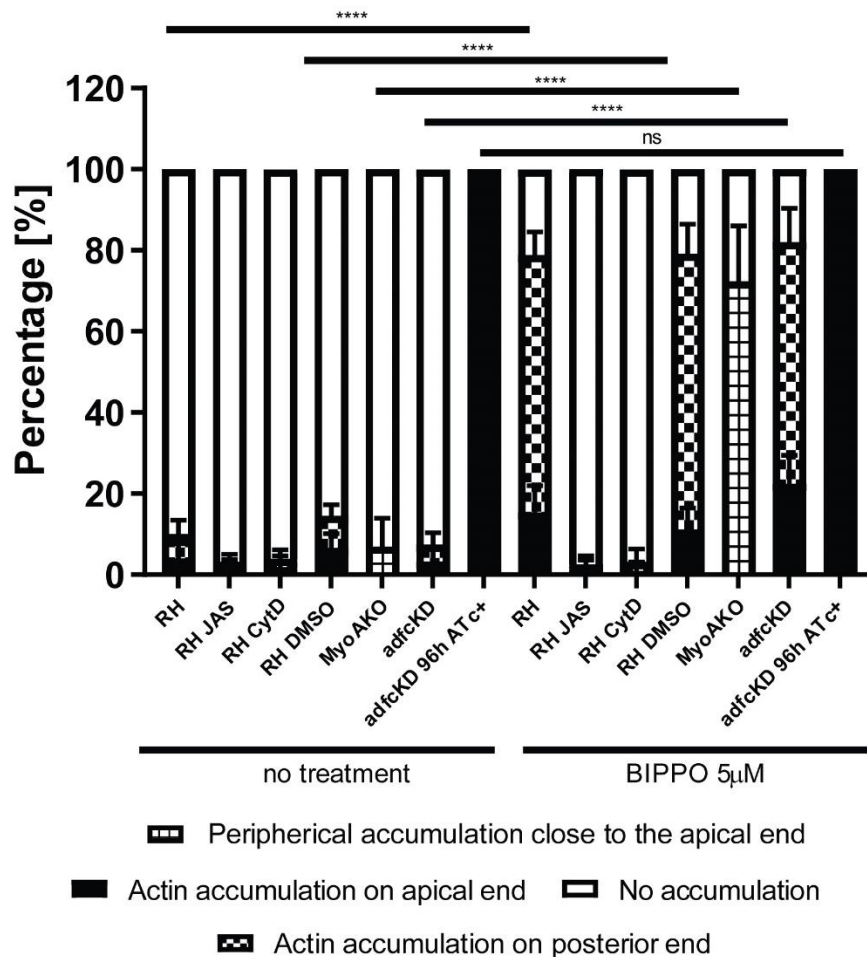
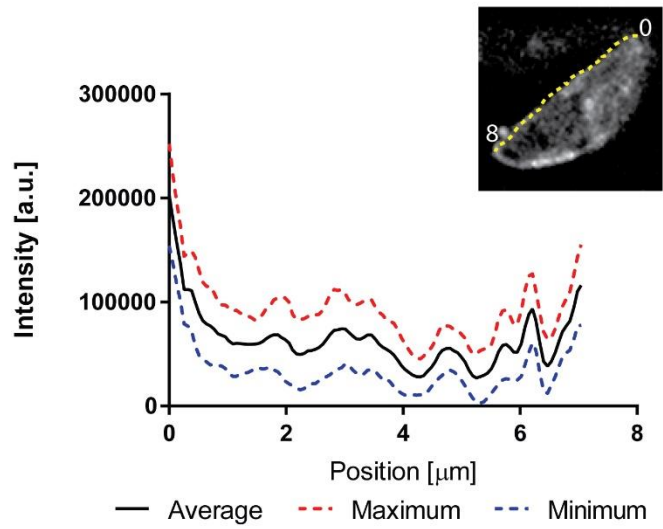
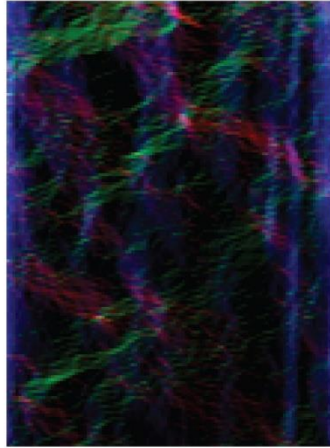


Figure 4-11 Extracellular actin dynamics are shifted upon addition of A23187 or BIPPO.

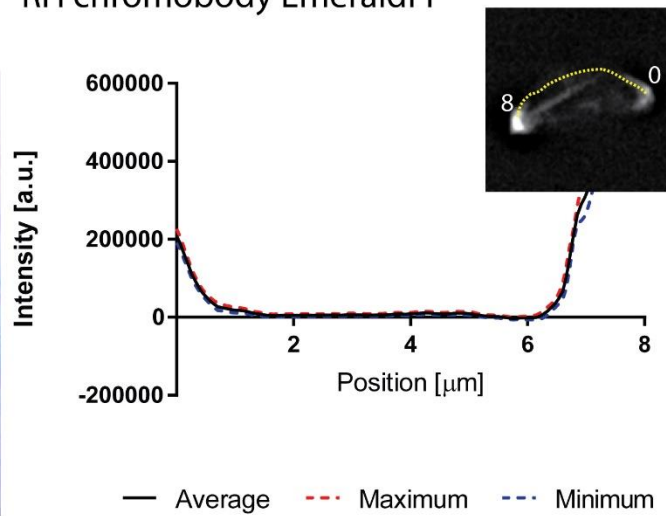
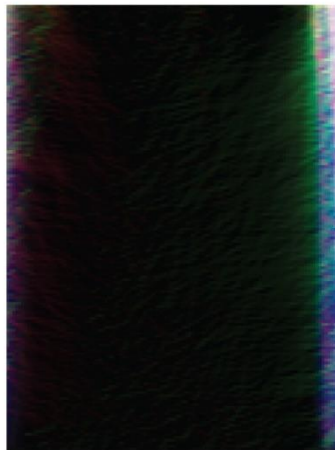
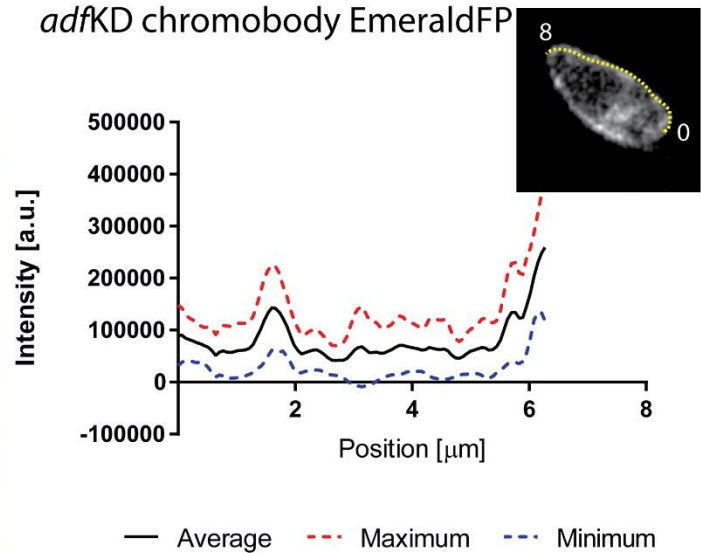
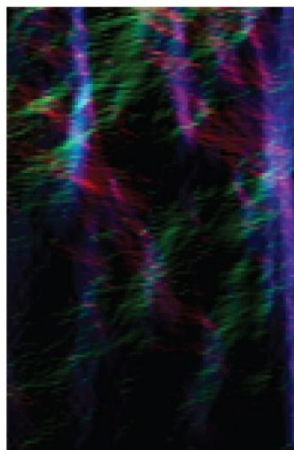
A. Top three rows: Parasites expressing Cb EmeraldFP along with MyoA-SNAP before and after Ca^{2+} -ionophore (A23187) or BIPPO treatment. The parasites were also treated with 2 μM of Cytochalasin D or DMSO (as control) for 30 min. After addition of A23187, preferential relocalisation of actin can be observed at the apical tip, while BIPPO presented more cases with F-actin accumulation in the basal end. 4th row: *myoAKO* parasites expressing Cb-EmeraldFP before and after treatment with A23187 and BIPPO. While no apical accumulation of F-actin is observed, some peripheral location of F-actin occurs in presence of A23187 or BIPPO. Bottom row: *adf cKD* parasites expressing Cb-EmeraldFP before and after treatment with Ca^{2+} ionophore or BIPPO. No apparent change in F-actin localisation can be seen upon treatment. Representative still from Movie S2. **B.** Skeletonization of movies shown in A. Before addition of A23187 or BIPPO, RH and *myoA* KO parasites behave similar with no accumulation of F-actin at the apical tip. After treatment with A23187, preferential accumulation of F-actin at the apical tip can be observed for RH, while BIPPO presented preferential accumulation in the basal end. In *myoA* KO, some relocalisation of actin is observed at the periphery of the parasite. In the case of *adf cKD*, no relocalisation occurs. **C.** Quantification of actin accumulation before and after treatment with Ca^{2+} ionophore or BIPPO. The parasites were counted for F-actin accumulation after adding Ca^{2+} ionophore or BIPPO using SiR tubulin to discriminate parasite orientation. Numbers were generated by counting total number of parasites and then number of parasites with Actin accumulation on the apical or basal tip. A minimum of 200 parasites were counted upon 3 biological replicates. Two-way ANOVA was used for statistical analysis and Tukey's multiple comparisons test. p value <0.0001 . Stills generated from MovieS9. Numbers indicate minutes:seconds; and Scale bars represent 5 μm .

A

No treatment



RH chromobody EmeraldFP

*adfKD* chromobody EmeraldFP*myoAKO* chromobody EmeraldFP

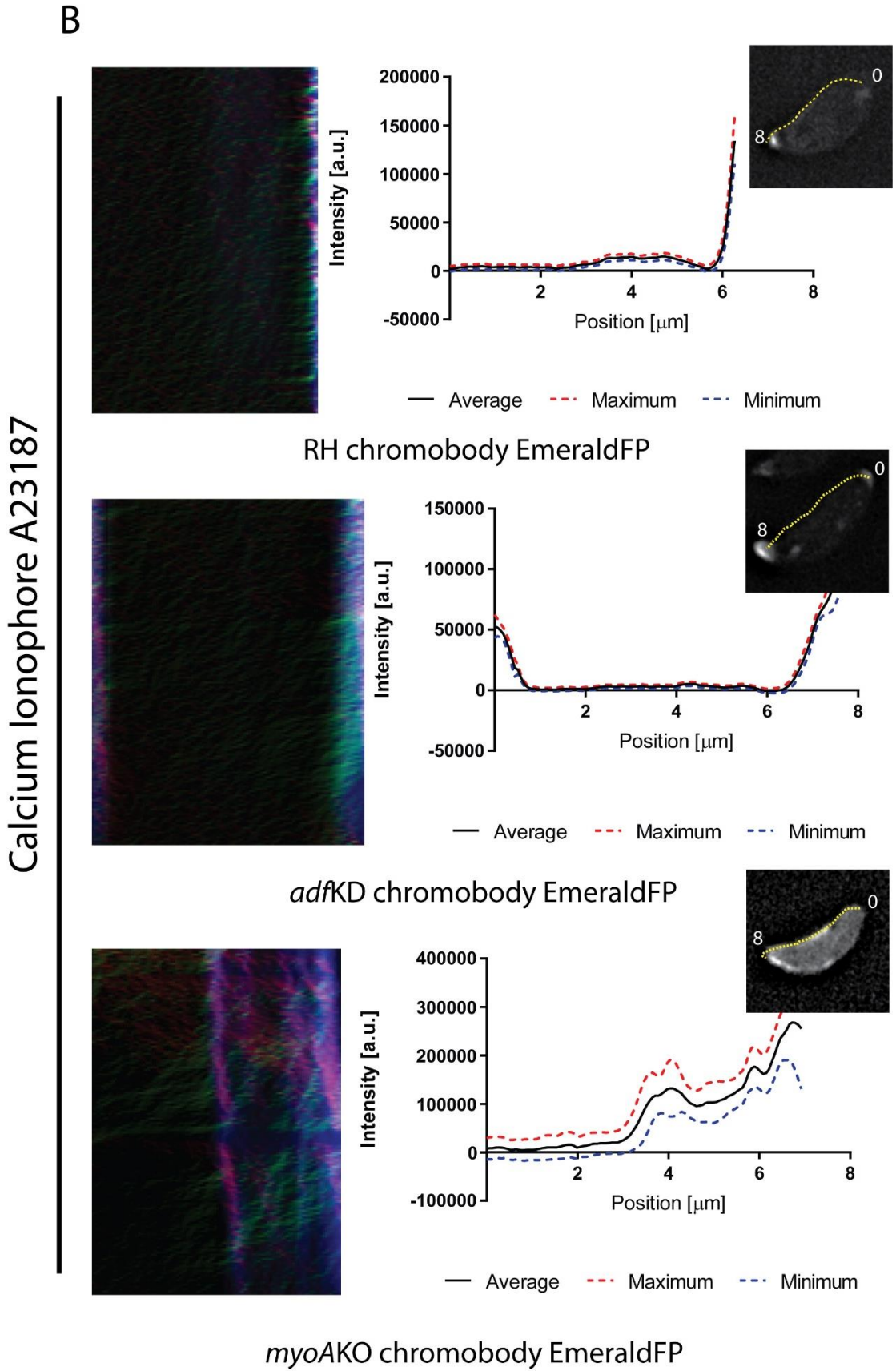


Figure 4-12 Kymograph analysis of actin flow upon addition of A23187.

A, B. Kymograph flow analysis examples done in RH chromobody EmeraldFP parasites with and without Ca^{2+} Ionophore treatment. Before treatment, the parasite appears to show dynamic actin behaviour across the entire periphery, yet upon addition of Ca^{2+} Ionophore strong actin accumulation can be observed in the apical tip as represented in the kymograph measurement. Kymograph flow analysis examples done in *myoA* KO chromobody EmeraldFP parasites with and without Ca^{2+} Ionophore treatment. Before treatment, the parasite appears to show dynamic actin behaviour across the entire periphery similar to *wt*, yet upon addition of Ca^{2+} Ionophore strong actin accumulation can be observed in the periphery close to the apical tip and covering approximately half of the parasite peripheral length as represented in the kymograph measurement. Kymograph flow analysis examples done in *adf* KD chromobody EmeraldFP parasites with and without Ca^{2+} Ionophore treatment. Before treatment, the parasite appears to lack dynamic actin behaviour across the entire periphery unlike *wt* and *myoA* KO, upon addition of Ca^{2+} Ionophore no further change is detected. The colour-coded kymograph represents forward movement (red), backwards movement (green) and static (blue). Numbers indicate minutes:seconds; and Scale bars represent 5 μm .

4.8 Discussion

The analysis of the dynamic behaviour of molecules is a complex process that becomes more difficult when multiple molecules are analysed (Saxton and Jacobson, 2002; Chenouard *et al.*, 2010). The quality of the data captured by microscopy will dictate how viable any follow-up analysis is, thus it is critical to maintain the best possible conditions when obtaining microscopy data. Once this initial step is followed, subsequent analysis becomes less problematic.

Several methods can be used to analyse the dynamic behaviour of molecules. However, different dynamics will require different methods. If analysis of well-defined molecules is desired, particle tracking software is readily available in both free and premium software (Saxton and Jacobson, 2002; Jaqaman *et al.*, 2008). However, this method is not effective when many ill-defined particles are moving in different directions. Kymographs are a common solution for this type of dynamics, as it can effectively separate motion into their main components: time and space. However, this method can itself be flawed, as it mainly relies on user input, introducing bias into the analysis and compromising reproducibility (Chiba *et al.*, 2014; Mangeol, Prevo and Peterman, 2016).

Automatic detection methods that work for a wide variety of dynamics are uncommon but very valuable. Limiting user input bias is perhaps, the most important step to eliminate user error when analysing kymographs (Mangeol, Prevo and Peterman, 2016). KymographClear and KymographDirect are useful

tools for this end, and although flawed, can allow users to characterise the dynamic flow of F-actin in replicating *Toxoplasma gondii* parasites.

Kymograph generated using these processes elucidated that the F-actin flow dynamics goes in two directions and not one as previously suggested (Tosetti *et al.*, 2019), supporting the idea that it can allow the transport of other molecules during replication. The quantification data obtained from using automatic kymograph analysis also allow to point subtle differences in actin dynamics, as shown in Figure 4-9B-E, where even 0.1 μ M of JAS was enough to detect a change in actin dynamics by kymograph analysis while still not being very apparent by eye. Other studies have also shown cases where bi-directional movement of actin is present, such as bi-directional actin movement on myosin tracks *in vitro* (Toyoshima, Toyoshima and Spudich, 1989), circular movement that allows mitochondrial movement in *Arabidopsis thaliana* (Zhang *et al.*, 2014) and bi-directional movement facilitated by cytoskeletal components and microtubules in motility and axonal filopodia extension (Chetta *et al.*, 2015).

In recent reports, bidirectional F-actin dependent movement of vesicles and dense granules has been described (Heaslip, Nelson and Warshaw, 2016; Periz *et al.*, 2019), supporting our analysis. This bidirectional flow of F-actin appears to be not solely dependent on a single myosin, such as MyoA, but other myosin proteins such as MyoF are potentially involved, as the latter was suggested to be responsible for apicoplast and dense granule motility (Heaslip, Nelson and Warshaw, 2016; Fréchal, Jacot, *et al.*, 2017).

A continuation of this discussion can be found in the discussion chapter (chapter 6).

5 *Toxoplasma gondii* invasion dynamics: nuclear squeeze and the F-actin ring involvement in invasion

Parasites from the Apicomplexa phylum have evolved invasive stages that actively seek to enter host cells to survive. This process starts by an approach done by the parasite towards the host cell by gliding motility. Upon host cell recognition, the parasite reorients itself and starts the invasion process (Morisaki, Heuser and Sibley, 1995).

The invasion process starts by the formation of the tight junction (TJ) by establishing a junction ring in the contact point between the parasite and the host cell membrane. The TJ ring is a protein complex assembled by the sequential secretion of secretory organelles known as micronemes and rhoptries, where rhoptry neck proteins (RONs) are subsequently inserted into the host cell plasma membrane (Besteiro, Dubremetz, and Lebrun 2011; Reese, Shah, and Boothroyd 2014). Different rhoptry neck proteins (for example, RON2) are also involved in the formation of the TJ complex on the outside the parasite, by binding to the exposed micronemal transmembrane microneme protein AMA1 on the surface of the host cell (Besteiro, Dubremetz and Lebrun, 2011; Egarter *et al.*, 2014).

This process is further supported by de novo F-actin formation from the parasite entry site in the host cell (Gonzalez *et al.*, 2009; Bichet *et al.*, 2014). Accumulation at this point occurs due to the insertion of Toxofilin, a protein complex believed to be responsible for recruitment of actin nucleation factors in the host cell to further stabilize the TJ (Delorme-Walker *et al.*, 2012). Furthermore, the parasite's own F-actin dynamics play a key role during the invasion process paired with the parasite's acto-myosin system in the form of a linear motor that powers actin treadmilling in order to generate force for invasion (Meissner, Schlüter and Soldati, 2002; Drewry and Sibley, 2015; Heintzelman, 2015). However, KO mutants lacking key elements of this motor remain invasive, although at reduced levels, suggesting the model is incomplete (Egarter *et al.*, 2014; Gras *et al.*, 2017; Whitelaw *et al.*, 2017).

5.1 *Toxoplasma gondii* suffers mechanical stress during invasion

During invasion, *Toxoplasma gondii* suffers mechanical stress as the parasite deforms while going through the TJ (Figure 5-1 A). This process facilitates parasite entry into the host cell by deforming its horizontal width as only a small entry point is created during invasion. Deformation was assessed by measuring the diameters of free parasites both outside the host cell and mid-invasion. Measurement of the average diameter of parasites prior to invasion (extracellular 2.5-3 μm) and during invasion (TJ mid-invasion 1.5-2 μm) show significant body compression in order to fit through the TJ (Figure 5-1 B). Following the same trend, analysis of the average diameter of the nucleus during pre and mid invasion yielded similar results, where the nucleus was significantly constricted on about 50% of its regular diameter while going through the TJ in comparison to extracellular parasites (Figure 5-1 B).

Several deletion mutant lines for key components of the actomyosin system present a loss in invasiveness (*myoA* KO, *mlc1* cKO, *act1* cKO and *adf* cKD). However, mutant parasite lines lacking one of these components can still invade, albeit at a much reduced rate (~ 20%). This residual invasion was often the subject of debate (Egarter *et al.*, 2014; Drewry and Sibley, 2015; Whitelaw *et al.*, 2017), as it was initially believed that core components of the actomyosin system were essential for invasion (Fr nal *et al.*, 2010; Heintzelman, 2015). Invasion analysis done in mutants such as the *myoA* KO demonstrated a stop-and-go manner of invasion that leads to extended invasion times (Egarter *et al.*, 2014; Whitelaw *et al.*, 2017). This was also shown to trigger different behaviours of entry into the host cell, such as partial invasion by the parasite, followed by host cell membrane outward projection to complete the “invasion” process, behaviour similar to micropinocytosis (Bichet *et al.*, 2016). Furthermore, the strong forces exerted in some cases might also cause the parasite to remain trapped in the TJ and eventually die.

When parasites lacking components of the actomyosin system (*myoA* KO and *adf* cKD) were measured, different dynamics were recognised as extracellular parasites and the ones mid-invasion presented different constriction levels across the mutants (Figure 5-1 C). Every parasite line presented similar width while

extracellular, with a measurement around 2.5 - 3 μm . However, the *myoA* KO presented a higher level of TJ constriction mid-invasion when compared to wt (all parasite lines but *myoA* KO at $\sim 2\mu\text{m}$, while *myoA* KO is at $\sim 1.6\mu\text{m}$) (Figure 5-1 C). On the other hand, the nucleus deformation changed from 1.7 to 2.5 μm in extracellular parasites to a less compressed state in the *adf* cKD with $\sim 1.7\mu\text{m}$, while wt, un-induced *adf* cKD and *myoA* KO presented a constriction of $\sim 1.3\mu\text{m}$ (Figure 5-1 D).

Taken together, these data suggest the actomyosin motor could have a limited effect in the invasion process from a mechanical point of view. The deformation the parasite body suffers during invasion can be altered to a limited degree with the introduction of actomyosin mutants. These actomyosin elements could also play a role in counteracting the pressure exerted by the host cell in the entry site. The lack of either *myoA* KO or *adf* cKD lead to a slight change in the constriction in the body of the parasite or its nucleus, respectively. However, the junction ring can be considered constant upon interference with the acto-myosin system of the parasite.

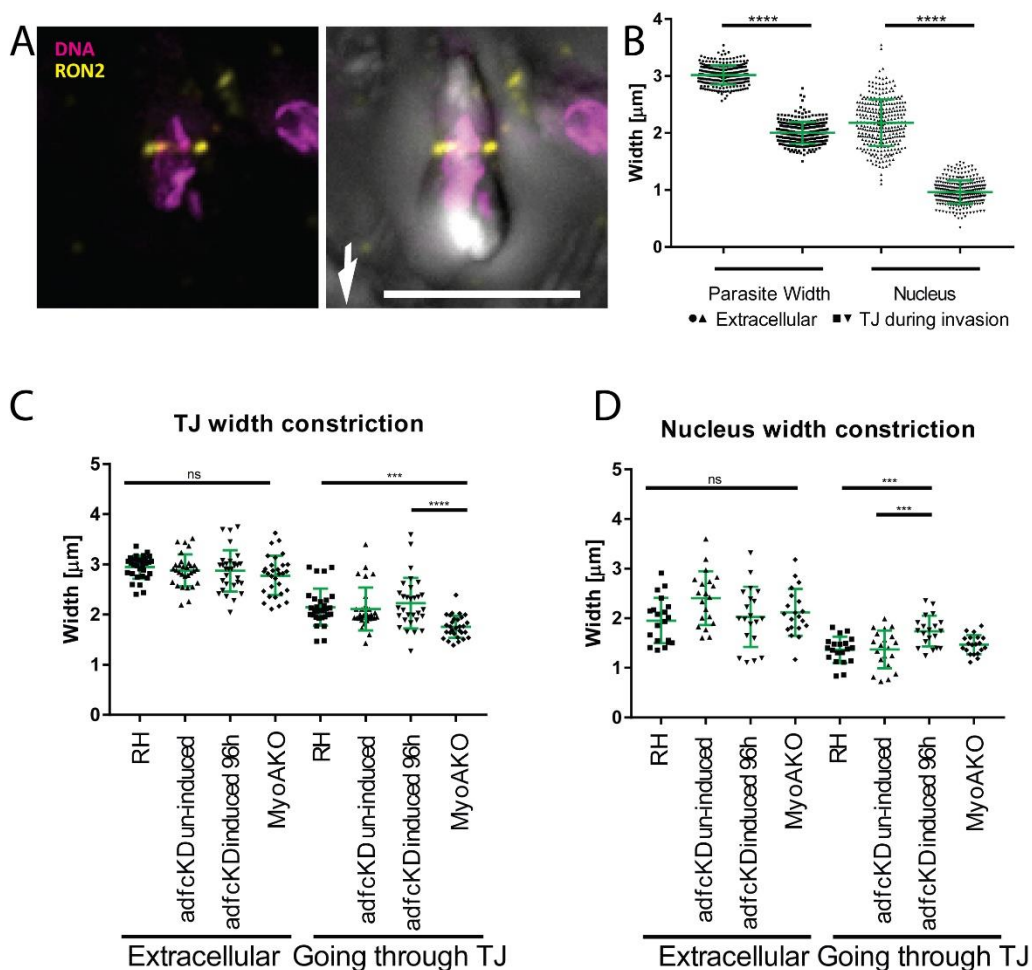


Figure 5-1 The parasite and its nucleus are deformed during invasion.

A. Representative image of wild Type RH parasites mid-invasion. A tight junction assay was carried out by allowing freshly egressed parasite to invade host cells and then fixed with 4% PFA. Immunofluorescence labelled the TJ with anti-Ron2 (yellow) and DAPI (magenta) for the nucleus. Scale bar represents 5 μ m. **B.** Graph depicting mechanical deformation of invading and non-invading parasites and its nucleus. 100 parasites found mid-invasion were counted in triplicate and compared to extracellular, freshly egressed parasites. One-way ANOVA was used for statistical analysis. p value equals <0.0001. **C,D.** Graph depicting deformation of parasites and its nucleus during extracellular life and invasion. The *adf* cKD strain was compared in both induced and non-induced state. 30 parasites were counted for each condition in triplicate. One-way ANOVA was used for statistical analysis and Tukey's multiple comparisons test were carried out. p value <0.0001.

5.2 The nucleus acts as a limiting factor for parasite invasion; a potential explanation for abortive events

Based on the hypothesis previously detailed, live invasion processes were analysed where *wt* and inducible *act1* KO parasites were allowed to invade host cells (Figure 5-2). Two main conditions were tested: *wt* parasites where actin is present and *act1* KO parasites that lack actin, a major component of the actomyosin motor (Figure 5-2 A). Invasion by *wt* parasites starts with an initial rapid invasion step (Penetration step), followed by a pause when $\sim 1/3$ of the body is inside the host cell (Speed decrease), and a second acceleration until the parasite is fully inside the host cell (Finalisation) (*RH*, Figure 5-2 A, B, Movie S10). Induced *act1* KO parasites after 72 hours of RAPA treatment also managed to invade host cells, albeit in lower numbers. However, the time lapse between the fast-initial penetration (Penetration initiation) and the finalisation of invasion lag to around 1 minute for the speed decrease step (*act1* KO, Figure 5-2 A, B, Movie S11). In rare cases, invading parasites are known to be pushed out of the host cell during this stalled stage (Figure 5-2 C, Movie S12). These results could support the notion that a limitation during invasion is present and can act as a barrier for successful invasion. Since actomyosin mutants provided different invasion dynamics in the deformation of both the body and nucleus of the parasite, the nucleus acting as a limitation for invasion needs to be explored further. Given the promiscuous nature of *T. gondii*, it is possible that the invasion process is not universal, requiring some degree of adaption to the host cell membrane, which can present varying degrees of invasion easiness. This hypothesis would fit previous data that showed that mutants lacking key glideosomal proteins invade host cells at varying speeds, with slow invaders that can take several minutes to finish the invasive process (Whitelaw *et al.*, 2017).

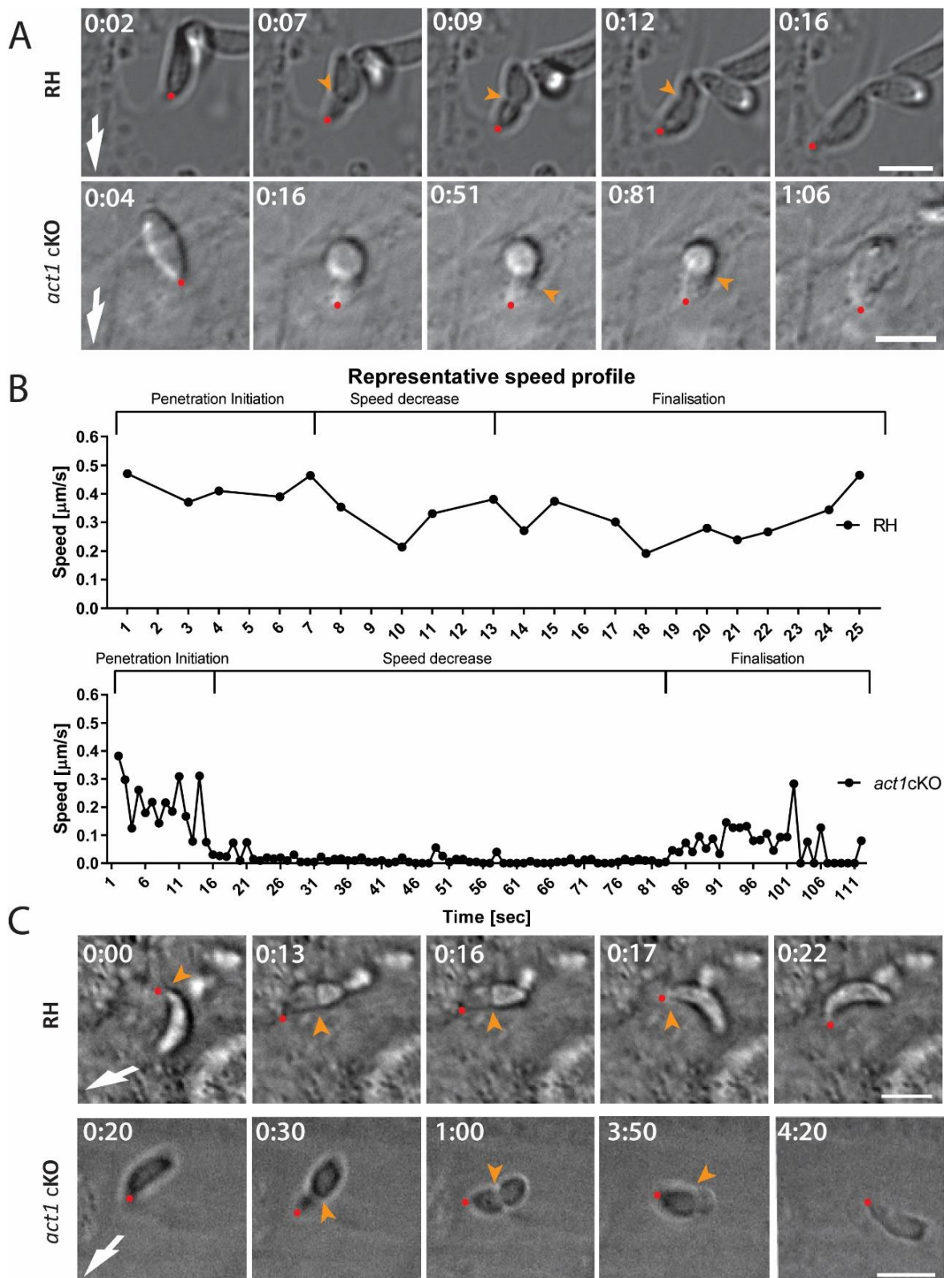


Figure 5-2 *T.gondii* nucleus can act as a limiting factor for invasion.

A. Time-lapse microscopy analysis of RH Wild type (upper row) and *act1* cKO (bottom row) tachyzoites invading HFFs cells. Time was determined from the onset of invasion. White arrow points at invasion direction; yellow arrow points at tight junction; red dot follows the apical pole of the parasite. **B.** Representative example of speed profiles of invading parasites where the apical tip of the parasite was followed during the penetration process. The relative displacement of the apical tip

over time allowed speed calculations. Individual stages were named in regard to the invasion step (Penetration initiation, Speed decrease and finalisation). Invasion was analysed with Icy Image Processing Software (Pasteur Institut) using the Manual Tracking plugin by analysing each movie 5 times and averaging the measurements. **C.** Time-lapse analysis showing abortive invasion of wild type and *act1* cKO parasites. Time was determined from the onset of invasion. White arrow points at invasion direction; yellow arrow points at tight junction; red dot follows the apical pole of the parasite. Stills generated from MovieS10-12. The *Act1* KO mutants used here corresponds to the original DiCre strain that possesses a floxed *Act1* gene. Numbers indicate minutes:seconds; and Scale bars represent 5 μm . The time-lapse was captured by Dr. Jamie Whitelaw and Dr. Fernanda LaTorre-Barragan and then analysed by the author (Meissner Lab).

5.3 The F-actin ring is not present in all cases of invasion; parasite mutant lines invasion behaviour

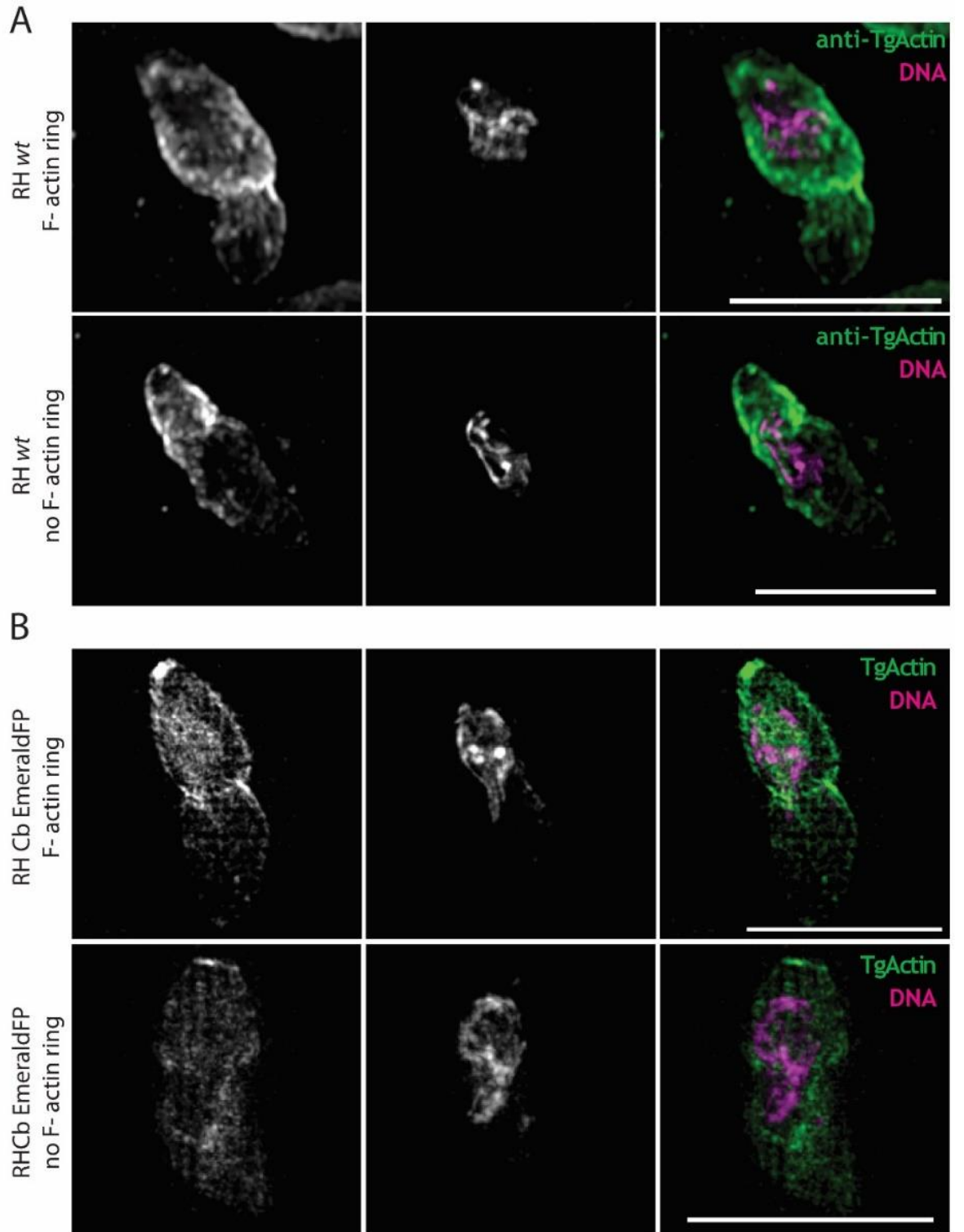
F-actin in *Apicomplexa* parasites is believed to occur as short filaments that are translocated between the Inner Membrane Complex (IMC) and the plasma membrane (PM) (Meissner, Schlüter and Soldati, 2002; Fréchal *et al.*, 2010). The aforementioned linear motor model states that these short actin filaments would interact with micronemal transmembrane proteins at the PM. These micronemal transmembrane proteins are then translocated in linear fashion to the posterior pole by the concerted action of the actomyosin complex, that would generate the force for this displacement (Fréchal *et al.*, 2010). Given that actin would in this case remain enclosed between the IMC and the PM, the nucleus would be expected to passively enter the host cell during invasion without major involvement of F-actin. However, this directly contradicts the observations already made, where F-actin pools are known to be located across the cytoplasm of the cell and also in the TJ (Periz *et al.*, 2017). This led to hypothesise that F-actin is able to assist in nucleus passage during invasion, as has been described in other eukaryotic cells during migration through a constricted environment (Gomes, Jani and Gundersen, 2005; Guilluy *et al.*, 2014; Petrie and Yamada, 2015; Isogai and Innocenti, 2016; Jayo *et al.*, 2016).

As previously described using anti-filamentous actin antibodies, *Plasmodium* merozoites presented a ring like structure in the TJ during invasion (Riglar *et al.*, 2011; Angrisano, Riglar, *et al.*, 2012). However, no data regarding this ring was found by using antibodies against actin in *Toxoplasma gondii*. By synchronising parasites using Endo buffer (ENDO *et al.*, 1987) and then allowing them to invade for 5 minutes, visualisation mid-invasion was possible. Fixation for this assay required a cytoskeleton buffer with 4%PFA (CB-4%PFA), since, as mentioned in the

previous chapter, actin structures are often lost depending on the fixative used. By doing Structure Illumination Super Resolution Microscopy (SR-SIM), the same F-actin ring was visualised. However, in some cases no F-actin ring was observed during invasion (Figure 5-3 A). When this assay was repeated with F-actin chromobody expressing parasites, the same phenomenon was observed, with a majority of cases showing an F-actin ring, and a few without (Figure 5-3 B).

By expressing F-actin chromobodies in a variety of mutants possessing defects in the actomyosin motor (*adf* KD, *act1* KO and *myoA* KO) and then allowing them to invade, a change was observed in the proportion of the formation of the F-actin ring (Figure 5-3 C). Since the previous *LoxP-Act1* DiCre mutant expresses a GFP cassette upon *Act1* excision, a different non-fluorescent version was employed using Cas9 to create a frame shift in the gene, obtaining an *Act1* KO strain upon co-expression of the Cas9 and *Act1* gRNAs. From this point in this thesis and on, this Cas9 *Act1* cKO strain is used, as it allows co-expression of chromobody EmeraldFP proteins. In the majority of cases in the *wt* (76%) the F-actin ring was present, while in the remaining ~24% no significant accumulation was detectable (red arrowheads, Figure 5-3 C,D). In the case of the mutants, all actomyosin impaired mutants lacked an F-actin ring, leading to a hypothesis that F-actin is more dynamic and performs more functions than previously described (Figure 5-3 C,D). It is noteworthy that the percentage of the population not showing an F-actin ring during invasion fits well with the residual invasion observed in glideosome impaired mutants, suggesting the presence of an actin-independent invasion mechanism. In addition, every invasion event was accompanied by F-actin accumulation in the posterior pole of the parasite, with the exception of the *act1* KO that lacks actin and the *myoA* KO (Figure 5-3 E).

Following fixed assays, live invasion time-lapse microscopy was carried out for comparison (Figure 5-4 A). In the case of RH chromobody EmeraldFP, as previously described, the F-actin rings appear from the onset of invasion (red arrowhead, upper row panels, Figure 5-4 A). As seen in fixed assays, invasions were also detected where no F-actin accumulated at the junction (red arrowhead, middle row panels, Figure 5-4 A). However, in both cases actin accumulated in the posterior pole of the parasite (orange arrowheads, upper and middle panels, Figure 5-4 A).



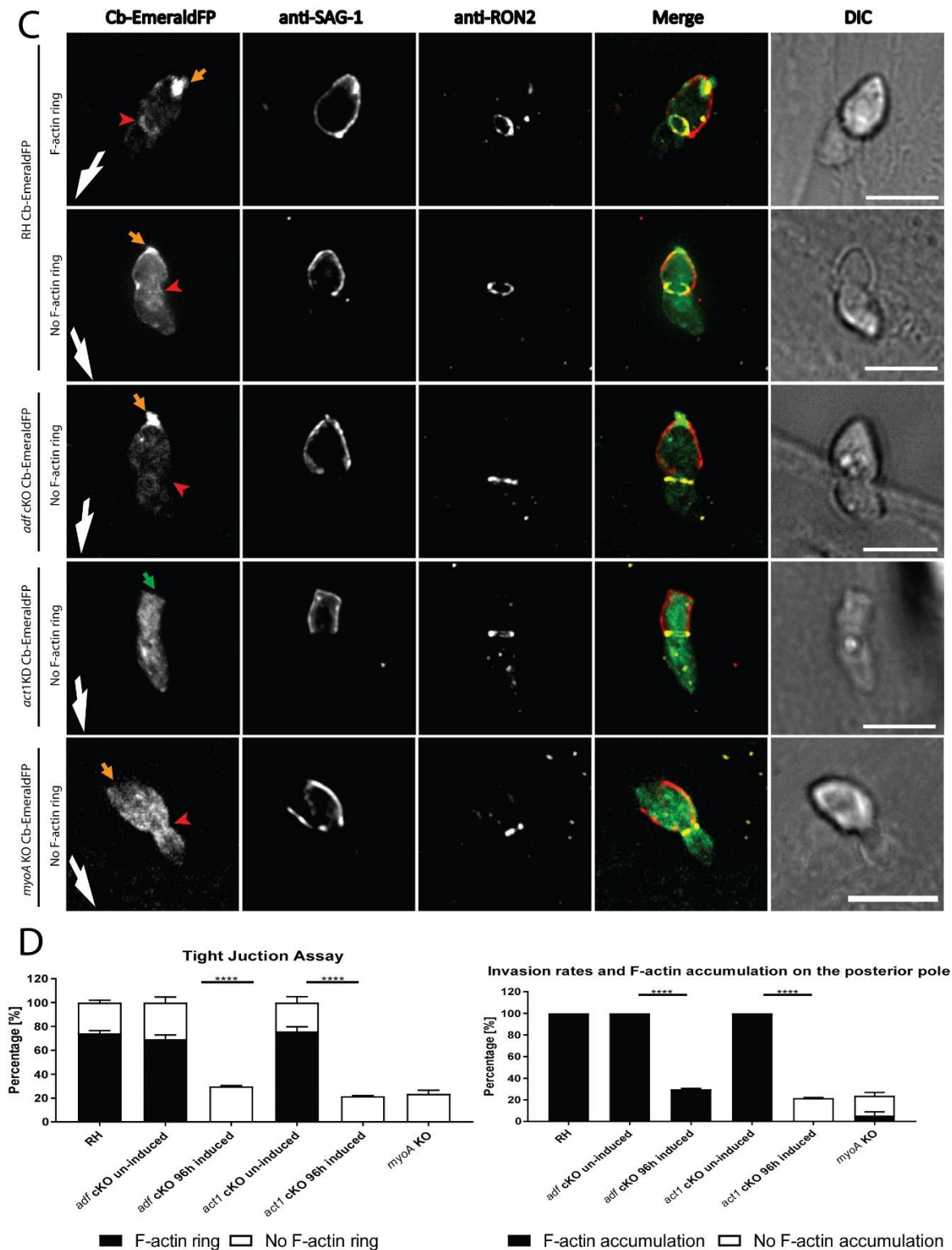


Figure 5-3 F-actin dynamics during *Toxoplasma gondii* invasion during fixed and live imaging.

A. SR-SIM depicting wild type parasites using anti-actin antibodies previously used in Angrisano et al. 2012. In the upper panel an actin ring is shown during invasion. In the lower panel, no F-actin ring was found during the invasion process. **B.** SR-SIM depicting transgenic (wild type) parasites expressing actin chromobody EmeraldFP. The upper panel depicts a parasite mid-invasion with the presence of an F-actin ring. The lower panel presents a parasite mid-invasion without detecting an F-actin ring. **C.** Representative immunofluorescence staining of tachyzoites during host cell penetration. The majority of wild type parasites presented an F-actin ring detected at the junction. For *adf* cKO, *act1* cKO and *myoA* KO, no F-actin ring was detected. SAG1 staining was performed prior to permeabilisation to stain only the extracellular portion of the parasite. Antibodies against

Ron2 were used to stain the TJ. Red arrowhead: position of the TJ. Orange arrow: posterior pole of the parasite. For the *act1* cKO mutant, only cytoplasmic signal can be observed, corresponding to the cytosolic expressed CB-EmeraldFP. Note the posterior deformation of the parasite, when compared to parasites still expressing *act1* (green arrow). In the case of *myoA* KO CB-EmeraldFP, very little to no accumulation of F-actin occurs at the posterior pole (yellow arrow). Instead, F-actin appears to accumulate at the apical pole with stronger signal in the periphery in proximity to the TJ (red arrowhead). White arrows point to direction of invasion. Scale bars represent 5 μm . **D.** Quantification of F-actin accumulation at the TJ as detected in time lapse analysis. The values are expressed as percentage. 28 total parasite invasion events were captured across three different biological replicates. **E.** Tight Junction assay on fixed samples (as shown in (A)) depicting invasion rates of indicated parasites. Note that the number of total invasion events for *adf* cKD, *act1*cKO and *myoA*KO correlates to the number of invasion events, seen for RH without F-actin ring formation. No F-actin ring could be seen for these mutants. Three biological replicates were done with 300 parasites counted for each biological replicate. One-way ANOVA analysis was performed for each graph. p value <0.0001.

Since in the case of the *adf* KD, F-actin is relocated to both poles, no major actin dynamics can be seen during invasion (orange arrowhead, lower panels, Figure 5-4 A, Movie S13). The invasion speed also appears to lessen, validating data previously published where the *adf* KD mutant was able to invade, albeit in a slower and less efficient way (Mehta and Sibley, 2011).

The previous actin accumulation during invasion was also assessed by tracing ROI lines to generate an intensity profile (Figure 5-4 B). Confirming previous data, the F-actin ring, if formed during invasion can be easily distinguished as a distinct peak; in contrast, no peaks are present when no F-actin accumulates at the junction (red arrowhead). Posterior F-actin accumulation is always observed as another distinct peak in intensity (orange arrowhead) in all cases. The *adf* KD also presented a distinct intensity peak corresponding to the stabilised actin on the posterior (orange arrowhead) and apical pole.

In good accordance with the fixed assays, around ~78% of the parasites presented a detectable F-actin ring (Figure 5-4 C). It is noteworthy to mention that rare invasion events known as “capping invasion” (Bichet *et al.*, 2016) have been described, wherein parasites are able to invade the host cell through a static or capped TJ that depends on the host cell plasma membrane retraction or engulfment to fully internalise the invader. In an independent analysis of F-actin dynamics during invasion with capped invasion, the parasite still formed an F-actin ring at the TJ, suggesting two possible mechanism: invasion either relies on F-actin traction forces regardless of the type of invasion, or the ring-like F-actin

structure is stabilising the entry point counteracting potential host cell pressure in the entry site (Del Rosario *et al.*, accepted).

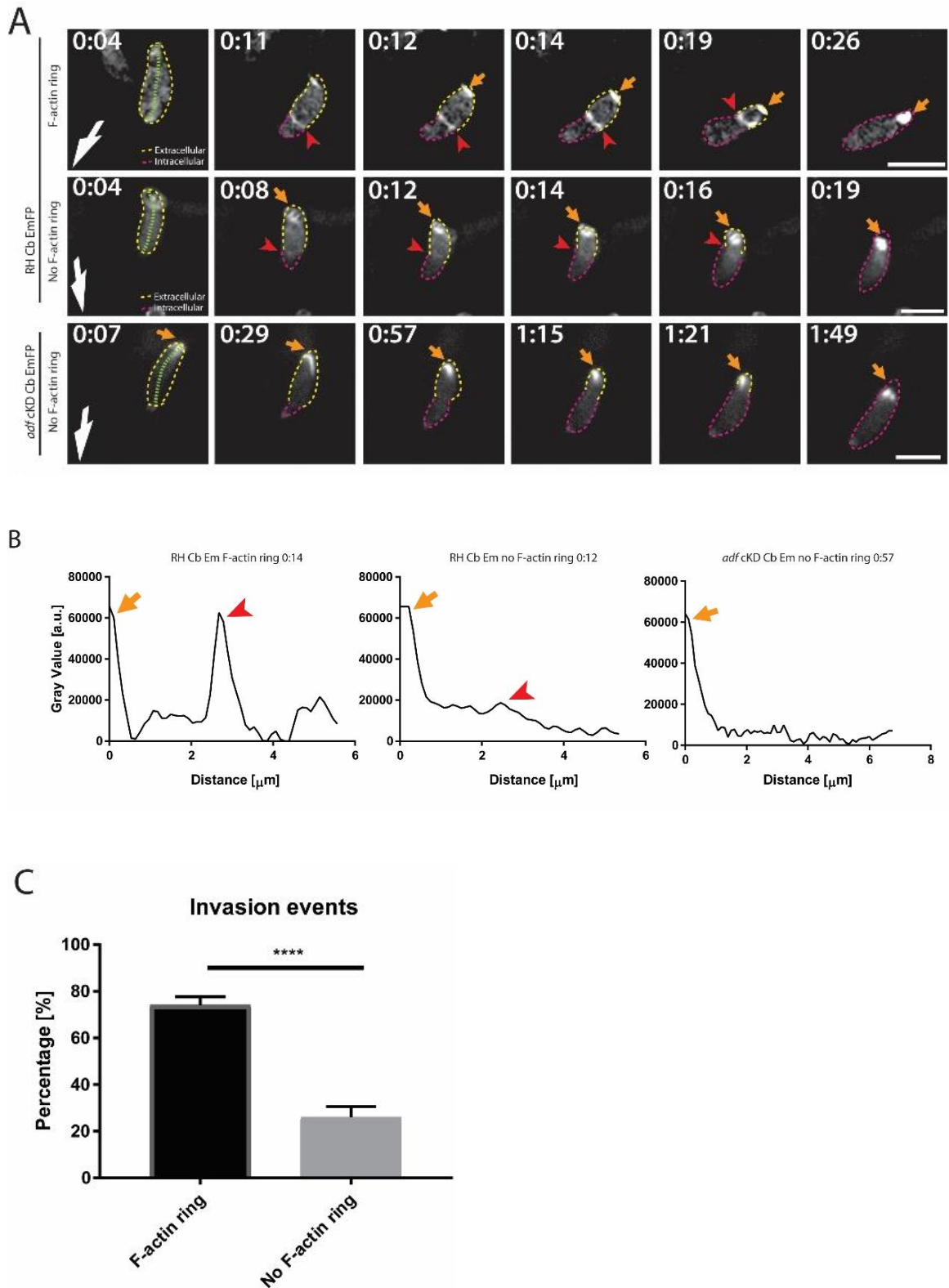


Figure 5-4 F-actin dynamics during *Toxoplasma gondii* invasion.

A. Time-lapse analysis depicting invading RH Cb-EmeraldFP parasites. During invasion, an F-actin ring can be observed at the TJ in the majority of cases (red arrowheads, upper panel). Invasion can also occur without significant formation of an F-actin ring (middle panel). Invasion of *adf* cKD parasites occurs without formation of an F-actin ring despite clear deformation of the parasite body

(lower panel). During the entire invasion event F-actin accumulation is observed at the posterior pole of the parasite in all cases (orange arrows). Green segmented lines depict the area that was measured for generation of intensity plot profiles shown in (b). Yellow and purple dotted lines indicate the extra- and intracellular part of the parasite during the entry process respectively. **B.** Intensity plot profiles of the time lapse analysis shown in (a). Depicted plots correlate to half-invaded parasites. In the case of F-actin ring formation, two distinct peaks are detected, correlating to the F-actin ring at the TJ (red arrowhead) and the posterior pole of the parasite (orange arrow). In the case of no F-actin ring, no accumulation at the TJ can be observed; only the peak correlating to posterior F-actin can be detected. For *adf* cKD, a major peak can be seen corresponding to the posterior pole of the parasite. **C.** Quantification of F-actin accumulation in wt parasites at the TJ as detected in time lapse analysis. The values are expressed as percentage. 28 total parasite invasion events were captured across three different biological replicates. White arrows point to direction of invasion. Stills generated from MovieS13. Numbers indicate minutes:seconds. Scale bars represent 5 μm .

5.4 *In vivo* analysis of F-actin dynamics and nuclear squeeze during *Toxoplasma gondii* invasion.

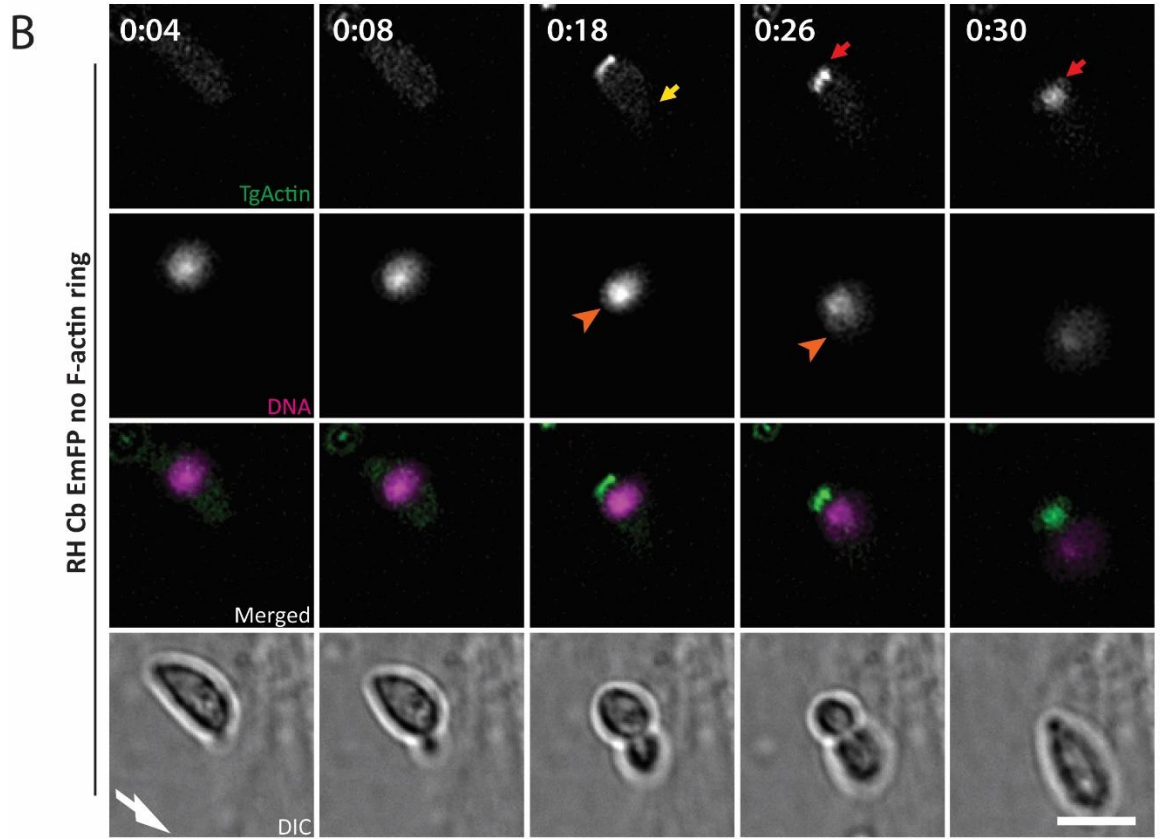
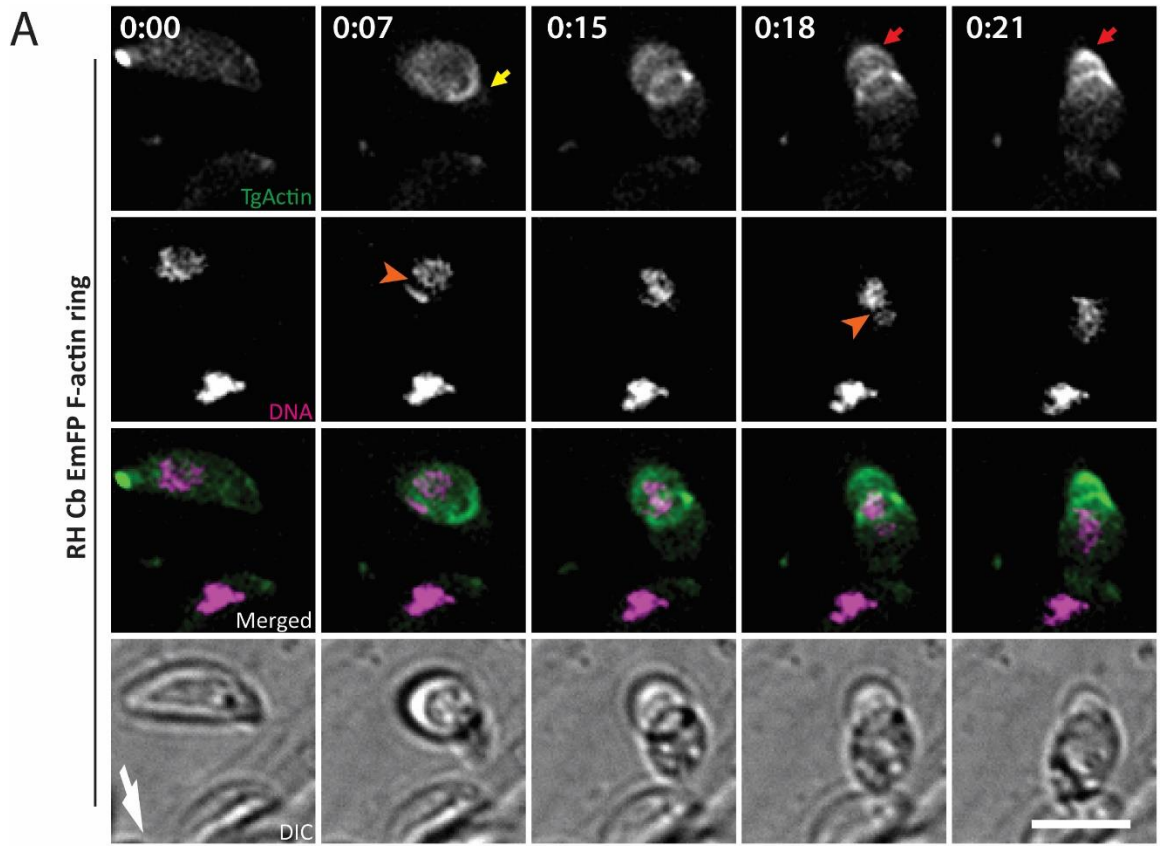
Given that live F-actin dynamics presented similar behaviour to fixed samples during invasion, simultaneous visualisation of F-actin dynamics and the nucleus were characterised. Following previous descriptions during invasion, the F-actin ring appears at the beginning of invasion followed by intense accumulation of F-actin in the TJ once the nucleus is close. This accumulation becomes prominent once the nucleus reaches the TJ (yellow arrowhead, Figure 5-5 A, Movie S14). Interestingly, the nucleus shape remains rounded before it reaches the TJ (orange arrowhead). Once the nucleus passes through the TJ, a visible constriction of the nucleus is encountered (orange arrowhead, second 18). Additionally, posterior actin accumulation forming a cup-like structure is evident that increases in intensity and appears to shape the posterior pole during the last stage of invasion (red arrowhead, seconds 18 - 21).

The nuclear signal can also be binarized and followed through the invasion process using a process that recognises and measures the shape or contour of the structure. The Icy imaging software plugin called “Contour Analysis” allows the analysis of a wide variety of factors, including speed, shape and diameter in 2D imaging (De Chaumont *et al.*, 2012). By using this tool, the nucleus diameter was measured by a horizontal transversal in the middle depicting nucleus constriction upon passing through the TJ (seconds 14 - 18, orange arrowhead, Figure 5-5 C). By using a similar procedure for the body of the parasite, the posterior pole of the parasite can also be measured and followed through invasion. This analysis yielded a posterior pole with a diameter that is reduced once the nucleus needs to go

through. This reduction becomes more apparent once the nucleus is finishing passing through the TJ and it is usually defined as the deformability index in cellular transmigration (Muller, 2013) (Figure 5-5 D).

In cases where an F-actin ring is not apparent (yellow arrowhead, second 18, Figure 5-5 B, Movie S14), strong F-actin accumulation still occurs at the posterior pole (red arrowheads). The nucleus on the other hand, appears to be not or less constricted (orange arrowheads). By posterior contour analysis, the nucleus appears to not possess a constriction phase (Figure 5-5 E), while the posterior pole does present a decrease in the diameter (Figure 5-5 F).

Together, these data suggest *Toxoplasma gondii* actin contributes to invasion by creating a continuous structure along the F-actin ring in the TJ with the posterior end where a cup-like structure is formed to allow pushing of the nucleus during invasion. Since the F-actin accumulation in the posterior pole of the parasite is present regardless of a visible F-actin ring, it could suggest a pushing mechanism that is important for the overall invasion process.



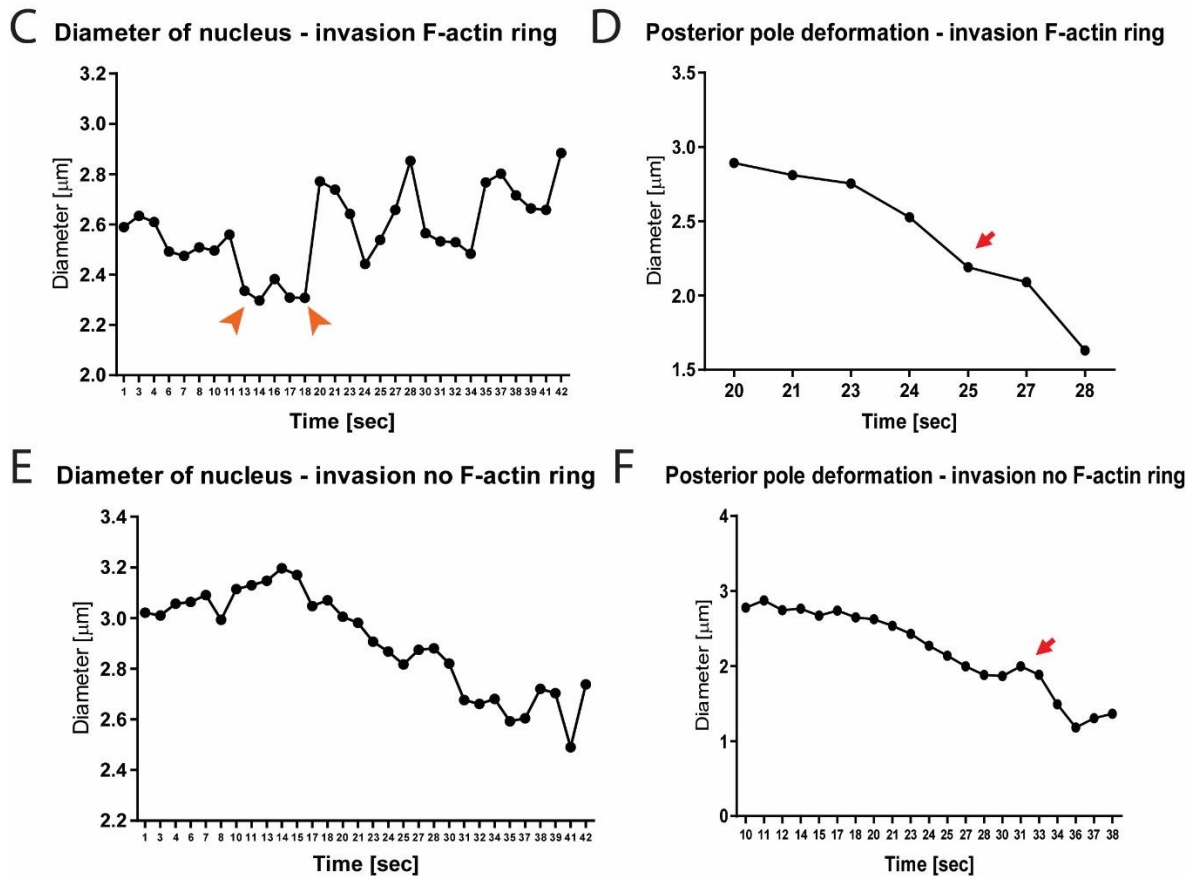


Figure 5-5 Time lapse analysis of parasites that show accumulation of F-actin at the junction. **A.** Time-lapse analysis of invading RH Cb-EmeraldFP parasites. During penetration, an F-actin ring is formed at the TJ. The nucleus (purple) is squeezed through the TJ (red arrowhead) and posterior F-actin appears to be directly connected to the nucleus. Actin accumulation at the posterior pole of the parasite (blue arrow). **B.** During penetration, no F-actin ring is formed at the TJ and the nucleus (purple) is squeezed through the TJ (red arrowhead) and posterior F-actin appears to be directly connected to the nucleus. Actin accumulation at the posterior pole of the parasite. **C, E.** Analysis of nucleus deformation during live imaging shown in A and B. The nucleus appears to constrict once its passing through the TJ F-actin ring as show above (A). This is represented by a decrease of around 300nm in the diameter of the nucleus (red arrow). In the case of no F-actin ring, the nucleus appears to not change shape during this process. **D, F.** The posterior end of the parasite also deforms during the invasion process. F-actin is accumulated during invasion, with the posterior end acquiring a more rounded shape. This changes once the nucleus has passed through the TJ in both cases. Scale bar represents 5 μm . Stills generated from MovieS14. Numbers indicate minutes:seconds. Scale bar represents 5 μm . White arrow points to direction of invasion.

5.5 Super-resolution SIM analysis of invading parasites

Super-resolution Structure Illumination Microscopy (SR-SIM) was also applied to fixed samples of invading parasites. During this process, perinuclear F-actin is detected in connection to both the F-actin ring and the posterior actin cup (green arrowhead, Figure 5-6 A). This association appears to not depend on the presence of the F-actin ring at the TJ (Figure 5-6 A).

Higher eukaryotic cells present complex dynamics during migration (Petrie and Yamada, 2015). The nucleus is usually positioned at the back of the cell during migration with actomyosin contractility as a requirement for this nuclear position. Additionally, an F-actin cage is generated by the help of formins and Arp2/3 complexes along with microtubule (MT) structures surrounding the actin cage (Gomes, Jani and Gundersen, 2005; Gundersen *et al.*, 2006; Renkawitz and Sixt, 2016; Schiffhauer *et al.*, 2016; Thiam *et al.*, 2016; Hons *et al.*, 2018). Since *Toxoplasma gondii* cells presented similar dynamics during invasion, the location of microtubules (MT) were assessed.

In *T. gondii*, the MTs cover 2/3 of the parasite body creating a rigid structure starting from the apical tip (Figure 5-6, Movie S15-16). During invasion, this MT structure was deformed when the tachyzoite passed through the TJ (white arrows, Figure 5-6). Once most of the MTs were through the junction, the nucleus was squeezed (orange arrowheads). In some cases, the MTs extended far beyond their normal reach to follow the nucleus (white arrow). These extensions seemed to be depolymerised during the invasion process, as they appeared segmented (white arrow). Interestingly, the microtubules closely aligned to the part of the nucleus that entered through the TJ, while F-actin closely aligned to the posterior part of the nucleus, resulting in a highly polarised cytoskeletal organisation. It is plausible that, akin to other eukaryotes, a coordinated action of microtubule and F-actin based mechanisms supports nuclear entry and deformation through the TJ. F-actin was localised surrounding the nucleus at all times and was particularly apparent at times where the nucleus was squeezed halfway (DNA, orange arrowheads, Figure 5-6 A-C). As previously mentioned, in some cases the F-actin ring was not always present at the TJ, indicating that F-actin accumulation at the TJ is highly dynamic.

Additionally, in the *adf* KD strain, MTs behaved similarly to *wt* although F-actin was severely affected (green arrowheads, Figure 5-6 B, Movie S15-16). In the case of the *myoA* KO, a similar F-actin reorganisation similar to the one described in the Figure 4-2 occurred during invasion. Where F-actin signal appeared to accumulate in the peripheral areas adjacent to the TJ without extending further (green arrowheads).

To summarise, the combined data from fixed invasion assays and SR-SIM imaging demonstrate that the parasite's nucleus is surrounded by F-actin. The filaments appear to adapt a cytoskeletal conformation designed to deform and push the nucleus inside the host cell. It is likely that during invasion, the glideosome provides the traction force for general movement of the parasite through the TJ, while perinuclear actin is critical in order to facilitate nuclear entry. This phenomenon would explain the delayed invasion seen in these mutants as F-actin cannot generate the required force to achieve efficient invasion.

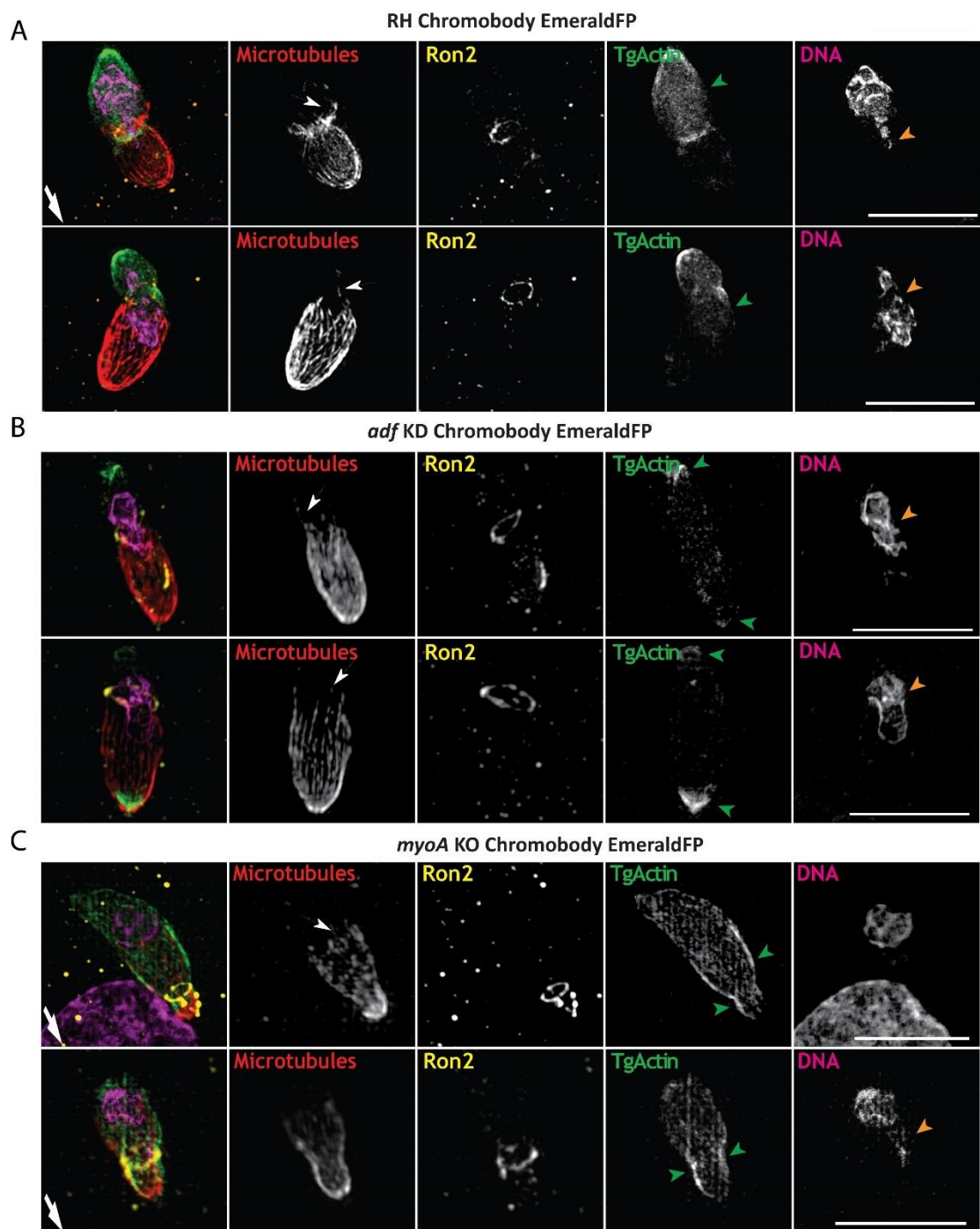


Figure 5-6 Super-resolution microscopy demonstrates formation of a F-actin cage around the nucleus during invasion.

A. SR-SIM images showing three stages of invading wt parasites. SiR-tubulin staining for microtubules (in red) was performed prior to fixation to specifically label microtubules in the parasite. During invasion, the microtubules (MT) are deformed in the TJ area. The nucleus passes through the TJ once most of the MTs have passed. However, the MTs appear to follow the direction of the nucleus where they seem to de-polymerise (white arrow). Accumulation of actin (green arrow) in the posterior still extracellular portion of the parasite forms a polarised F-actin mesh. The nucleus is deformed when it goes across the TJ area as expected (orange arrowhead). **B.** Analysis of AdfKD during invasion. The MTs are deformed in the TJ area and follow the direction of the nucleus. F-actin is accumulated on both ends of the parasite (green arrowheads), with little to no signal anywhere else. This is due to the depletion of the ADF protein, which causes F-actin stabilization upon depletion. The nucleus also appears to suffer less constriction when passing through the TJ. Note that this also coincides with an absence of an F-actin ring. **C.** In the case of the *myoA* KO strain, the MTs also deform when passing through the TJ. However, instead of the usual F-actin distribution during invasion, F-actin appears to be accumulated on the apical end of the parasite and shows a more cytosolic, non-polarised distribution. This signal is particularly strong in the peripheral area where the TJ is located. Even though accumulation of F-actin in the peripheral area is present, no apparent F-actin ring can be observed. Little to no F-actin accumulation can be found on the posterior end of the parasite as well. Scale bar represents 5 μm . See Movie S15-16 for 3D render models. White arrow points to direction of invasion. Images taken alongside Dr. Javier Periz (Meissner Lab).

5.6 Correlative Light-Electron Microscopy analysis of F-actin bundles association with the nucleus

Super-resolution analysis provided important information to complete our model. However, precision is key in order to understand the true location of F-actin during invasion. For this end, correlative light-electron microscopy (CLEM) was performed on parasites expressing Cb-EmeraldFP. This process involved two different microscopy techniques: light microscopy where the sample is prepared as any other immunofluorescence sample and then a specific event is imaged by SR microscopy followed by sample treatment and sectioning for Electronic Transmission Microscopy (TEM) in the same event (Loussert, Forestier and Humbel, 2012; Sueters-Di Meo, Kruit and Hoogenboom, 2016). Both processes need to be applied to the same events in order to combine the two for analysis. Similarly, previous results where F-actin structures were visualised around the nucleus in invading chromobody EmeraldFP parasites in SR-SIM were found. However, TEM microscopy yielded ambiguous results with no apparent actin filaments, although some breakdown products of filamentous actin might be present beneath the IMC (arrows, Figure 5-7 A). The same case was found to be in wt parasites not expressing chromobody EmeraldFP, where possible breakdown filamentous structures are present, yet remain ambiguous whether they are actual filaments and no other membrane structures (Figure 5-7 B).

The ambiguity of the samples and the apparent lack of clear filamentous actin structures can be explained by fast depolymerisation prompted by fixation of the sample. As previously described in chapter 4, sample fixation can create severe effects on the preservation of protein structures, particularly F-actin as the filamentous structures are often less stable than conventional membranes and are prone to depolymerisation.

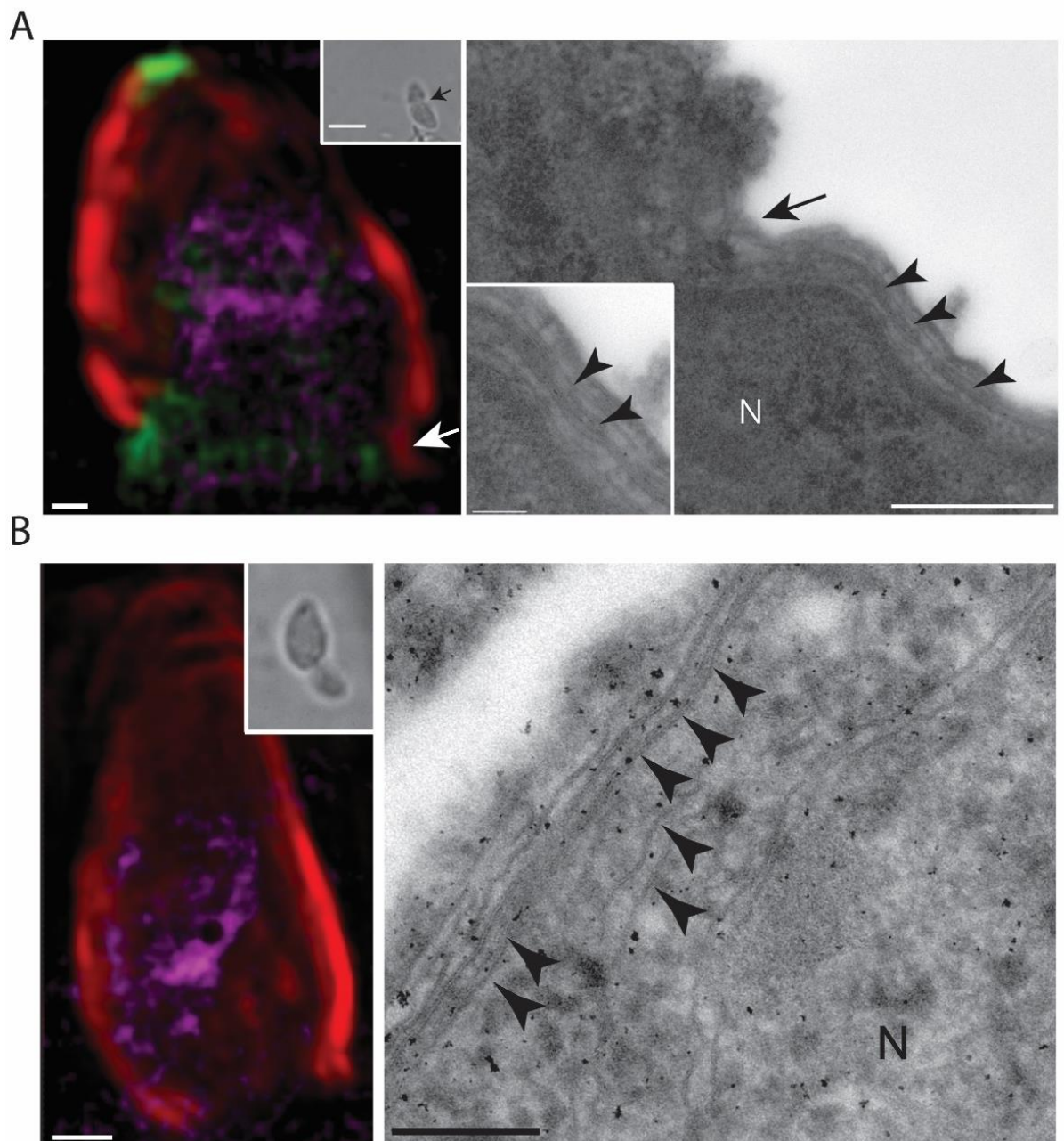


Figure 5-7 Correlative Light and Electron microscopy during invasion.

A. CLEM of invading EmeraldFP. SAG1 staining (in red) indicates the membrane part still outside during penetration; magenta indicates the parasites' nucleus (N). Black arrow shows the constriction during invasion (bright field insets). Note the accumulation of actin (in green) at the tight-junction area (white arrow). A thin section of the same constriction area is shown, in TEM. Although breakdown products of F-actin might be present (black arrowheads) beneath the IMC of the parasite,

no F-actin is visible between the IMC and the plasma membrane. **B.** CLEM of invading *wt* parasites. A thin section of the same constriction area is shown, in TEM. Although potential breakdown products of F-actin appear to be present (black arrowheads) beneath the IMC of the parasite, no F-actin is visible between the IMC and the plasma membrane. Scale bars represent 200nm. CLEM done by Dr. Leandro Lemgruber (III Institute, University of Glasgow).

5.7 *Toxoplasma gondii* F-actin-nucleus association

As previously described in *Plasmodium falciparum* parasites (Angrisano, Riglar, *et al.*, 2012), the F-actin accumulation in the TJ occurs slightly behind the RON complex junctional ring (light blue arrow, Figure 5-8 B). However, this association is not exclusive with the TJ as the F-actin ring strongly appears along the portion of the parasite's body that remains outside during invasion (white arrow, Figure 5-8 A). This association is more apparent when several sections (Z) are visualised (Z=0 and Z=6).

During the invasion process a rigid structure such as the nucleus needs to go through the TJ, which as shown previously is much smaller in diameter (Guilluy *et al.*, 2014). To manage this task, the nucleus is constricted when going through the TJ. During this process, F-actin appears to be localised in the vicinity of the nucleus reminiscent of higher eukaryotic cells during migration (Thiam *et al.*, 2016). During higher eukaryotic cell migration, a concerted action of formins and Arp2/3 complexes are known to generate a cage-like structure around the nucleus that has been associated with nuclear protection and force generation for nucleus displacement when migrating through tight spaces (Guilluy *et al.*, 2014; Petrie and Yamada, 2015; Schiffhauer *et al.*, 2016; Thiam *et al.*, 2016). Since *Toxoplasma gondii* parasites exhibit a similar behaviour to higher eukaryotes during migration, and since F-actin appears to form a continuum across the extracellular portion of the parasite during invasion, association with the nucleus during the invasion process was also assessed based on observation. Invading parasites were fixed mid invasion and a tight junction assay was carried out. F-actin signal accumulation in close proximity to the nucleus was then analysed and counted as positives (Figure 5-8 C). RH parasites along with uninduced *adf* KD parasites showed the largest percentage of invading parasites presenting F-actin association with the nucleus, showing ~60% of positive cases. However, once ADF was depleted upon ATc treatment, no association was observed. When *myoA* KO

parasites were assessed, half of positive events were found (~30%) when compared to the wt.

Given these results, circumstantial evidence points out that F-actin might be forming a supportive structure around the nucleus during invasion which leads to the hypothesis that *Toxoplasma gondii* parasites are exhibiting a similar behaviour as higher eukaryotic migrating cells. This behaviour has also been described in Red-Blood Cells (RBCs), where they need to deform to pass through narrow capillaries (Dobbe *et al.*, 2002). Although RBCs lack a nucleus, the cell body still represents a major obstacle to allow cell movement.

It is possible that F-actin might be forming a cage or a cup-like structure in order to push the nucleus through the TJ and also protecting it from the mechanical forces during invasion. However, the nature of this phenomenon is still unclear, and more work is needed to elucidate the nature of these events.

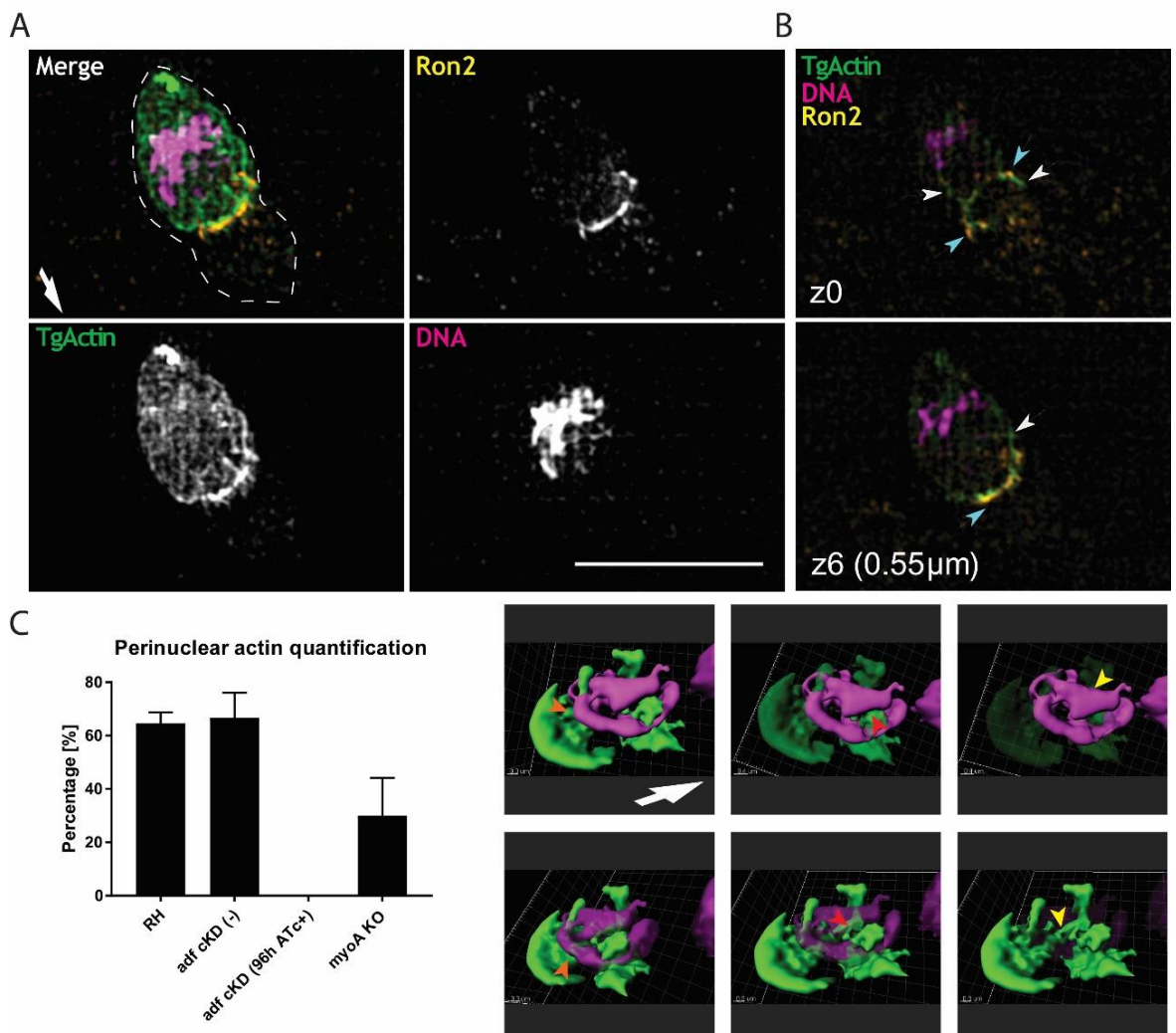


Figure 5-8 Super-resolution microscopy demonstrates formation of a F-actin cage around the nucleus during invasion.

A. SR image of an invading parasite. The F-actin mesh is apparent on the portion that is still outside the host cell and is most likely supporting the nucleus during the invasion process. **B.** F-actin localisation in relation to the TJ during invasion. F-actin is closely associated to the Ron2 ring in the TJ during invasion. **C.** Quantification of perinuclear actin. A minimum of 15 parasites were counted by assessing chromobody EmeraldFP signal as an actin marker around or in the vicinity of the nucleus. Still images to the right represent what was considered as F-actin – nucleus association. The orange arrowhead points to F-actin surrounding the nucleus in the posterior end of the parasite, the red and yellow arrowhead shows F-actin in the vicinity of the nucleus, suggesting a close interaction between the two. Scale bar represents 5 μm . White arrow points to direction of invasion. Analysis of A and B were done by Dr. Javier Periz (Meissner Lab).

5.8 F-actin and nuclear squeeze invasion dynamics in other *Apicomplexan* parasites

In the previous section, *Toxoplasma gondii* invasion processes and F-actin dynamics were assessed. However, these dynamics on *Plasmodium* parasites remained uncharacterised during invasion. In a past study, the roles of actin during the asexual life cycle of both *Toxoplasma gondii* and *Plasmodium falciparum* were found to be different, with actin having a major impact in invasion for *Plasmodium*, as deletion of the *act1* gene resulted in a complete block in invasion (Das *et al.*, 2017).

Invasion assays and localisation analysis of F-actin during merozoite invasion showed a similar distribution of F-actin at the TJ, around the nucleus and at the posterior pole of the parasite (Figure 5-9 A). Fixed immunofluorescence imaging of merozoites in the process of invasion were analysed for F-actin distribution. As with *P. falciparum* and *T. gondii*, F-actin can be detected at the junction, at the onset of invasion (Figure 5-9 A) and supporting our overall observations, F-actin in the merozoite clearly accumulates at the posterior pole during *Plasmodium* invasion of the erythrocyte, in direct contact with the nucleus (Figure 5-9 B). These findings were also found in *Plasmodium knowlesi*, which behaved exactly as *P. falciparum*. The *Plasmodium falciparum* assays were carried out by Sujaan Das from the Meissner Lab and the *Plasmodium knowlesi* experiments by Oliver Lyth from the Baum lab.

These finding could imply that the F-actin dynamics surrounding the invasion process, and the mechanical deformation of the nucleus are conserved mechanism across at least two major *Apicomplexan* groups.

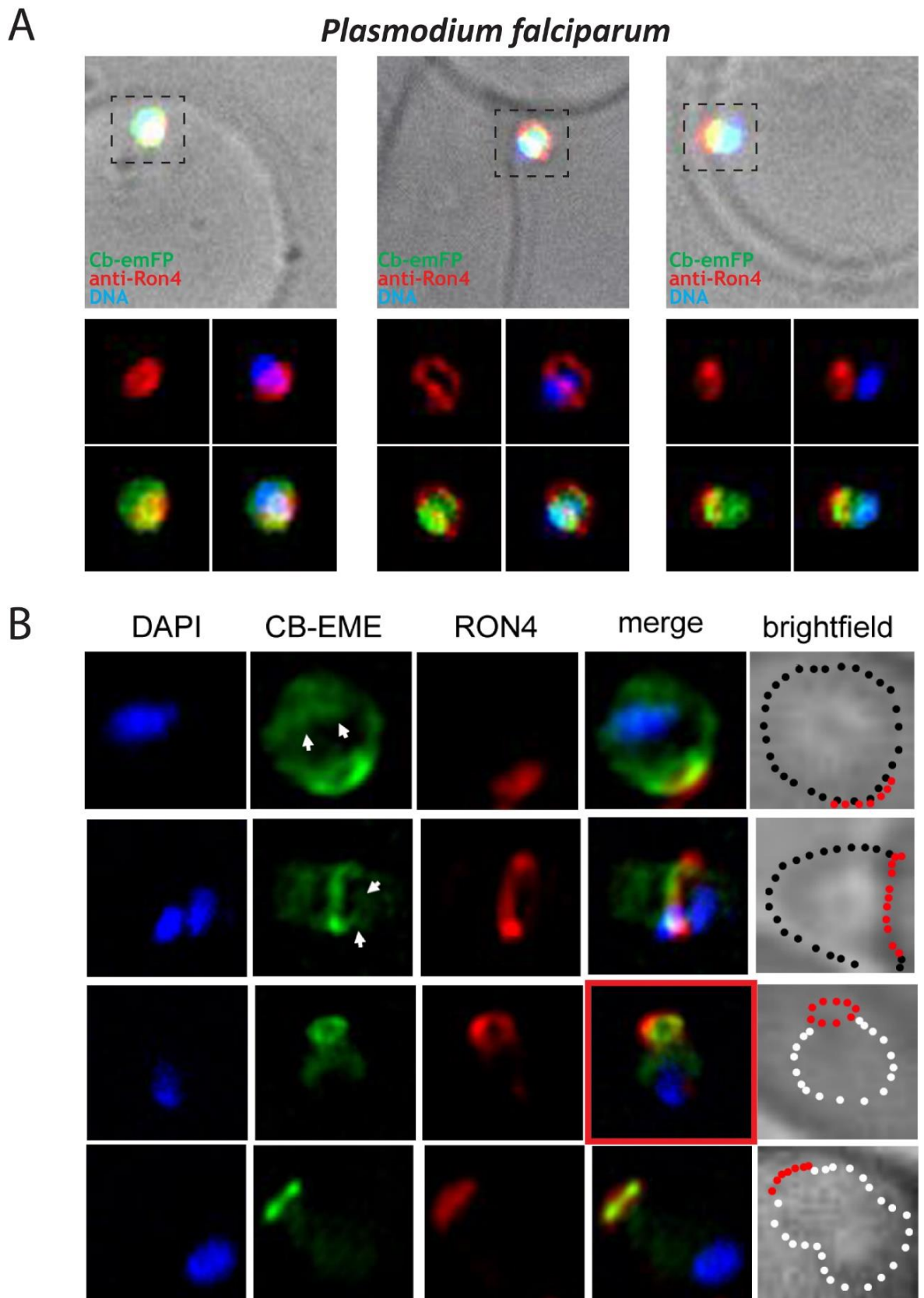


Figure 5-9 Plasmodium spp F-actin dynamics during invasion.

A. IFA showing various stages of invasion of erythrocytes by *P. falciparum* merozoites expressing Cb-EmeraldFP. DAPI labels the nucleus (DNA), Cb-EmeraldFP labels actin filaments (CB-EME, green) and the invasion junction is marked with an anti-RON4 antibody (red). Left panel: a merozoite beginning invasion; note the formation of an F-actin ring (green) behind the RON4 junction (red). Middle panel: A merozoite in the middle of the invasion event; note the constriction of the nucleus (blue) as it passes through the RON4 junction and F-actin colocalising with it (green). Right panel: A

merozoite completing the process of invasion; note the F-actin ring beyond the RON4-junction and actin filaments colocalising with the nucleus. **B.** Super-resolution images showing various stages of invasion of erythrocytes by *P. falciparum* merozoites expressing Cb-EmeraldFP. DAPI labels the nucleus (blue), Cb-EmeraldFP labels actin filaments (CB-EME, green) and the invasion junction is marked with an anti-RON4 antibody (red). Brightfield images have been marked with red dots depicting the junction, black dots depicting merozoite boundary still outside the erythrocyte and white dots depicting a merozoite that has penetrated the host cell. Top panel shows an attached merozoite beginning the process of invasion, the second panel during the process of invasion and the bottom two panels show merozoites completing the process of invasion. White arrows depict actin filaments that colocalise with the nucleus. *Plasmodium spp.* assays were done by Dr. Sujaan Das (Meissner Lab) and Dr. Oliver Lyth (Baum Lab) and presented in Del Rosario et al. 2019.

5.9 Discussion

These results demonstrate similarities in F-actin dynamics between apicomplexan and other eukaryote systems during motility. In other eukaryote systems, the nucleus is actively pushed and pulled along the cell by a concerted action of retrograde actin flow mediated by myosin II, nesprins and other interface proteins between the nucleus and actin, fascin and formins (Gomes, Jani and Gundersen, 2005; Gundersen *et al.*, 2006; Guilluy *et al.*, 2014; Arsenovic *et al.*, 2016; Jayo *et al.*, 2016; Thiam *et al.*, 2016). These complexes mediate intricate perinuclear F-actin structures that are also associated with microtubules. These mechanisms facilitate nuclear movement by pushing and pulling the organelle along with protection and constriction (when going through tight gaps) (Gundersen *et al.*, 2006; Gardel *et al.*, 2010; Petrie and Yamada, 2015; Jayo *et al.*, 2016). *Toxoplasma gondii*, as it needs to invade host cells through a constricted environment, the junction will similarly suffer mechanical deformation of both the cell body and the nucleus. within good agreement, we detected strong perinuclear F-actin and F-actin accumulation in the back of the parasite. Given these similarities between these lower and higher eukaryotes, it is not far-fetched to speculate of a somewhat conserved migration/invasion mechanism across diverse orders of eukaryotes. This is also somewhat apparent when other cell behaviour is analysed such as RBCs, where they need to deform to pass through capillaries (Dobbe *et al.*, 2002) limited only by their size, as their deformability index depends on the size of the cell (Park *et al.*, 2016). Other cells such as leukocytes, need to reach damaged tissues to promote healing. During tissue damage events, neutrophils leave the blood vessels to the location of the injury in a phenomenon termed leukocyte extravasation (Muller, 2013).

Beside the parallels between apicomplexan parasites and other eukaryote systems, these results allow to reconcile discrepancies in the phenotypic characteristics of invasion and the role of actin and the glideosome. During invasion, the actomyosin complex localised in the sub-pellicular compartment between the IMC and PM generates traction forces at the TJ to initiate and allow invasion. However, the nucleus presents a notable barrier for this invasion process that very likely requires the concerted action of cytoplasmic actin sources to allow deformation and pushing. This very likely also requires subpellicular microtubules to allow the nucleus to go through as a barrier to be deformed and pushed into the host cell.

A more detailed discussion of all resulting data can be found in the next chapter, where all data contained in this thesis is consolidated in a proposed model for F-actin dynamics during invasion.

6 Discussion

Actin in Apicomplexa was originally linked to gliding motility and invasion during extracellular life and apicoplast inheritance during the intracellular stage (Poupel and Tardieux, 1999; Gaskins *et al.*, 2004; Heintzelman, 2015; Periz *et al.*, 2017). Although critical for efficient motility and invasion, recent results demonstrated that parasites are still able to move and invade in the absence of critical components of the glideosome, which has been attributed to redundancies in the repertoire of myosins. However, even depletion of *Act1* did not completely block motility and invasion, suggesting additional/alternative mechanisms that can partially compensate for the loss of the linear motor. Previously it was impossible to correlate the suggested function of F-actin with its localisation during these processes (Andenmatten *et al.*, 2013; Egarter *et al.*, 2014; Whitelaw *et al.*, 2017).

By expressing chromobodies that recognise actin in apicomplexan parasites, our group managed to uncover previously unknown actin functions and structures during the lytic cycle (Periz *et al.*, 2017). Despite initial scepticism regarding the physiological relevance of the chromobody signal in *Toxoplasma gondii*, emerging studies have proven its usefulness (Del Rosario *et al.*, accepted; Periz *et al.*, 2017, 2019; Felix Stortz *et al.*, 2019; Tosetti *et al.*, 2019). However, establishment of new pipelines for data acquisition and analysis will be required to reach the state of the art seen in other model systems analysing the dynamic and function of actin. Additionally, more in-depth characterisation of the chromobody is needed as no information regarding the exact molecular dynamics of the actin nanobody - actin interaction currently exists. For this end, in vitro assays are possibly the best way to assess polymerisation rates and determine whether the chromobody causes significant interference in regular actin dynamics.

The data gathered in this thesis uses several approaches to dissect the dynamics of F-actin during invasion and replication, from classical genetical manipulation to complex super-resolution microscopy analysis. This approach allowed us to generate a new model of how *Toxoplasma gondii* actin dynamics work throughout the asexual cycle of the parasite, ranging from the bi-directional flow of actin during replication that can sustain different functions including vesicular trafficking and recycling, to mechanical constriction and displacement of the nucleus during invasion. From this study it became obvious that, similar to other

eukaryotes, F-actin in apicomplexan parasites fulfils multiple functions, from vesicular transport, organellar division to motility and invasion.

6.1 F-actin flow, nucleation points and parasite replication.

During parasite replication, actin dynamics were observed behaving in flow-like patterns, where directionality is not easily distinguishable by eye. However, three accumulation points are easily identifiable as they appear to be brighter than the rest of the signal in the parasite body (Figure 3-3). The F-actin appeared to concentrate at the apical tip of the parasite (yellow arrowhead), the central or Golgi area (red arrowhead) and the residual body (green arrowhead). Moreover, recent studies reanalysed the localisation of these formins, showing correlation with these nucleation centres with FRM1 located in the apical tip, FRM2 in the central region and FRM3 in the residual body (Tosetti et al. 2019; Stortz et al. 2019). From these nucleation centres, both the central (FRM2) and the residual body (FRM3) centre appeared to be the brightest during replication. However, the flow itself can be seen moving to and from these sources without a well-defined direction. To solve this issue, kymograph analysis was adapted that allows the tracking of F-actin flow in the areas where it was apparent (Figure 4-8 A, C), confirming that the actin flow was bi-directional.

This bi-directionality actin flow allows the translocation of F-actin and potentially its cargo across the whole parasite body. Initial data found in Periz et al, 2017 suggested that these filamentous actin structures could permit displacement of different molecules using actin to support cargo transport, which would suit this bi-directional movement. In a recent study, these filamentous actin tracks have been shown to associate with micronemes within the parasite that are transported along F-actin. In addition, it is very likely that these filamentous structures also support communication between daughter cells, allowing recycling of molecules (Periz et al. 2019).

How the short F-actin filaments are translocated is currently unknown. 13 myosins have been described for *Toxoplasma gondii* (Sharma and Chitnis, 2013) and could

fulfil overlapping functions to ensure F-actin dynamics, as suggested previously for MyoA (Fréchal *et al.*, 2014). Albeit myosin-powered translocation of F-actin is possible, the fast-directed movement observed during time-lapse microscopy could also be based in a rapid polymerisation and de-polymerisation rate of apicomplexan actin itself (Kumpula *et al.*, 2017, 2018). Interestingly, analysis of myosin A null-mutants expressing chromobody EmeraldFP failed to show a significant difference in F-actin flow, as long as microneme secretion or gliding motility was not stimulated. This result supports the idea that myosin A is involved in processes related to motility (Egarter *et al.*, 2014; Whitelaw *et al.*, 2017), as F-actin dynamics were comparatively different upon stimulation of microneme secretion and gliding motility.

As expected, genetic manipulation or use of drugs targeting actin or actin polymerisation affected actin flow. Jasplakinolide is a drug that stabilises actin on relatively low concentrations (0.25 μM for 30 min). This effect manifests as an accumulation of F-actin in both the apical and posterior end, and relatively little to no flow can be detected at the periphery or in the cytoplasm. The effect of *adf* KD presented a similar effect, with strong accumulation of actin in both ends as published previously (Mehta and Sibley 2011; Periz *et al.*, 2017). Even though the effects on F-actin dynamics caused by JAS and the depletion of *adf* are similar, the cause is probably different. JAS has been described as forming new binding sites between actin monomers, promoting stabilisation and limiting actin depolymerisation (Gavin and Holzinger, 2003; Tannert *et al.*, 2010; Pospich *et al.*, 2017). This effect likely forms long filamentous structures that cannot be depolymerised or severed, which are then transported to both ends where they accumulate (Gavin and Holzinger, 2003). In the case of the depletion of ADF, unrestrained polymerisation due to the absence of filament severing likely results in a very low monomeric to filamentous actin ratio (G:F-actin). ADF/cofilin has been shown to enhance the rate of actin filament turnover due to their depolymerisation action that allows faster replenishment of actin monomers in the available pool. For this reason, lack of severing lead to the accumulation of actin filamentous structures as reported in other eukaryotes. Curiously, the unstable nature of *T. gondii* filamentous actin would suggest a different scenario, as rapid depolymerisation of actin filaments were expected. However, accumulation in both ends of the parasite mimics phenotypes observed in other

eukaryotes, that reported filamentous actin structures (stress fibers predominantly) accumulation associated with enlarged focal adhesion sites at the plasma membrane (Hotulainen *et al.*, 2004; Kanellos *et al.*, 2015).

How these filaments end up specifically at both ends could be explained by the actin flow. During replication, three nucleation centres appear in the parasite. However, the central nucleation centre appears to present more prevalent dynamics that feeds the peripheral area and the RB. In a previous study FRM1 was associated with motility and invasion, as a KO in FRM1 led to a decrease in invasion events, while FRM2 and FRM3 showed no effect (Tosetti *et al.*, 2019). Due to FRM2 localization in the central area close to the Golgi or apicoplast and FRM3 in the RB, it is likely that actin is predominantly polymerised in the central nucleation centre as *T.gondii* FRM2 KOs presented a lack of central polymerisation centre (Stortz *et al.*, 2019). From this nucleation centre, F-actin is translocated to the periphery where it will accumulate in the apical end. This nucleation centre could help polymerise actin further, which will then flow towards the posterior end. It is important to note that this F-actin flow goes in both directions (bi-directional), with stronger retrograde flow supporting trafficking of molecules along the way. For this reason, it is possible to hypothesise that once F-actin reaches the posterior end, it is likely to remain there with some filaments going in an anterograde manner towards the apical end and some others translocated to the RB and then onto other daughter cells by the action of myosin F, as myosin F was suggested to allow parasite-to-parasite connection during replication (Jacot, Daher and Soldati-Favre, 2013; Frénal, Jacot, *et al.*, 2017). Additionally, F-actin likely depolymerises at the posterior end, as the accumulation in the posterior end of the parasite disappears following invasion. This model would explain why F-actin is accumulated when it is stabilised, as both ends of the parasite appear to allow F-actin accumulation (Figure 6-1). Future experiments will be able to address the polymerisation and depolymerisation events at the accumulation centres in detail. Initial efforts were done by using Fluorescence recovery after photobleaching (FRAP and photo-switchable proteins experiments, but the size of the sample, the speed of the dynamics and the resolution limit lead to inconclusive results (Dr. Javier Periz and Prof. Markus Meissner, *personal communication*).

The exact nature of the actin transport during this process remains to be identified. However, myosins L or G are likely candidates as they are present in the periphery and the cytoplasm, respectively (Frénal, Jacot, *et al.*, 2017). For future studies, genetic manipulation to KO these myosins would benefit this model, especially considering that myosin A KO parasites present regular F-actin flow dynamics in non-stimulated parasites. It is also important to dissect the role of the FRMs during replication, as KO mutants in both FRM2 and 3 could provide important information to validate this model.

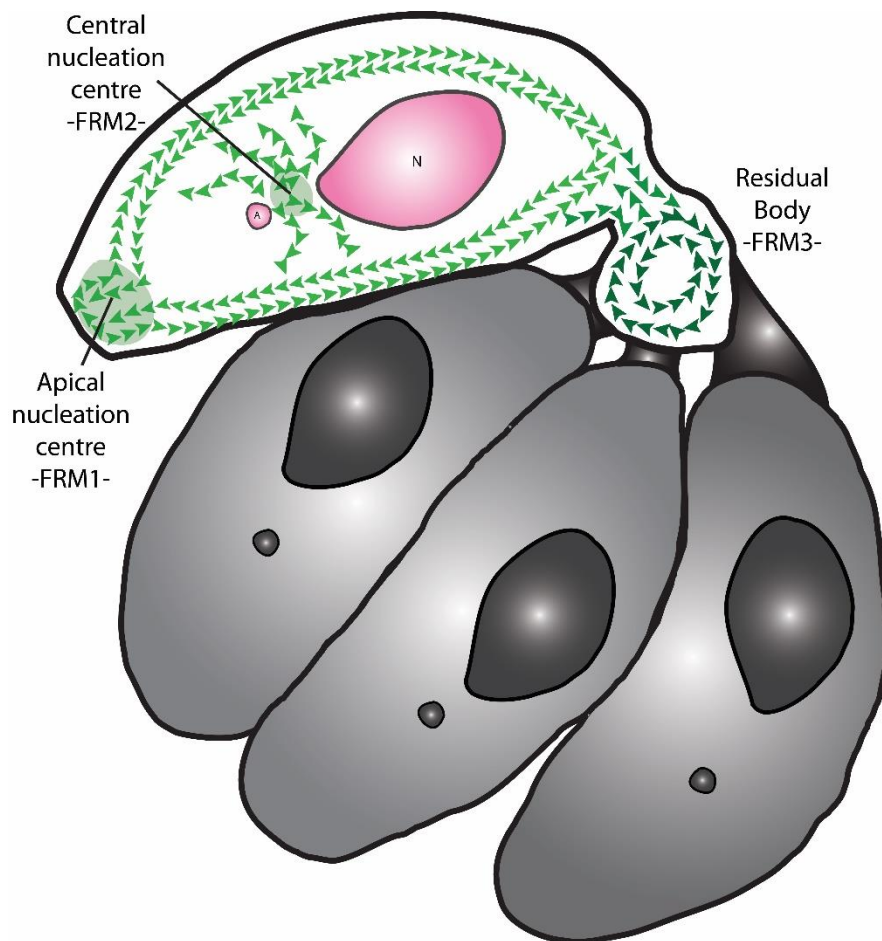


Figure 6-1 *Toxoplasma gondii* filamentous actin flow model in replicating parasites.

During parasite replication, F-actin flows from the Central nucleation centre towards the periphery. The bi-directional flow would then translocate actin filaments towards both ends where actin can be accumulated. The F-actin that accumulates in the posterior end can then be translocated to the RB and other daughter cells by the actions of myosin F. A - apicoplast; N - nucleus. Darker actin in the RB points to more intense actin signal.

6.2 Immobile extracellular parasites and actin flow

The major function of actin in extracellular parasites appears to be the promotion of motility and host cell invasion, while in intracellular parasites it plays critical roles for apicoplast division and organellar recycling (Periz et al. 2019). As shown in the previous section, during replication, parasites display a flow in two directions, with emphasis towards a retrograde flow. Once the parasites egress and initiate gliding, strong accumulation occurs at the apical and posterior end. Interestingly, these accumulation points correlate well with the focal adhesion points described for *Plasmodium* sporozoites measured with RICM and TFM, where the sporozoite glides by using a combination of both ends of its body as strong attachment points while the rest of the body engages in weaker attachment, leading to a model, called stick-and-slip that proposes that parasite motility depends on the fast turnover of attachment sites at the posterior and apical pole of the parasite (Münter *et al.*, 2009). An additional point to come to terms with this model is to hypothesise that the observed F-actin accumulation points are enriched with adhesin proteins, such as MIC2 to allow attachment. This is further supported by the fact that mutants for components of the acto-myosin system, such as Act1, MLC1 or MIC2 are reduced in attachment strength (Whitelaw *et al.*, 2017). Thus, actin would flow from the cytoplasm to the focal adhesion points to allow formation of attachment sites. Subsequently posterior attachment sites are formed at the posterior end, allowing motility by stick-and-slip. However, the exact nature of the actin flow and turnover of attachment sites during gliding remains to be described. This remains challenging, as rapidly moving parasites move in and out of the plane of focus abruptly, making imaging difficult; the application of image stabilisation processes to measure actin flow may aid in these experiments. In addition, the force needed to achieve attachment remains poorly understood. Analysis by TFM (Traction Force Microscopy) would be able to measure and characterised the force exertion from the parasite to allow attachment. The protein-to-protein interaction in these attachment points also remain unknown. Analysis by TIRF (Total Internal Reflection Fluorescence Microscope) microscopy could provide insight on the nature of the actin-adhesion interplay that facilitates traction. A combination of the two, such as STFM (Super-Resolved Traction Force Microscopy) would allow to accurately discern the forces at play along with 3D

motility assays, as the parasite has shown different gliding behaviour in a 3D matrix.

If parasites are allowed to rest in conditions where no serum is present, no gliding motility occurs and the actin flow appears similar to the description in Figure 6-1, akin to intracellular parasites (Figure 6-2 A). The nucleation centres appear to re-arrange upon the addition of drugs that interact with the calcium signalling pathway of the parasites. Calcium signalling and stable calcium ion levels are important throughout the lytic cycle of apicomplexan parasites, and have been linked to gliding motility, invasion and egress (Garrison *et al.*, 2012; McCoy *et al.*, 2012; Lourido and Moreno, 2015). If this pathway is activated, for example through calcium ionophore A23187 treatment, strong relocalisation of F-actin to the apical and basal end occurs in wild type parasites. (Figure 6-2 B). A23187 is a calcium homeostasis-altering drug that triggers egress by affecting Na^+/H^+ exchangers (NHEs) which are localised in the plasma membrane of the parasite (Koltzschner *et al.*, 2003; Arrizabalaga *et al.*, 2004). Comparatively, when a different drug is added such BIPPO (Howard *et al.*, 2015), strong relocalisation of F-actin towards both ends of the parasite occurs with basal accumulation as the more prevalent type of accumulation. (Figure 6-2 E). BIPPO has been suggested as being responsible in the activation of microneme secretion and egress by modulating the signal pathway of PKG-dependant processes. Since both A23187 and BIPPO trigger microneme secretion and egress, a similar effect was expected. Furthermore, the parasites resting in serum-free media were not triggered by A23187 for motility, although actin was translocated to the apical or posterior end. BIPPO appears to weakly prime the parasite for motility in serum-free conditions as more gliding events were observed.

In the case of *adf* KD, actin is stabilised and dynamics completely disappears, impeding further relocation events even when stimulated by both A23187 and BIPPO (Figure 6-2 C, F). This effect is likely due to the inability to relocate actin due to stabilisation as *adf* KD parasite were also primed for gliding upon BIPPO treatment. If *myoA* KO parasites are treated with either A23187 or BIPPO, relocalisation of actin occurs towards the apical end. However, the actin flow appears to become arrested at the periphery close to the apical end without further movement. This effect can be hypothesised to occur due to the lack of

myosin A, a myosin involved in both gliding and invasion. FRM1 would nucleate F-actin in the apical end and, since myosin A is no longer present in the periphery, F-actin cannot easily migrate through and becomes stuck (Figure 6-2 D, G). This would explain why the parasite still manages to present correct attachment, as the apical end can be used for this function; or small actin pools in the cytoplasm could be redirected towards the posterior end as in rare cases, some invading *myoA* KO mutants presented actin accumulation in the posterior end (Figure 5-3, E).

Lastly, the F-actin flow appears to occur within the cytosol of the parasite and skeleton analysis suggests that short F-actin filaments are transported, forming a continuous “network” within the cytosol. Even in case of *MyoAKO* parasites F-actin filaments seen at the periphery appear to be formed in the cytosol. However, more work is needed to elucidate these dynamics, perhaps by a combination of IMC markers, actin chromobodies and high-speed super-resolution microscopy, to correctly trace filamentous actin networks.

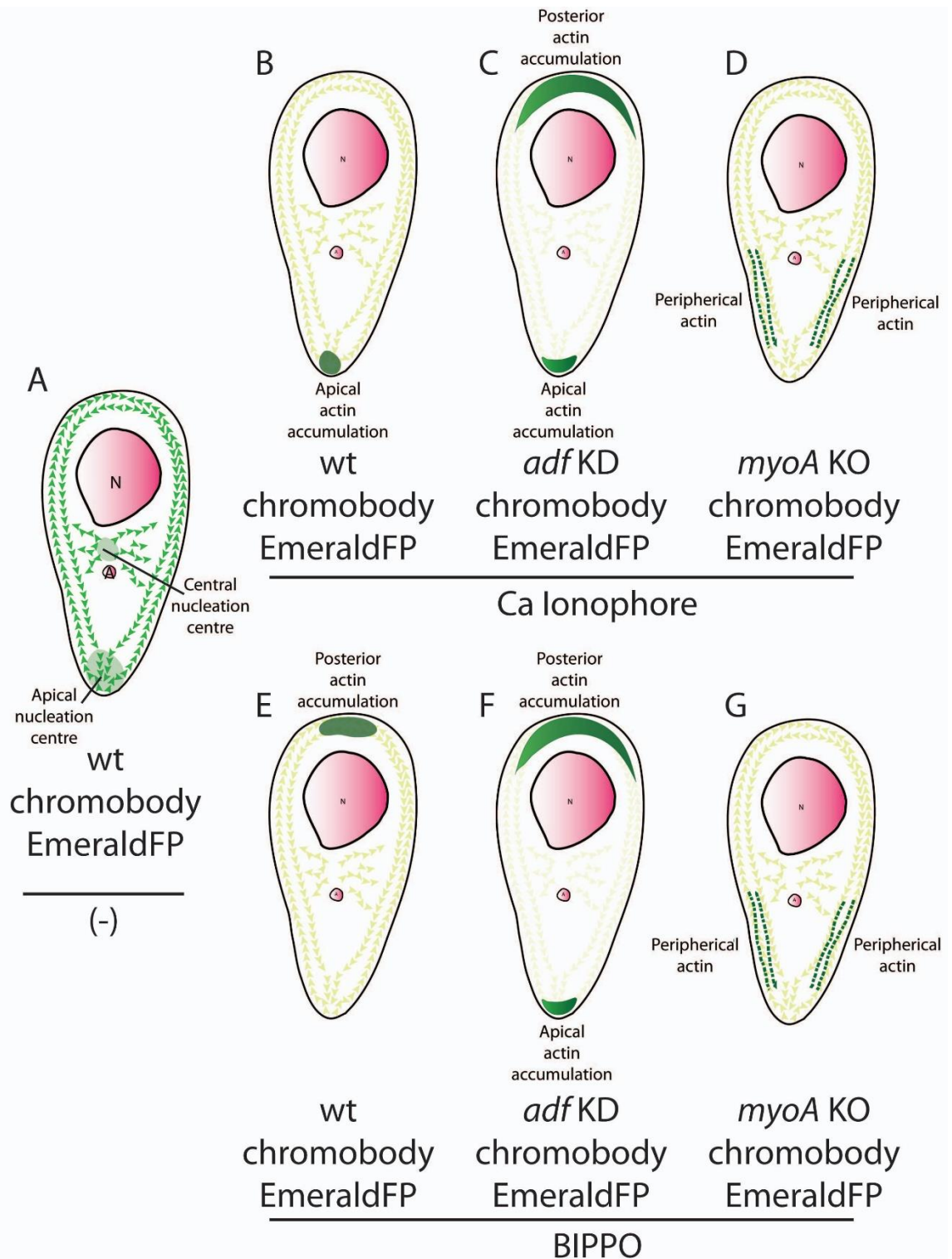


Figure 6-2 *Toxoplasma gondii* flow model in extracellular parasites.

A. Wild type parasite expressing chromobody EmeraldFP without drug treatments. **B.** Wild type parasite expressing chromobody EmeraldFP with Ca ionophore treatment. Note the accumulation is more prominent in the apical end. **C.** *adf* KD parasites expressing chromobody EmeraldFP with Ca ionophore treatment. Strong F-actin stabilisation occurs with the depletion of ADF, which in turn stops further actin re-arrangement even when drugs that target egress and invasion pathways are present. **D.** *myoA* KO parasites expressing chromobody EmeraldFP with Ca ionophore treatment. F-actin accumulates to the periphery close to the apical end. Myosin A has been associated with gliding and invasion, resulting in the inability to translocate actin to generate force for movement. **E.** Wild type parasite expressing chromobody EmeraldFP with BIPPO treatment. Note the accumulation in the posterior end. **F.** *adf* KD parasites expressing chromobody EmeraldFP with BIPPO treatments same

effect as (C). **G.** *myoA* KO parasites expressing chromobody EmeraldFP with BIPPO treatment. Same effect as seen in (D). A - apicoplast; N - nucleus.

6.3 *Toxoplasma gondii* invasion: new perspectives on actin dynamics during invasion

During invasion, the parasite suffers mechanical deformation that is likely detrimental to its fitness unless a compensatory mechanism to deal with the potential damage or stress is present (Del Rosario *et al.*, accepted; Bichet *et al.*, 2016). During invasion, both *Toxoplasma gondii* and *Plasmodium falciparum* parasites suffer physical deformation when passing through the TJ. This deformation also affects other organelles large enough to require shape changes on their own, such as the nucleus. Other eukaryotic cells, such as mammalian ones, experience similar issues during migration, particularly when cells need to traverse tight gaps such as spaces between cells or blood vessels (Gundersen *et al.*, 2006; Petrie and Yamada, 2015; Schwarz and Leube, 2016). Several studies have observed the deformation indexes needed for RBCs to pass through small capillaries (Dobbe *et al.*, 2002; Fu *et al.*, 2012; Davidson *et al.*, 2014). Additionally, extravasation of leukocytes from blood capillaries into tissues to reach sites of cellular damage in an event called transmigration, represents another example of cells actively regulating its shape and suffering physical deformation in order to perform a function (Stoitzner *et al.*, 2002; Muller, 2013).

This is done by a concerted action of actin flow mediated by nucleation factors such as formin, Arp2/3 and coronin, polymerisation factors such as profilin and depolymerisation factors such as ADF/cofilin and gelsolin but also by type II myosins that translocate the flow in a specific direction and interface proteins that link actin and the nucleus such as nesprin and SUN proteins in the LINC (Linker of Nucleoskeleton and Cytoskeleton) complex regulating the nucleus movement and mechanotransduction (Goley and Welch, 2006; Guilluy *et al.*, 2014; Arsenovic *et al.*, 2016; Jayo *et al.*, 2016; Thiam *et al.*, 2016). All these factors together allow the formation of intricate perinuclear F-actin structures connected to microtubule cages allowing extra support to the structure.

The complex interplay of the previously mentioned factors is in place to protect the nucleus and allow ease of movement during cell migration. Additionally, actomyosin complexes allow pushing and pulling of this cage, effectively moving the nucleus along with the cell (Petrie and Yamada, 2015; Thiam *et al.*, 2016). As apicomplexan parasites encounter similar mechanical deformation during motility through tissue or, especially during host cell invasion, it is possible that a conserved mechanism exists between disparate eukaryotes to counteract these forces and prevent cellular damage while undergoing deformation. Lastly, the nucleus piston-like mechanism described in mammalian cells to allow nucleus translocation in tight gaps (Petrie, Koo and Yamada, 2014) along with the osmotic stress-force generation (Petrie *et al.*, 2012) by the translocation of the nucleus propose an interesting concept to pursue in apicomplexan parasites, given that both eukaryotic cells appear to behave similarly in these migratory conditions.

Several discrepancies exist about the role of actin and the complex machinery behind gliding and invasion in apicomplexan parasites; the present work provides an opportunity to reconcile some of them (Drewry and Sibley, 2015; Heintzelman, 2015; Bichet *et al.*, 2016). Although computational F-actin flow dynamics were not analysed in moving parasites, the effects exhibited from the use of drugs such as A23187 and BIPPO along with the *myoA* KO mutant in extracellular resting ones shows that the flow of actin in extracellular parasites is more likely one-directional, from the nucleation centre in the apical tip (FRM1) towards the rear of the parasite. Upon reaching the posterior end of the parasite, this actin flow would be ready to interact and connect to other F-actin pools in the cytoplasm, forming a continuous dynamic structure, as observed in the super resolution microscopy presented in this work (Figure 5-3 A, Figure 5-7 A). Once the cytoplasmatic pools are connected, F-actin association with the nucleus would occur (Figure 6-3 A). The very same F-actin dynamics appears to be also involved in the accumulation of F-actin at the TJ, as both SR-SIM and CLEM imaging showed close association of filamentous actin with the nucleus below the IMC (Figure 5-8 A, Figure 5-9 A, B). Whether this F-actin ring structure facilitates nuclear constriction remains to be fully tested. However, mutants lacking an F-actin ring appear to present a slight decrease in nuclear constriction, although more biophysical experiments need to be done to fully support this hypothesis (Figure

5-1 D). Another possible explanation is that the F-actin ring works as a supportive structure, counteracting the forces exerted by the host cell on the TJ.

The continuous F-actin meshwork at the posterior end also contracts during the invasion process, in similar fashion to other migrating eukaryotic cells. Since this is a characterised phenomenon in mammalian cells, it is possible that the cytoplasmic pools of F-actin in *Toxoplasma gondii* accumulate in the posterior end to allow the pushing of the nucleus in order to pass through the TJ (Figure 6-3 C).

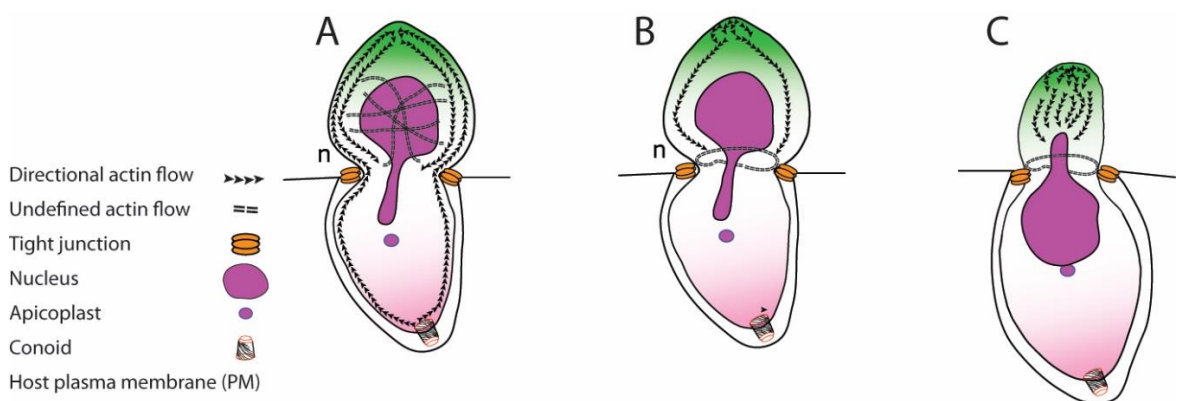


Figure 6-3 Model of actin flow in highly polarised parasites during penetration.

A. FRM1 mediated F-actin polymerisation is translocated by myosin A towards the posterior end. The F-actin pool would then join cytoplasmic actin pools to form perinuclear actin structures. **B.** Cytoplasmic actin originating in the apical tip likely forms the F-actin ring during the beginning of invasion. **C.** The F-actin accumulation in the posterior end of the parasite during invasion can exert force to push the nucleus through the TJ.

Given the results obtained in this study, the model this thesis proposes is that F-actin exists as cytoplasmic pools that could be employed to push the nucleus and control cell shape. Whether this process is linked to potential actin dynamics encountered between the PM and the IMC as suggested by the linear motor goes beyond the scope of this study. However, both processes could exist and synergistically interact during gliding and invasion.

Following the same hypothesis, the proposed model speculates that during invasion, once the parasite reorients and initiates penetration, F-actin is newly polymerised by FRM1 at the apical tip. This newly actin-enriched point would then form a F-actin ring closely associated to the newly formed TJ (Figure 6-4 A, B).

Actin would then be transported via myosin A at the periphery towards the posterior end, as *myoA* KO mutants appears to show peripheral F-actin “trapped” in the peripheral area close to the TJ. Upon reaching the posterior end, it forms a continuum joining other pools of F-actin in the cytoplasm (Figure 6-4 B). The actin filaments would then associate to the nucleus in perinuclear actin structures and the ring would allow physical constriction of the nucleus by a concerted action of a hypothetical actin-nucleus interface proteins, such as the LINC complex in other eukaryotes (Lämmermann *et al.*, 2008; Jayo *et al.*, 2016).

During invasion, the parasite presents a polarised state of actin, with stronger F-actin signal in the portion that is still extracellular and a weaker signal in the portion of the parasite that is intracellular. This continuous F-actin structure in the posterior end can potentially shape the form of the parasite, as parasite lacking F-actin present a distinct bullet-shaped posterior pole (Figure 5-3 C). Since the nucleus also needs to enter through the TJ, another F-actin pool in the posterior end would alter the shape of the parasite and would push the nucleus through the TJ (Figure 6-4 C, D). At this point it is unclear, why ~20% of parasites appear to enter the host cell without formation of an F-actin ring at the TJ. One explanation could be that since the parasite initiates invasion in a seemingly random area of the host cell, it is likely that the resistance it encounters will vary. In areas with less resistance, the host cell membrane would exert less force towards the TJ and, thus, no F-actin ring would be needed. In this case, the nucleus would not be severely constricted, and invasion would appear in a smoother manner without a speed decrease stage shown in cases where an actin ring is present (Figure 5-1 B) (Figure 6-4 E). During the initial invasion step, the F-actin enriched parasite tip is crucial for the initial invasion step, as *myoH* mutants are unable to initiate invasion (Graindorge *et al.*, 2016). Whether this initial actin polymerisation in the apical end of the parasite is necessary for an initial bout of force generation is currently unknown. However, given the nature of the initial fast parasite invasion dynamic depicted in this work, it is a possibility that needs to be analysed. Moreover, given the presence or absence of the F-actin ring at this point, mechanosensing proteins are likely localised in this area (Gregor *et al.*, 2014; Tang, Mehta and Gunst, 2017). These mechanosensing proteins would gauge the permissibility of the host cell membrane (Gregor *et al.*, 2014) and would rapidly alter the dynamics of actin polymerisation at the initial step of invasion.

This mechanism would be particularly useful in events of cellular transmigration, as the parasite would need to travel across different host cell types and having a mechanism to help it discern the correct tool for the cell it's about to invade would prove beneficial to the parasite survival.

The parasite microtubules also appear to play a role in stability during invasion, as they appear to form continuous structures with actin. This function could also be extended to function as a stabiliser allowing the maintenance of cell shape during invasion to correctly manage forces to allow efficient penetration.

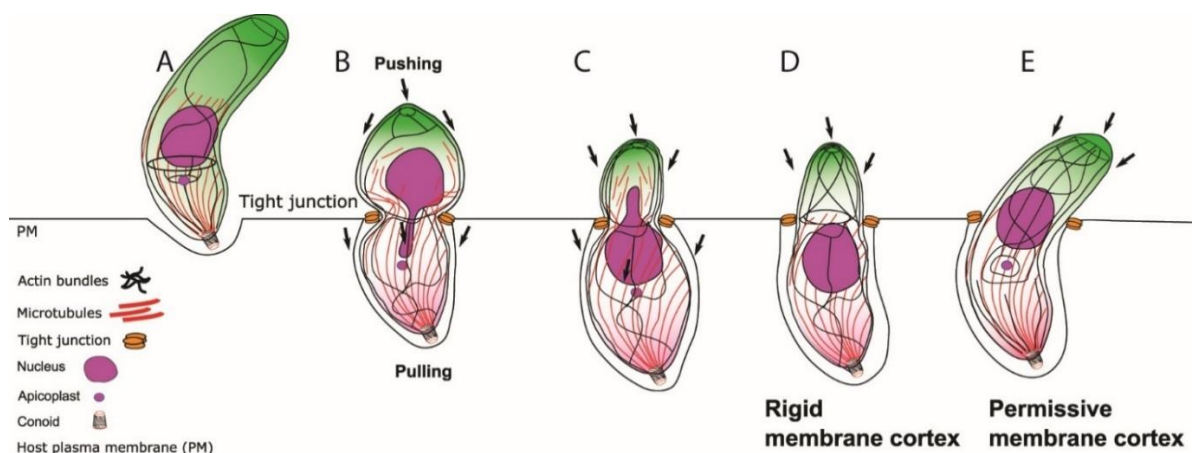


Figure 6-4 Model of the proposed nuclear squeeze mechanism during apicomplexan invasion.

A-D. Once the parasite manages to attach to the surface of a host cell, F-actin strongly accumulates at the posterior pole and at the apical end. During penetration, the junctional complex is formed that contributes to the attachment and stabilisation of the parasite to the host cell in the TJ. F-actin at the TJ provides stability for nuclear entry, while posterior F-actin might provide pushing force to allow nuclear entry. At the same time microtubules might facilitate nuclear entry by pulling the nucleus through the TJ. According to this model, the nucleus is squeezed through the TJ by a pushing-pulling mechanism controlled by actin and potentially microtubules. There is a strong indication that F-actin is polarised during this step, forming a mesh that facilitates control of the parasite portion that is still outside. **E.** In some cases (for example due to more permissive host cells or upon modulation of F-actin dynamics), a F-actin ring at the junction is not required/formed and the nucleus can passively enter the host cell. Model drawn by Dr. Javier Periz and further modified by the author.

6.4 Summary on findings and outlook.

The data presented in this study allow for reconciliation of discrepancies in the phenotypic characteristic of invading parasites for the first time. It also presents previously uncharacterised actin dynamics during replication, gliding and invasion, broadening current knowledge on the subject.

More work remains to be done to complete the characterisation of actin dynamics in the lytic cycle pertaining to both intra- and extracellular parasites. The creation of formin tagged inducible mutants would allow dissection of the nature of the nucleation centres and assign roles, if they exist, to specific stages. It is also necessary to further characterise the functionality of the actin flow, as trafficking and recycling has been shown to depend on F-actin dynamics (Periz *et al.*, 2019).

The intricate interplay of actin factors and the nucleus also remains a broad subject to be studied further. Information regarding functional proteins that interface actin and the nucleus is non-existent and identifying them is the first step to understanding the complex dynamics between actin and the nucleus at play during invasion. One particular set of proteins correspond to the LINC complex that is associated with the inner and outer membranes of the nucleus and enables the transmission of mechanical stimuli to the nuclear envelope. In other eukaryotes, members of this complex such as nesprin, are directly involved in the cell's response to mechanical stress and the interplay of nesprin/actin or nesprin/plectin is essential for nuclear mechanotransduction. Additionally, mechanical stress upon the nucleus is known to trigger epigenetic events altering gene expression, either as a stress response or to change cellular functions. Since apicomplexan parasites need to go through several layers of tissues and are at the same time able to invade through a wide variety of them, it would be interesting to see if mechanical stress can modify genetic expression. This is particularly interesting given the nature of *Plasmodium falciparum* parasites, as they need to transmigrate to establish infection. This transmigration event would trigger epigenetic changes due to the physical deformation of the nucleus, leading to changes in the parasite stage or mechanisms for invasion. This hypothetical effect could be the initial trigger to change the machinery from extracellular parasites into intracellular ones, or even a method of regulation between life cycle stages.

Another point of interest resulting from this work is the consideration of how the parasite reacts to physical stimuli, particularly those pertaining to invasion. Studying the forces involved in invasion and how the parasite transforms these mechanical stimuli into chemical ones remains an important aspect to study, as it has the potential to broaden the knowledge of how cells invade other ones. This could in turn one day generate better strategies to combat invading parasites.

7 Bibliography

Adl, S. M. *et al.* (2007) 'Diversity, Nomenclature, and Taxonomy of Protists', *Systematic Biology*. doi: 10.1080/10635150701494127.

Adl, S. M. *et al.* (2019) 'Revisions to the Classification, Nomenclature, and Diversity of Eukaryotes', *Journal of Eukaryotic Microbiology*. doi: 10.1111/jeu.12691.

Agop-Nersesian, C. *et al.* (2009) 'Rab11A-Controlled Assembly of the Inner Membrane Complex Is Required for Completion of Apicomplexan Cytokinesis', *PLoS Pathogens*. Edited by L. D. Sibley, 5(1), p. e1000270. doi: 10.1371/journal.ppat.1000270.

Agop-Nersesian, C. *et al.* (2010) 'Biogenesis of the inner membrane complex is dependent on vesicular transport by the alveolate specific GTPase Rab11B', *PLoS Pathogens*. doi: 10.1371/journal.ppat.1001029.

Agrawal, S. *et al.* (2009) 'Genetic evidence that an endosymbiont-derived endoplasmic reticulum-associated protein degradation (ERAD) system functions in import of apicoplast proteins', *Journal of Biological Chemistry*. doi: 10.1074/jbc.M109.044024.

Ajioka, W. and Boothroyd, J. C. (2009) 'NIH Public Access', *Microbiology*, 314(5806), pp. 1780-1783. doi: 10.1126/science.1133690.Polymorphic.

Alexander, D. L. *et al.* (2005) 'Identification of the moving junction complex of *Toxoplasma gondii*: A collaboration between distinct secretory organelles', *PLoS Pathogens*. doi: 10.1371/journal.ppat.0010017.

Altschul, S. F. *et al.* (1990) 'Basic local alignment search tool', *Journal of Molecular Biology*. doi: 10.1016/S0022-2836(05)80360-2.

Andenmatten, N. *et al.* (2013) 'Conditional genome engineering in *Toxoplasma gondii* uncovers alternative invasion mechanisms.', *Nature methods*, 10(2), pp. 125-7. doi: 10.1038/nmeth.2301.

- Angrisano, F., Delves, M. J., *et al.* (2012) 'A GFP-Actin reporter line to explore microfilament dynamics across the malaria parasite lifecycle', *Molecular and Biochemical Parasitology*, 182(1-2), pp. 93-96. doi: 10.1016/j.molbiopara.2011.11.008.
- Angrisano, F., Riglar, D. T., *et al.* (2012) 'Spatial Localisation of Actin Filaments across Developmental Stages of the Malaria Parasite', *PLoS ONE*. Edited by T. J. Templeton, 7(2), p. e32188. doi: 10.1371/journal.pone.0032188.
- Arber, S. *et al.* (1998) 'Regulation of actin dynamics through phosphorylation of cofilin by LIM-kinase.', *Nature*, 393(6687), pp. 805-9. doi: 10.1038/31729.
- Arganda-Carreras, I. *et al.* (2010) '3D reconstruction of histological sections: Application to mammary gland tissue', *Microscopy Research and Technique*. doi: 10.1002/jemt.20829.
- Arrizabalaga, G. *et al.* (2004) 'Ionophore-resistant mutant of *Toxoplasma gondii* reveals involvement of a sodium/hydrogen exchanger in calcium regulation', *Journal of Cell Biology*. doi: 10.1083/jcb.200309097.
- Arsenovic, P. T. *et al.* (2016) 'Nesprin-2G, a Component of the Nuclear LINC Complex, Is Subject to Myosin-Dependent Tension', *Biophysical Journal*. doi: 10.1016/j.bpj.2015.11.014.
- Baker, L. and Straube, A. (2013) *Actin dynamics*. Available at: https://warwick.ac.uk/fac/sci/moac/people/students/2013/lewis_baker/msc_year/actin_dynamics/ (Accessed: 2 February 2019).
- Bamburg, J. R. (1999) 'Proteins of the ADF/cofilin family: essential regulators of actin dynamics', *Annual Review of Cell and Developmental Biology*, 15, pp. 185-230. doi: 10.1146/annurev.cellbio.15.1.185.
- Bane, K. S. *et al.* (2016) 'The Actin Filament-Binding Protein Coronin Regulates Motility in Plasmodium Sporozoites', *PLOS Pathogens*. Edited by R. Tewari, 12(7), p. e1005710. doi: 10.1371/journal.ppat.1005710.

- Bargieri, D. Y. *et al.* (2013) 'Apical membrane antigen 1 mediates apicomplexan parasite attachment but is dispensable for host cell invasion', *Nature Communications*. doi: 10.1038/ncomms3552.
- Baum, J. *et al.* (2008) 'A Malaria Parasite Formin Regulates Actin Polymerization and Localizes to the Parasite-Erythrocyte Moving Junction during Invasion', *Cell Host & Microbe*, 3(3), pp. 188-198. doi: 10.1016/j.chom.2008.02.006.
- Beck, J. R. *et al.* (2014) 'RON5 Is Critical for Organization and Function of the Toxoplasma Moving Junction Complex', *PLoS Pathogens*. doi: 10.1371/journal.ppat.1004025.
- Behnke, M. S. *et al.* (2011) 'Virulence differences in Toxoplasma mediated by amplification of a family of polymorphic pseudokinases', *Proceedings of the National Academy of Sciences*. doi: 10.1073/pnas.1015338108.
- Behnke, M. S. *et al.* (2012) 'The Polymorphic Pseudokinase ROP5 Controls Virulence in Toxoplasma gondii by Regulating the Active Kinase ROP18', *PLoS Pathogens*. doi: 10.1371/journal.ppat.1002992.
- Behnke, M. S. *et al.* (2015) 'Rhoptry Proteins ROP5 and ROP18 Are Major Murine Virulence Factors in Genetically Divergent South American Strains of Toxoplasma gondii', *PLoS Genetics*. doi: 10.1371/journal.pgen.1005434.
- Besteiro, S. *et al.* (2009) 'Export of a Toxoplasma gondii rhoptry neck protein complex at the host cell membrane to form the moving junction during invasion', *PLoS Pathogens*. doi: 10.1371/journal.ppat.1000309.
- Besteiro, S., Dubremetz, J. F. and Lebrun, M. (2011) 'The moving junction of apicomplexan parasites: A key structure for invasion', *Cellular Microbiology*. doi: 10.1111/j.1462-5822.2011.01597.x.
- Bichet, M. *et al.* (2014) 'The toxoplasma-host cell junction is anchored to the cell cortex to sustain parasite invasive force', *BMC Biology*, 12(1), p. 773. doi: 10.1186/s12915-014-0108-y.

- Bichet, M. *et al.* (2016) 'Genetic impairment of parasite myosin motors uncovers the contribution of host cell membrane dynamics to *Toxoplasma* invasion forces', *BMC Biology*. doi: 10.1186/s12915-016-0316-8.
- Bindschadler, M. *et al.* (2004) 'A Mechanistic Model of the Actin Cycle', *Biophysical Journal*. doi: 10.1016/S0006-3495(04)74326-X.
- Birbach, A. (2008) 'Profilin, a multi-modal regulator of neuronal plasticity', *BioEssays*, pp. 994-1002. doi: 10.1002/bies.20822.
- Bisio, H. *et al.* (2019) 'Phosphatidic acid governs natural egress in *Toxoplasma gondii* via a guanylate cyclase receptor platform', *Nature Microbiology*. doi: 10.1038/s41564-018-0339-8.
- Black, M. *et al.* (1995) 'Restriction enzyme-mediated integration elevates transformation frequency and enables co-transfection of *Toxoplasma gondii*', *Molecular and Biochemical Parasitology*. doi: 10.1016/0166-6851(95)02483-2.
- Black, M. W. and Boothroyd, J. C. (2000) 'Lytic cycle of *Toxoplasma gondii*.' , *Microbiology and molecular biology reviews : MMBR*, 64(3), pp. 607-623. doi: 10.1128/MMBR.64.3.607-623.2000.
- Blader, I. J. *et al.* (2015) 'Lytic Cycle of *Toxoplasma gondii* : 15 Years Later ', *Annual Review of Microbiology*. doi: 10.1146/annurev-micro-091014-104100.
- Borges-Pereira, L. *et al.* (2015) 'Calcium signaling throughout the *Toxoplasma gondii* lytic cycle a study using genetically encoded calcium indicators', *Journal of Biological Chemistry*. doi: 10.1074/jbc.M115.652511.
- Bosch, J. *et al.* (2012) 'Crystal structure of GAP50, the anchor of the invasion machinery in the inner membrane complex of *Plasmodium falciparum*', *Journal of Structural Biology*. doi: 10.1016/j.jsb.2012.02.009.
- Bradley, P. J. *et al.* (2005) 'Proteomic analysis of rhoptry organelles reveals many novel constituents for host-parasite interactions in *Toxoplasma gondii*', *Journal of Biological Chemistry*. doi: 10.1074/jbc.M504158200.

Brangwynne, C. P., MacKintosh, F. C. and Weitz, D. A. (2007) 'Force fluctuations and polymerization dynamics of intracellular microtubules', *Proceedings of the National Academy of Sciences*. doi: 10.1073/pnas.0703094104.

Braun, L. *et al.* (2019) 'The Toxoplasma effector TEEGR promotes parasite persistence by modulating NF- κ B signalling via EZH2', *Nature Microbiology*. doi: 10.1038/s41564-019-0431-8.

Bubb, M. R. *et al.* (2002) 'Effects of Jasplakinolide on the Kinetics of Actin Polymerization', *Journal of Biological Chemistry*. doi: 10.1074/jbc.275.7.5163.

Bugyi, B. and Carlier, M.-F. (2010) 'Control of Actin Filament Treadmilling in Cell Motility', *Annual Review of Biophysics*. doi: 10.1146/annurev-biophys-051309-103849.

Bullen, H. E. *et al.* (2016) 'Phosphatidic Acid-Mediated Signaling Regulates Microneme Secretion in Toxoplasma', *Cell Host & Microbe*, 19(3), pp. 349-360. doi: 10.1016/j.chom.2016.02.006.

Burg, J. L. *et al.* (1988) 'Molecular analysis of the gene encoding the major surface antigen of Toxoplasma gondii', *Journal of Immunology*.

Butcher, B. a. *et al.* (2011) 'Toxoplasma gondii rhoptry kinase rop16 activates stat3 and stat6 resulting in cytokine inhibition and arginase-1-dependent growth control', *PLoS Pathogens*, 7(9). doi: 10.1371/journal.ppat.1002236.

Caldas, L. A., de Souza, W. and Attias, M. (2010) 'Microscopic analysis of calcium ionophore activated egress of Toxoplasma gondii from the host cell', *Veterinary Parasitology*. doi: 10.1016/j.vetpar.2009.09.051.

Campellone, K. G. and Welch, M. D. (2010) 'A nucleator arms race: Cellular control of actin assembly', *Nature Reviews Molecular Cell Biology*. doi: 10.1038/nrm2867.

Carey, K. L. *et al.* (2004) 'The Toxoplasma gondii Rhoptry Protein ROP4 Is Secreted into the Parasitophorous Vacuole and Becomes Phosphorylated in

Infected Cells', *Eukaryotic Cell*. doi: 10.1128/ec.3.5.1320-1330.2004.

Carrier, M. F. and Pantaloni, D. (1997) 'Control of actin dynamics in cell motility', *Journal of Molecular Biology*. doi: 10.1006/jmbi.1997.1062.

Del Carmen, M. G. *et al.* (2009) 'Induction and regulation of conoid extrusion in *Toxoplasma gondii*', *Cellular Microbiology*. doi: 10.1111/j.1462-5822.2009.01304.x.

Carruthers, V. B. (2002) 'Host cell invasion by the opportunistic pathogen *Toxoplasma gondii*', *Acta Tropica*, pp. 111-122. doi: 10.1016/S0001-706X(01)00201-7.

Carruthers, V. B. and Tomley, F. M. (2008) 'Receptor-ligand interaction and invasion: Microneme proteins in Apicomplexans', *Sub-cellular biochemistry*. doi: 10.1007/978-0-387-78267-6_2.

Carruthers, V. and Boothroyd, J. C. (2007) 'Pulling together: an integrated model of *Toxoplasma* cell invasion', *Current Opinion in Microbiology*. doi: 10.1016/j.mib.2006.06.017.

Chacko, J. V., Zanicchi, F. C. and Diaspro, A. (2013) 'Probing cellular structures by coupling optical super resolution and atomic force microscopy techniques for a correlative approach.', *Cytoskeleton (Hoboken, N.J.)*, (2013), pp. 1-19. doi: 10.1002/cm.

Chan, K. T., Creed, S. J. and Bear, J. E. (2011) 'Unraveling the enigma: Progress towards understanding the coronin family of actin regulators', *Trends in Cell Biology*. doi: 10.1016/j.tcb.2011.04.004.

Charras, G. T. *et al.* (2006) 'Reassembly of contractile actin cortex in cell blebs', *The Journal of Cell Biology*, 175(3), pp. 477-490. doi: 10.1083/jcb.200602085.

Charron, A. J. and Sibley, L. D. (2004) 'Molecular partitioning during host cell penetration by *Toxoplasma gondii*', *Traffic*. doi: 10.1111/j.1600-

0854.2004.00228.x.

De Chaumont, F. *et al.* (2012) 'Icy: An open bioimage informatics platform for extended reproducible research', *Nature Methods*. doi: 10.1038/nmeth.2075.

Checkley, W. *et al.* (2015) 'A review of the global burden, novel diagnostics, therapeutics, and vaccine targets for cryptosporidium', *The Lancet Infectious Diseases*. doi: 10.1016/S1473-3099(14)70772-8.

Chen, Y. *et al.* (2012) 'Aquaporin 2 Promotes Cell Migration and Epithelial Morphogenesis', *Journal of the American Society of Nephrology*, 23(9), pp. 1506-1517. doi: 10.1681/ASN.2012010079.

Chenouard, N. *et al.* (2010) 'Curvelet analysis of kymograph for tracking bi-directional particles in fluorescence microscopy images', in *Proceedings - International Conference on Image Processing, ICIP*. doi: 10.1109/ICIP.2010.5652479.

Chetta, J. *et al.* (2015) 'Bidirectional actin transport is influenced by microtubule and actin stability', *Cellular and Molecular Life Sciences*. doi: 10.1007/s00018-015-1933-z.

Chhabra, E. S. and Higgs, H. N. (2007) 'The many faces of actin: Matching assembly factors with cellular structures', *Nature Cell Biology*. doi: 10.1038/ncb1007-1110.

Chi, Q. *et al.* (2014) 'Rear actomyosin contractility-driven directional cell migration in three-dimensional matrices: a mechano-chemical coupling mechanism', *Journal of The Royal Society Interface*, 11(95), pp. 20131072-20131072. doi: 10.1098/rsif.2013.1072.

Chiba, K. *et al.* (2014) 'Simple and Direct Assembly of Kymographs from Movies Using KYMOMAKER', *Traffic*. doi: 10.1111/tra.12127.

Chomik, A. *et al.* (1997) 'Quantification in optical sectioning microscopy: a comparison of some deconvolution algorithms in view of 3D image

segmentation', *Journal of Optics*.

Chow, C. W. K., Davey, D. E. and Mulcahy, D. E. (1997) 'Signal filtering of potentiometric stripping analysis using Fourier techniques', *Analytica Chimica Acta*. doi: 10.1016/S0003-2670(96)00441-2.

Le Clainche, C. and Carlier, M.-F. (2008) 'Regulation of Actin Assembly Associated With Protrusion and Adhesion in Cell Migration', *Physiological Reviews*. doi: 10.1152/physrev.00021.2007.

Cleveland, D. W. (2004) 'Treadmilling of tubulin and actin', *Cell*. doi: 10.1016/0092-8674(82)90048-4.

Cooper, J. A. *et al.* (1983) 'Kinetic Evidence for a Monomer Activation Step in Actin Polymerization', *Biochemistry*. doi: 10.1021/bi00278a021.

Craig, S. W. and Pollard, T. D. (1982) 'Actin-binding proteins', *Trends in Biochemical Sciences*. doi: 10.1016/0968-0004(82)90153-0.

Daher, W. *et al.* (2010) 'Concerted action of two formins in gliding motility and host cell invasion by *Toxoplasma gondii*.', *PLoS Pathog*, 6(10), p. e1001132. doi: 10.1371/journal.ppat.1001132.

Daher, W. *et al.* (2012) 'Molecular characterization of *toxoplasma gondii* formin 3, an actin nucleator dispensable for tachyzoite growth and motility', *Eukaryotic Cell*, 11(3), pp. 343-352. doi: 10.1128/EC.05192-11.

Dahl, K. N. (2004) 'The nuclear envelope lamina network has elasticity and a compressibility limit suggestive of a molecular shock absorber', *Journal of Cell Science*. doi: 10.1242/jcs.01357.

Dahl, K. N., Ribeiro, A. J. S. and Lammerding, J. (2008) 'Nuclear shape, mechanics, and mechanotransduction', *Circulation Research*. doi: 10.1161/CIRCRESAHA.108.173989.

Das, S. *et al.* (2017) 'Multiple essential functions of *Plasmodium falciparum* actin-1 during malaria blood-stage development', *BMC Biology*. doi:

10.1186/s12915-017-0406-2.

Davidson, P. M. *et al.* (2014) 'Nuclear deformability constitutes a rate-limiting step during cell migration in 3-D environments', *Cellular and Molecular Bioengineering*. doi: 10.1007/s12195-014-0342-y.

Delorme-Walker, V. *et al.* (2012) 'Toxofilin upregulates the host cortical actin cytoskeleton dynamics, facilitating Toxoplasma invasion', *Journal of Cell Science*, 125(18), pp. 4333-4342. doi: 10.1242/jcs.103648.

Desjardins, P. and Conklin, D. (2010) 'Nanodrop microvolume quantification of nucleic acids', *Journal of Visualized Experiments*. doi: 10.2307/1521521.

Ding, M., Clayton, C. and Soldati, D. (2000) 'Toxoplasma gondii catalase: Are there peroxisomes in Toxoplasma', *Journal of Cell Science*.

Dobbe, J. G. G. *et al.* (2002) 'Analyzing red blood cell-deformability distributions', *Blood Cells, Molecules, and Diseases*. doi: 10.1006/bcmd.2002.0528.

Dobrowolski, J. M., Niesman, I. R. and Sibley, L. D. (1997) 'Actin in the parasite toxoplasma gondii is encoded by a single copy gene, act1 and exists primarily in a globular form', *Cell Motility and the Cytoskeleton*. doi: 10.1002/(SICI)1097-0169(1997)37:3<253::AID-CM7>3.0.CO;2-7.

Doggett, T. M. and Breslin, J. W. (2011) 'Study of the Actin Cytoskeleton in Live Endothelial Cells Expressing GFP-Actin', *Journal of Visualized Experiments*. doi: 10.3791/3187.

Dominguez, R. and Holmes, K. C. (2011) 'Actin structure and function.', *Annual review of biophysics*, 40(April), pp. 169-86. doi: 10.1146/annurev-biophys-042910-155359.

Donald, R. G. and Roos, D. S. (2006) 'Stable molecular transformation of Toxoplasma gondii: a selectable dihydrofolate reductase-thymidylate synthase marker based on drug-resistance mutations in malaria.', *Proceedings of the*

National Academy of Sciences. doi: 10.1073/pnas.90.24.11703.

van Dooren, G. G., Kennedy, A. T. and McFadden, G. I. (2012) 'The Use and Abuse of Heme in Apicomplexan Parasites', *Antioxidants & Redox Signaling*. doi: 10.1089/ars.2012.4539.

Doube, M. *et al.* (2010) 'BoneJ: Free and extensible bone image analysis in ImageJ', *Bone*. doi: 10.1016/j.bone.2010.08.023.

Dougherty, G. (2018) 'Fundamentals of digital image processing', in *Digital Image Processing for Medical Applications*. Cambridge University Press, pp. 123-154. doi: 10.1017/CBO9780511609657.006.

Dowse, T. and Soldati, D. (2004) 'Host cell invasion by the apicomplexans: The significance of microneme protein proteolysis', *Current Opinion in Microbiology*. doi: 10.1016/j.mib.2004.06.013.

Drewry, L. L. and Sibley, L. D. (2015) 'Toxoplasma actin is required for efficient host cell invasion', *mBio*. doi: 10.1128/mBio.00557-15.

Dubey, J. P., Lindsay, D. S. and Speer, C. A. (1998) 'Structures of *Toxoplasma gondii* tachyzoites, bradyzoites, and sporozoites and biology and development of tissue cysts', *Clinical Microbiology Reviews*.

Dubey, J. P., Miller, N. L. and Frenkel, J. K. (1970) 'The *Toxoplasma gondii* oocyst from cat feces.', *The Journal of experimental medicine*.

Dunn, J. D. *et al.* (2008) 'The *Toxoplasma gondii* dense granule protein GRA7 is phosphorylated upon invasion and forms an unexpected association with the rhoptry proteins ROP2 and ROP4', *Infection and Immunity*. doi: 10.1128/IAI.01667-07.

Dupin, I., Sakamoto, Y. and Etienne-Manneville, S. (2011) 'Cytoplasmic intermediate filaments mediate actin-driven positioning of the nucleus', *Journal of Cell Science*. doi: 10.1242/jcs.076356.

Egarter, S. *et al.* (2014) 'The toxoplasma acto-myosin motor complex is important

but not essential for gliding motility and host cell invasion', *PLoS ONE*, 9(3). doi: 10.1371/journal.pone.0091819.

ENDO, T. *et al.* (1987) 'Effects of Extracellular Potassium on Acid Release and Motility Initiation in *Toxoplasma gondii*', *The Journal of Protozoology*. doi: 10.1111/j.1550-7408.1987.tb03177.x.

Etienne-Manneville, S. (2013) 'Microtubules in Cell Migration', *Annual Review of Cell and Developmental Biology*. doi: 10.1146/annurev-cellbio-101011-155711.

Evangelista, M. (2003) 'Formins: signaling effectors for assembly and polarization of actin filaments', *Journal of Cell Science*. doi: 10.1242/jcs.00611.

Felix Stortz, J. *et al.* (2019) 'Formin-2 drives polymerisation of actin filaments enabling segregation of apicoplasts and cytokinesis in *Plasmodium falciparum*', *eLife*. doi: 10.7554/elife.49030.

Flegr, J. *et al.* (2014) 'Toxoplasmosis - A global threat. Correlation of latent toxoplasmosis with specific disease burden in a set of 88 countries', *PLoS ONE*. doi: 10.1371/journal.pone.0090203.

Frénal, K. *et al.* (2010) 'Functional dissection of the apicomplexan glideosome molecular architecture', *Cell Host and Microbe*. doi: 10.1016/j.chom.2010.09.002.

Frénal, K. *et al.* (2014) 'Plasticity between MyoC- and MyoA-Glideosomes: An Example of Functional Compensation in *Toxoplasma gondii* Invasion', *PLoS Pathogens*. Edited by F. Frischknecht, 10(11), p. e1004504. doi: 10.1371/journal.ppat.1004504.

Frénal, K., Dubremetz, J. F., *et al.* (2017) 'Gliding motility powers invasion and egress in Apicomplexa', *Nature Reviews Microbiology*. doi: 10.1038/nrmicro.2017.86.

Frénal, K., Jacot, D., *et al.* (2017) 'Myosin-dependent cell-cell communication controls synchronicity of division in acute and chronic stages of *Toxoplasma*

gondii', *Nature Communications*, 8, p. 15710. doi: 10.1038/ncomms15710.

Frenkel, J. K., Dubey, J. P. and Miller, N. L. (1970) 'Toxoplasma gondii in cats: Fecal stages identified as coccidian oocysts', *Science*. doi: 10.1126/science.167.3919.893.

Fu, Y. *et al.* (2012) 'Nuclear deformation during breast cancer cell transmigration', *Lab on a Chip*. doi: 10.1039/c2lc40477j.

Fukata, Y. *et al.* (2001) 'Rho-Rho-kinase pathway in smooth muscle contraction and cytoskeletal reorganization of non-muscle cells', *Trends in Pharmacological Sciences*. doi: 10.1016/S0165-6147(00)01596-0.

Gajria, B. *et al.* (2008) 'ToxoDB: An integrated toxoplasma gondii database resource', *Nucleic Acids Research*. doi: 10.1093/nar/gkm981.

Gardel, M. L. *et al.* (2010) 'Mechanical Integration of Actin and Adhesion Dynamics in Cell Migration', *Annual Review of Cell and Developmental Biology*. doi: 10.1146/annurev.cellbio.011209.122036.

Garg, S. *et al.* (2015) 'In silico analysis of calcium binding pocket of perforin like protein 1: insights into the regulation of pore formation', *Systems and Synthetic Biology*. doi: 10.1007/s11693-015-9166-x.

Garrels, J. I. and Gibson, W. (1976) 'Identification and characterization of multiple forms of actin', *Cell*. doi: 10.1016/0092-8674(76)90142-2.

Garrison, E. *et al.* (2012) 'A Forward Genetic Screen Reveals that Calcium-dependent Protein Kinase 3 Regulates Egress in Toxoplasma', *PLoS Pathogens*, 8(11). doi: 10.1371/journal.ppat.1003049.

Garweg, J. G., De Groot-Mijnes, J. D. F. and Montoya, J. G. (2011) 'Diagnostic approach to ocular toxoplasmosis', *Ocular Immunology and Inflammation*. doi: 10.3109/09273948.2011.595872.

Gaskins, E. *et al.* (2004) 'Identification of the membrane receptor of a class XIV myosin in Toxoplasma gondii', *Journal of Cell Biology*. doi:

10.1083/jcb.200311137.

Gavin, R. H. and Holzinger, A. (2003) 'Jasplakinolide: An Actin-Specific Reagent that Promotes Actin Polymerization', in *Cytoskeleton Methods and Protocols*. doi: 10.1385/1-59259-051-9:109.

Georgatos, S. D., Maroulakou, I. and Blobel, G. (1989) 'Lamin A, lamin B, and lamin B receptor analogues in yeast', *Journal of Cell Biology*. doi: 10.1083/jcb.108.6.2069.

Gilk, S. D. *et al.* (2009) 'GAP45 phosphorylation controls assembly of the Toxoplasma myosin XIV complex', *Eukaryotic Cell*. doi: 10.1128/EC.00201-08.

Gold, D. A. *et al.* (2015) 'The Toxoplasma dense granule proteins GRA17 and GRA23 mediate the movement of small molecules between the host and the parasitophorous vacuole', *Cell Host and Microbe*. doi: 10.1016/j.chom.2015.04.003.

Goley, E. D. and Welch, M. D. (2006) 'The ARP2/3 complex: an actin nucleator comes of age.', *Nature reviews. Molecular cell biology*, 7(10), pp. 713-26. doi: 10.1038/nrm2026.

Gomes, E. R., Jani, S. and Gundersen, G. G. (2005) 'Nuclear movement regulated by Cdc42, MRCK, myosin, and actin flow establishes MTOC polarization in migrating cells', *Cell*. doi: 10.1016/j.cell.2005.02.022.

Gonzalez, V. *et al.* (2009) 'Host Cell Entry by Apicomplexa Parasites Requires Actin Polymerization in the Host Cell', *Cell Host & Microbe*, 5(3), pp. 259-272. doi: 10.1016/j.chom.2009.01.011.

Goyal, P. *et al.* (2013) 'Cofilin Oligomer Formation Occurs In Vivo and Is Regulated by Cofilin Phosphorylation', *PLoS ONE*, 8(8). doi: 10.1371/journal.pone.0071769.

Gozalet, R. C. and Woods, R. E. (2013) 'Digital Image Processing, 3rd edition', *IEEE Transactions on Biomedical Engineering*. doi: 10.1109/TBME.2009.2017027.

- Graindorge, A. *et al.* (2016) 'The Conoid Associated Motor MyoH Is Indispensable for *Toxoplasma gondii* Entry and Exit from Host Cells', *PLoS Pathogens*. doi: 10.1371/journal.ppat.1005388.
- Gras, S. *et al.* (2017) 'Parasites lacking the micronemal protein MIC2 are deficient in surface attachment and host cell egress, but remain virulent in vivo', *Wellcome Open Research*. doi: 10.12688/wellcomeopenres.11594.2.
- Gras, S. *et al.* (2019) 'An endocytic-secretory cycle participates in *Toxoplasma gondii* in motility', *PLOS Biology*. Edited by M. T. Laub, 17(6), p. e3000060. doi: 10.1371/journal.pbio.3000060.
- Green, J. L. *et al.* (2017) 'Compositional and expression analyses of the glideosome during the *Plasmodium* life cycle reveal an additional myosin light chain required for maximum motility', *Journal of Biological Chemistry*, 292(43), pp. 17857-17875. doi: 10.1074/jbc.M117.802769.
- Gregor, M. *et al.* (2014) 'Mechanosensing through focal adhesion-anchored intermediate filaments', *FASEB Journal*. doi: 10.1096/fj.13-231829.
- Gu, Z. *et al.* (2011) 'Integrins traffic rapidly via circular dorsal ruffles and macropinocytosis during stimulated cell migration', *Journal of Cell Biology*. doi: 10.1083/jcb.201007003.
- Gubbels, M. J., White, M. and Szatanek, T. (2008) 'The cell cycle and *Toxoplasma gondii* cell division: Tightly knit or loosely stitched?', *International Journal for Parasitology*. doi: 10.1016/j.ijpara.2008.06.004.
- Guilluy, C. *et al.* (2014) 'Isolated nuclei adapt to force and reveal a mechanotransduction pathway in the nucleus', *Nature Cell Biology*. doi: 10.1038/ncb2927.
- Gundersen, G. G. *et al.* (2006) 'Regulation of Microtubules by Rho GTPases in Migrating Cells', in. doi: 10.1002/047001766x.ch10.
- Hakansson, S. *et al.* (2013) 'Time-Lapse Video Microscopy of Gliding Motility in

- Toxoplasma gondii Reveals a Novel, Biphasic Mechanism of Cell Locomotion', *Molecular Biology of the Cell*. doi: 10.1091/mbc.10.11.3539.
- Hanboonkunupakarn, B. and White, N. J. (2016) 'The threat of antimalarial drug resistance', *Tropical Diseases, Travel Medicine and Vaccines*, 2(1), p. 10. doi: 10.1186/s40794-016-0027-8.
- Harding, C. R. *et al.* (2016) 'Gliding Associated Proteins Play Essential Roles during the Formation of the Inner Membrane Complex of Toxoplasma gondii', *PLoS Pathogens*. doi: 10.1371/journal.ppat.1005403.
- Harding, C. R. *et al.* (2019) 'Alveolar proteins stabilize cortical microtubules in Toxoplasma gondii', *Nature Communications*. doi: 10.1038/s41467-019-08318-7.
- Hatch, A. L. *et al.* (2016) 'Actin filaments as dynamic reservoirs for Drp1 recruitment.', *Molecular biology of the cell*, 27(20), pp. 3109-3121. doi: 10.1091/mbc.E16-03-0193.
- Hatch, A. L., Gurel, P. S. and Higgs, H. N. (2014) 'Novel roles for actin in mitochondrial fission', *Journal of Cell Science*. doi: 10.1242/jcs.153791.
- Heaslip, A. T. *et al.* (2010) 'TgMORN1 is a key organizer for the basal complex of Toxoplasma gondii', *PLoS Pathogens*. doi: 10.1371/journal.ppat.1000754.
- Heaslip, A. T. *et al.* (2011) 'The motility of a human parasite, toxoplasma gondii, is regulated by a novel lysine methyltransferase', *PLoS Pathogens*. doi: 10.1371/journal.ppat.1002201.
- Heaslip, A. T., Ems-McClung, S. C. and Hu, K. (2009) 'TgICMAP1 Is a Novel Microtubule Binding Protein in Toxoplasma gondii', *PLoS ONE*. Edited by D. Davis, 4(10), p. e7406. doi: 10.1371/journal.pone.0007406.
- Heaslip, A. T., Nelson, S. R. and Warshaw, D. M. (2016) ' Dense granule trafficking in Toxoplasma gondii requires a unique class 27 myosin and actin filaments ', *Molecular Biology of the Cell*. Edited by G. Steinberg, 27(13), pp. 2080-2089. doi: 10.1091/mbc.E15-12-0824.

- Heintzelman, M. B. (2015) 'Gliding motility in apicomplexan parasites.', *Seminars in cell & developmental biology*. Elsevier Ltd, 46, pp. 135-142. doi: 10.1016/j.semcdb.2015.09.020.
- Herman, I. M. (1993) 'Actin isoforms', *Current Opinion in Cell Biology*. doi: 10.1016/S0955-0674(05)80007-9.
- Higgs, H. N. and Peterson, K. J. (2005) 'Phylogenetic analysis of the formin homology 2 domain.', *Molecular biology of the cell*. doi: 10.1091/mbc.e04-07-0565.
- Hill, D. E., Chirukandoth, S. and Dubey, J. P. (2005) 'Biology and epidemiology of *Toxoplasma gondii* in man and animals', *Animal Health Research Reviews*, 6(1), pp. 41-61. doi: 10.1079/AHR2005100.
- Hlavac, V. (2011) 'Fundamentals of Image Processing', in *Optical and Digital Image Processing: Fundamentals and Applications*. doi: 10.1002/9783527635245.ch4.
- Hons, M. *et al.* (2018) 'Chemokines and integrins independently tune actin flow and substrate friction during intranodal migration of T cells', *Nature Immunology*. doi: 10.1038/s41590-018-0109-z.
- Horzum, U., Ozdil, B. and Pesen-Okvur, D. (2014) 'Step-by-step quantitative analysis of focal adhesions', *MethodsX*. Elsevier B.V., 1(1), pp. 56-59. doi: 10.1016/j.mex.2014.06.004.
- Hotulainen, P. *et al.* (2004) 'Actin-depolymerizing Factor and Cofilin-1 Play Overlapping Roles in Promoting Rapid F-Actin Depolymerization in Mammalian Nonmuscle Cells', *Molecular Biology of the Cell*. doi: 10.1091/mbc.e04-07-0555.
- Howard, B. L. *et al.* (2015) 'Identification of potent phosphodiesterase inhibitors that demonstrate cyclic nucleotide-dependent functions in apicomplexan parasites', *ACS Chemical Biology*. doi: 10.1021/cb501004q.
- Howe, D. K. and Sibley, L. D. (1995) '*Toxoplasma gondii* comprises three clonal

lineages: correlation of parasite genotype with human disease.’, *The Journal of infectious diseases*, 172(6), pp. 1561-1566. doi: 10.1093/infdis/172.6.1561.

Hu, K. (2002) ‘Daughter Cell Assembly in the Protozoan Parasite *Toxoplasma gondii*’, *Molecular Biology of the Cell*. doi: 10.1091/mbc.01-06-0309.

Hunt, A. *et al.* (2019) ‘Differential requirements of cyclase associated protein (CAP) for actin turnover during the lytic cycle of’, *BioRxiv*. doi: 10.1101/569368.

Hunter, C. A. and Sibley, L. D. (2012) ‘Modulation of innate immunity by *Toxoplasma gondii* virulence effectors.’, *Nature reviews. Microbiology*. doi: 10.1038/nrmicro2858.

Huynh, M.-H. and Carruthers, V. B. (2009) ‘ Tagging of Endogenous Genes in a *Toxoplasma gondii* Strain Lacking Ku80 ’, *Eukaryotic Cell*. doi: 10.1128/ec.00358-08.

Huynh, M. H. *et al.* (2003) ‘Rapid invasion of host cells by *Toxoplasma* requires secretion of the MIC2-M2AP adhesive protein complex’, *EMBO Journal*. doi: 10.1093/emboj/cdg217.

Huynh, M. H., Boulanger, M. J. and Carruthers, V. B. (2014) ‘A conserved apicomplexan microneme protein contributes to *Toxoplasma gondii* invasion and virulence’, *Infection and Immunity*, 82(10), pp. 4358-4368. doi: 10.1128/IAI.01877-14.

Ilagan, R. P. *et al.* (2010) ‘A new bright green-emitting fluorescent protein - Engineered monomeric and dimeric forms’, *FEBS Journal*. doi: 10.1111/j.1742-4658.2010.07618.x.

Isermann, P. and Lammerding, J. (2013) ‘Nuclear mechanics and mechanotransduction in health and disease’, *Current Biology*. doi: 10.1016/j.cub.2013.11.009.

Isogai, T. and Innocenti, M. (2016) ‘New nuclear and perinuclear functions of formins’, *Biochemical Society Transactions*, 44(6), pp. 1701-1708. doi:

10.1042/BST20160187.

Iyer, K. V. *et al.* (2012) 'Mechanical activation of cells induces chromatin remodeling preceding MKL nuclear transport', *Biophysical Journal*. doi: 10.1016/j.bpj.2012.08.041.

Jacot, D. *et al.* (2016) 'An Apicomplexan Actin-Binding Protein Serves as a Connector and Lipid Sensor to Coordinate Motility and Invasion', *Cell Host & Microbe*, 20(6), pp. 731-743. doi: 10.1016/j.chom.2016.10.020.

Jacot, D., Daher, W. and Soldati-Favre, D. (2013) 'Toxoplasma gondii myosin F, an essential motor for centrosomes positioning and apicoplast inheritance', *The EMBO Journal*, 32(12), pp. 1702-1716. doi: 10.1038/emboj.2013.113.

Jameson, D. *et al.* (2009) 'Information management for high content live cell imaging', *BMC Bioinformatics*. doi: 10.1186/1471-2105-10-226.

Jaqaman, K. *et al.* (2008) 'Robust single-particle tracking in live-cell time-lapse sequences', *Nature Methods*. doi: 10.1038/nmeth.1237.

Jayo, A. *et al.* (2016) 'Fascin Regulates Nuclear Movement and Deformation in Migrating Cells', *Developmental Cell*. doi: 10.1016/j.devcel.2016.07.021.

Jewett, T. J. and Sibley, L. D. (2003) 'Aldolase forms a bridge between cell surface adhesins and the actin cytoskeleton in apicomplexan parasites', *Molecular Cell*. doi: 10.1016/S1097-2765(03)00113-8.

JIMÉNEZ-RUIZ, E. *et al.* (2014) 'Advantages and disadvantages of conditional systems for characterization of essential genes in *Toxoplasma gondii*', *Parasitology*, 141(11), pp. 1390-1398. doi: 10.1017/S0031182014000559.

Jones, T. C. and Hirsch, J. G. (1972) 'The interaction between *Toxoplasma gondii* and mammalian cells. II. The absence of lysosomal fusion with phagocytic vacuoles containing living parasites.', *The Journal of experimental medicine*.

Kabsch, W. *et al.* (1990) 'Atomic structure of the actin: DNase I complex', *Nature*. doi: 10.1038/347037a0.

- Kafsack, B. F. C. *et al.* (2009) 'Rapid membrane disruption by a perforin-like protein facilitates parasite exit from host cells', *Science*. doi: 10.1126/science.1165740.
- Kallio, J. P. and Kursula, I. (2014) 'Recombinant production, purification and crystallization of the *Toxoplasma gondii* coronin WD40 domain', *Acta Crystallographica Section F: Structural Biology Communications*. International Union of Crystallography, 70(4), pp. 517-521. doi: 10.1107/S2053230X14005196.
- Kamerkar, S. and Davis, P. H. (2012) 'Toxoplasma on the brain: Understanding host-pathogen interactions in chronic CNS infection', *Journal of Parasitology Research*, 2012. doi: 10.1155/2012/589295.
- Kanellos, G. *et al.* (2015) 'ADF and Cofilin1 Control Actin Stress Fibers, Nuclear Integrity, and Cell Survival', *Cell Reports*, 13(9), pp. 1949-1964. doi: 10.1016/j.celrep.2015.10.056.
- Kanellos, G. and Frame, M. C. (2016) 'Cellular functions of the ADF/cofilin family at a glance.', *Journal of cell science*, 129(17), pp. 3211-8. doi: 10.1242/jcs.187849.
- Katoh, K. *et al.* (2002) 'Arrangement of radial actin bundles in the growth cone of *Aplysia* bag cell neurons shows the immediate past history of filopodial behavior', *Proceedings of the National Academy of Sciences*. doi: 10.1073/pnas.96.14.7928.
- Katris, N. J. *et al.* (2014) 'The Apical Complex Provides a Regulated Gateway for Secretion of Invasion Factors in *Toxoplasma*', *PLoS Pathogens*. doi: 10.1371/journal.ppat.1004074.
- Keeley, A. and Soldati, D. (2004) 'The glideosome: A molecular machine powering motility and host-cell invasion by Apicomplexa', *Trends in Cell Biology*. doi: 10.1016/j.tcb.2004.08.002.
- Kessler, H. *et al.* (2008) 'Microneme protein 8 - a new essential invasion factor in *Toxoplasma gondii*', *Journal of Cell Science*. doi: 10.1242/jcs.022350.

- Khan, A. *et al.* (2011) 'Genetic analyses of atypical *Toxoplasma gondii* strains reveal a fourth clonal lineage in North America', *International Journal for Parasitology*. doi: 10.1016/j.ijpara.2011.01.005.
- Kheir, W. A. (2005) 'A WAVE2-Abi1 complex mediates CSF-1-induced F-actin-rich membrane protrusions and migration in macrophages', *Journal of Cell Science*. doi: 10.1242/jcs.02638.
- Kibbe, W. A. (2007) 'OligoCalc: An online oligonucleotide properties calculator', *Nucleic Acids Research*. doi: 10.1093/nar/gkm234.
- Kim, K. and Boothroyd, J. C. (1995) 'Toxoplasma gondii: stable complementation of sag1 (p30) mutants using SAG1 transfection and fluorescence-activated cell sorting.', *Experimental parasitology*, 80(1), pp. 46-53. doi: 10.1006/expr.1995.1006.
- King, C. A. (1988) 'Cell motility of sporozoan protozoa', *Parasitology Today*, 4(11), pp. 315-319. doi: 10.1016/0169-4758(88)90113-5.
- Kissinger, J. C. *et al.* (2003) 'ToxoDB: Accessing the *Toxoplasma gondii* genome', *Nucleic Acids Research*. doi: 10.1093/nar/gkg072.
- Koltzschner, M. *et al.* (2003) 'Ca²⁺-dependent Binding and Activation of Dormant Ezrin by Dimeric S100P', *Molecular Biology of the Cell*, 14(September), pp. 2372-2384. doi: 10.1091/mbc.E02.
- Kong, L. *et al.* (2012) 'Lamin A/C protein is overexpressed in tissue-invading prostate cancer and promotes prostate cancer cell growth, migration and invasion through the PI3K/AKT/PTEN pathway', *Carcinogenesis*. doi: 10.1093/carcin/bgs022.
- Kovar, D. R. *et al.* (2006) 'Control of the assembly of ATP- and ADP-actin by formins and profilin', *Cell*. doi: 10.1016/j.cell.2005.11.038.
- Kovar, D. R. (2006) 'Molecular details of formin-mediated actin assembly', *Current Opinion in Cell Biology*, pp. 11-17. doi: 10.1016/j.ceb.2005.12.011.

Kovar, D. R. and Pollard, T. D. (2004) 'Progressing actin: Formin as a processive elongation machine.', *Nature cell biology*, 6(12), pp. 1158-1159. doi: 10.1038/ncb1204-1158.

Krause, M. and Wolf, K. (2015) 'Cancer cell migration in 3d tissue: Negotiating space by proteolysis and nuclear deformability', *Cell Adhesion and Migration*. doi: 10.1080/19336918.2015.1061173.

Kremer, K. *et al.* (2013) 'An Overexpression Screen of *Toxoplasma gondii* Rab-GTPases Reveals Distinct Transport Routes to the Micronemes', *PLoS Pathogens*, 9(3). doi: 10.1371/journal.ppat.1003213.

Kucera, K. *et al.* (2010) 'Structure-Based Analysis of *Toxoplasma gondii* Profilin: A Parasite-Specific Motif Is Required for Recognition by Toll-Like Receptor 11', *Journal of Molecular Biology*. doi: 10.1016/j.jmb.2010.09.022.

Kudryashev, M. *et al.* (2010) 'Geometric constraints for detecting short actin filaments by cryogenic electron tomography', *PMC Biophysics*. doi: 10.1186/1757-5036-3-6.

Kumpula, E.-P. *et al.* (2018) 'Atomic view into Plasmodium actin polymerization, ATP hydrolysis, and phosphate release', *BioRxiv*, pp. 1-35.

Kumpula, E.-P. and Kursula, I. (2015) 'Towards a molecular understanding of the apicomplexan actin motor: on a road to novel targets for malaria remedies?', *Acta Crystallographica Section F Structural Biology Communications*. doi: 10.1107/s2053230x1500391x.

Kumpula, E. P. *et al.* (2017) 'Apicomplexan actin polymerization depends on nucleation', *Scientific Reports*. doi: 10.1038/s41598-017-11330-w.

Laemmli, U. K. (1970) 'Cleavage of structural proteins during the assembly of the head of bacteriophage T4', *Nature*. doi: 10.1038/227680a0.

Lamarque, M. *et al.* (2011) 'The RON2-AMA1 interaction is a critical step in moving junction-dependent invasion by apicomplexan parasites', *PLoS*

Pathogens. doi: 10.1371/journal.ppat.1001276.

Lammerding, J. (2011) 'Mechanics of the nucleus', *Comprehensive Physiology*. doi: 10.1002/cphy.c100038.

Lämmermann, T. *et al.* (2008) 'Rapid leukocyte migration by integrin-independent flowing and squeezing', *Nature*. doi: 10.1038/nature06887.

Lautscham, L. A. *et al.* (2015) 'Migration in Confined 3D Environments Is Determined by a Combination of Adhesiveness, Nuclear Volume, Contractility, and Cell Stiffness', *Biophysical Journal*. doi: 10.1016/j.bpj.2015.07.025.

Lei, T. *et al.* (2014) 'ROP18 is a key factor responsible for virulence difference between *Toxoplasma gondii* and *Neospora caninum*', *PLoS ONE*, 9(6), pp. 1-10. doi: 10.1371/journal.pone.0099744.

Leriche, M. A. and Dubremetz, J. F. (1991) 'Characterization of the protein contents of rhoptries and dense granules of *Toxoplasma gondii* tachyzoites by subcellular fractionation and monoclonal antibodies', *Molecular and Biochemical Parasitology*. doi: 10.1016/0166-6851(91)90092-K.

Leung, J. M. *et al.* (2014) 'Disruption of TgPHIL1 alters specific parameters of *Toxoplasma gondii* motility measured in a quantitative, three-dimensional live motility assay', *PLoS ONE*. doi: 10.1371/journal.pone.0085763.

Li, A. *et al.* (2010) 'The Actin-Bundling Protein Fascin Stabilizes Actin in Invadopodia and Potentiates Protrusive Invasion', *Current Biology*. doi: 10.1016/j.cub.2009.12.035.

Lim, L. and McFadden, G. I. (2010) 'The evolution, metabolism and functions of the apicoplast', *Philosophical Transactions of the Royal Society B: Biological Sciences*. doi: 10.1098/rstb.2009.0273.

Lippert, D. N. D. and Wilkins, J. A. (2012) 'Glia maturation factor gamma regulates the migration and adherence of human T lymphocytes', *BMC Immunology*. doi: 10.1186/1471-2172-13-21.

Liu, J. *et al.* (2013) 'Novel Thioredoxin-Like Proteins Are Components of a Protein Complex Coating the Cortical Microtubules of *Toxoplasma gondii*', *Eukaryotic Cell*. doi: 10.1128/ec.00082-13.

Liu, Y.-J. *et al.* (2015) 'Confinement and Low Adhesion Induce Fast Amoeboid Migration of Slow Mesenchymal Cells', *Cell*, 160(4), pp. 659-672. doi: 10.1016/j.cell.2015.01.007.

Liu, Z. *et al.* (2015) 'Immune homeostasis enforced by co-localized effector and regulatory T cells', *Nature*. doi: 10.1038/nature16169.

Lourido, S. and Moreno, S. N. J. (2015) 'The calcium signaling toolkit of the Apicomplexan parasites *Toxoplasma gondii* and *Plasmodium spp*', *Cell Calcium*. doi: 10.1016/j.ceca.2014.12.010.

Loussert, C., Forestier, C.-L. and Humbel, B. M. (2012) *Correlative light and electron microscopy in parasite research.*, *Methods in cell biology*. doi: 10.1016/B978-0-12-416026-2.00004-2.

Machesky, L. M. and Gould, K. L. (1999) 'The Arp2/3 complex: A multifunctional actin organizer', *Current Opinion in Cell Biology*. doi: 10.1016/S0955-0674(99)80014-3.

Maciver, S. K. and Hussey, P. J. (2002) 'The ADF/cofilin family: actin-remodeling proteins.', *Genome biology*, 3(5), p. reviews3007. doi: 10.1186/gb-2002-3-5-reviews3007.

Maenz, M. *et al.* (2014) 'Ocular toxoplasmosis past, present and new aspects of an old disease', *Progress in Retinal and Eye Research*. doi: 10.1016/j.preteyeres.2013.12.005.

Maier, J., Traenkle, B. and Rothbauer, U. (2016) 'Visualizing epithelial-mesenchymal transition using the chromobody technology', *Cancer Research*, pp. 5592-5596. doi: 10.1158/0008-5472.CAN-15-3419.

Maiuri, P. *et al.* (2015) 'Actin flows mediate a universal coupling between cell

speed and cell persistence', *Cell*. doi: 10.1016/j.cell.2015.01.056.

Mak, M., Reinhart-King, C. A. and Erickson, D. (2013) 'Elucidating mechanical transition effects of invading cancer cells with a subnucleus-scaled microfluidic serial dimensional modulation device', *Lab on a Chip*. doi: 10.1039/c2lc41117b.

Mangeol, P., Prevo, B. and Peterman, E. J. G. (2016) 'KymographClear and KymographDirect: two tools for the automated quantitative analysis of molecular and cellular dynamics using kymographs', *Molecular Biology of the Cell*, 27(12), pp. 1948-1957. doi: 10.1091/mbc.E15-06-0404.

Mann, T. and Beckers, C. (2001) 'Characterization of the subpellicular network, a filamentous membrane skeletal component in the parasite *Toxoplasma gondii*', *Molecular and Biochemical Parasitology*. doi: 10.1016/S0166-6851(01)00289-4.

Manuscript, A. (2015) 'Ménage à Trois of ROPs', 15(5), pp. 517-518. doi: 10.1016/j.chom.2014.05.002.*Toxoplasma*.

Markham, J. and Conchello, J. A. (2001) 'Artefacts in restored images due to intensity loss in three-dimensional fluorescence microscopy', *Journal of Microscopy*. doi: 10.1046/j.1365-2818.2001.00961.x.

MBINFO (2019) *Cytoskeleton Dynamics*. Available at:

<https://www.mechanobio.info/cytoskeleton-dynamics/what-is-the-cytoskeleton/what-are-actin-filaments/what-factors-influence-actin-filament-length-and-treadmilling/#what-factors-influence-actin-filament-length-and-treadmilling> (Accessed: 10 April 2019).

McCoy, J. M. *et al.* (2012) 'TgCDPK3 Regulates Calcium-Dependent Egress of *Toxoplasma gondii* from Host Cells', *PLoS Pathogens*, 8(12). doi: 10.1371/journal.ppat.1003066.

McFadden, G. I. (2001) 'PRIMARY AND SECONDARY ENDOSYMBIOSIS AND THE ORIGIN OF PLASTIDS', *Journal of Phycology*, 37(6), pp. 951-959. doi: 10.1046/j.1529-8817.2001.01126.x.

McGregor, A. L., Hsia, C.-R. and Lammerding, J. (2016) 'Squish and squeeze – the nucleus as a physical barrier during migration in confined environments', *Current Opinion in Cell Biology*, 40, pp. 32-40. doi: 10.1016/j.ceb.2016.01.011.

Mckee, F. D., Kirschner, M. W. and Caput, D. (1986) 'Homologies in both primary and secondary structure between nuclear envelope and intermediate filament proteins', *Nature*. doi: 10.1038/319463a0.

Mehta, S. and Sibley, L. D. (2011) 'Actin depolymerizing factor controls actin turnover and gliding motility in *Toxoplasma gondii*', *Molecular Biology of the Cell*. Edited by Y.-L. Wang, 22(8), pp. 1290-1299. doi: 10.1091/mbc.e10-12-0939.

Meissner, M. *et al.* (2001) 'Modulation of myosin A expression by a newly established tetracycline repressor-based inducible system in *Toxoplasma gondii*.' , *Nucleic acids research*, 29(22), p. E115. doi: 10.1093/nar/29.22.e115.

Meissner, M. *et al.* (2005) 'Tetracycline analogue-regulated transgene expression in *Plasmodium falciparum* blood stages using *Toxoplasma gondii* transactivators', *Proceedings of the National Academy of Sciences*. doi: 10.1073/pnas.0500112102.

Meissner, M., Ferguson, D. J. P. and Frischknecht, F. (2013) 'Invasion factors of apicomplexan parasites: essential or redundant?', *Current Opinion in Microbiology*. Elsevier Ltd, 16(4), pp. 438-444. doi: 10.1016/j.mib.2013.05.002.

Meissner, M., Schlüter, D. and Soldati, D. (2002) 'Role of *Toxoplasma gondii* myosin a in powering parasite gliding and host cell invasion', *Science*. doi: 10.1126/science.1074553.

Melatti, C. *et al.* (2019) 'A unique dynamin-related protein is essential for mitochondrial fission in *Toxoplasma gondii*', *PLOS Pathogens*, 15(4), p. e1007512. doi: 10.1371/journal.ppat.1007512.

Melo, M. B. *et al.* (2013) 'Transcriptional Analysis of Murine Macrophages Infected with Different *Toxoplasma* Strains Identifies Novel Regulation of Host

Signaling Pathways', *PLoS Pathogens*. Edited by D. L. Sacks, 9(12), p. e1003779. doi: 10.1371/journal.ppat.1003779.

Mendez, M. G., Kojima, S.-I. and Goldman, R. D. (2010) 'Vimentin induces changes in cell shape, motility, and adhesion during the epithelial to mesenchymal transition', *The FASEB Journal*. doi: 10.1096/fj.09-151639.

Mercier, C. (2002) 'Biogenesis of Nanotubular Network in Toxoplasma Parasitophorous Vacuole Induced by Parasite Proteins', *Molecular Biology of the Cell*. doi: 10.1091/mbc.e02-01-0021.

Mercier, C. *et al.* (2005) 'Dense granules: Are they key organelles to help understand the parasitophorous vacuole of all apicomplexa parasites?', *International Journal for Parasitology*. doi: 10.1016/j.ijpara.2005.03.011.

Minot, S. *et al.* (2012) 'Admixture and recombination among *Toxoplasma gondii* lineages explain global genome diversity', *Proceedings of the National Academy of Sciences of the United States of America*. doi: 10.1073/pnas.1117047109.

Mital, J. (2005) 'Conditional Expression of *Toxoplasma gondii* Apical Membrane Antigen-1 (TgAMA1) Demonstrates That TgAMA1 Plays a Critical Role in Host Cell Invasion', *Molecular Biology of the Cell*. doi: 10.1091/mbc.e05-04-0281.

Montoya, J. G. (2002) 'Laboratory Diagnosis of *Toxoplasma gondii* Infection and Toxoplasmosis', *The Journal of Infectious Diseases*. doi: 10.1086/338827.

Montoya, J. G. and Remington, J. S. (2008) 'Clinical Practice: Management of *Toxoplasma gondii* Infection during Pregnancy', *Clinical Infectious Diseases*. doi: 10.1086/590149.

Morejohn, L. C. *et al.* (1987) 'Oryzalin, a dinitroaniline herbicide, binds to plant tubulin and inhibits microtubule polymerization in vitro', *Planta*. doi: 10.1007/BF00394595.

Morgado, P. *et al.* (2011) '*Toxoplasma gondii* Induces B7-2 Expression through Activation of JNK Signal Transduction', *Infection and Immunity*, 79(11), pp.

4401-4412. doi: 10.1128/IAI.05562-11.

Morisaki, J. H., Heuser, J. E. and Sibley, L. D. (1995) 'Invasion of *Toxoplasma gondii* occurs by active penetration of the host cell.', *Journal of cell science*, 108 (Pt 6, pp. 2457-2464.

Morrisette, N. (2015) 'Targeting *Toxoplasma* tubules: Tubulin, microtubules, and associated proteins in a human pathogen', *Eukaryotic Cell*. doi: 10.1128/EC.00225-14.

Morrisette, N. S., Murray, J. M. and Roos, D. S. (1997) 'Subpellicular microtubules associate with an intramembranous particle lattice in the protozoan parasite *Toxoplasma gondii*.' , *Journal of cell science*.

Morrisette, N. S. and Sibley, L. D. (2002) 'Cytoskeleton of apicomplexan parasites.' , *Microbiology and molecular biology reviews : MMBR*.

Mukherjee, A. *et al.* (2011) 'Automated kymograph analysis for profiling axonal transport of secretory granules', *Medical Image Analysis*. doi: 10.1016/j.media.2010.12.005.

Muller, W. A. (2013) 'Getting Leukocytes to the Site of Inflammation', *Veterinary Pathology*. doi: 10.1177/0300985812469883.

Mullins, R. D. *et al.* (2013) 'Arp2/3 Complex from *Acanthamoeba* Binds Profilin and Cross-links Actin Filaments', *Molecular Biology of the Cell*. doi: 10.1091/mbc.9.4.841.

Münter, S. *et al.* (2009) 'Plasmodium Sporozoite Motility Is Modulated by the Turnover of Discrete Adhesion Sites', *Cell Host & Microbe*, 6(6), pp. 551-562. doi: 10.1016/j.chom.2009.11.007.

Murakami, K. *et al.* (2010) 'Structural Basis for Actin Assembly, Activation of ATP Hydrolysis, and Delayed Phosphate Release', *Cell*. doi: 10.1016/j.cell.2010.09.034.

Murakami, Y. (2013) 'Heterochromatin and Euchromatin', in *Encyclopedia of*

Systems Biology. doi: 10.1007/978-1-4419-9863-7_1413.

Muyldermans, S. *et al.* (2009) 'Camelid immunoglobulins and nanobody technology', *Veterinary Immunology and Immunopathology*. doi: 10.1016/j.vetimm.2008.10.299.

Nair, S. C. *et al.* (2012) 'Apicoplast isoprenoid precursor synthesis and the molecular basis of fosmidomycin resistance in *Toxoplasma gondii*', *The Journal of Experimental Medicine*. doi: 10.1084/jem.201100392095c.

Niedelman, W. *et al.* (2012) 'The rhoptry proteins ROP18 and ROP5 mediate *Toxoplasma gondii* evasion of the murine, but not the human, interferon-gamma response', *PLoS Pathogens*. doi: 10.1371/journal.ppat.1002784.

Nishi, M. *et al.* (2008) 'Organelle dynamics during the cell cycle of *Toxoplasma gondii*', *Journal of Cell Science*. doi: 10.1242/jcs.021089.

Nishida, E. and Sakai, H. (1983) 'Kinetic analysis of actin polymerization', *Journal of Biochemistry*. doi: 10.1093/oxfordjournals.jbchem.a134224.

Oelz, D. B., Rubinstein, B. Y. and Mogilner, A. (2015) 'A Combination of Actin Treadmilling and Cross-Linking Drives Contraction of Random Actomyosin Arrays', *Biophysical Journal*, 109(9), pp. 1818-1829. doi: 10.1016/j.bpj.2015.09.013.

de Oliveira, G. B. *et al.* (2016) 'Cerebral toxoplasmosis in patients with acquired immune deficiency syndrome in the neurological emergency department of a tertiary hospital', *Clinical Neurology and Neurosurgery*. doi: 10.1016/j.clineuro.2016.08.014.

Olshina, M. A. *et al.* (2015) 'Plasmodium falciparum coronin organizes arrays of parallel actin filaments potentially guiding directional motility in invasive malaria parasites', *Malaria Journal*. doi: 10.1186/s12936-015-0801-5.

Otterbein, L. R., Graceffa, P. and Dominguez, R. (2001) 'The crystal structure of uncomplexed actin in the ADR state', *Science*. doi: 10.1126/science.1059700.

- Ou, G. *et al.* (2005) 'Functional coordination of intraflagellar transport motors', *Nature*. doi: 10.1038/nature03818.
- Pantaloni, D., Carlier, M. F. and Coue, M. (1984) 'The critical concentration of actin in the presence of ATP increases with the number concentration of filaments and approaches the critical concentration of actin.ADP', *Journal of Biological Chemistry*.
- Pantaloni, D., Le Clainche, C. and Carlier, M. F. (2001) 'Mechanism of actin-based motility', *Science*. doi: 10.1126/science.1059975.
- Panza, P. *et al.* (2015) 'Live imaging of endogenous protein dynamics in zebrafish using chromobodies', *Development*, 142(10), pp. 1879-1884. doi: 10.1242/dev.118943.
- Pappas, G., Roussos, N. and Falagas, M. E. (2009) 'Toxoplasmosis snapshots: Global status of *Toxoplasma gondii* seroprevalence and implications for pregnancy and congenital toxoplasmosis', *International Journal for Parasitology*, 39(12), pp. 1385-1394. doi: 10.1016/j.ijpara.2009.04.003.
- Park, H. *et al.* (2016) 'Measuring cell surface area and deformability of individual human red blood cells over blood storage using quantitative phase imaging', *Scientific Reports*. doi: 10.1038/srep34257.
- Pavlou, G. *et al.* (2018) 'Toxoplasma Parasite Twisting Motion Mechanically Induces Host Cell Membrane Fission to Complete Invasion within a Protective Vacuole', *Cell Host and Microbe*. doi: 10.1016/j.chom.2018.06.003.
- Periz, J. *et al.* (2017) 'Toxoplasma gondii F-actin forms an extensive filamentous network required for material exchange and parasite maturation', *eLife*, 6. doi: 10.7554/eLife.24119.
- Periz, J. *et al.* (2019) 'A highly dynamic F-actin network regulates transport and recycling of micronemes in *Toxoplasma gondii* vacuoles', *Nature Communications*, 10(1), p. 4183. doi: 10.1038/s41467-019-12136-2.

Pernas, L. *et al.* (2014) 'Toxoplasma Effector MAF1 Mediates Recruitment of Host Mitochondria and Impacts the Host Response', *PLoS Biology*. doi: 10.1371/journal.pbio.1001845.

Petrie, R. J. *et al.* (2012) 'Nonpolarized signaling reveals two distinct modes of 3D cell migration', *The Journal of Cell Biology*, 197(3), pp. 439-455. doi: 10.1083/jcb.201201124.

Petrie, R. J., Koo, H. and Yamada, K. M. (2014) 'Generation of compartmentalized pressure by a nuclear piston governs cell motility in a 3D matrix', *Science*. doi: 10.1126/science.1256965.

Petrie, R. J. and Yamada, K. M. (2015) 'Fibroblasts Lead the Way: A Unified View of 3D Cell Motility', *Trends in Cell Biology*, 25(11), pp. 666-674. doi: 10.1016/j.tcb.2015.07.013.

Petrie, R. J. and Yamada, K. M. (2016) 'Multiple mechanisms of 3D migration: the origins of plasticity', *Current Opinion in Cell Biology*, 42, pp. 7-12. doi: 10.1016/j.ceb.2016.03.025.

Plattner, F. *et al.* (2008) 'Toxoplasma Profilin Is Essential for Host Cell Invasion and TLR11-Dependent Induction of an Interleukin-12 Response', *Cell Host & Microbe*, 3(2), pp. 77-87. doi: 10.1016/j.chom.2008.01.001.

Pollard, T. D. (1984) 'Polymerization of ADP-actin', *Journal of Cell Biology*, 99(3), pp. 769-777. doi: 10.1083/jcb.99.3.769.

Pollard, T. D. (1986) 'Rate constants for the reactions of ATP- and ADP-actin with the ends of actin filaments', *Journal of Cell Biology*. doi: 10.1083/jcb.103.6.2747.

Pollard, T. D. (2007) 'Regulation of Actin Filament Assembly by Arp2/3 Complex and Formins', *Annual Review of Biophysics and Biomolecular Structure*. doi: 10.1146/annurev.biophys.35.040405.101936.

Pollard, T. D. (2016) 'Actin and actin-binding proteins', *Cold Spring Harbor*

Perspectives in Biology, 8(8). doi: 10.1101/cshperspect.a018226.

Pollard, T. D., Blanchoin, L. and Mullins, R. D. (2002) 'Molecular Mechanisms Controlling Actin Filament Dynamics in Nonmuscle Cells', *Annual Review of Biophysics and Biomolecular Structure*. doi: 10.1146/annurev.biophys.29.1.545.

Pollard, T. D. and Borisy, G. G. (2003) 'Cellular motility driven by assembly and disassembly of actin filaments', *Cell*, 112(4), pp. 453-465. doi: 10.1016/S0092-8674(03)00120-X.

Pollard, T. D. and Cooper, J. A. (2009) 'Actin, a Central Player in Cell Shape and Movement', *Science*, 326(5957), pp. 1208-1212. doi: 10.1126/science.1175862.

Pospich, S. *et al.* (2017) 'Near-atomic structure of jasplakinolide-stabilized malaria parasite F-actin reveals the structural basis of filament instability', *Proceedings of the National Academy of Sciences*. doi: 10.1073/pnas.1707506114.

Poupel, O. and Tardieux, I. (1999) 'Toxoplasma gondii motility and host cell invasiveness are drastically impaired by jasplakinolide, a cyclic peptide stabilizing F-actin', *Microbes and Infection*. doi: 10.1016/S1286-4579(99)80066-5.

Radke, J. R. *et al.* (2001) 'Defining the cell cycle for the tachyzoite stage of *Toxoplasma gondii*', *Molecular and Biochemical Parasitology*. doi: 10.1016/S0166-6851(01)00284-5.

Ramakrishnan, S. *et al.* (2012) 'Apicoplast and endoplasmic reticulum cooperate in fatty acid biosynthesis in apicomplexan parasite *Toxoplasma gondii*', *Journal of Biological Chemistry*. doi: 10.1074/jbc.M111.310144.

Reese, M. L., Shah, N. and Boothroyd, J. C. (2014) 'The *Toxoplasma* Pseudokinase ROP5 Is an Allosteric Inhibitor of the Immunity-related GTPases', *Journal of Biological Chemistry*, 289(40), pp. 27849-27858. doi: 10.1074/jbc.M114.567057.

Reid, A. J. (2015) 'Large, rapidly evolving gene families are at the forefront of host-parasite interactions in Apicomplexa.', *Parasitology*, (Suppl 1), pp. S57-70. doi: 10.1017/S0031182014001528.

Dos Remedios, C. G. *et al.* (2003) 'Actin Binding Proteins: Regulation of Cytoskeletal Microfilaments', *Physiological Reviews*. doi: 10.1152/physrev.00026.2002.

Renkawitz, J. and Sixt, M. (2016) 'Formin' a Nuclear Protection', *Cell*, pp. 1448-1449. doi: 10.1016/j.cell.2016.11.024.

Revach, O. Y. *et al.* (2015) 'Mechanical interplay between invadopodia and the nucleus in cultured cancer cells', *Scientific Reports*. doi: 10.1038/srep09466.

Ridley, A. J. (2011) 'Life at the Leading Edge', *Cell*, 145(7), pp. 1012-1022. doi: 10.1016/j.cell.2011.06.010.

Riedl, J. *et al.* (2008) 'Lifeact: a versatile marker to visualize F-actin.', *Nature methods*, 5(7), pp. 605-7. doi: 10.1038/nmeth.1220.

Riglar, D. T. *et al.* (2011) 'Super-resolution dissection of coordinated events during malaria parasite invasion of the human erythrocyte', *Cell Host and Microbe*. doi: 10.1016/j.chom.2010.12.003.

Rocchetti, A., Hawes, C. and Kriechbaumer, V. (2014) 'Fluorescent labelling of the actin cytoskeleton in plants using a cameloid antibody.', *Plant methods*, 10, p. 12. doi: 10.1186/1746-4811-10-12.

Roiko, M. S., Svezhova, N. and Carruthers, V. B. (2014) 'Acidification Activates *Toxoplasma gondii* Motility and Egress by Enhancing Protein Secretion and Cytolytic Activity', *PLoS Pathogens*. Edited by L. J. Knoll, 10(11), p. e1004488. doi: 10.1371/journal.ppat.1004488.

Roos, D. S. *et al.* (1999) 'Origin, targeting, and function of the apicomplexan plastid', *Current Opinion in Microbiology*. doi: 10.1016/S1369-5274(99)80075-7.

Del Rosario, M. *et al.* (no date) 'Apicomplexan F-actin is required for efficient

nuclear entry during host cell invasion', *Submitted*.

Rothbauer, U. *et al.* (2006) 'Targeting and tracing antigens in live cells with fluorescent nanobodies', *Nature Methods*. doi: 10.1038/nmeth953.

Rueden, C. T. *et al.* (2017) 'ImageJ2: ImageJ for the next generation of scientific image data', *BMC Bioinformatics*. doi: 10.1186/s12859-017-1934-z.

Russell, D. G. and Burns, R. G. (1984) 'The polar ring of coccidian sporozoites: a unique microtubule-organizing centre', *J Cell Sci*.

Sadak, A. *et al.* (1988) 'Characterization of a family of rhoptry proteins of *Toxoplasma gondii*', *Molecular and Biochemical Parasitology*. doi: 10.1016/0166-6851(88)90075-8.

Sadhu, R. K. and Chatterjee, S. (2016) 'Actin filaments growing against a barrier with fluctuating shape', *Physical Review E - Statistical, Nonlinear, and Soft Matter Physics*, 93(6), pp. 1-11. doi: 10.1103/PhysRevE.93.062414.

Sahai, E. and Marshall, C. J. (2003) 'Differing modes of tumour cell invasion have distinct requirements for Rho/ROCK signalling and extracellular proteolysis', *Nature Cell Biology*, 5(8), pp. 711-719. doi: 10.1038/ncb1019.

Sahoo, N. (2005) 'Unusual Kinetic and Structural Properties Control Rapid Assembly and Turnover of Actin in the Parasite *Toxoplasma gondii*', *Molecular Biology of the Cell*. doi: 10.1091/mbc.e05-06-0512.

Sailem, H. Z., Cooper, S. and Bakal, C. (2016) 'Visualizing quantitative microscopy data: History and challenges', *Critical Reviews in Biochemistry and Molecular Biology*. doi: 10.3109/10409238.2016.1146222.

Salamun, J. *et al.* (2014) 'Structure of *Toxoplasma gondii* coronin, an actin-binding protein that relocalizes to the posterior pole of invasive parasites and contributes to invasion and egress', *FASEB Journal*. doi: 10.1096/fj.14-252569.

Saxton, M. J. and Jacobson, K. (2002) 'SINGLE-PARTICLE TRACKING: Applications to Membrane Dynamics', *Annual Review of Biophysics and Biomolecular*

Structure. doi: 10.1146/annurev.biophys.26.1.373.

Schäpe, J. *et al.* (2009) 'Influence of lamin A on the mechanical properties of amphibian oocyte nuclei measured by atomic force microscopy', *Biophysical Journal*. doi: 10.1016/j.bpj.2009.02.048.

Scherlach, K. *et al.* (2010) 'The chemistry and biology of cytochalasins', *Natural Product Reports*. doi: 10.1039/b903913a.

Schiffhauer, E. S. S. *et al.* (2016) 'Mechanoaccumulative Elements of the Mammalian Actin Cytoskeleton', *Current Biology*. doi: 10.1016/j.cub.2016.04.007.

Schindelin, J. *et al.* (2012) 'Fiji: an open-source platform for biological-image analysis.', *Nature methods*. doi: 10.1038/nmeth.2019.

Schmitz, S. *et al.* (2005) 'Malaria parasite actin filaments are very short', *Journal of Molecular Biology*. doi: 10.1016/j.jmb.2005.03.056.

Schmitz, S. *et al.* (2010) 'Malaria Parasite Actin Polymerization and Filament Structure', *Journal of Biological Chemistry*, 285(47), pp. 36577-36585. doi: 10.1074/jbc.M110.142638.

Schoenwaelder, S. M. and Burridge, K. (1999) 'Bidirectional signaling between the cytoskeleton and integrins', *Current Opinion in Cell Biology*. doi: 10.1016/S0955-0674(99)80037-4.

Schreiner, S. M. *et al.* (2015) 'The tethering of chromatin to the nuclear envelope supports nuclear mechanics', *Nature Communications*. doi: 10.1038/ncomms8159.

Schwarz, N. and Leube, R. (2016) 'Intermediate Filaments as Organizers of Cellular Space: How They Affect Mitochondrial Structure and Function', *Cells*, 5(3), p. 30. doi: 10.3390/cells5030030.

Seeber, F. and Soldati-Favre, D. (2010) 'Metabolic pathways in the apicoplast of apicomplexa', *International Review of Cell and Molecular Biology*. doi:

10.1016/S1937-6448(10)81005-6.

Sellers, J. R. (2000) 'Myosins: A diverse superfamily', *Biochimica et Biophysica Acta - Molecular Cell Research*. doi: 10.1016/S0167-4889(00)00005-7.

Sharma, P. and Chitnis, C. E. (2013) 'Key molecular events during host cell invasion by Apicomplexan pathogens', *Current Opinion in Microbiology*. Elsevier Ltd, 16(4), pp. 432-437. doi: 10.1016/j.mib.2013.07.004.

Shastri, A. J. *et al.* (2014) 'GRA25 is a novel virulence factor of toxoplasma gondii and influences the host immune response', *Infection and Immunity*, 82(6), pp. 2595-2605. doi: 10.1128/IAI.01339-13.

Shaw, M. K. *et al.* (2000) 'Microtubules, but not actin filaments, drive daughter cell budding and cell division in *Toxoplasma gondii*.' , *Journal of cell science*.

Shaw, M. K. and Tilney, L. G. (1999) 'Induction of an acrosomal process in *Toxoplasma gondii*: Visualization of actin filaments in a protozoan parasite', *Proceedings of the National Academy of Sciences*, 96(16), pp. 9095-9099. doi: 10.1073/pnas.96.16.9095.

Sheiner, L. *et al.* (2010) 'Toxoplasma gondii transmembrane microneme proteins and their modular design', *Molecular Microbiology*. doi: 10.1111/j.1365-2958.2010.07255.x.

Sheiner, L., Dowse, T. J. and Soldati-Favre, D. (2008) 'Identification of trafficking determinants for polytopic rhomboid proteases in *Toxoplasma gondii*', *Traffic*. doi: 10.1111/j.1600-0854.2008.00736.x.

Shen, B. *et al.* (2014) 'Functional analysis of rhomboid proteases during *Toxoplasma* invasion', *mBio*. doi: 10.1128/mBio.01795-14.

Shen, B. and Sibley, L. D. (2014) 'Toxoplasma aldolase is required for metabolism but dispensable for host-cell invasion ', *Proceedings of the National Academy of Sciences*. doi: 10.1073/pnas.1315156111.

Shwab, E. K. *et al.* (2014) 'Geographical patterns of *Toxoplasma gondii* genetic

diversity revealed by multilocus PCR-RFLP genotyping', *Parasitology*. doi: 10.1017/S0031182013001844.

Sibley, L. D. *et al.* (2009) 'Genetic diversity of *Toxoplasma gondii* in animals and humans.', *Philosophical transactions of the Royal Society of London. Series B, Biological sciences*, 364(1530), pp. 2749-2761. doi: 10.1098/rstb.2009.0087.

Sibley, L. and Niesman, I. (1995) 'Regulated secretion of multi-lamellar vesicles leads to formation of a tubulo-vesicular network in host-cell vacuoles occupied by *Toxoplasma gondii*', *Journal of Cell ...*

Siden-Kiamos, I., Louis, C. and Matuschewski, K. (2012) 'Evidence for filamentous actin in ookinetes of a malarial parasite', *Molecular and Biochemical Parasitology*. doi: 10.1016/j.molbiopara.2011.11.002.

Skillman, K. M. *et al.* (2013) 'The unusual dynamics of parasite actin result from isodesmic polymerization.', *Nature communications*. Nature Publishing Group, 4, p. 2285. doi: 10.1038/ncomms3285.

Smal, I. *et al.* (2010) 'Microtubule dynamics analysis using kymographs and variable-rate particle filters', *IEEE Transactions on Image Processing*. doi: 10.1109/TIP.2010.2045031.

Snow, J. J. *et al.* (2004) 'Two anterograde intraflagellar transport motors cooperate to build sensory cilia on *C. elegans* neurons', *Nature Cell Biology*. doi: 10.1038/ncb1186.

Soldati, D., Dubremetz, J. F. and Lebrun, M. (2001) 'Microneme proteins: Structural and functional requirements to promote adhesion and invasion by the apicomplexan parasite *Toxoplasma gondii*', *International Journal for Parasitology*, pp. 1293-1302. doi: 10.1016/S0020-7519(01)00257-0.

Speer, C. A. and Dubey, J. P. (1998) 'Ultrastructure of early stages of infections in mice fed *Toxoplasma gondii* oocysts', *Parasitology*. doi: 10.1017/S0031182097001959.

- Stehbens, S. and Wittmann, T. (2012) 'Targeting and transport: How microtubules control focal adhesion dynamics', *Journal of Cell Biology*. doi: 10.1083/jcb.201206050.
- Stoitzner, P. *et al.* (2002) 'A close-up view of migrating Langerhans cells in the skin', *Journal of Investigative Dermatology*. doi: 10.1046/j.0022-202x.2001.01631.x.
- Stortz, J. F. *et al.* (2019) 'Formin-2 drives polymerisation of actin filaments enabling segregation of apicoplasts and cytokinesis in *Plasmodium falciparum*', *eLife*, 8. doi: 10.7554/eLife.49030.
- Stricker, J., Falzone, T. and Gardel, M. L. (2010) 'Mechanics of the F-actin cytoskeleton', *Journal of Biomechanics*, 43(1), pp. 9-14. doi: 10.1016/j.jbiomech.2009.09.003.
- Stroka, K. M. *et al.* (2014) 'Water permeation drives tumor cell migration in confined microenvironments', *Cell*. doi: 10.1016/j.cell.2014.02.052.
- Suarez, C. E. *et al.* (2017) 'Advances in the application of genetic manipulation methods to apicomplexan parasites', *International Journal for Parasitology*. doi: 10.1016/j.ijpara.2017.08.002.
- Sueters-Di Meo, J., Kruit, P. and Hoogenboom, J. (2016) 'Improving 3d correlation in integrated correlated light and electron microscopy using confocal laser scanning microscopy', in *European Microscopy Congress 2016: Proceedings*. doi: 10.1002/9783527808465.emc2016.6525.
- Suss-Toby, E., Zimmerberg, J. and Wardt, G. E. (1996) *Toxoplasma invasion: The parasitophorous vacuole is formed from host cell plasma membrane and pinches off via a fission pore (cell capacitance/intracellular parasite/endocytosis)*, *National Institutes of Health*.
- Sweeney, K. R. *et al.* (2010) 'Host Cell Invasion by *Toxoplasma gondii* Is Temporally Regulated by the Host Microtubule Cytoskeleton', *Eukaryotic Cell*, 9(11), pp. 1680-1689. doi: 10.1128/EC.00079-10.

- Tanaka, K. (2000) 'Formin family proteins in cytoskeletal control.', *Biochemical and biophysical research communications*, 267(2), pp. 479-81. doi: 10.1006/bbrc.1999.1707.
- Tang, D. D. and Gerlach, B. D. (2017) 'The roles and regulation of the actin cytoskeleton, intermediate filaments and microtubules in smooth muscle cell migration', *Respiratory Research*. doi: 10.1186/s12931-017-0544-7.
- Tang, D., Mehta, D. and Gunst, S. J. (2017) 'Mechanosensitive tyrosine phosphorylation of paxillin and focal adhesion kinase in tracheal smooth muscle', *American Journal of Physiology-Cell Physiology*. doi: 10.1152/ajpcell.1999.276.1.c250.
- Tang, Q. *et al.* (2014) 'Calcium-dependent phosphorylation alters class XIVa myosin function in the protozoan parasite *Toxoplasma gondii*', *Molecular Biology of the Cell*. doi: 10.1091/mbc.e13-11-0648.
- Tannert, R. *et al.* (2010) 'Synthesis and structure-activity correlation of natural-product inspired cyclodepsipeptides stabilizing F-actin', *Journal of the American Chemical Society*. doi: 10.1021/ja9095126.
- Tardieux, I. and Baum, J. (2016) 'Reassessing the mechanics of parasite motility and host-cell invasion', *The Journal of Cell Biology*, 214(5), pp. 507-515. doi: 10.1083/jcb.201605100.
- Thiam, H. R. *et al.* (2016) 'Perinuclear Arp2/3-driven actin polymerization enables nuclear deformation to facilitate cell migration through complex environments', *Nature Communications*. doi: 10.1038/ncomms10997.
- Thomas, D. G. *et al.* (2015) 'Non-muscle myosin IIB is critical for nuclear translocation during 3D invasion', *Journal of Cell Biology*. doi: 10.1083/jcb.201502039.
- Tinevez, J.-Y. *et al.* (2009) 'Role of cortical tension in bleb growth', *Proceedings of the National Academy of Sciences*, 106(44), pp. 18581-18586. doi: 10.1073/pnas.0903353106.

- Tosetti, N. *et al.* (2019) 'Three F-actin assembly centers regulate organelle inheritance , cell-cell communication and motility in *Toxoplasma gondii*', pp. 1-32.
- Toyoshima, Y. Y., Toyoshima, C. and Spudich, J. A. (1989) 'Bidirectional movement of actin filaments along tracks of myosin heads', *Nature*.
- Tran, J. Q. *et al.* (2012) 'SPM1 Stabilizes Subpellicular Microtubules in *Toxoplasma gondii*', *Eukaryotic Cell*, 11(2), pp. 206-216. doi: 10.1128/EC.05161-11.
- Trivedi, N. *et al.* (2014) 'Leading-process actomyosin coordinates organelle positioning and adhesion receptor dynamics in radially migrating cerebellar granule neurons', *Neural development*. doi: 10.1186/1749-8104-9-26.
- Van Troys, M. *et al.* (2008) 'Ins and outs of ADF/cofilin activity and regulation', *European Journal of Cell Biology*, pp. 649-667. doi: 10.1016/j.ejcb.2008.04.001.
- Vahokoski, J. *et al.* (2014) 'Structural Differences Explain Diverse Functions of Plasmodium Actins', *PLoS Pathogens*. doi: 10.1371/journal.ppat.1004091.
- Vallotton, P. and Small, J. V. (2009) 'Shifting views on the leading role of the lamellipodium in cell migration: speckle tracking revisited', *Journal of Cell Science*. doi: 10.1242/jcs.042036.
- Villari, G. *et al.* (2015) 'A direct interaction between fascin and microtubules contributes to adhesion dynamics and cell migration', *Journal of Cell Science*. doi: 10.1242/jcs.175760.
- Visa, N. and Percipalle, P. (2010) 'Nuclear functions of actin.', *Cold Spring Harbor perspectives in biology*. doi: 10.1101/cshperspect.a000620.
- Vogel, D. Y. *et al.* (2014) 'Macrophages migrate in an activation-dependent manner to chemokines involved in neuroinflammation.', *Journal of neuroinflammation*. *Journal of Neuroinflammation*, 11(1), p. 23. doi: 10.1186/1742-2094-11-23.

Waller, R. F. and McFadden, G. I. (2005) 'The apicoplast: A review of the derived plastid of apicomplexan parasites', *Current Issues in Molecular Biology*.

Wang, R., Li, Q. and Tang, D. D. (2006) 'Role of vimentin in smooth muscle force development', *American Journal of Physiology-Cell Physiology*. doi: 10.1152/ajpcell.00097.2006.

Wang, Y. *et al.* (2013) 'Phosphorylation of cofilin regulates extinction of conditioned aversive memory via AMPAR trafficking.', *Journal of Neuroscience*, 33(15), pp. 6423-6433. doi: 10.1523/JNEUROSCI.5107-12.2013.

Waterman-Storer, C. M. and Salmon, E. (1999) 'Positive feedback interactions between microtubule and actin dynamics during cell motility', *Current Opinion in Cell Biology*. doi: 10.1016/S0955-0674(99)80008-8.

Weber, A. P. M. and Linka, N. (2011) 'Connecting the Plastid: Transporters of the Plastid Envelope and Their Role in Linking Plastidial with Cytosolic Metabolism', *Annual Review of Plant Biology*, 62(1), pp. 53-77. doi: 10.1146/annurev-arplant-042110-103903.

Wei, Q. *et al.* (2012) 'The BBSome controls IFT assembly and turnaround in cilia', *Nature Cell Biology*. doi: 10.1038/ncb2560.

Welch, M. D. and Mullins, R. D. (2002) 'Cellular Control of Actin Nucleation', *Annual Review of Cell and Developmental Biology*. doi: 10.1146/annurev.cellbio.18.040202.112133.

Wesseling, J. G. *et al.* (1988) 'Nucleotide sequence and deduced amino acid sequence of a Plasmodium falciparum actin gene', *Molecular and Biochemical Parasitology*. doi: 10.1016/0166-6851(88)90051-5.

Wetzel, D. M. *et al.* (2003) 'Actin Filament Polymerization Regulates Gliding Motility by Apicomplexan Parasites', *Molecular Biology of the Cell*. Edited by J. Lippincott-Schwartz, 14(2), pp. 396-406. doi: 10.1091/mbc.e02-08-0458.

Whitelaw, J. A. *et al.* (2017) 'Surface attachment, promoted by the actomyosin

system of *Toxoplasma gondii* is important for efficient gliding motility and invasion', *BMC Biology*, 15(1), p. 1. doi: 10.1186/s12915-016-0343-5.

Wichroski, M. J. *et al.* (2002) 'Clostridium septicum alpha-toxin is active against the parasitic protozoan *Toxoplasma gondii* and targets members of the SAG family of glycosylphosphatidylinositol-anchored surface proteins', *Infection and Immunity*. doi: 10.1128/IAI.70.8.4353-4361.2002.

Wiggin, O. *et al.* (2012) 'ADF/Cofilin Regulates Actomyosin Assembly through Competitive Inhibition of Myosin II Binding to F-Actin', *Developmental Cell*, 22(3), pp. 530-543. doi: 10.1016/j.devcel.2011.12.026.

Williams, M. J. *et al.* (2015) 'Two Essential Light Chains Regulate the MyoA Lever Arm To Promote *Toxoplasma* Gliding Motility', *mBio*. doi: 10.1128/mbio.00845-15.

Wilson, M. H. and Holzbaun, E. L. F. (2012) 'Opposing microtubule motors drive robust nuclear dynamics in developing muscle cells', *Journal of Cell Science*. doi: 10.1242/jcs.108688.

Wolf, K. *et al.* (2003) 'Compensation mechanism in tumor cell migration', *The Journal of Cell Biology*, 160(2), pp. 267-277. doi: 10.1083/jcb.200209006.

Wolf, M. *et al.* (2015) 'ADF/Cofilin controls synaptic actin dynamics and regulates synaptic vesicle mobilization and exocytosis', *Cerebral Cortex*, 25(9), pp. 2863-2875. doi: 10.1093/cercor/bhu081.

Wolffe, A. P. and Hayes, J. J. (1999) 'Chromatin disruption and modification', *Nucleic Acids Research*, pp. 711-720. doi: 10.1093/nar/27.3.711.

Wu, J. *et al.* (2014) 'Actomyosin pulls to advance the nucleus in a migrating tissue cell', *Biophysical Journal*. doi: 10.1016/j.bpj.2013.11.4489.

Xiao, H. *et al.* (2010) 'Post-translational modifications to *Toxoplasma gondii* α - and β -tubulins include novel C-terminal methylation', *Journal of Proteome Research*. doi: 10.1021/pr900699a.

Yadav, R. *et al.* (2011) 'Solution structure and dynamics of ADF from *Toxoplasma gondii*', *Journal of Structural Biology*. doi: 10.1016/j.jsb.2011.07.011.

Yang, N. *et al.* (2013) 'Genetic basis for phenotypic differences between different *Toxoplasma gondii* type I strains.', *BMC genomics*. *BMC Genomics*, 14(1), p. 467. doi: 10.1186/1471-2164-14-467.

Yarmola, E. G. and Bubb, M. R. (2006) 'Profilin: emerging concepts and lingering misconceptions', *Trends in Biochemical Sciences*, 31(4), pp. 197-205. doi: 10.1016/j.tibs.2006.02.006.

Yeh, E. and DeRisi, J. L. (2011) 'Chemical rescue of malaria parasites lacking an apicoplast defines organelle function in blood-stage *Plasmodium falciparum*', *PLoS Biology*. doi: 10.1371/journal.pbio.1001138.

Yi, J. *et al.* (2012) 'Actin retrograde flow and actomyosin II arc contraction drive receptor cluster dynamics at the immunological synapse in Jurkat T cells', *Molecular Biology of the Cell*. doi: 10.1091/mbc.e11-08-0731.

Yoon, H. S. *et al.* (2002) 'The Single, Ancient Origin of Chromist Plastids', *Journal of Phycology*, 38(s1), pp. 40-40. doi: 10.1046/j.1529-8817.38.s1.8.x.

Yusuf, N. A. *et al.* (2015) 'The *Plasmodium* Class XIV Myosin, MyoB, Has a Distinct Subcellular Location in Invasive and Motile Stages of the Malaria Parasite and an Unusual Light Chain', *Journal of Biological Chemistry*, 290(19), pp. 12147-12164. doi: 10.1074/jbc.M115.637694.

Zhang, Y. *et al.* (2014) 'The circular F-actin bundles provide a track for turnaround and bidirectional movement of mitochondria in *Arabidopsis* root hair', *PLoS ONE*. doi: 10.1371/journal.pone.0091501.

Zhao, S. H. *et al.* (2013) 'Profilin-1 promotes the development of hypertension-induced cardiac hypertrophy', *Journal of Hypertension*. doi: 10.1097/HJH.0b013e32835d6a56.